THE UNIVERSITY OF QUEENSLAND

AUSTRALIA

Neuroligins and Neurexins in Alzheimer's disease

Ikhlas Abdulaziz Sindi

B. Biochem., M. MolBio.

A thesis submitted for the degree of Doctor of Philosophy at

The University of Queensland in 2014

School of Medicine

Abstract

Alzheimer's disease (AD) is a progressive neurodegenerative disorder and a main cause of dementia in the elderly. The main pathological hallmarks of AD are the accumulation of insoluble aggregates of amyloid-β-peptides (Aβ), which are proteolytic cleavage products of the amyloid-β precursor protein, and insoluble filaments composed of hyperphosphorylated tau protein. Familial forms of AD can raise the production of Aβ peptides.

Synaptic damage is a critical aspect of AD, and the best correlate with cognitive impairment ante mortem. Synapses, the loci of communication between neurons, are characterized by signature protein combinations arrayed at tightly apposed pre- and post-synaptic sites. The most widely studied trans-synaptic junctional complexes, which direct synaptogenesis and foster the maintenance and stability of the mature terminal, are conjunctions of presynaptic neurexins and postsynaptic neuroligins. The presynaptic neurexins bind with the neuroligins on the postsynaptic membrane. This pairing is implicated in synaptic signalling and the determination of whether a synapse will be excitatory or inhibitory. At the postsynaptic density, neuroligin-1 is specific for glutamatergic synapses, whereas neuroligin-2 is indicative of a GABAergic synapse. The neuroligins mediate connection with the presynaptic terminal mainly through β-neurexin, which occurs in different isoforms derived from alternatively spliced transcripts. Fluctuations in the levels of neuroligins and neurexins can sway the balance between excitatory and inhibitory neurotransmission in the brain, and could lead to damage of synapses and dendrites.

The main objective of the research set out below was to investigate possible disruptions of nerve-cell connections in AD through assay of the trans-synaptic neurexin and neuroligin proteins. The project explored differences in neuroligin and neurexin expression across different brain regions at various stages of the progression of the disease. I also investigated whether any differences occurred at the level of transcription or translation of the proteins. Additional work focused on a genetic study and the association between the *NRXN-3* gene and AD.

To identify the differences in the level of protein expression, a sensitive immunodetection-assay using recombinant protein standards was developed to measure concentrations of neuroligin-1, neuroligin-2 and β-Neurexin-1 in AD cases and matched controls. Two regions that are pathologically affected in the AD brain, the hippocampus and the inferior temporal cortex, and one relatively spared region, the occipital cortex, were studied. Quantification showed higher expression in AD cases than in controls of both post-synaptic neuroligin-1 and pre-synaptic β-neurexin-1. The expression of neuroligin-1 and β-neurexin-1 was higher in AD hippocampus than in this region in controls, but the difference only reached significance for neuroligin-1. In contrast, the expression of neuroligin-2 protein was lower overall in AD cases than in controls. Lower expression in AD cases was seen in all areas and reached statistical significance in inferior temporal cortex.

A mass spectrometry approach was employed to validate the quantification of these proteins using with two novel methods, multiple reaction monitoring (MRM) and sequential window acquisition of all theoretical fragment ion spectra (SWATH). Using these high-throughput techniques I identified several hundred synaptic proteins, including neuroligins and neurexins. However, an insufficient number of peptides was identified for each of these proteins, which precluded their quantification by these approaches.

Protein data from the immunodetection assay were correlated with mRNA transcript levels by using quantitative real-time PCR assays, which were established for neuroligin-1, neuroligin-2 and β-neurexin-1 transcripts in the same areas of AD cases and controls. Quantification revealed significantly lower expression of all three transcripts in AD hippocampus and inferior temporal cortex, but no difference in occipital cortex, compared with controls. Expression of the three transcripts was found to correlate with disease progression as indexed by the AD pathological markers Aβ, neurofibrillary tangles, and neuronal loss. However, APOE genotype had no effect on mRNA transcript levels.

To look for a genetic association between the *β–NRXN-3* gene and AD, I attempted to replicate a published report that the single nucleotide polymorphism rs17757879 was a tag for the

gene in a Spanish cohort. AD cases and controls were genotyped by a Taqman assay to explore the association between rs17757879 in *β–NRXN-3* and AD in an Australian Caucasian population. Overall, the data did not show a significant association between rs17757879 and AD. When the subjects were partitioned by gender, there was a trend toward a significant association between rs17757879 and the disease in males only. When alleles were divided according to the presence or absence of the T allele (CT plus TT compared with CC) association reached significance, and indicated that the T allele was protective against AD in males.

The data from this project provides further understanding of the molecular characteristics of the neurexin-neuroligin complex in AD. An understanding of the roles of these molecules will likely open new therapeutic avenues for the treatment of AD.

Declaration by author

This thesis is composed of my original work, and contains no material previously published or written by another person except where due reference has been made in the text. I have clearly stated the contribution by others to jointly-authored works that I have included in my thesis.

I have clearly stated the contribution of others to my thesis as a whole, including statistical assistance, survey design, data analysis, significant technical procedures, professional editorial advice, and any other original research work used or reported in my thesis. The content of my thesis is the result of work I have carried out since the commencement of my research higher degree candidature and does not include a substantial part of work that has been submitted to qualify for the award of any other degree or diploma in any university or other tertiary institution. I have clearly stated which parts of my thesis, if any, have been submitted to qualify for another award.

I acknowledge that an electronic copy of my thesis must be lodged with the University Library and, subject to the General Award Rules of The University of Queensland, immediately made available for research and study in accordance with the *Copyright Act 1968*.

I acknowledge that copyright of all material contained in my thesis resides with the copyright holder(s) of that material. Where appropriate I have obtained copyright permission from the copyright holder to reproduce material in this thesis.

Publications during candidature

Sindi, I. A., Tannenberg, R. K. & Dodd, P. R. 2014. A role for the neurexin-neuroligin complex in Alzheimer's disease. *Neurobiol. Aging*, 35, 746–56.

Sindi, I. A., Tannenberg, R. K. & Dodd, P. R. 2014. Higher expression of neuroligin-1 in Alzheimer's disease. *J. Alzheimers Dis.*, submitted.

Conference Abstracts: Oral Presentations

Sindi, I. A., Tannenberg, R. K., Byrne, G. & Dodd, P. R. 2013. A role for the neurexin-neuroligin complex in Alzheimer's disease. Presented at the 9th Annual Postgraduate Symposium, School of Chemistry and Molecular Bioscience, The University of Queensland, 21 November.

Conference Abstracts: Poster Presentations

Sindi, I. A., Tannenberg, R. K., Byrne, G. & Dodd, P. R. 2012. A role for the neurexin-neuroligin complex in Alzheimer's disease. Presented at Australian Neuroscience Society (ANS) Annual Meeting, Gold Coast, Australia, 29 January to 1 February.

Sindi, I. A., Tannenberg, R. K., Byrne, G. & Dodd, P. R. 2012. A role for the neurexin-neuroligin complex in Alzheimer's disease. Presented at the 4th Brain Plasticity Symposium at the Queensland Brain Institute, The University of Queensland, 3–5 September.

Sindi, I. A., Tannenberg, R. K., Byrne, G. & Dodd, P. R. 2012. A role for the neurexin-neuroligin complex in Alzheimer's disease. Presented at International Postgraduate Symposium In Biomedical Sciences at University of Queensland, 24 September.

Sindi, I. A., Tannenberg, R. K., Byrne, G. & Dodd, P. R. 2013. A role for the neurexin-neuroligin complex in Alzheimer's disease. Presented at Australasian Neuroscience Society (ANS) Annual Meeting, Melbourne, Australia, 3–6 February.

Sindi, I. A., Tannenberg, R. K., Byrne, G. & Dodd, P. R. 2013. A role for the neurexin-neuroligin complex in Alzheimer's disease. Presented at the Society for Neuroscience Annual Meeting, San Diego, U.S.A., 8–12 November.

Publications included in this thesis

Sindi, I. A., Tannenberg, R. K. & Dodd, P. R. 2014. A role for the neurexin-neuroligin complex in Alzheimer's disease. *Neurobiol Aging*, 35, 746-56.

Incorporated in parts of Chapter 1.

Contributor	Statement of contribution
Author Sindi, I. A. (Candidate)	I was responsible for 100% of research material, planning and writing the text and preparing the figures for the paper.
Author Tannenberg, R. K.	Provided laboratory guidance and advice.
Dodd, P. R.	Offered critical advice and editing of the manuscript prior submission

Sindi, I. A., Tannenberg, R. K. & Dodd, P. R. 2014. Higher expression of neuroligin-1 in Alzheimer's disease. *J. Alzheimers Dis*., submitted.

Partially incorporated in some paragraphs in chapter 3.

Contributor	Statement of contribution
Author Sindi, I. A. (Candidate)	I was responsible for 100% of research material, planning and writing the text and preparing the figures for the paper.
Author Tannenberg, R. K.	Provided laboratory guidance and advice.
Dodd, P. R.	Offered critical advice and editing of the manuscript prior submission

Contributions by others to the thesis

Dr. Rudi Tannenberg, Mentor, hands-on laboratory training and advice.

A/Prof. Peter Dodd, Lab chief and mentor, research and experimental design, statistical analysis training and advice.

Professor Gerard Byrne, Principal supervisor, clinical advice.

Research design advice and training:

Dr. Mathew Hynd

Dr. Michael Nefedov

Dr. Ada Ho

Laboratory experimental advice:

Dr. Rudi Tannenberg

Dr. Naomi Etheridge

Statement of parts of the thesis submitted to qualify for the award of another degree

None

Acknowledgments

My Ph.D. study has been a wonderful and often overwhelming experience. It is hard to say whether it has been grappling with the topic itself, which has been the real learning experience, or grappling with how to write papers, give talks, work in a group, stay up and stay focused. However, I am grateful to many people for making the time working on my Ph.D. an unforgettable experience. Firstly, I am deeply thankful to my supervisor A/Professor Peter Dodd. Working with you has been a real pleasure to me, with heaps of fun and excitement. You have been a steady influence throughout my Ph.D.; you have oriented and supported me with promptness and care, and have always been patient and encouraging in times of new ideas and difficulties; you have listened to my ideas and discussions with you frequently led to key insights. Your capability to select and to approach scientific problems, your high scientific standards, and your hard work set an example. Above all, you made me feel a friend and I am thankful from my heart. In addition, I am very grateful to my other supervisors Professor Gerard Byrne and Dr. Rudi Tannenberg for helpful comments during my Ph.D. lab work and in this thesis. In addition, I am very privileged to work with many other great lab members who became friends over the last several years: Dr. Naomi Etheridge, Dr. Ada Ho, Crystal Higgs, and Rachel Chang. I learned a lot from you in my research and how to tackle new problems and how to develop techniques to solve them. I have greatly enjoyed the opportunity to work with Dr. Amanda Nouwens, who supervised me for the mass spectrometer study and provided me technical with very useful technical advice.

To my family, Mom (Mrs. Nagat Alghamdy) and Dad (Mr. Abdulaziz Sindi) thank you for being so supportive over the past few years. Thank you for keeping yourselves healthy, and sparing me from family responsibilities, so that I could enjoy this adventure without worries. This will probably be the only page you will understand so I want you to know you mean the world to me.

This project could not be completed without the support and love from my lovely husband Dr. Emad Saig, words do not justice the appreciation I have for his love and support during my PhD work at SCMB building and home. Special thank for my little sons Ahmed Saig and Abdulaziz Saig

for being in my life and encourage me to work hard and gain the degree for both of them. Last but not least special thanks for my lovely sisters and brothers for supporting me during my study.

Keywords

Alternative splicing, cell adhesion molecules, excitatory synapses, inhibitory synapses, neurodegeneration, acetylcholinesterase (AChE).

Australian and New Zealand Standard Research Classifications (ANZSRC)

ANZSRC code: 060105 Cell Neurochemistry, 20%

ANZSRC code: 060405 Gene Expression, 60%

ANZSRC code: 060109 Proteomics and Intermolecular Interactions, 20%

Fields of Research (FoR) Classification

FoR code: 0604 Genetics, 50%

FoR code: 1109 Neuroscinces, 50%

List of Figures

List of Tables

List of Abbreviations

Aβ	Amyloid protein
AD	Alzheimer's disease
APP	Amyloid precursor protein
AMPA	α-amino-3-hydroxyl-5-methyl-4-isoxazole-propionate
ANCOVA	Analysis of covariance
α-NRXN-1	α-Neurexin-1
APOE	Apilopoprotein E gene
ApoE	Apilopoprotein E protein
β-NRXN-1	β-Neurexin-1
BSA	Bovine serum albumin
CAM	Cell adhesion molecules
CNS	Central nervous system
C_T	Cycle threshold
DOC	Deoxycholate
DNA	Deoxyribonucleic acid
E. coli	*Escherichia coli*
FAD	Familial Alzheimer's disease
gDNA	Genomic deoxyribonucleic acid
HPLC	High-performance liquid chromatography
IPTG	Isopropyl-1-thio-β-D-galactopyranoside
LB	Luria broth
LTP	Long-term potentiation
MCI	Mild cognitive impairment
mRNA	Messenger ribonucleic acid
MRM	Multiple reaction mentoring
NFT	Neurofibrillary tangles

NLGN-1	Neuroligin-1
NLGN-2	Neuroligin-2
NLGN-3	Neuroligin-3
NLGN-4	Neuroligin-4
NMDA	*N*-methyl-D-aspartate
NRXN-3	Neurexin-3
PBS	Phosphate buffered saline
PBST	Phosphate buffered saline plus Tween-20
PCR	Polymerase chain reaction
PDZ	PSD-95/Discs large/Zona occludens-1
PMD	Post-mortem delay
PS	Pathological severity
PSD	Post-synaptic density
PSD-95	Post-synaptic density protein of 95 kDa
PSEN1	Presenilin-1
PSEN2	Presenilin-2
PVDF	Polyvinylidenefluoride
qRT-PCR	Quantitative reverse-transcription polymerase chain reaction
RIN	RNA integrity number
RPL13	60S ribosomal protein L13
RT	Room temperature
RT-PCR	Reverse-transcription polymerase chain reaction
SP	Senile plaques
SWATH	Sequential Window Acquisition of all THeoretical mass spectra
TCA	Trichloroacetic acid

Chapter 1

1 Introduction

1.1 Epidemiology and history

Alzheimer's disease (AD) is the most common form of organic dementia. It affects more than 20% of people aged 65 years or older. It ultimately leads to the death of affected individuals on average 9 years after diagnosis (Reynolds, 2001). Worldwide, approximately 27 million individuals are affected by the disease (Ferri et al., 2005); and 4.6 million new cases arise every year. 8% of all medical costs in the United States of America are related to dementia. Between regional populations of 60 years old, people from North America and Western Europe are thought to show the highest prevalence and incident rate of AD, followed by people from Latin America and china (Fig. 1.1). Among western societies, prevalence and increase display with a cohort effect with individuals born later having a lower risk than individuals born earlier in the past century (Christensen et al., 2013, Matthews et al., 2013, Rocca et al., 2011, Schrijvers et al., 2012). The mortality from AD is predicted to increase dramatically over the next two to three decades as achievements in treating cancer and heart disease allow more individuals to reach the age of risk for dementias (Morgan, 2010).

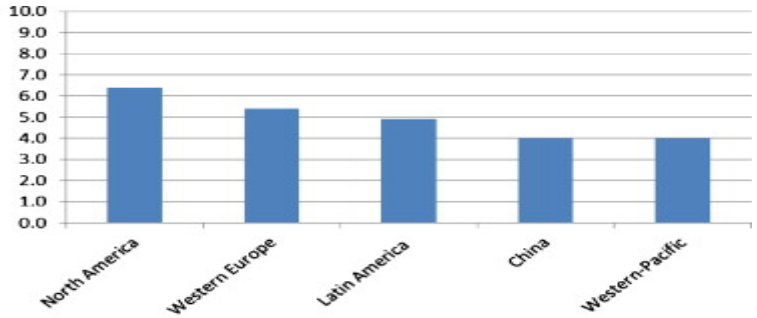

Fig. 1.1. Global prevalence of AD

The story of Alzheimer's disease begins at the beginning of the 20th century, on November 25, 1901 when a 51-year-old woman, her name Auguste D, was admitted to the Frankfurt State Asylum where she was examined by young psychiatrist Alois Alzheimer. The patient had a striking

group of symptoms such as cognitive impairment, loss of social appropriateness, a progressive decline in memory, and loss of capacity to communicate. Doctor Alzheimer remained interested in Auguste D's case until her death in Frankfurt on April 8, 1906. Alzheimer requested the patient brain to be sent to Munich to study in his new neuropathology laboratory and he described the clinical and pathological findings at a conference in Tubingen on November 3, 1906. The title of his presentation was 'On a peculiar disease process of the cerebral cortex' and the reports of this conference were published the following year (Alzheimer et al., 1995). Alzheimer reported that on post-mortem examination of Auguste's autopsy brain he found plaques, tangles and atherosclerotic alterations. The novel aspect in the 1906 case was their occurrence in an unusually young patient; however, Alzheimer did not claim to have discovered a new disease. Alzheimer's case notes were missing for approximately a century but were revealed in the basement of the University of Munich by Konrad Maurer, which led to one of the basic publications of recent times about AD (Maurer et al., 1997) comprising a photograph of Auguste D and examples of Alzheimer's handwritten notes on Auguste's cognitive status. Two years later Professor Manuel Gräber and his team extracted and tested DNA and found that Auguste did not carry the ε4 allele of the apolipoprotein E gene (Gräber et al., 1998), however the team were not able to screen for genetic mutations associated with early onset disease.

The main feature of AD is memory loss. Memory is now considered to be a collection of mental abilities that use multiple systems and components within the brain. Memory researchers have characterised six major memory systems, which are: Episodic memory, Semantic memory, Short-term memory, Simple classical conditioning (which involves the pairing of two stimuli), Procedural memory, and Priming (which occurs when a prior encounter with a particular item changes the response to the current item). In AD, cognitive researcher found some of the six major memory systems to be highly impaired and others to be relatively preserved (Gold and Budson, 2008). Episodic memory, which is critical for remembering new events, is considered to be the most clinically relevant in patients; its impairment is one of the earliest symptoms of AD (Gold and Budson, 2008). Other studies have shown semantic memory to be impaired in AD, with patients exhibiting particular deficits in naming categorized items (Tippett et al., 2007). The impairment of

semantic memory has often been related to pathology in the anterior and inferolateral temporal lobes and the frontal lobes, which leads to a loss of the dendritic arbor on neurons in these cortical regions (Davies et al., 2004). Other features of AD such as cognitive decline appear after the development of memory impairment. Language function and visuospatial skills are affected relatively early. Language dysfunction includes reduced vocabulary in spontaneous speech. However, impairment of motor functions usually only appears at late disease stages.

1.1.1 Diagnosis (Clinical and post mortem)

The clinical criteria usually used for the diagnosis of AD are based on the Diagnostic Manual of Mental Disorders, Fourth Edition (DSM- IV) and follow the criteria of the National Institute of Neurological and Communicative Disorders and Stroke and the Alzheimer's Disease and Related Disorders Association (NINCDS-ADRDA; McKhann et al., 1984). Different screening tests have been established during the last years, however the Mini Mental State Examination (MMSE) is the most widely used. The Community Screening Instrument for Dementia (CSI-D) was developed to be used in cross-cultural studies. It is composed of language expression, attention and calculation, orientation to place and time, language comprehension, and memory recall. The CSI-D instrument correlates with the Mini Mental State Examination (MMSE) and 10-word-list–learning task (Liu et al., 2005).

A general neurologic examination is usually normal in the demented patient with AD. Continuing gait problems can occur in the severe stages of AD, with a noticeably increased risk for falls. At present no laboratory test is available to confirm the diagnosis of AD. The main neuropathologic criteria for AD are those propagated by the National Institute on Aging (NIA) and National Institute of Neurological and Communicative Disorders and Stroke (NINCDS; Mirra et al., 1993).

Both DSM-IV and NINCDS-ADRDA criteria are based on history and neurologic examination, and current indication proposes that both have fallen behind because of new advances in scientific knowledge. Different biomarkers have been identified based on structural Magnetic

Resonance Imaging (MRI), molecular imaging and cerebrospinal fluid (CSF) analyses Structural MRI in patients with AD displays atrophy in the hippocampus that is predictive of future cognitive decline.

On the other hand, post-mortem diagnosis of AD needs proof of the existence of neurofibrillary tangles (NTF) and β-amyloid (Aβ) in the brain and cases of dementia without these alterations must be classified as non-Alzheimer dementias. Brain alterations found in cases clinical diagnosed with AD often include both Aβ and NFT (Braak et al., 2011). The main method used for staining Aβ uses thioflavine S, which is insensitive and can determine NFT changes as well. Specific antibodies for the pathologic proteins are commercially available; yet, practical considerations limit their application to small sections and well-equipped laboratories. The use of modern silver methods that take advantage of the physical development of the nucleation sites and avoid variable ammoniacal silver solutions known as Gallyas techniques is recommended (Braak et al., 1988, Braak and Braak, 1991b). These methods are simpler to use and much more reliable, and can be applied to routinely fixed autopsy material even if it has been stored for decades in formaldehyde.

1.2 Genetics of AD

The first study signifying a genetic factor for AD was published when early reports focused on the constant progress of AD-like disease in Down's syndrome patients after age 40, and the increased risk of disease in family members of AD patients (Harris, 1982). However, there are two different types of AD genetics, which are early onset AD (EOAD) and late onset AD (LOAD).

1.2.1 EOAD genetics

Genetic linkage studies and candidate gene analysis led to the identification of the three early onset familial AD (EOFAD) genes. The amyloid precursor protein (APP) gene on chromosome 21 was the first one found to have a mutation that causes EOFAD (Goate et al., 1991). The association between Trisomy 21 (Down's Syndrome) and AD allowed the researchers to focus on chromosome 21 as the possible locus for an AD gene. Linkage of one locus on chromosome 21 was found in extended AD families with the autosomal dominant form of EOAD (St George-Hyslop et al., 1987).

A missense mutation in the APP gene at exon 17, which partially encoded the Aβ peptide and led to a valine to isoleucine change at amino acid 717, was identified in some of the families included in the study (Goate et al., 1991). Afterward, 26 other mutations have been identified within *APP* from 74 EOFAD families (Theuns et al., 2006). These studies delivered strong support for the amyloid hypothesis discussed in detail in the related section of this thesis.

Linkage analysis studies led to the characterization of the second EOFAD gene, Presenilin-1 *PSEN1* on chromosome 14. Genome-wide studies found a significant association of a locus on chromosome 14 with EOFAD (Mullan et al., 1992, Schellenberg et al., 1992, St George-Hyslop et al., 1992). *PSEN1* mutations are the most common known genetic mutations that lead to EOFAD, with 157 pathogenic *PSEN1* mutations identified among 347 EOFAD families. The *PSEN2* gene was found in a linkage study associated with EOFAD. A candidate gene study of *PSEN2* identified sequence homology to *PSEN1* that had a segregating mutation resulting in an asparagine to isoleucine substitution (Asn141Ile; Levy-Lahad et al., 1995). Simultaneously, a candidate gene study found different missense mutations in the same gene (Rogaev et al., 1995).

1.2.2 LOAD genetics

A genome search conducted among both EOAD and LOAD families found a novel locus on chromosome 19 that has a strong effect on LOAD (Pericak-Vance et al., 1991). Biochemical studies of lipids in AD brains using an antibody to Apolipoprotein E (APOE), a protein which has special relevance to nervous tissue, found that APOE immunoreactivity was associated with amyloid in both senile plaques and neurofibrillary tangles (Namba et al., 1991). Given that the *APOE* gene mapped to the locus recognized by the Pericak-Vance et al. (1991) linkage study, this allowed investigation of the genetic and biological associations of APOE with AD. *In vitro* studies showed that APOE binds Aβ and that *APOE* ε4, a particular allelic form of *APOE*, is found at a higher frequency in LOAD cases than in controls. The *APOE* gene is polymorphic, including three alleles, ε2, ε3 and ε4, which differ at the 112^{th} and 158^{th} residues. These genes encode the corresponding apolipoproteins APOE2, APOE3 and APOE4, and produce six possible genotypes (Zannis et al., 1981, Zuo et al., 2006). APOE proteins have significant functions in mediating the uptake and distribution of cholesterol, and

each isoform is associated with specific lipoprotein elements (Puglielli et al., 2003). The ε3 allele is the most common, found among 70–80% of the population. The corresponding APOE3 protein is involved in multiple functions in neuronal biology including neuronal remodelling and repair following injury (Boyles et al., 1989, Corder et al., 1993, Mahley, 1988). The ε4 allele found in 12% of individuals. It is related to memory deficit and significantly increases the risk of AD. The APOE4 protein inhibits dendrite outgrowth (Corder et al., 1993, Nathan et al., 1994). The ε2 allele, found in 5% of the population, could have a protective effect against the development of AD. The *APOE* ε2 allele has been shown to reduce cortical Aβ, senile plaques and NFTs (Corder et al., 1994, Nagy et al., 1995, West et al., 1994). A population based prospective study found that 55% of AD cases are in the *APOE* ε4/ε4 group (Myers et al., 1996), while 27% of people who carry *APOE* ε3/ε4 develop the disease and 9% of APOE ε3/ε3 carriers develop AD.

Genome-wide association studies on AD on 6,000 cases and 10,000 controls showed associations of two new genes, *CLU* and *PICALM*, with LOAD as well as *APOE* (Lambert et al., 2009, Harold et al., 2009). *CLU* encodes the protein clusterin, which has important roles in the clearance of cellular debris and mechanisms of apoptosis, lipid metabolism and cell proliferation (Rosenberg and Silkensen, 1995, Viard et al., 1999, Wong et al., 1994). *PICALM* encodes the protein phosphatidylinositol binding clathrin assembly protein, which has significant functions in the dynamics of endocytosis (Tebar et al., 1999). Nevertheless, different published findings have shown contradictory results between research groups and ethnic populations; and effect sizes are generally very modest. *APOE* is the gene with the most significant association with AD and the most studied gene in AD pathophysiology.

In addition, a recent study found that a rare functional variant (R47H) in the *TREM2* gene had a similar effect size to the ε4 risk allele of apolipoprotein E in AD. *TREM2* encodes a type I membrane protein that creates a receptor-signalling complex with the TYRO protein tyrosine kinase-binding protein (TYROBP), which activates the immune responses in macrophages and dendritic cells (Paloneva et al., 2002). *TREM2* is expressed throughout the central nervous system, and shows high concentrations in white matter, hippocampus and neocortex. An association was found between

R47H and LOAD in North American and European populations (Niemitz, 2013). An additional study detected the R47H variant in GWAS on an Icelandic LOAD population (Guerreiro et al., 2013). Since the *TREM2* risk variant modifies TREM2 protein function, these results suggest that TREM2 impairment could reduce phagocytic clearance of amyloid proteins and thus impair a protective mechanism in the brain.

1.3 Pathological hallmarks of AD

1.3.1 Neurofibrillary tangles

Neurofibrillary tangles are a neuropathological hallmark of AD. They are composed of abnormally phosphorylated microtubule-associated protein τ (MAPT). The MAPT gene is located on chromosome 17. Alternative splicing of exons 2, 3, and 10 leads to the production of six MAPT isoforms that are differentially expressed during brain development (Sergeant et al., 2005). The phosphorylation of MAPT controls its binding to microtubules and enhances their assembly. A normal level of phosphorylation is needed for optimal MAPT activity, while hyperphosphorylation disrupts its biological function. This modifies various processes that are controlled by the appropriate organization of the microtubule network (Alonso et al., 1994, Li et al., 2007). The relationship between Aβ and MAPT in pathogenesis is not well understood. It has been suggested that changes in ion homeostasis and oxidative stress due to Aβ aggregation destabilize phosphatases and kinases that control MAPT phosphorylation. As a result, MAPT hyperphosphorylation leads to synaptic dysfunction and neuron loss (Butner and Kirschner, 1991, Goode and Feinstein, 1994).

Neurofibrillary tangles occur in other AD brain lesions, i.e., thickened neurites in senile plaques and neuropil threads. They are also found in other neurodegenerative diseases, such as progressive supranuclear palsy, dementia pugilistica, corticobasal degeneration, Pick's disease, Downs syndrome, and Parkinson's disease, which has led to the hypothesis that they are responsible, at least in part, for the neuronal damage (Joachim et al., 1987, Wood et al., 1986). This hypothesis is strengthened by the observation that mutations in the MAPT gene lead to the accumulation of paired

helical filaments in frontotemporal dementia with parkinsonism linked to chromosome 17 (FTDP-17; Clark et al., 1998, Hong et al., 1998, Hutton et al., 1998).

There is older evidence that dementia correlates with intracellular NFT (Cummings et al., 1998). Clinicopathological research related tangle load in the frontal cortex with agitation and aberrant motor behaviour (Tekin et al., 2001). Semi-quantitative post-mortem measurements of NFT in the hippocampus from demented patients showed that increased tangle load was linked to increased severity of aggressive behaviours and the presence of chronic aggression. These results suggest a pathogenic link between neurofibrillary tangle load in hippocampus and aggressive behaviours in dementia patients (Lai et al., 2010). Nevertheless, as discussed further below, current opinion strongly endorses synaptic loss as the key pathogenic feature of AD (Selkoe, 2002).

In recent years several approaches have been made in animal models to therapeutically target tau pathology (Brunden et al., 2009). Different specific approaches aim to inhibit the creation of tau oligomers and fibrils, such as Targeting tau aggregation, Targeting microtubule stabilization, Targeting tau folding and Targeting tau phosphorylation. Blocking tau/tau aggregation with small-molecule drugs is difficult because of the large surface areas that are involved in such interactions (Brunden et al., 2009). Targeting microtubule stabilization was performed by treating mice that had axonopathy and amyotrophy with the microtubule-stabilizing drug paclitaxel. These latter mice showed significant improvement of fast axonal transport (Ishihara et al., 1999). However, none of these approaches has yet been translated into clinical practice. In contrast, the clinically used drug Memantine, which is a non-competitive NMDA receptor antagonist, does sway the excitation-inhibition balance away from over-excitation in AD cases.

1.3.2 β-Amyloid

The second component essential for AD diagnosis is the senile plaque. Glenner and Wong (1984a, 1984b) and Masters et al. (1985) reported that the 42-residue amyloid β-peptide, Aβ42, is the main constituent of senile plaques. There are two main forms of β-amyloid, a 40- (Aβ40) and a 42- (Aβ42) amino acid peptide, although peptide length can range from 39 to 43 amino acids. There

is an additional N-terminally truncated species (Ingelsson et al., 2004). Aβ42 builds up earlier in amyloid plaques and aggregates into fibrils more quickly than Aβ40 *in vitro* (Jarrett et al., 1993, Roher et al., 1993). Aβ is derived from a large amyloid precursor protein (APP) that undergoes multiple proteolytic cleavages. APP is an integral membrane protein that moves to the endoplasmic reticulum *via* its signal peptide and is subject to post-translational modifications. Heterogeneous forms of APP result from alternative splicing and different post-translational modifications (Hung and Selkoe, 1994, Selkoe et al., 1988, Weidemann et al., 1989). Neurons express high levels of the 695-residue isoform (Haass et al., 1991). The enzyme α-secretase first works on APP to cleave off a large soluble ectodomain fragment, sAPPα, located in the lumen/extracellular space, and to leave an 83-residue C-terminal fragment (CTF83) within the membrane. APP molecules not cleaved by α-secretase can be cleaved by β-secretase to generate sAPPβ and C-terminal fragment 99 (CTF99), a 99-residue peptide in the membrane (Seubert et al., 1993). The latter is then cleaved by γ-secretase to produce Aβ and a 55-residue cytosolic peptide, the APP intracellular domain (AICD; Selkoe, 2001).

Amyloid deposits may be present in AD brain up to a decade before the emergence of cognitive symptoms (Ingelsson et al., 2004, Mintun et al., 2006). Since Amyloid was a key component of Alzheimer's own seminal paper some authorities require the presence of Aβ for a diagnosis of AD, but tissue loads of plaques do not correlate well with dementia. The dominance of Aβ in theories of AD pathogenesis derives from genetic studies on mutations of *APP* and presenilin (*PS*) genes in familial AD cases. Possession of the disease allele of any one of these genes leads to greater production of Aβ or to a predominance of the Aβ42 form, which has a propensity for misfolding and aggregation (Chapman et al., 2001, Selkoe, 1998). Several AD transgenic mice have been produced that have the mutant forms of human *APP* and *PS1* or *PS2* genes. They develop amyloid aggregates in the brain and show cognitive impairment (Ashe, 2001), although neuronal loss requires additional transgenic influence.

1.3.3 Synaptic loss and synaptic proteins in AD

While there is a significant negative correlation of synapse numbers and synaptic markers with cognitive decline in AD, neither neurofibrillary tangles nor senile plaques show strong

statistical association with clinical AD severity (Terry et al., 1991). Assays of synapses and synaptic markers in the AD brain (Bancher et al., 1993) and in transgenic mouse models (Buttini et al., 2005) support the hypothesis that synaptic degeneration and damage take place early in the development of the disease. Light and electron microscopy were used to study the form and density of synapses in the dentate gyrus of double-transgenic *APP/PS1* mice. Both the numbers of synapses per unit volume and the morphology of the remaining synapses are affected in plaque-free regions of these animals (Alonso-Nanclares et al., 2013). Disrupted synaptic connections would result in neural dysfunction, and lead to the dementia and cognitive impairment observed in AD and other neurodegenerative disorders (Terry et al., 1991). Loss of synaptic connectivity could follow changes in pre- or post-synaptic proteins. These proteins are located in synaptic vesicles, the cytoplasm, and the terminal membranes. Proteins may be altered differentially in different diseases. There is a link between changes in synaptic proteins and terminal loss in AD (Reddy et al., 2005, Tannenberg et al., 2006). Neuroimaging of autopsy brain supports a link between grey matter loss and synaptic protein reduction (Heindel et al., 1994). Nonetheless, synaptic proteins are dynamic, and their levels can be changed in animal models by memory and learning training, behavioural tasks, or administration of drugs (Sindi et al., 2014). Not all synaptic proteins are equally affected in specific brain regions in AD: these proteins are located in different compartments of synaptic terminals, play different roles, and can be enriched differentially in excitatory and inhibitory terminal classes.

Levels of synaptic proteins vary among brain regions. The hippocampus is affected earlier than other regions in AD progression, and is the most affected region in late stages of the disease (Honer et al., 1992, Perdahl et al., 1984, Sze et al., 1997). Frontal cortex synaptic protein levels are lower in AD brain than in control brain; reported differences between AD frontal cortex and other AD brain regions are inconsistent (Lassmann et al., 1992, Sze et al., 1997, Tannenberg et al., 2006).

1.3.4 Synaptic disruption by β-amyloid

Mechanisms underlying the failure of synaptic plasticity and the disruption of memory in AD are not clearly understood. Two opposing notions have been put forward to explicate this issue. Under normal physiological conditions, Aβ may play a role in synaptic plasticity, and its deficiency,

through aggregation, could lead to abnormal functioning of the synapse. Alternatively, Aβ could be responsible for synaptic disruption in AD. In the normal synapse, neuronal activity might regulate the production and secretion of Aβ by controlling APP processing upstream of γ-secretase activity (Kamenetz et al., 2003). Aβ levels in brain interstitial fluid are influenced by synaptic activity on a time scale of minutes to hours (Cirrito et al., 2005). In an acute brain slice model, the impact of synaptic activity on Aβ levels is linked to synaptic vesicle exocytosis. Synaptic activity can alter Aβ metabolism and area-specific Aβ accumulation (Cirrito et al., 2005). Inhibiting β- and γ-secretase activity may result in reduced levels of Aβ that would enhance toxicity and the death of neurons, should Aβ promote neuronal survival (Plant et al., 2003).

Conversely, *in vitro* and *in vivo* studies have explored possible molecular and signalling mechanisms that promote synaptotoxic effects of Aβ (Dinamarca et al., 2008, Haass and Selkoe, 2007, Klyubin et al., 2005, Rowan et al., 2007, Selkoe, 2008). Koh et al. (1990) demonstrated that Aβ peptides and glutamate are together more neurotoxic to cultured neurons than either agent alone. The mechanism of Aβ synaptic toxicity is complex, because different multimeric forms of Aβ exhibit effects ranging from reversible alterations in synaptic form and function to neuronal loss. High levels of Aβ reduce glutamatergic synaptic transmission and lead to synaptic loss (Hsia et al., 1999, Kamenetz et al., 2003, Mucke et al., 2000). Intracerebroventricular injection of soluble synthetic Aβ40 dimers rapidly reduces the plasticity of excitatory synaptic transmission at doses (10–42 pmol) comparable to natural Aβ concentrations (Hu et al., 2008).

1.3.5 Oligomeric Aβ and excitatory synapses

Koffie et al. (2009) used Array tomography to assess the impact of free Aβ on synaptic loss in double-transgenic *APP/PS1* mice. They showed that amyloid plaques in these mice are enclosed by a halo of oligomeric Aβ. Examination of more than 14,000 synapses revealed a 60% loss of excitatory synapses contiguous to the halo. Deposits of oligomeric Aβ were linked to a subset of excitatory synapses that were smaller than those that did not interact with oligomeric Aβ. In green fluorescent protein (GFP) Tg2576 *APP* mice, multiphoton live imaging revealed disruption of neurons and a lower dendritic spine density than in age-matched controls (Spires et al., 2005).

Axonal immunostaining and colocalization studies of synaptophysin and PSD-95 proteins showed a similar loss of pre- and post-synaptic partners near plaques in human autopsy brain (Spires et al., 2005).

Aβ can affect the role of glutamate NMDA receptors (NMDARs) and eliminate induction of NMDAR-dependent LTP in the neuron (Shankar et al., 2007, Snyder et al., 2005). When NMDARs were quantified by biotinylation in cultured cortical neurons treated with Aβ, there was an 80% reduction in subunit protein. Application of a γ-secretase inhibitor reduced the Aβ concentration and returned NMDAR levels to normal. Aβ oligomers also induce the endocytosis of NMDARs by a mechanism involving α7-nicotinic acetylcholine receptors (Snyder et al., 2005). Ronicke et al. (2011) showed that NMDAR-2B activation mediates Aβ-induced LTP disruption. Application of an NMDAR-2B antagonist to hippocampal slice treated with Aβ oligomer abolished the disruption.

1.3.6 Oligomeric Aβ and prion proteins

Lauren et al. (2009) showed that the cellular prion protein PrP^c is a receptor for Aβ oligomers with nanomolar affinity. The binding of PrP^c to Aβ oligomers leads to loss of LTP. In hippocampal slices, anti-PrP^c antibodies reduce the binding of oligomeric Aβ to PrP^c and prevent synaptic disruption. Deletion of PrP^c improves cognitive function in transgenic mice over-expressing mutant APP (APPswe and PS1ΔE9), reduces premature neuronal death, and reverses the memory deficit (Gimbel et al., 2010). Antibody blockade prevents the PrP^c-enhanced neurotoxicity of Aβ oligomers (Kudo et al., 2012).

1.3.7 Other Aβ synaptic targets

Excitatory synapses are formed and maintained by the homophilic trans-synaptic binding of N-cadherin (Fannon and Colman, 1996). A luciferase-complementation assay was used to show that N-cadherin enhances APP dimerization and the production of Aβ (Asada-Utsugi et al., 2011). Application of Aβ down-regulates N-cadherin expression, which weakens synapses and can further increase Aβ production *via* interaction with the PS1 complex (Ando et al., 2011, Andreyeva et al., 2012).

Other synaptic junction proteins play roles in Aβ production. Expression of α4 and β3 integrin is increased in neurons in the vicinity of plaques and tangles in AD autopsy brain tissue (Akiyama et al., 1991, Van Gool et al., 1994). Studies using integrin-blocking antibodies revealed that Aβ accumulation and neurotoxicity in human cortical primary neurons are mediated by α2β1 and α5β1 integrins. The α2β1 and α5β1 integrin signalling pathways may be critical to Aβ neurotoxicity in AD (Wright et al., 2007).

1.4 Cell adhesion molecules

Protein complexes that link pre- and post-synaptic membranes have significant functions in regulating neural networks. Neurotransmitters released from the presynaptic terminal acting on receptors located on the post-synaptic membrane convey information between neurons at synapses (Dalva et al., 2007). Signalling can be facilitated by adhesion molecules, which cooperate across the synaptic junction (Bamji et al., 2003, Dalva et al., 2000, Graf et al., 2004, Hall et al., 2000, Scheiffele et al., 2000, Umemori et al., 2004). Synaptically localized cell adhesion molecules (CAMs) modulate the function of synapses through protein–protein interactions and signalling cascades, and also direct the formation of new synapses. Various CAMs organize synapse formation, control dendritic spine morphology, amend synaptic plasticity, and alter synaptic receptor function. These molecules arbitrate function and physical interactions between neurons at several stages in the life of a synapse (Fig. 1.2).

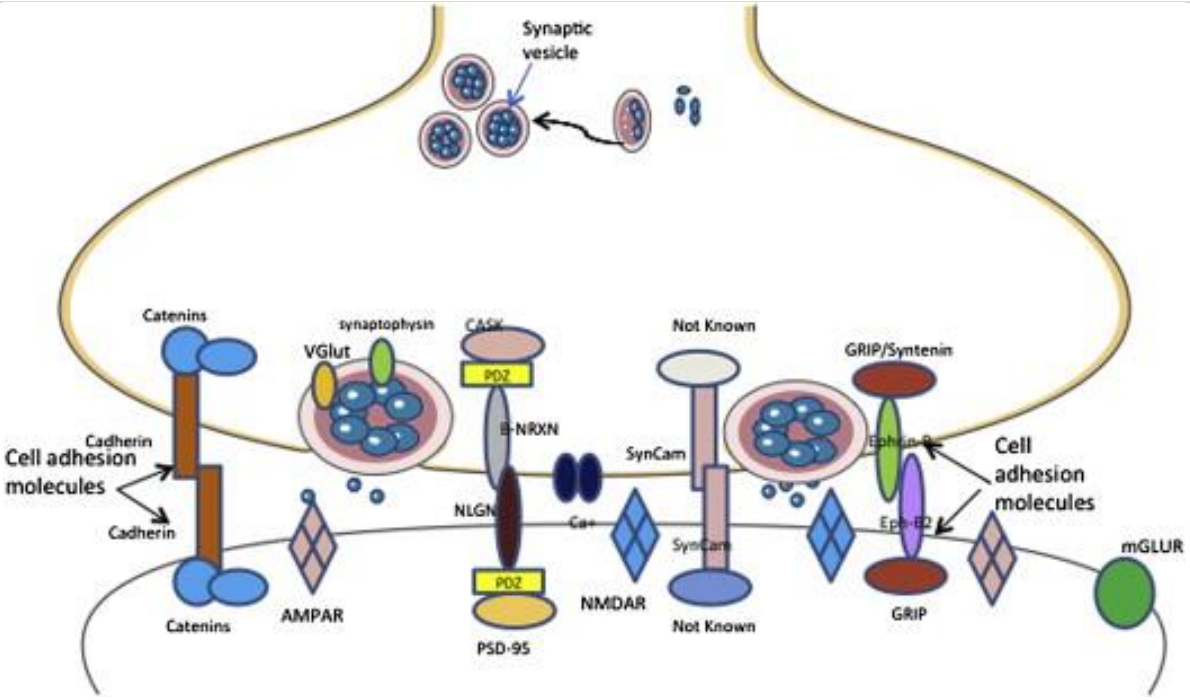

Fig. 1.2. The function of cell adhesion molecules at the synapse. During synaptogenesis, synaptic CAMs help stabilize contacts between neurons and recruit synaptic proteins *via* specific cytoplasmic or extracellular motifs such as PDZ-binding domains. Contacts among adhesion molecules may guide the activation of intracellular signalling events that lead to synapse maturation. In the mature synapse, synaptic CAMs work together with channels and other synaptic proteins to modulate their function. VGLUT (Vesicular glutamate transporter), CASK (Calcium/calmodin-dependent serine protein kinase), AMPAR (α-amino-3-hydroxy-5-methyl-4-isoxazolepropionic acid receptor), GRIP (Glutamate receptor-interacting protein) mGLUR (metabotropic Glutamate receptors).

Different classes of CAMs play differing roles in synapses. CAMs include neurexins and neuroligins, N-cadherin, synaptic cell adhesion molecule-1 (SynCAM-1), and the ephrinB-receptor–ephrinB system. The most widely described CAM pairing implicated in synaptogenesis and nerve-terminal stability is the interface between neurexins and neuroligins that are located at pre-synaptic and post-synaptic sites respectively.

1.4.1 Neurexin–neuroligin complex

The neurexin family was discovered in 1992 after the recognition that one member of the family is a receptor for α-latrotoxin, a component of black widow spider venom that causes massive neurotransmitter release from the presynaptic terminal (Ushkaryov et al., 1992). Further studies over two decades delineated neurexins and their binding ligands, the neuroligins (Ichtchenko et al., 1995, 1996). Scheiffele et al. (2000) showed that neuroligins occur on the surface of non-neuronal cells. In neurons they stimulate synaptic vesicle formation during functional pre-synaptic differentiation in contacting axons. Over-expression and knockdown studies *in vitro* have revealed that neurexin-neuroligin complexes are key discriminants in GABAergic and glutamatergic synaptogenesis, and that patterns of differences in isoform binding affinities and localization determine this specificity and differentiation.

1.4.2 Structures of neurexins and neuroligins

1.4.2.1 Neurexins

Neurexins are a family of highly polymorphic brain-specific proteins that are products of the three neurexin genes *NRXNI, NRXNII,* and *NRXNIII*. Each gene encodes two transcripts, α-neurexin and β-neurexin, which are expressed from upstream and downstream promoters of the same gene respectively (Fig. 1.3).

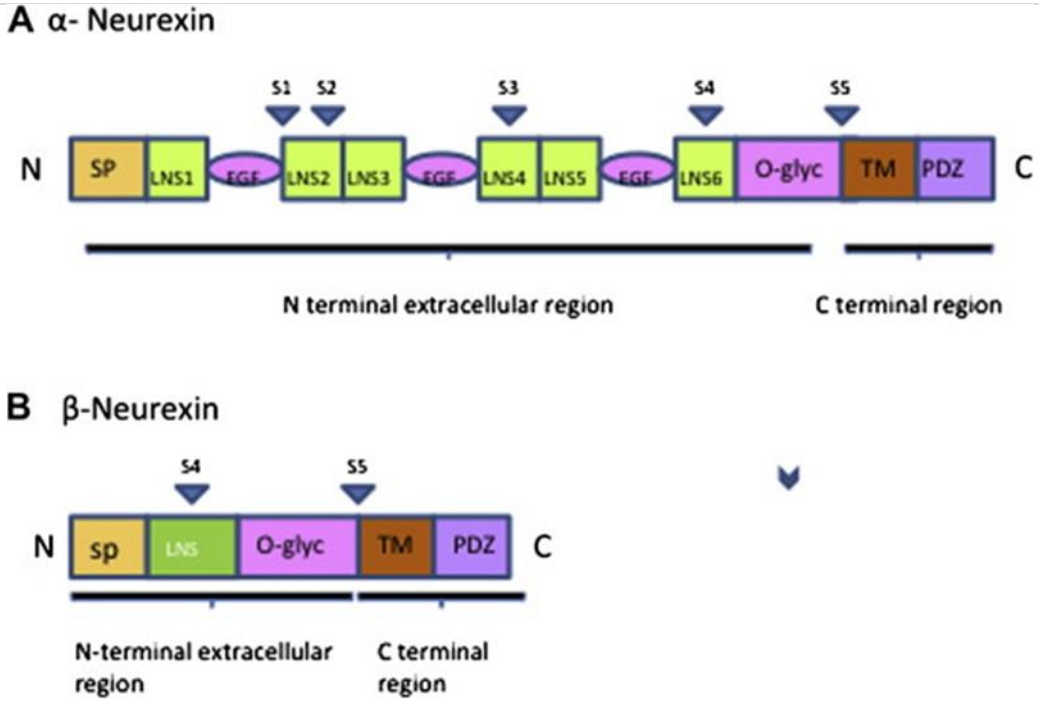

Fig. 1.3. Structure of α- and β-neurexins. **A**, α-Neurexins consist of an N-terminal extracellular sequence containing the following: a signal peptide (SP); six laminin A, neurexin, and sex hormone binding protein (LNS) domains, three epidermal growth factor (EGF)–like sequences, and an O-glycosylation region (O-Glyc). There are five sites of alternative splicing in the extracellular sequence (S1–S5), which are indicated by arrowheads. The N-terminal extracellular region is followed by a carboxy-terminal sequence, which contains a transmembrane (TM) region as well as a short cytoplasmic region that comprises the PDZ II interaction site. **B**, The N-terminal extracellular sequence in β-neurexins consists of a signal peptide, one LNS domain, and an O-Glyc region. There are only two alternative splice sites in β-neurexins, as indicated.

Molecular studies of *NRXN* transcripts have identified two alternative splice sites in the β-neurexins and five in the α-neurexins. In consequence, at least six neurexins isoforms can be generated from these different genes: three α-*NRXN*s, Iα, IIα and IIIα, and three β-*NRXN*s, Iβ, IIβ and IIIβ (Jarrett et al., 1993, Ullrich et al., 1995, Ushkaryov et al., 1994). The five alternative splice sites in α-*NRXN* (S1-S5) are scattered among six laminin–neurexin–sex-hormone–binding protein (LNS) and three epidermal growth factor (EGF)–like domains (Fig. 1.3). β-*NRXNs* are usually

truncated forms of α-*NRXNs* containing a single LNS domain (Fig. 1.3). Alternative splicing and *N*- and *O*-glycosylation add additional diversity to produce up to 1000 isoforms (Missler et al., 1998). As will be discussed later, alternative splicing of neurexins controls their roles at synapses. The range of alternative splicing provides a potent cellular mechanism for constructing a huge number of different cell-surface proteins that could be expressed in sub-populations of cells, giving specificity and variety for processes such as adhesion and recognition between cells as well as ligand–receptor interactions. *In situ* hybridization studies have shown that mRNA encoding both α- and β-neurexins can be expressed in the same neuron. Conversely, different types of *NRXN*s are widely distributed among diverse types of neurons (Ichtchenko et al., 1995). Immunofluorescence analysis and the roles of neurexins as α-latrotoxin receptors show that the localization of neurexins is predominantly pre-synaptic (Sugita et al., 1999, Ushkaryov et al., 1992). Nevertheless, it has not been confirmed whether this localization is exclusive: some studies indicate that the deletion of genes encoding α-neurexins also has post-synaptic effects (Kattenstroth et al., 2004, Taniguchi et al., 2007).

1.4.2.2 Neuroligins

There are three sets of neurexin-binding ligands in the mammalian brain: dystroglycan, neurexophilins, and neuroligins (NLGNs). The most intensively studied ligands are the neuroligins, which were discovered by affinity purification (Ichtchenko et al., 1995). Three genes coding neuroligins, *NLGN1*, *NLGN2*, and *NLGN3*, have been found in mice and rats; they are mostly expressed in the central nervous system (CNS; Ichtchenko et al., 1996). Five genes encoding neuroligin family members have been detected in human tissues, *NLGN1*, *NLGN2*, *NLGN3*, *NLGN4*, and *NLGN4Y*, with a sequence identity in their extracellular domains of more than 70% (Ylisaukko-oja et al., 2005a). All neuroligin isoforms are post-synaptic transmembrane proteins. Neuroligin-1 is usually expressed in neurons at excitatory postsynaptic sites and found connected to NMDAR, postsynaptic density–95 (PSD-95) and synaptic scaffolding molecule (S-SCAM) at the synaptic junction and postsynaptic densities (Hirao et al., 1998, Ichtchenko et al., 1995, Kurschner et al., 1998, Song et al., 1999). Neuroligin-2 is expressed mainly at inhibitory neuronal sites in CNS but is also expressed in pancreas, lung endothelia, and colon (Varoqueaux et al., 2004). Human neuroligin-

3 is expressed in glia and dorsal root ganglia cells (Gilbert et al., 2001, Philibert et al., 2000). Expression of *NLGN4* mRNA in human tissues is at its highest level in the heart; it is expressed only at low levels in the brain, pancreas, skeletal muscle, and liver (Bolliger et al., 2001, Nguyen and Südhof, 1997). Neuroligin-4Y, the gene for which is located in the Y chromosome, differs from neuroligin-4 by 19 amino acids and has also diverged in sequences within its introns (Bolliger et al., 2001, Jamain et al., 2003; Fig. 1.4).

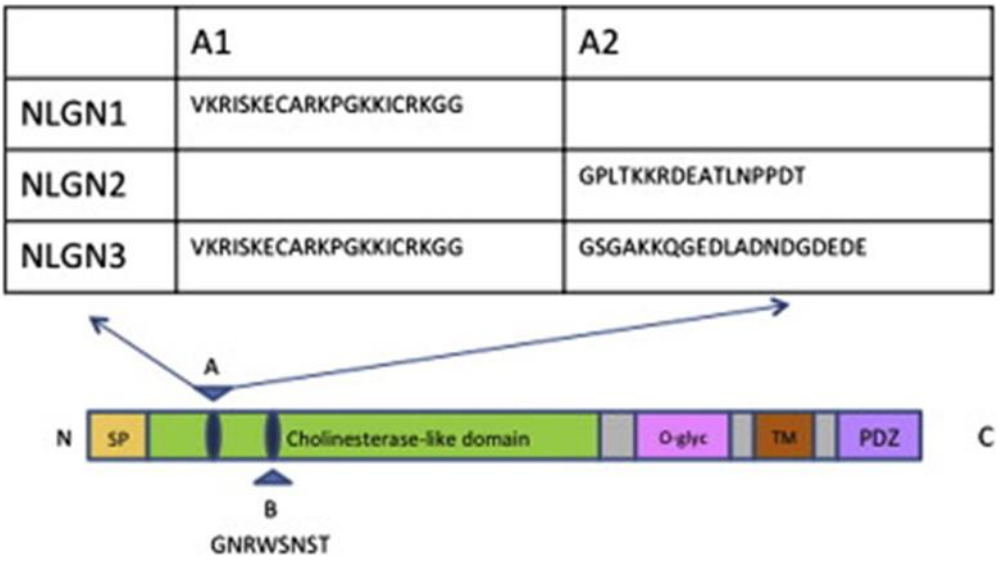

Fig. 1.4. Neuroligin structure. The N-terminal extracellular sequence of neuroligins consists of a signal peptide (SP), cholinesterase-like domain (CLD) and a carbohydrate-attachment region for O-linked glycosylation (O-Glyc). The cholinesterase-like domain of neuroligin-1 contains two alternative splice sites (**A** and **B**) with insert sequence A1 and B, whereas neuroligin-2 contains one splice site (**A**) with insert sequence A2. Neuroligin-3 has one alternative splice site (**A**) with two insert sequences, one homologous to A1, the second homologous with A2 (**A**). The C-termini of all neuroligins are identical and consist of a single transmembrane region as well as a short cytoplasmic sequence containing a type I PDZ-recognition motif.

The extracellular domain of neuroligin-1 has two alternative splice sites (A and B), whereas neuroligin-2, neuroligin-3 and neuroligin-4 have one conserved alternative splice site (A). The variations among family members are due to differences in the insert sequences. In neuroligin-1, the insert at site A, called A1, has a calculated charge of+8 and an internal disulfide bond between

Cys172 and Cys181, whereas the insert at site B, which is unique to neuroligin-1, contains an *N*-glycosylation consensus sequence at Asn303 (Hoffman et al., 2004). Neuroligin-2 has one insert at site A called A2; it has a calculated charge of –5 and lacks an internal disulfide bond. Neuroligin-3 has two inserts at splice site A: one is homologous with the neuroligin-1 insert, and the second is homologous with neuroligin-2 insert (Ichtchenko et al., 1995, 1996; Fig. 3). Neuroligin-4 inserts have not yet been clearly delineated.

Neuroligins are members of a protein family that possess a cholinesterase-like domain (CLD), and are known as cholinesterase-like adhesion molecules (CLAMs). All family members (glutactin, neurotactin, and gliotactin, as well as the neuroligins) lack one or more of the residues that are essential for catalytic activity. The function of the N-terminal sequence in neuroligins is heterophilic adhesion. Hence, this domain mediates the interaction between receptor and ligand, rather than the interaction between enzyme and substrate. Neuroligins lack a serine residue that is essential for enzymatic function in cholinesterases; important nearby residues are histidine and glutamic acid, which are close to the third disulfide loop (Holmquist, 2000, Hoffman et al., 2004). Two of the three disulfide loops in all members of CLAM family are conserved in acetylcholinesterases (Zeev-Ben-Mordehai et al., 2003).

Members of the CLAM family form 3D structures that are very similar to that of acetylcholinesterase (AChE). Approximately 65% of the CLD is conserved between the cholinesterase superfamily and CLAM family members. The structure of AChE has three loops, which are stabilized by disulfide bonds that permit the right positioning of the enzyme active site. The first part of CLD is totally conserved between the families; it includes the first and second disulfide-bonded loops. The second part of the CLD is conserved only in the area of the cysteine residue. The majority of the conserved structures in CLAM proteins are those essential for shaping the α- and β-hydrolase folds and positioning the first component of the active site in the enzyme. The second part of the conserved CLD structure positions the other two components at the catalytic site and forms the mouth of the catalytic gorge. CLAM proteins differ from AChE by either total or partial loss of the third disulfide-bonded loop, which appreciably changes the conformation of the

gorge mouth and hence abrogates catalytic site function (Fig. 1.5). The review by Gilbert and Auld (2005) gives more detail on the 3D structure of the CLD in AChE and CLAM family proteins.

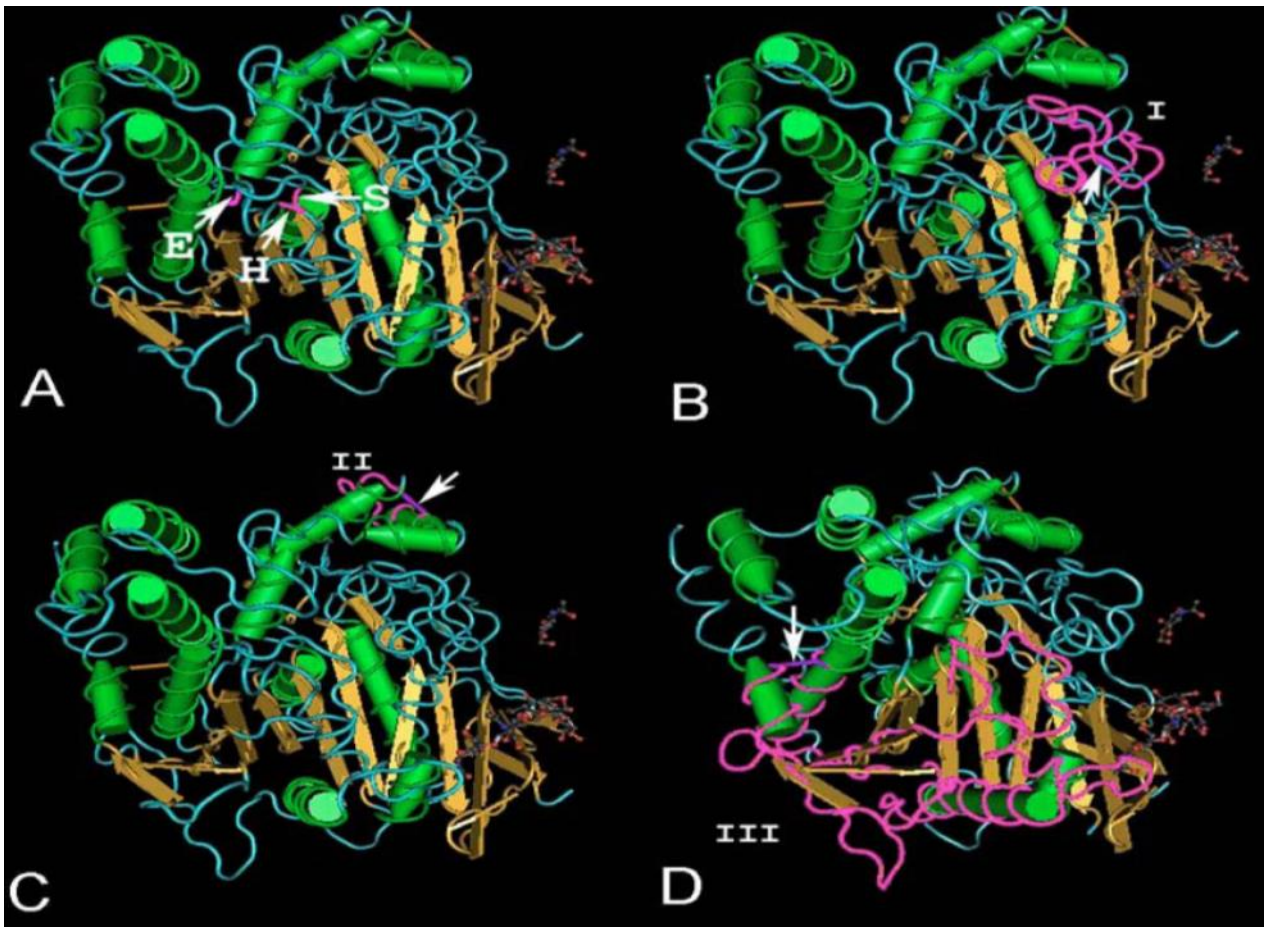

Fig. 1.5. The 3D structure of CLD models of CLAM family protein in Drosophila acetylcholinesterase. **A,** the catalytic site; **B,** the first disulfide-bonded loop; **C,** the second disulfide-bonded loop; and **D,** the third disulfide-bonded loop. The domain in the third loop in the CLAM family is the most divergent in sequence. In vertebrates the neuroligin third loop is reduced in size, resulting in a considerably shorter loop, while this loop is not present at all in invertebrate neuroligins.

Comparisons of the structures of cholinesterase family members with neuroligins have significantly increased our understanding of the relationship between structure and function in the neuroligins (Hoffman et al., 2004). Consideration of 2- and 3-dimensional analyses indicates that the CLD is a possible target for ligands to associate with CLAM family members, particularly to mediate neuroligin–neurexin binding. Over-expression of AChE decreases β-neurexin levels *in vitro* and *in*

vivo, as well as having a negative effect on glutamatergic synapses *in vitro*, which suggests there is crosstalk between the neuroligin–neurexin complex and AChE (Andres et al., 1997).

1.4.3 Neuroligin–neurexin interactions

The neuroligin–neurexin interaction is controlled by different molecular and cellular mechanisms, including oligomerization, calcium binding, and alternative splicing.

1.4.3.1 Oligomerization mechanisms

Neuroligin-1 has five *N*-glycosylation sites as well as a domain rich in serine and threonine residues next to the transmembrane sequence that contains a number of sites for *O*-linked glycosylation (Ichtchenko et al., 1995). Blocking *N*-glycosylation in neuroligin-1 enhances its binding to neurexin to form the neuroligin–neurexin oligomer (Comoletti et al., 2003). In contrast, deglycosylation of neurexins does not influence neuroligin binding affinity.

1.4.3.2 Calcium-dependent mechanisms

The extracellular domains of neuroligin and neurexin bind to each other in the presence of calcium ion (Ca^{2+}; Ichtchenko et al., 1995). With recombinant neuroligin-1 and β-neurexins, binding occurs at differing concentrations of Ca^{2+} for different alternatively spliced isoforms (Nguyen and Südhof, 1997). Structural studies of the α-neurexin LNS2 domain show that a splice site generates highly variable surfaces surrounded by Ca^{2+} ions (Sheckler et al., 2006). Ca^{2+} binding has low affinity and is decreased below detectable levels by the addition of 8- to 15-residue splice inserts. In consequence, Ca^{2+}-dependent interactions of neurexins may be affected by changes in Ca^{2+} concentration that are within the estimated variations within the synapse as a result of synaptic activity (Nguyen and Südhof, 1997).

1.4.3.3 Alternative splicing mechanisms

Neurexins exhibit a great deal of alternative splicing that produces more than 2,000 variants (Tabuchi and Südhof, 2002). The splice insert sequences and their locations are preserved between *NRXN* genes and between species, indicating that alternative splicing plays a significant role. Alternative splicing is not as extensive in neuroligin, but it takes place in the significant CLD

domain. The alternatively spliced regions in neuroligins and neurexins are the sites of interactions between them (Fig. 1.6). Alternative splicing changes binding affinity, and affects synapse development and neuronal functions *in vitro* (Boucard et al., 2005, Chih et al., 2006, Graf et al., 2006).

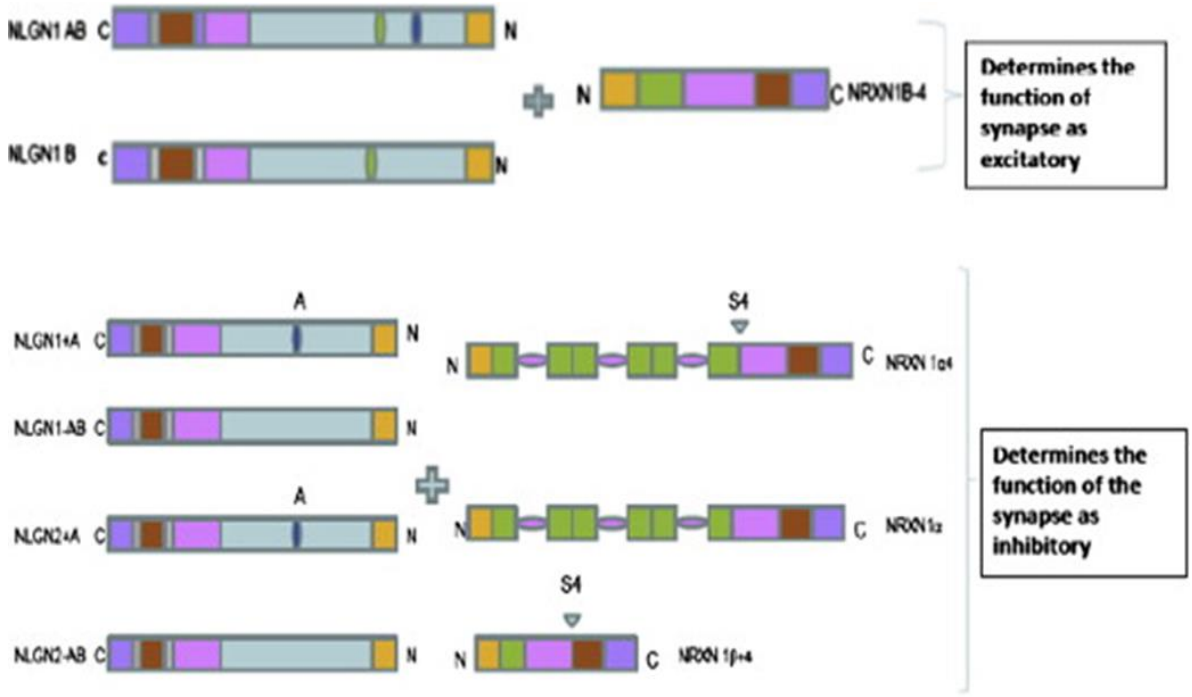

Fig. 1.6. Neurexin–neuroligin splice sites and the possible binding pairs. Splicing at site B in neuroligin and at site 4 in β-neurexin-1 controls binding affinity and synapse function. In β-neurexin, the presence of the 30-residue insert at site 4 decreases the affinity of binding, especially with neuroligin-1, which has an insert at site B (+B). This sequence can maintain high-affinity binding with neuroligin-1, which does not have an insert at site B (–B), or with neuroligin-2, which also does not have a B splice site. Similarly, α-neurexins that do or do not contain an insert at site 4 can attach to B+ neuroligins (with splice site B included). In this case, the regulation of the interaction between the two proteins does not occur due to the presence of the B insert (9 amino acids), but takes place as a result of its N-linked glycosylation. Additional studies are required to verify how alternative splicing of neuroligin-1 (at site B) and β-neurexins (at site 4) controls the binding of particular isoforms of these proteins as well as their adhesive properties.

1.4.3.4 Neuroligin/neurexin interactions and synaptic localization

The roles of neuroligins and neurexins in specifying synapse formation as either excitatory or inhibitory have been delineated by studies conducted *in vitro*. Over-expression of neuroligin proteins increases synapse numbers, whereas knockdown of the same proteins decreases synapse numbers (Chih et al., 2005). Scheiffele et al. (2000) showed that expressing neuroligins in normal cells can stimulate pre-synaptic differentiation in contacting axons. On the other hand, the expression of neurexins in neurons can lead to clustering of proteins in post-synaptic dendrites (Graf et al., 2004).

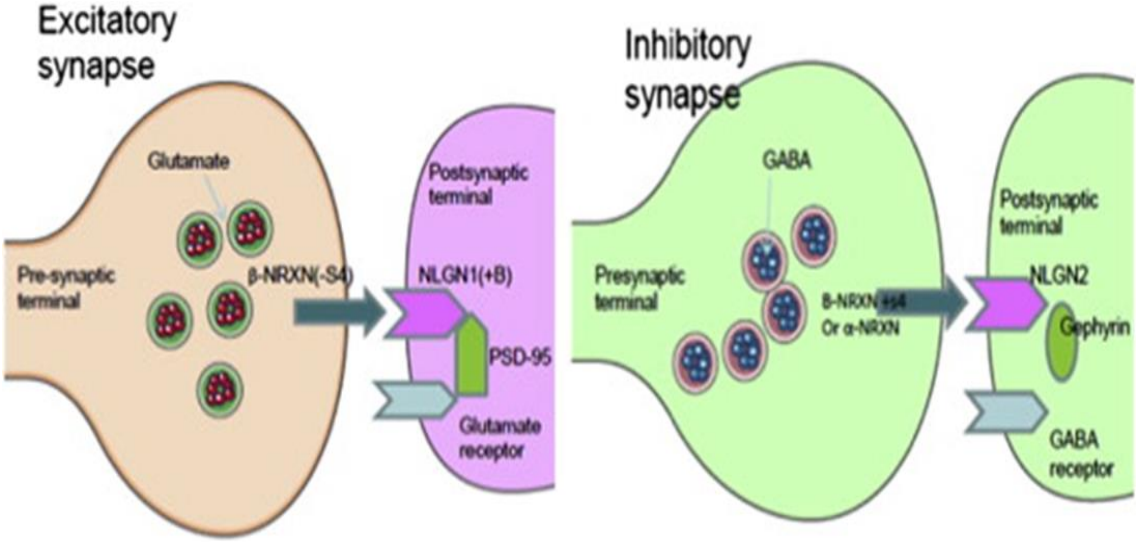

Fig. 1.7. The role of alternative splicing of the neurexin–neuroligin complex in determining synaptic function as either excitatory or inhibitory. Neurexins and neuroligins possess extracellular domains that are modified at different locations by alternative splicing. Splice site 4 (S4) of β-neurexin and location B of neuroligin-1 change the proteins' binding specificity for their neuroligin or neurexin partners and change their capability to stimulate glutamatergic over GABA (γ-aminobutyric acid)–mediated synaptogenesis. Each neurexin isoform binds a specific neuroligin isoform that guides the creation of specialized synapses. β-neurexin that does not have the alternative splice site S4 (β-neurexin1 [–S4]) pairs neuroligin-1s that has the inclusion of splice site B (neuroligin-1+B). The addition of the S4 in β-neurexin prevents neuroligin-1 pairing and decreases accumulation of post-synaptic proteins that are specific to glutamatergic synapses. Conversely, β-neurexin with an S4 (+S4) has high

affinity for neuroligin-2 and guides the formation of GABA-signaling synapses. On the post-synaptic membrane, neuroligin-1+B isoforms interact with β-neurexin. On the other hand, –B isoforms can pair both neurexin types. neuroligin-1+B is confined to glutamatergic synapses. The majority of neuroligin-2 proteins that lack the B site have an alternative splice site at location A to guide their specific localization to the GABAergic synapse.

In consequence, neuroligin–neurexin binding *in vitro* can control both the pre- and post-synaptic sides of the synapse. The organization of synapse configuration as excitatory or inhibitory is controlled by the diverse neurexin and neuroligin types incorporated, as well as the splice variants that occur in the extracellular domain. Neuroligin-1 is located in excitatory synapses and supports the development of excitatory specializations, depending on alternative splicing (Fig. 1.6). Conversely, neuroligin-2 is located in inhibitory synapses and preferentially stimulates the formation of inhibitory contacts (Chih et al., 2005). Alternative splicing in the extracellular domain of neuroligins guides neuroligin–neurexin binding between neurons, and controls excitatory/inhibitory synapse formation (Boucard et al., 2005, Chih et al., 2006; Fig. 1.7).

1.4.4 A role for the neuroligin–neurexin complex in triggering amyloid deposition in AD?

Acetylcholinesterase interacts with senile plaques in AD brain. Both bovine AChE and human and murine recombinant AChE accelerate the accumulation of either wild-type or mutant Aβ peptide as amyloid. The interaction of AChE and Aβ does not depend on the subunit composition of the enzyme or on the presence of the AChE active site (Inestrosa et al., 1996). The neurotoxicity elicited by AChE–Aβ complexes is more than that induced by the Aβ alone (Inestrosa et al., 1996). Affinity-purified AChE increases the accumulation of APP in glial cells in selective brain regions in a concentration-dependent manner. The increased expression of APP in astrocytes and microglia induced by AChE is due to the activation of glial cells (von Bernhardi et al., 2003). Tg2576 mice, which express human APP and develop plaques at 9 months, crossed with transgenic mice expressing human AChE, produce F1 animals that express both transgenes in the brain. The F1 cerebral cortex displays plaques at 6 months that are stained by thioflavin S and antibodies against

Aβ40 and Aβ42. Plaques accumulate in the hybrid mice 50% sooner than in the parental line and plaque quantity increases with age (Rees et al., 2003).

Given that neuroligins have an extracellular sequence containing a domain that is homologous with AChE, and given that the CLD site in neuroligin lacks important residues (Scholl and Scheiffele, 2003), neuroligin has been proposed as a synaptic protein candidate that may affect Aβ accumulation in AD. Fluorescence spectroscopy and surface plasmon resonance analysis show an interaction between oligomeric forms of Aβ and the extracellular domain of neuroligin-1 with a K_d in the nanomolar range (Dinamarca et al., 2011, 2012), whereas the interaction between Aβ and neuroligin-2 is very weak. Immunoprecipitation assays confirmed that Aβ oligomers react with neuroligin-1 but not with neuroligin-2. Studies of Aβ polymerization in a thioflavin-T assay showed that neuroligin-1 stabilized Aβ accumulation *in vitro*. Neuroligin-1 behaved as a nucleating factor for Aβ accumulation by inducing the formation of Aβ oligomers (Dinamarca et al., 2012). These data suggested that neuroligin-1 stabilizes oligomeric assemblies of Aβ in the glutamatergic synapse, where they may bind to neuroligin-1 in the post-synaptic membrane. This complex might then act as a local aggregation seed for more Aβ oligomers that affect the post-synaptic region and promote synaptic toxicity in AD.

1.4.4.1 Proteolytic processing of neuroligins and neurexins in AD

Several studies have demonstrated that AD-related proteolytic enzymes can regulate synaptic efficacy by processing synaptic CAMs (Cartier et al., 2009, Mabb and Ehlers, 2010, Malinverno et al., 2010). Metalloproteases and γ-secretase are intramembrane aspartyl proteases that cleave single-transmembrane proteins; both are implicated in AD. They cleave a range of substrates, the most extensively studied of which is APP. Other substrates include proteins involved in synapse maintenance such as EphRs, ephrins, cadherins, and nectin. PS1/γ-secretase can cleave full-length E-cadherin and a transmembrane C-terminal fragment, which is a key regulator of the Wnt signaling pathway (Marambaud et al., 2002). PS1/γ-secretase regulates the processing of nectins in PS1-/- and+/+ primary hippocampal neurons. Lack of PS1/γ-secretase inhibits the processing of nectin-1 and nectin-3 to their C-terminal fragments and leads to the accumulation of the full-length proteins

(Kim et al., 2011). PS1-dependent intramembrane cleavage followed by nectin shedding takes place at synapses, and is regulated during synaptic plasticity. In mice and rats, metalloproteases and γ-secretase reduce the levels of synaptic proteins on both sides of the synapse to weaken synaptic transmission (Restituito et al., 2011). Activity-dependent substrate cleavage by these enzymes is a novel mechanism of synaptic regulation to alter synaptic transmission.

A number of neuroligin-1 peptide fragments have been detected by immunoblotting in rat and mouse neuronal cultures (Suzuki et al., 2012), which indicates that neuroligin-1 undergoes proteolysis. The metalloproteinase ADAM10 cleaves the amino-terminus, extracellular domain of neuroligin-1, while the carboxy-terminus region is cleaved by γ-secretase. Addition of NMDA and soluble β-neurexin to the medium in cell culture experiments increases the quantity of neuroligin-1 N-terminal fragments (Suzuki et al., 2012), suggesting that neuroligin-1 cleavage can be stimulated by neuronal activity. The overstimulation of glutamate receptors that occurs in excitotoxic environments, such as AD-affected brain areas, could mediate synaptic damage.

Increased neuron activity *in vivo* decreases synaptic levels of neuroligin-1. Reducing the action of metalloproteases by inhibitors like MMP9 blocks this effect, probably by mitigating the activity-induced cleavage of neuroligin-1 (Peixoto et al., 2012). This finding may provide a treatment avenue for neuroligin-mediated synaptic damage in AD. Peixoto et al. (2012) showed that cleavage of neuroligin-1 occurs at single activated dendritic spines and involves NMDA receptors and Ca^{2+}-calmodulin-dependent kinase (CaMK) signaling leading to the destabilization of presynaptic β-neurexin1. The cleavage of neuroligin-1 weakens the synapse by rapidly decreasing presynaptic transmitter release (Suzuki et al., 2012). Together, these data suggest that the acute activity stimulated by cleavage of neuroligin-1 is a local homeostatic mechanism to control structural and functional synaptic plasticity.

The mechanism that controls neurexin function at synapses is not fully understood. The PS/γ-secretase complex can process neurexins and inactivation of the complex stimulates the accumulation of neurexin at the pre-synaptic terminal *in vivo* and *in vitro*. Different familial AD

mutations in PS1 affect β-neurexin-1 processing differently: some stimulate the processing of β-neurexin-1, whereas others have the opposite effect. Inhibition of PS and neurexin accumulation at sites controlled by neuroligin-1 suggests that PS organizes the processing of neurexins at glutamatergic synapses, and that impairment of neurexin processing by PS could involve at least part of a proposed familial AD pathogenesis pathway (Saura et al., 2011). Processing of neurexin-3β by α-secretase produces an ~80-kDa extracellular N-terminal domain designated soluble neurexin-3β and the transmembrane C-terminal fragment neurexin-3β-CTF. Further processing of the C-terminal fragment by γ-secretase produces a 12-kDa intracellular domain neurexin-3β-ICD (Bot et al., 2011). Mutated forms of PS1 that are associated with familial AD include PS1-L166P, PS1-P436Q, and PS1-9, which alter the catalytic core of γ-secretase and lead to a partial loss of enzyme function. The effect of these mutations on neurexin-3 processing has been elucidated by over-expressing them in Chinese hamster ovary cells stably expressing neurexin-3. The mutated proteins increase neurexin-3β-CTF levels and decrease neurexin-3β-ICD formation (Bot et al., 2011). These data suggest that mutated forms of PS1/γ-secretase impair neurexin-3 processing and may cause the accumulation of the intracellular neurexin-3 C-terminal fragment.

1.4.4.2 Neuroligins and neurexins in learning and memory

Experiments on transgenic mice have revealed that overexpression of neuroligin-1 protein elicits learning and memory deficits, impairment of the induction of long-term potentiation (LTP), alterations in spine morphology, and reduced synaptic plasticity by altering the excitatory to inhibitory synapse ratio in hippocampus (Dahlhaus et al., 2010). Silencing of neuroligin-1 in the amygdala of mice showed that this protein plays an essential role in the storage of associative fear memory (Kim et al., 2008). Subsequent physiological experiments revealed that the lower neuroligin-1 levels weaken NMDA receptor-mediated currents and inhibit LTP (Jung et al., 2010). neuroligin-1 knockout mice show abnormalities in spatial learning and memory that are associated with impaired hippocampal LTP and a reduced NMDA/AMPA receptor ratio at corticostriatal synapses (Blundell et al., 2010). These data suggest that steady neuroligin-1 levels are essential for NMDA receptor-mediated synaptic transmission, which plays a central role in synaptic plasticity and

long-term memory formation in the amygdala of adult animals (Kim et al., 2008). *NLGN3* R451C mutant mice exhibit impaired social interactions but improved spatial learning. Unexpectedly, these behavioural changes are induced by the stimulation of inhibitory synaptic transmission, with no effect at excitatory synapses. On the other hand, deletion of *NLGN3* did not cause much alteration, indicating that the R451C substitution is a gain-of-function mutation. These results suggest that increased inhibitory synaptic transmission could play an important role in autism spectrum disorders (Taniguchi et al., 2007). Hines et al. (2008) manipulated transgenic mice overexpressing neuroligin-1 and neuroligin-2 under the control of the Thy1 promoter, which leads to expression in various brain regions at early stages of development. Several abnormalities resulted from an increased expression of neuroligin-2, but not of neuroligin-1. A slight alteration in neuroligin-2 expression culminated in distended contacts at frontal cortex synapses and a general reduction in the excitatory to inhibitory synaptic ratio. These animals also showed impaired social behaviour and anxiety. A study using neuroligin-1 and neuroligin-3 knockdown showed that neuroligin-1 alternatively spliced at site B is required for LTP expression in young CA1 pyramidal cells, but that neuroligin-3 does not appear essential for LTP support (Shipman and Nicoll, 2012).

Neurexin and neuroligin proteins at sensory-to-motor neuron synapses play roles in the gill-withdrawal reflex in *Aplysia*, which exhibits sensitization (Shipman and Nicoll, 2012, Choi et al., 2011). Reducing neurexin in the presynaptic sensory neuron or neuroligin in the postsynaptic motor neuron eliminates long-term facilitation and enhances the associated presynaptic growth elicited by frequent pulses of serotonin. These data suggest that activity-dependent regulation of the neurexin-neuroligin contact could govern trans-synaptic signalling that is essential for the storage of long-term memory. An altered function of synaptic cell-adhesion molecules that leads to reduced excitatory synaptic transmission is a potential treatment target for neurological disorders. Such alterations may provide the neural basis for an imbalance in excitatory and inhibitory transmission and the behavioural changes related to disorders such as AD. Neuroligin-1 expression can modulate synapse morphology and LTP; abnormal synapse morphology, reduced synaptic plasticity, and deficits in learning occur in several neurological disorders, including AD.

1.5 Thesis outline

1.5.1 Chapter 2

Fluctuations in the levels of the synaptic proteins neuroligin-1 or neuroligin-2 in relation to synaptic loss in AD. This chapter describes the development of an immunodetection assay to quantify neuroligin-1 and neuroligin-2 proteins in autopsy brain tissues. Truncated versions of neuroligin-1 and neuroligin-2 were constructed, cloned, expressed, and purified. Different concentrations of the engineered protein were mixed with constant amounts of native protein extracted from tissue. Recombinant truncated protein separated clearly from the target protein as a sharp band. A standard curve with multiple points was created to show band intensity against quantity of standard in the different lanes on the same gel. The chapter then shows the successful use of the immunodetection assay in achieving precise estimates of the quantities of neuroligin-1 and neuroligin-2 present in each sample.

1.5.2 Chapter 3

Using the immunodetection assay from Chapter 2, concentrations of neuroligin-1 and neuroligin-2 were accurately quantified in hippocampus, inferior temporal cortex and occipital cortex autopsy tissue from 15 AD cases and 15 controls. These concentrations were compared between the two groups. Further statistical analyses assessed the effects of sex and the pathological severity of the disease on neuroligin-1 and neuroligin-2 protein levels. In addition, a similar immunodetection assay was used to quantify β-neurexin in hippocampus, inferior temporal cortex and occipital cortex autopsy tissue from 15 AD cases and 15 controls.

1.5.3 Chapter 4

The aim of this chapter was to validate the data obtained from quantification of neuroligin-1, neuroligin-2 and β-neurexin by using multiple reaction monitoring MRM assays, which are based on mass spectrometry and SWATH techniques, in AD cases and controls. This included sample preparation, validation and optimization of the best transitions and the actual quantification of the neuroligin and neurexin isoforms.

1.5.4 Chapter 5

This chapter describes the development of a real time PCR assay to quantify neuroligin-1, neuroligin-2 and β-neurexin transcripts in human autopsy brain tissues. The concentrations of theses transcripts were measured in hippocampus, inferior temporal cortex and occipital cortex from 14 AD cases and 14 controls, and then compared.

1.5.5 Chapter 6

The aim of this chapter was to confirm the association between Alzheimer disease and the single nucleotide polymorphism (SNP) rs17757879 in *NRXN3β* in an Australian Caucasian population using a case-control association approach, by using genomic DNA from the Queensland Brain Bank.

1.5.6 Chapter 7

Conclusions and future directions.

Chapter 2

2 Development of an immunoassay to quantify neuroligin-1 and neuroligin-2

2.1 Aim of the research

1. To develop an immune-detection assay to quantify neuroligin-1 and neuroligin-2.
2. To clone, express and purify recombinant truncated neuroligin-1 and neuroligin-2 protein standards.

2.2 Introduction

The use of brain autopsy tissues in neurobiological research has increased in recent years. Biochemical and proteomic experiments on human tissue are an essential component in establishing the roles that many proteins and pathways play in neurological disorders. Estimates of protein levels in autopsy brain tissue from cases and controls contribute to our understanding of the pathogenesis of disease. Recent developments in technology have been responsible for massive amounts of data on protein expression in different diseases, and have helped to delineate several drug targets. These approaches require that the molecular and biochemical state of the tissue is well maintained. Ideally, the target proteins should be undamaged and biologically active. Several studies have assessed the stability of transcripts and proteins isolated from human autopsy brain tissues (Johnson and Ferris, 2002, Johnston et al., 1997, Köpke et al., 1993, Yasojima et al., 2001). Various factors affect post mortem yields of DNA, mRNA and protein, such as the method of tissues preparation, tissue pH, storage conditions, time in storage, and post-mortem interval (PMI; Kingsbury et al., 1995, Leonard et al., 1993, Ludes et al., 1993, Lukiw et al., 1990, Palmer et al., 1988, Schramm et al., 1999). It has been shown that cells can be obtained from human autopsy brain tissues and maintained alive in culture (Verwer et al., 2002).

Proteomics uses several quantitative and qualitative techniques to detect the proteins in a tissue that differ in expression, for example in response to a disease. These include 2-dimensional differential gel electrophoresis (2D-DIGE), mass spectrometry (MS) and Western blotting. 2D-DIGE

has a limited capacity to detect alterations in expression or post-translational modification in low-abundance proteins. Mass spectrometry needs high expression levels for protein quantification and requires large amount of starting material, which is an issue for work on human tissue. It also involves various steps that could affect protein integrity or lead to degradation.

Western blotting (immunoblotting) is used to detect the presence of a particular protein in a complex biological extract. Although quantification can be problematic, immunoblotting can be effective in finding statistically significant alterations in the levels of protein linked to disease. As in gene expression, minor changes in protein expression in the brain might have major consequences in the tightly regulated CNS. More-complicated proteomic techniques may be unable to detect small significant differences in protein regulation, and simpler but more sensitive biochemical techniques needed to confirm any alterations found. Immunoblotting depends on three basic steps: (1) gel electrophoresis to separate a mixture of protein based on size; (2) effective transfer of separated proteins to a solid support; and (3) precise recognition of the protein of interest by selective primary and secondary antibodies. The band of the target protein is then visualized on the blotting membrane by using either X-ray film or an imaging system.

Immunoblotting is one of the most common laboratory techniques due to its advantages in time, simplicity, and cost. Data obtained from immunoblotting are simple to interpret, distinctive, and unmistakable. Often when a result does not match expectations, there can be indications of what must be investigated to find the reason. Nevertheless, there are several limitations of the method, such as incomplete protein transfer from the gel to the membrane, the availability of specific antibodies for protein recognition, and the small number of proteins that can be detected in one assay.

In this chapter I develop an immune-detection assay to specifically quantify neuroligin-1 and neuroligin-2 proteins in human autopsy brain tissue. β-NRXN protein was purchase from Life Technology Company, therefore was not included in this chapter. The strategy to sensitively and precisely quantify neuroligin-1 and neuroligin-2 concentrations used known amounts of recombinant

expressed truncated versions of neuroligin-1 and neuroligin-2 respectively to construct standard curves. I used this to identify small but significant differences between cases and controls, which might not have been detected by other techniques due to large variations in the levels of individual proteins. These measures of the exact molar concentrations of the proteins in my data set allowed me to assess and contrast alterations in levels of synaptic adhesion molecules at the synapse.

2.3 Materials and Methods

Truncated recombinant versions of the proteins that contained the relevant epitopes for the primary antibodies used, in the N-terminus of neuroligin-1 and the internal region of neuroligin-2, were constructed. This permitted me to accurately measure native protein levels in autopsy brain tissue by in-gel immunodetection. The truncated proteins were smaller than their target proteins to allow easy separation by electrophoresis. The engineered transcript proteins were expressed in a bacterial system and purified, and a known amount added to each AD case and control sample lane in the gel. Each truncated protein separated clearly from its target protein as a sharp band. A standard curve with multiple points was created derived from the band intensities produced by adding differing known quantities of standard to different lanes on the gel. This method was used to achieve very precise estimates of the quantities of neuroligin1 and neuroligin-2 present in each sample.

2.3.1 Recombinant neuroligin-1 and neuroligin-2 protein standards

A modified 5' end was integrated into the design of the forward primers to facilitate directional cloning into the vector from Invitrogen, which has a 4-nucleotide overhang sequence. The reverse primers were designed against the sequence upstream of the stop codon to permit expression of a downstream histidine tag. Using the Champion™ pET Directional TOPO® Expression Kit system (Life Technologies Pty Ltd, Invitrogen, Mulgrave, Vic, Australia), PCR products can be directionally cloned by adding four bases to the forward primer (CACC). The overhang in the cloning vector (GTGG) invades the 5' end of the PCR product, anneals to the added nucleotides, and results in production of a PCR product at the right orientation. With this system the PCR amplicon can be cloned at very high efficiency.

The forward and reverse primers sequences that were used to amplify a fragment of each protein are listed in Table 2.1.

The cDNA used to amplify the PCR product was prepared from frozen tissue that was stored at –80°C in 0.32 M sucrose. Pieces of frozen human autopsy tissue about 1 cm^3 were weighed and homogenized on ice in 10× (w/v) of TRIzol® (Invitrogen) using a motor-driven homogenizer (Polytron®, Kinematica, Bohemia, NY, USA). The homogenate was incubated for 5 min at room temperature and 0.2× (v/v) of chloroform was added and the incubation continued at RT for 2–3 min with shaking. The homogenate was centrifuged for 20 min at 10 000 × *g* at 4°C and the top layer transferred to a new tube. 0.1× (v/v) of isopropanol was added and the mixture incubated for 10 min at RT, then centrifuged at 10 000 × *g* for 15 min at 4°C. The pellet was resuspended in 1 ml of 75% ethanol and centrifuged at 20 000 × *g* for 20 min at 4°C. The final pellet was dried and resuspended in 50 µl of pure water and incubated at 60°C for an additional 10 min.

Table 2.1. *NLGN1* and *NLGN2* PCR and cloning details.

	NLGN1	*NLGN2*
Forward Primer	5'-CAC CAT GGC ACT GCC CAG AT-3'	5'-CAC CTA CGT GCA GAA CCA GAG C-3'
Reverse Primer	5'-ACC AGC TCG ATA CCA CAT AGC CTA A-3'	5'-CCG ACT ACC AGT CTC CCG TCT AA-3'
Size of PCR amplimer & recombinant protein	1069 bp between nucleotides 421 and 1491; 38 kDa	1035 bp between nucleotides 465 and 1510; 40 kDa
Location of epitope	Residues 33–61 near N-terminus	Internal region
Sizes of native form	4861bp	4621 bp

To reverse transcribe the RNA, DNase I was added to get rid of any contaminating genomic DNA. 1 µl of 10× DNase I reaction buffer (Fermentas Inc, Hanover, MD, USA) was added to 3 µg of RNA, then 40 U of RNase OUT (Fermentas) and 1 U of RNase-free DNase (Fermentas) were

added and the mixture incubated at 37°C for 30 min. EDTA was added to a final concentration of 2.27 mM and the mixture incubated at 75°C for 5 min. cDNA was formed by adding the following: 0.82 µg of DNase, 300 µM dNTPs (Promega Corp., Sydney, NSW Australia), 1 µg of Oligo (dT)12–18 primers (Promega), and 0.5 µg of random hexamers (Promega). Nuclease-free MilliQ H_2O was added to make the volume to 12 µl and the mixture incubated for 5 min at 65°C. The following reagents were added to perform the reverse transcriptase step: 5× first-strand buffer, 4.8 mM dithiothreitol (DTT), 40 U of RNaseOUT and 400 U of Superscript III Reverse Transcriptase® (Invitrogen). The mixture was incubated at 25°C for 5 min, then 50°C for 60 min and 70°C for 15 min. To eliminate any residual contamination by RNA, 2U of DNase-free ribonuclease H (Invitrogen) was added and the incubation continued for 20 min at 37°C. The cDNA was stored at –20°C.

The PCR product of *NLGN1* was amplified from cortical cDNA by incubating 1 µl of cDNA with 1 µl of 10 mM dNTPs, 1 µl of *NLGN1* 10 µM forward and reverse primers (final concentration 0.2 µM), 5 µl of 10× *Pfu* buffer without $MgSO_4$ (200 mM Tris-HCl, pH 8.8 at 25°C), 100 mM $(NH_4)_2SO_4$, 100 mM KCl, 1% (v/v) Triton X-100, 1 mg/ml BSA), 4 µl of 25 mM $MgSO_4$ (final concentration 2 mM) and 0.5 µl (1.25 U) of *Pfu* DNA polymerase. The PCR was performed using the following conditions: initial denaturation at 95°C for 2 min, then 35 cycles with denaturation at 95°C for 30s. A gradient PCR cycler was used to get different annealing temperatures for different reactions at 58°C and 62°C for 30s and extension at 72°C for 2 min. Final extension was at 72°C for 10 min. The PCR products were loaded onto a 1% agarose/ethidium bromide gel and run for 1h at 100V.

The PCR product of *NLGN2* was amplified from cortical cDNA by incubating 1 µl of cDNA with 10 mM dNTP mixture (final concentration of each dNTP 200 µM), 10 µl buffer B (60 mM Tris-SO_4, 18 mM $(NH_4)_2SO_4$, 2 mM $MgSO_4$, pH 9.1), 10 µM *NLGN2* forward and reverse primers (final concentration 200 nM), 1 µl of Elongase enzyme mix, finally topped up to 50 µl with MilliQ H_2O. The following conditions were used to perform the amplifications: pre-amplification denaturation at 94°C for 30s, then 35 cycles with denaturation at 94°C for 30s. A PCR gradient cycler was used to

get different annealing temperatures for different reactions for optimizations: 58°C, 60°C, 62°C and 64°C, with gradient annealing for 30s. Extension was performed at 68°C for 1 min. After the 35 cycles were completed a final extension at 68°C for 10 min was performed. The PCR products were loaded onto a 1% agarose/ethidium bromide gel and run for 1h at 100V.

2.3.1.1 PCR clean-up

To purify *NLGN1* and *NLGN2* PCR products from primers, nucleotides, polymerase and salt, and to obtain concentrated cDNA, I used the QIAquick PCR purification kit (QIAGEN Pty Ltd, Doncaster, VIC, Australia) as per the manufacturer's specification.

2.3.2 Topo cloning reaction

The purified PCR products of *NLGN1* and *NLGN2* were ligated into Topo vector at a 0.5:1 molar ratio of PCR product to vector. The ligation reaction was carried out in 6 µl total volume, which included 0.5 µl of purified PCR product, 1 µl salt solution, 1 µl Topo vector and 3.5 µl of MilliQ H_2O. The reaction was mixed gently and incubated for 5 min at room temperature. The mixture was placed on ice for the *E. coli* transformation (see next).

2.3.2.1 Transformation of E. coli

pET TOPO *NLGN1* and *NLGN2* constructs were transformed into competent *E. coli* (One Shot® TOP10 Chemically Competent *E. coli*; Invitrogen) by adding 3 µl of the TOPO® Cloning reaction product (previous section) into a vial of the *E. coli* preparation and the reaction mixed gently and incubated on ice for half an hour. Cells were heat-shocked for 30s at 42°C without shaking and the tubes immediately transferred to ice. 250 µl of Super Optimal broth with Catabolite repression (S.O.C.; 2% Tryptone, 0.5% Yeast Extract, 10 mM NaCl, 2.5 mM KCl, 10 mM $MgCl_2$, 10 mM $MgSO_4$, 20 mM glucose) was added to the vial at room temperature and the mixture shaken horizontally (200 rpm) at 37°C for 1h. 100 µl and 200 µl of each transformation reaction were spread on pre-warmed LB agar + carbenicillin plates and incubated overnight at 37°C.

2.3.2.2 PCR colony screening

Colonies obtained from the plates were streaked on new LB agar + carbenicillin plates and grown overnight at 37°C. Each growing colony was tip patched and incubated in a reaction containing 50 µl 2% Triton pH 12.4 (0.03 mM), 10 µl 6× loading dye (11 mM EDTA, 3.3 mM Tris-HCl, 0.017% SDS, 0.015% bromophenol blue, pH 8.0) and 50 µl of the bottom layer of a chloroform/phenol/isoamyl alcohol 25:24:1 saturated with 10 mM Tris and 1 mM EDTA, pH 8.0. Tubes were vortex and centrifuged for 10 min at 13,000 × *g*. The top layer of the mixture was loaded onto a 1% agarose/ethidium bromide gel with a 1 kbp ladder and run at 100V for 1h. Colonies with the right insert were identified from the banding pattern (Genomic DNA, Vector 5764 bp, insert *NLGN1* and *NLGN2* ~1000 bp).

2.3.2.3 Plasmid purification

A QIAprep Spin Miniprep Kit (QIAGEN) was used to purify high-copy plasmid DNA of *NLGN1* and *NLGN2* from 5 ml overnight cultures of *E. coli* in LB as per the manufacturer's specifications.

2.3.2.4 PCR screening

PCR screening was used to analyse positive transformants of *NLGN1* with the following reaction: 1 µl of 10 µM dNTPs, 1 µl of *NLGN1* 10 µM forward and reverse primers (final concentration 0.2 µM), 5 µl of 10× *Pfu* buffer without $MgSO_4$ (see above), 4 µl of 25 mM $MgSO_4$ (final concentration 2 mM) and 0.5 µl (1.25 U) of *Pfu* DNA polymerase. Colonies with inserts were resuspended into the reaction mixture and PCR performed using the following thermal cycling: initial denaturation step of 2 mins at 95°C, then 35 cycles of a 30s, 95°C denaturing step, 58 ± 4°C gradient annealing for 30s, and a 2 min, 72°C extension step which was followed by a final extension step of 72°C for 10 min.

2.3.2.5 Restriction enzyme analysis

Restriction analysis of purified *NLGN2* plasmid was conducted to confirm the presence and the correct orientation of the insert. The NEB cutter tool (New England BioLabs, Hitchin, UK) was

used to find non-overlapping open reading frames in DNA sequences of the *E. coli* genetic code and the sites for all Type II and commercially available Type III restriction enzymes that cut the sequence just once. Restriction enzyme APAI (New England Biolabs), which cut the insert at nucleotide 666 and cut the vector at nucleotide 5029, was used. The following reaction was conducted to perform *NLGN2* restriction analysis in 20 µl: 2 µl of 10× NEBuffer, 0.2 µl of BSA 100×, 5 µl of purified plasmid, 0.5 µl of APAI enzyme and 12.3 µl of sterile deionized water. The mixture was incubated for 3h at 37C in a water bath and then for additional 10 min at 70°C, then loaded into a 1% agaros/ethidium bromide gel and run for 1h at 100V.

2.3.2.6 Sequencing

NLGN1 and *NLGN2* constructs were sequenced using Illumina (San Diego, CA, USA) HiSeq2000 next generation sequencing at Australian Genome Research Centre to confirm that the *NLGN1* and *NLGN2* genes were in frame with the appropriate N-terminal or C-terminal fusion tags. The forward and reverse reaction mixtures of *NLGN1* and *NLGN2* were sent in 12 µl total volume (600 ng of plasmid and 0.6 µl of pET100/D-TOPO® T7 forward primer or 0.6 µl of reverse primer for pET100/D-TOPO® T7 reverse primer).

2.3.2.7 Expression

Successfully sequenced *NLGN1* and *NLGN2*-PET101/D-Topo clone (plasmid) were transformed into BL21 Star™ (DE3), which is included with each Champion™ pET directional TOPO® Expression Kit. 0.5 µl of each plasmid DNA was loaded into thawed vial of BL21 Star™ (DE3) and mixed gently. Cells were incubated on ice for 30 min, then heat-shocked for 30s at 42°C without shaking. The tubes were immediately transferred to ice and 250 µl of room temperature SOC medium was added to each tube. The mixtures were incubated at 37°C for 60 minutes with shaking (200 rpm). Each entire transformation reaction was added to 10 ml of LB containing 10 µl Ampicillin antibiotic and grown overnight at 37°C with shaking.

Because different recombinant proteins have different characteristics, pilot expression was performed in which a time course for expression was studied to determine the best condition for

protein expression. 500 µl of the overnight cultures were inoculated to 10 ml of LB containing 10 µl of Ampicillin and grown for 2h at 37°C with shaking (200 rpm) until the cells had reached mid-log phase (OD_{600} 0.5–0.8). Each culture was split into two (5 ml each) and 0.5 mM IPTG final concentration (250 µl of 200 µM) added to one sample to induce expression. 500 µl aliquots were taken from each culture as a zero time point sample and centrifuged for 1 min at 13,000 rpm. Supernatants were aspirated and pellets were then frozen at –20°C. Cultures were kept in the incubator at 37°C with shaking and aliquots taken every hour up to 4h. At each time point, 500 µl from the induced and uninduced cultures were taken and centrifuged for 1 min at 13,000 rpm, the supernatants were discarded, and the pellets stored at –20°C for analysis.

2.3.3 Analysing expression

To analyse the pilot expression of *NLGN1* and *NLGN2,* 10% of SDS separating gels were prepared by mixing 3.54 ml of MilliQ H_2O, 3.75 ml of 1M Tris (pH = 8.8), 100 µl of 10% SDS, 2.5 ml 40% Acrylamide, 100 µl of 10% APS (Ammonium persulfate) and 10 µl of TEMED (NNNN-tetramethylenediamine). 4% stacking gels were prepared by mixing 3.77 ml of MilliQ H_2O, 625 µl of 1M Tris (pH = 6.8), 50 µl of 10% SDS, 500 µl of 40% acrylamide, 50 µl of 10% APS and 5 µl of TEMED. Sample pellets from the pilot expression of *NLGN1* and *NLGN2* were thawed, suspended into 80 µl of 1× sample buffer, and boiled for 5 min at 100°C. 16 µl of each pellet and SDS-sample buffer mixture was loaded onto the gel and run for 45 min at 150V. Gels were stained with Coomassie Brilliant Blue (Sigma-Aldrich Pty Ltd, Castle Hill, NSW, Australia) in 50% methanol and 10% glacial acetic acid for 1h, then destained overnight with 45% methanol and 5% acetic acid. Gels were visualized on the Odyssey Infrared Imaging System (LI-COR Biotechnology, Cambridge, UK) at a scan intensity of 8 using the 700/800 nm fluorescence channel.

2.3.3.1 Scaling up expression for purification

To scale-up expression to 50 ml, 500 µl of overnight culture (previous step) was inoculated into 10 ml of LB containing 10 µl of ampicillin and grown overnight at 37°C with shaking (200 rpm) until the OD_{600} reached 1.0. One ml of the overnight culture was inoculated into 50 ml LB with 50 µl of Ampicillin and grown for 2h at 37°C with shaking (200rpm) until the cells reached mid-log phase

(OD_{600} = ~0.5). 1 mM IPTG was added to each culture to induce expression and the incubation continued at 37°C with shaking for 4h. Cells were harvested by centrifugation for 10,000 rpm for 10 minutes at +4°C.

2.3.3.2 Purification

Recombinant truncated neuroligin-1 and neuroligin-2 protein was purified under denaturating conditions using the Ni-NTA spin column kit (Qiagen) as per the manufacturer's instructions. Cells from 50 ml cultures of neuroligin-1 and neuroligin-2 were thawed for 15 min and pellets were resuspended and lysed in 1 ml of 1× PBS and 5 µl of 20 mg/ml lysozyme, 10 µl DNAase and 7 ml of buffer B, denaturing lysis/binding buffer (7 M urea, 100 mM NaH_2PO_4, 100 mM Tris-HCl, pH 8.0). The mixtures were agitated at room temperature for 1h until the solution become translucent. To pellet the cellular debris, 700 µl of lysates were centrifuged at 12,000 × g for 30 min at room temperature (25°C). The supernatant was collected and 20 µl of the cleared lysates saved for SDS-PAGE analysis.

2.3.3.3 Western blotting

To validate the expression and purification of neuroligin-1 and neuroligin-2 recombinant protein, western blotting was used. Proteins eluted from NI-NTA columns were mixed with 3× SDS-sample buffer (1:3 SDS buffer: protein) and loaded into 10% polyacrylamide gels. Proteins were separated for 30 min at 200V, then transferred to polyvinylidene difluoride (PVDF) membranes for 90 min at 100V. Membranes were blocked with 1% skim milk in PBST for 1h with shaking, then incubated overnight at 4°C with blocking solution plus mouse monoclonal primary antibody against neuroligin-1 (1:20000 Neuroligin-1 (A-4): sc-365110, Santa Cruz Biotechnology Inc, Dallas, TX, USA) or goat polyclonal primary antibody against neuroligin-2 (1:20000 Neuroligin-2 (R-16): sc-14089, Santa Cruz). Membranes were washed 3 × 10 min each in PBST and incubated at RT in the dark for 1h in skim milk blocking solution and PBST plus 1:20000 rabbit anti-goat 680 secondary antibodies (Invitrogen), then washed 3 × 10 min in PBST followed by 3 × 10 min in PBS. Finally, the membranes were dried and washed with methanol and visualized by the Odyssey infrared imaging system at λ = 700 nm.

2.3.4 Quantification of neuroligin-1 and neuroligin-2 recombinant proteins

The concentrations of neuroligin-1 and neuroligin-2 proteins were determined against a standard curve of BSA based on band intensity from the Odyssey imaging system.

2.3.4.1 Quantification of neuroligin-1 and neuroligin-2 endogenous protein

Variant amounts of purified neuroligin-1and neuroligin-2 were loaded onto separate SDS-PAGE gels. Standard curves were created by plotting the intensity of each neuroligin-1 and neuroligin-2 band from the Odyssey imaging system against known amounts of recombinant truncated neuroligin-1 and neuroligin-2 proteins respectively. This method allowed me to accurately quantify the the endogenous proteins using the standard curve present on each gel. This reduced both gel to gel and well to well variation during quantification (Agarwal et al., 2008).

2.4 Results

2.4.1 NLGN1 cloning

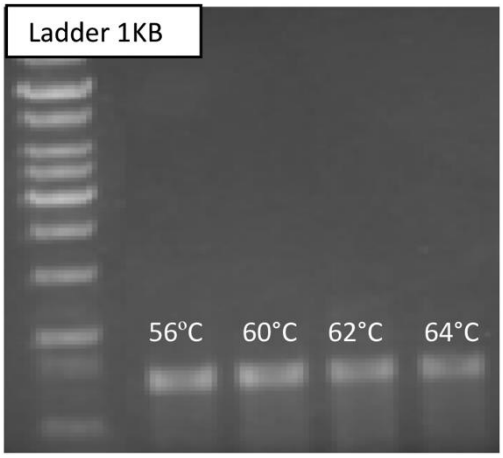

Fig. 2.1. Agarose ethidium bromide gel of *NLGN1* PCR products. Bands in lanes 2–5 represent temperature gradients 56–64°C. These bands represent the *NLGN1* amplicon and were identified at 1069 bp, which is the correct size, under UV.

To accurately quantify neuroligin-1 protein expression in human brain membrane samples, neuroligin-1 truncated protein was used as standard with different known concentrations. The fragment of neuroligin-1 amplified from occipital cortex cDNA corresponded to amino acids 421 to 1491, which contains the antigenic epitope amino acids 33 to 61 near the N-terminus recognised by

the Santa Cruz antibodies. Bands of the correct size (1069 bp) of the *NLGN1* amplicon were detected under UV light on an agarose ethidium bromide gel (Fig. 2.1).

PCR products of *NLGN1* were purified using the QIAquick PCR purification kit (Qiagen) and cloned into pET100/D-TOPO vector. The PET101/D-TOPO vector contains N-terminal or C-terminal polyhistidine (6×His) tags that facilitate the purification on a nickel column such as Ni-NTA. The pET TOPO® vectors have a T7/lac promoter to induce the expression of the protein of interest in high levels of IPTG. The T7lac promoter contains a lac operon sequence that assists in binding to lac repressor and has a role to further repress T7 RNA polymerase-induced basal transcription of the gene of interest in BL21 Star™(DE3) cells. The pET TOPO® vector has advantages for rapid directional cloning. Therefore, the vector was transformed into One Shot TOP10 *E. coli*. Quick screening for the successful insert of *NLGN1* into the TOPO vector was analysed by using phenol/chloroform/isoamyl alcohol (Fig. 2.2).

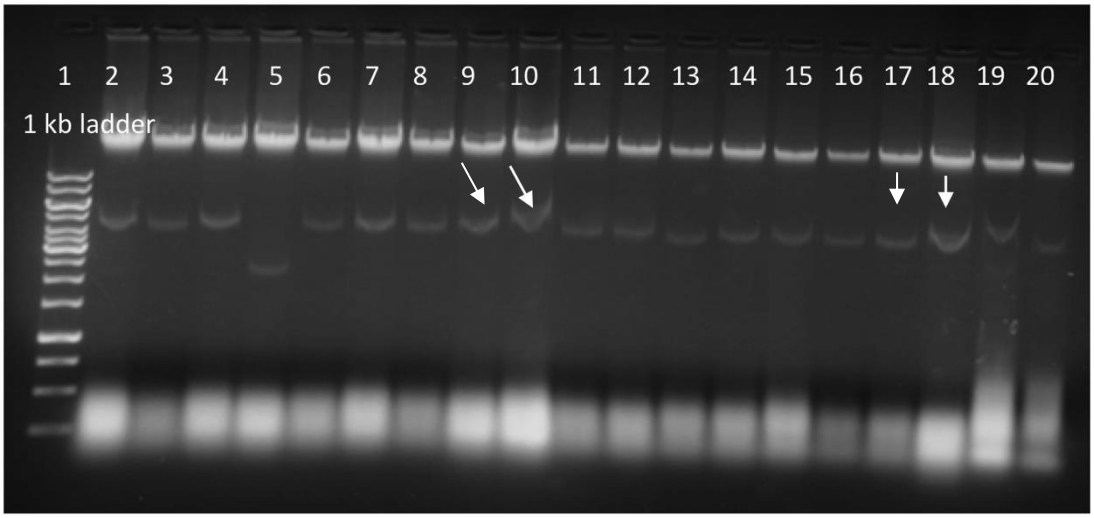

Fig. 2.2. Gel photo of quick screening for the successful insert (PCR product of neuroligin-1) into the TOPO vector. This technique gives rough confirmation of the successful ligation by the size of both insert and vector in the gel. Random selection of the colonies obtained from the transformation reaction in plates was done. These colonies were streaked on one plate and incubated overnight. Streaked patch colonies were treated with 2% Triton X-100 pH 12.4, then with phenol/chloroform/isoamyl alcohol (25:24:1) and loaded into the gel. The first lane in the gel represents the DNA

ladder standard, while lanes 2–19 show the treated colonies. Wells number 9 and 18 roughly show the successful ligation due to its size, which is slightly higher than the rest of the colonies in the gel.

To further analyse the successful transformation of *NLGN1*, analysis was conducted to confirm the presence and correct orientation of the insert by using a restriction enzyme with one specific site in the vector and one in the insert. NEB cutter from New England Biolabs was used to find the best restriction enzyme that cut the *NLGN1* insert. Plasmid digestion was performed as described in Section 2.3.2.5.

2.4.1.1 NLGN1 AGRF sequencing

AGRF sequencing was conducted to confirm the correct sequence and proper orientation of the insert for subsequent expression. See appendix for this chapter.

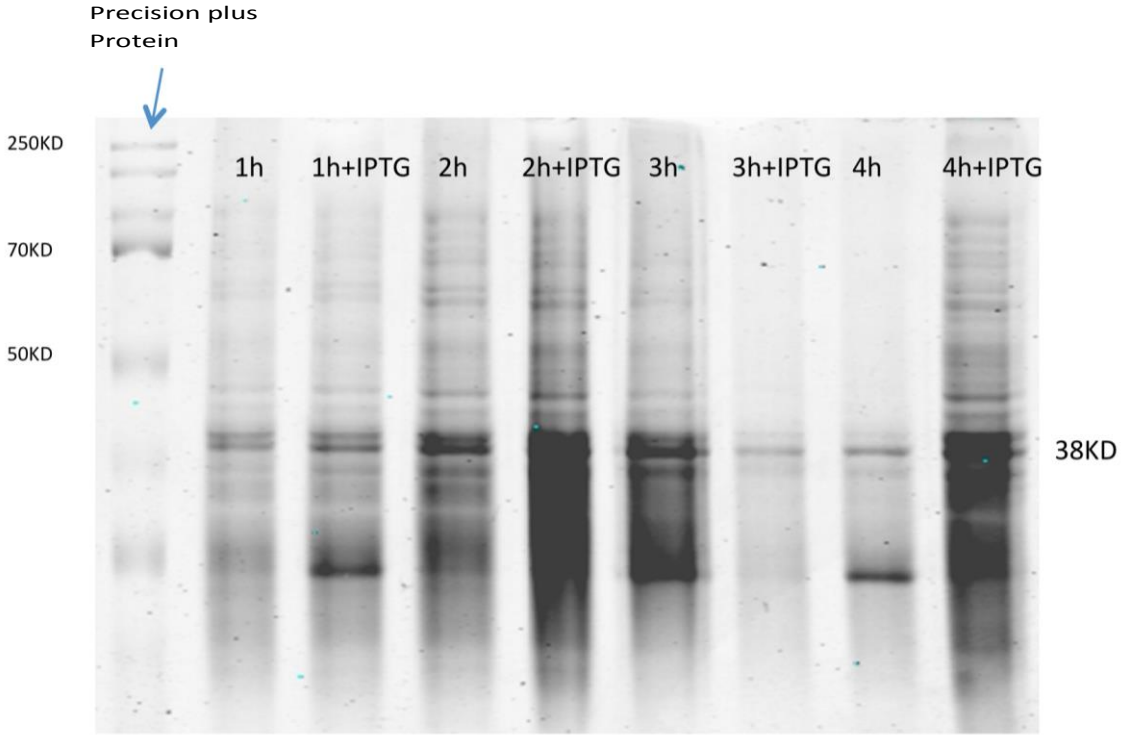

Fig. 2.3. SDS-PAGE of neuroligin-1 expression. Cultures were treated with or without IPTG to induce expression in (+) samples, and then run on SDS-PAGE for 45 minutes as described in Methods. Lane 1, protein marker; lanes 2, 4, 6 and 8, induced protein expression at 1, 2, 3, and 4h; lanes 1, 3, 5, and 7, no IPTG induction at 1–4h. The expected size of the recombinant truncated protein was 40 kDa.

2.4.1.2 Neuroligin-1 expression

The purified plasmid of pET100/D-TOPO constructs of neuroligin-1 were transformed into BL21 Star™(DE3) One Shot *E. coli* for the expression studies. A time course of expression up to 4 hours was performed to determine the best conditions for the expression neuroligin-1. SDS-PAGE was used to analyse neuroligin-1 expression and the Odyssey system used to visualize the Coomassie-stained gel (Fig. 2.3).

2.4.2 NLGN2 cloning

Neuroligin-2 recombinant truncated protein was used as a standard to accurately quantify neuroligin-2 native protein in human brain. PCR was used with human brain cDNA and primers (outlined in Table 1) to amplify a fragment of human neuroligin-2. The amplimer corresponds to amino acids 465 to 1510 and contains antigenic epitope. PCR optimization was done to generate the best conditions for amplifying *NLGN2* with the *Pfu* enzyme. Figure 2.4 shows the PCR products.

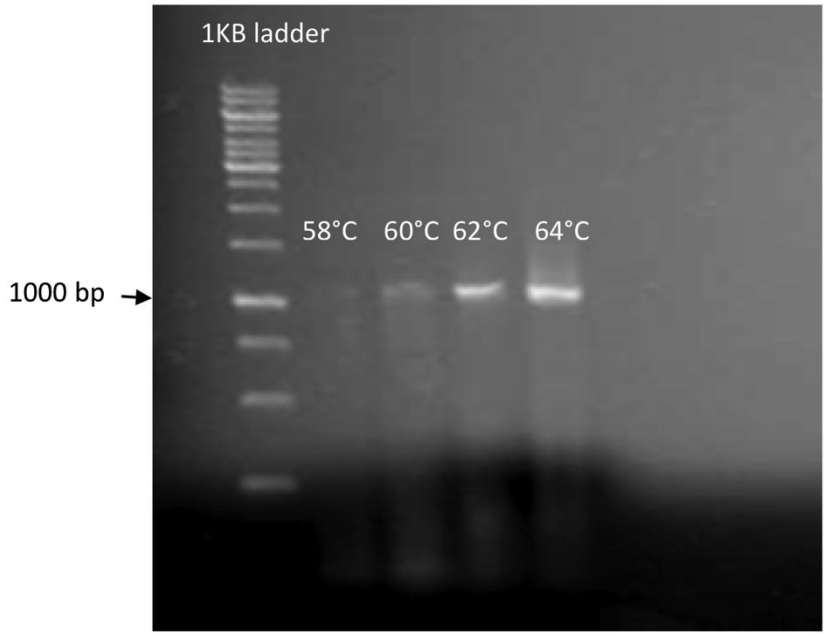

Fig. 2.4. PCR products of neuroligin-2. First lane is the 1 Kb ladder standard, lanes 2-4 are the PCR product of neuroligin-2 with annealing temperatures of 56, 58, 60, 62, and 64°C respectively.

Neuroligin-2 restriction analysis was conducted to confirm the presence and correct orientation of the insert by using a restriction enzyme with one specific site in the vector and one in the insert.

NLGN2 PCR products were purified and cloned as described in Methods. Quick screening for the successful insertion into the vector is shown in Fig. 2.5.

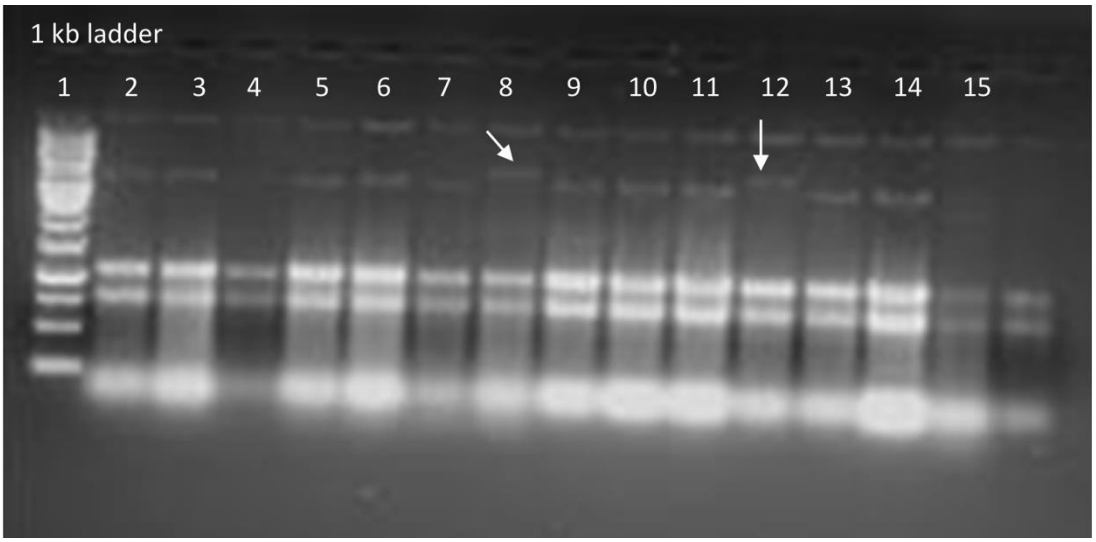

Fig. 2.5. Quick screening for the successful insert (PCR product of neuroligin-2) into the TOPO vector. Lane 1, DNA ladder, lanes 2–16, treated colonies. Wells #8 and 12 show successful ligation at slightly higher size than the rest of the extracts.

2.4.2.1 Neuroligin-2 expression

pET100/D-TOPO NLGN2 plasmid was transformed to BL21 Star™(DE3) One Shot *E. coli*. Pilot expression from 1–4 hours was conducted to determine the best expression conditions for neuroligin-2. Expression of neuroligin-2 protein was analysed by SDS-PAGE and Odyssey system was used to visualize the Coomassie-stained gel.

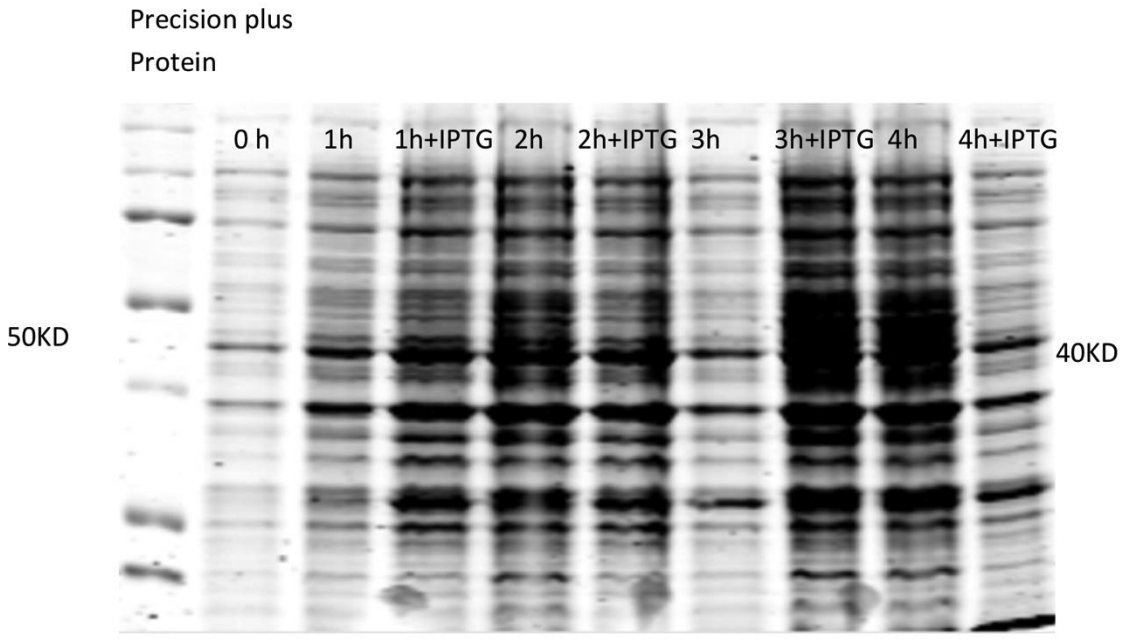

Fig. 2.6. SDS-PAGE of neuroligin-2 expression. Cultures were treated with (+) IPTG to induce expression, run on SDS-PAGE and stained as described in Methods. Lane 1, MW marker; lanes 2, 4, 5, 8, and 9, induced protein expression at 0, 1, 2, 3, and 4h; lanes 3, 6, 7, and 10, without IPTG induction at 1– 4h. The expected size of the recombinant protein is 40 kDa.

2.4.2.2 Neuroligin-1 and neroligin-2 purification

Maximum levels of recombinant neuroligin-1 and neuroligin-2 expression were attained at 4h after IPTG induction. Both proteins were purified on Ni-NTA columns from an upscale expression of 50 ml following 4h of IPTG addition (Figs 2.7 and 2.8).

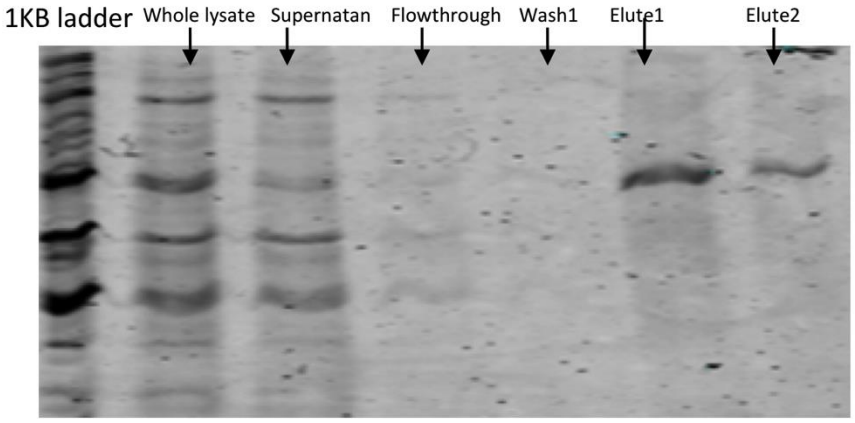

Fig. 2.7. Neuroligin-1 protein purificationon Ni-NTA columns. The second lane shows the whole lysate, the third lane the supernatant followed by flowthrough of the

supernatant, lanes 5 and 6 wash #1 and wash #2 respectively. The last two lanes that show the final eluates have the correct size of the recombinant truncated protein, 38KDa.

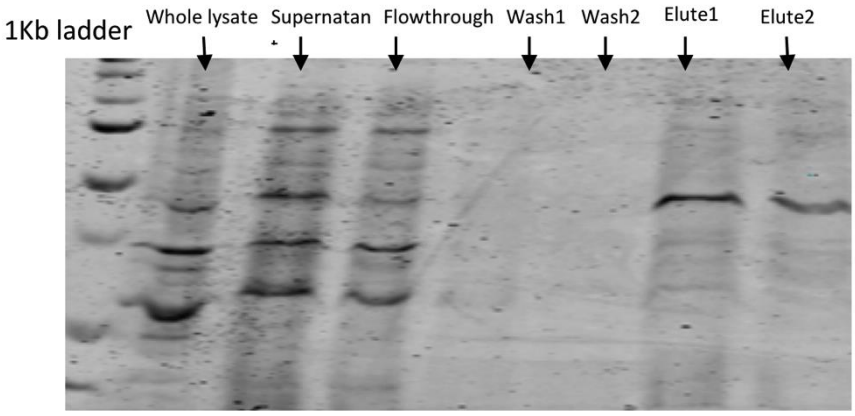

Fig. 2.8. Neuroligin-2 protein purification on Ni-NTA columns. Details as for Fig. 2.7; the last two lanes represent the final elutes and have the correct size of truncated recombinant protein, 40KDa.

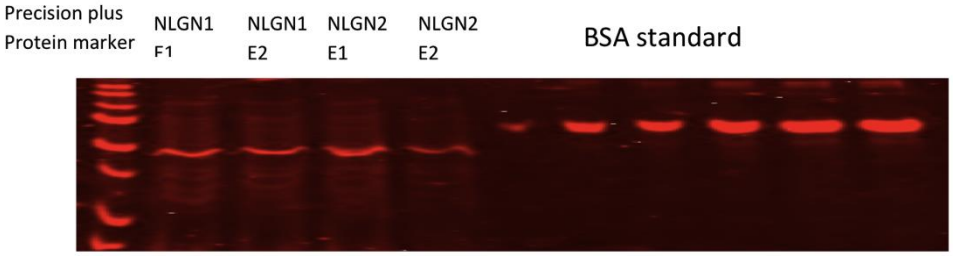

Fig. 2.9. Quantification of neuroligin-1 and neuroligin-2 recombinant proteins. The concentrations of neuroligin-1 and neuroligin-2 proteins were determined against a standard curve of known quantities of BSA based on band intensity in the Odyssey imaging system. The final concentration of neuroligin-1 was 21.39 ng/µl while the final concentration of neuroligin-2 was 24.27 ng/µl.

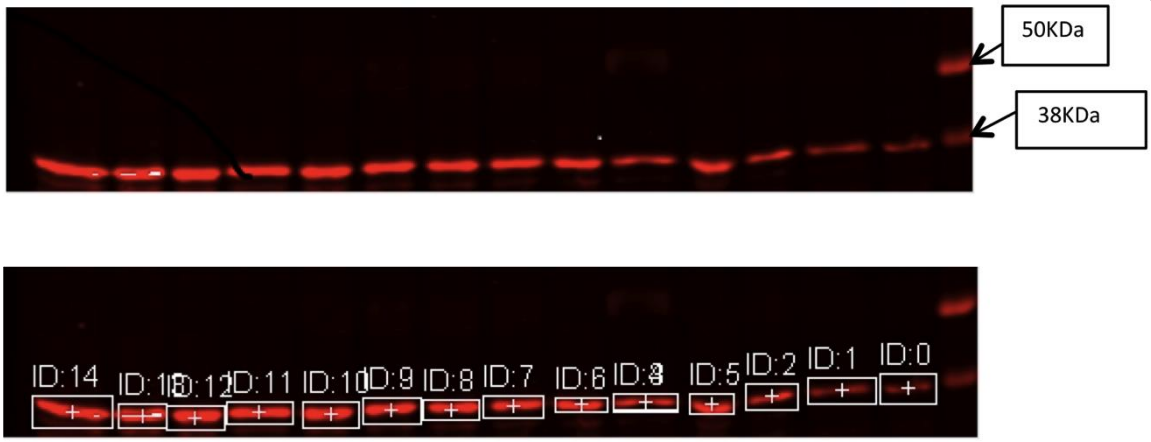

Fig. 2.10. Neuroligin-1 recombinant standard. Different concentrations of truncated recombinant neuroligin-1 were loaded onto the gel (10–100 ng). Details as Fig. 2.11.

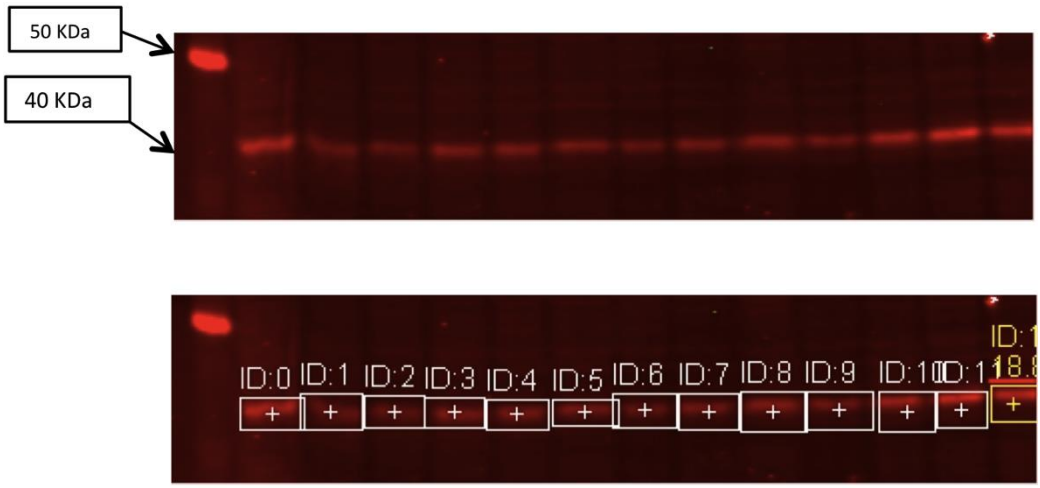

Fig. 2.11. Neuroligin-2 recombinant protein standard. Different concentrations of truncated recombinant neuroligin-2 were loaded onto the gel (10–100 ng). Details as for Fig. 2.11.

2.5 Discussion

Human post-mortem brain tissues have been used widely to find novel biomarkers in neurodegenerative disease, including AD. Different proteomic approaches can be used to find biomarkers and protein differences in AD, such as 2-dimensional gel electrophoresis, 2D-DIGE, and liquid chromatography based high-resolution tandem mass spectrometry, LCMS. The separation of a protein in 2-DIGE is based on the charge (isoelectric point) and the molecular weight. This separation leads to different pattern of protein spots that can then be recognized using MS methods to identify and quantify the proteins. 2-DIGE separation has good resolving power; utilization of

different dyes permits quantitative analysis, and allows increased sensitivity, reproducibility, and throughput in proteome analysis (Friedman et al., 2004, 2007). 2D-DIGE has a significant function in detecting proteins with posttranslational modifications (PTMs), because phosphorylation and glycosylation can have impacts on the isoelectric point and molecular weight of proteins. Hence, 2DIGE can be used to compare different samples, because the size (area) and intensity of spots alter according to variations in the expression of proteins. For these reasons, 2D-DIGE has been used to find biomarkers in CSF and plasma in neurodegenerative diseases such as AD (Castano et al., 2006, Davidsson et al., 2001, Hu et al., 2007).

An essential and informative phase in protein biomarker discovery is to identify quantitative differences in protein expression between diseased cases and controls. Utilizing 2-DIGE to quantify expression has limitations: it can't be used to quantify hydrophobic proteins such as membrane-bound proteins, and it is not applicable to proteins/peptides smaller than 15 kDa. It cannot detect differences when protein alterations are modest. This is a significant concern for studies of the human brain, where small changes in expression might have a marked impact over time.

There are simple and accurate proteomic techniques that can be used for validation, such as enzyme-linked immunosorbent assay (ELISA) and Western blotting. Western blotting is one of the less-expensive proteomic techniques, is quick to perform, sensitive, and needs less starting material, which are key considerations for work with human autopsy tissue. It can be used to identify and quantify a protein in a mixture by separating the protein in a gel based on its molecular weight. The protein is then transferred from the gel to a membrane, which is incubated with labelled antibodies specific to the protein of interest. Unbound antibody is washed off and the bands then visualized by an imaging system such as the Odyssey. If the primary antibodies are selective for the protein of interest, the visible band(s) represent that protein. The intensity of the band parallels to quantity of protein present. The use of a protein standard improves the quantification of the protein present.

Western blotting can give inaccurate results across gels. An internal control for protein quantification is essential for reliable, precise comparison of protein levels. Using a truncated

recombinant protein as standard in each gel minimizes errors due to the gel to gel variations. In this chapter, truncated recombinant human neuroligin-1 and neuroligin-2 proteins were successfully prepared to aid expression studies in human autopsy brain tissues. They allow accurate measurement of the native protein levels by in-gel immunodetection. The recombinant proteins are smaller than the native proteins; a known amount is added to each lane in the gel for use as a standard. The recombinant truncated protein separated clearly from their target proteins as sharp bands. A standard curve was created from the band intensities of standard in the different lanes on the gel; the use of the technique will be elucidated in the next chapter. It gives precise estimates of the quantities of neuroligin-1 and neuroligin-2 present in each sample, and can detect the proteins in the pmol per µg concentration range that is necessary to quantify proteins within the synapse. A comparison of the levels of neuroligin-1 and neuroligin-2 with other synaptic proteins is also possible with this method. The Odyssey infrared imaging system has a wide and linear dynamic range to quantify high and low signals on the same Western blot. It provides images with low background, high signal to noise detection, and clear, sharp, and reproducible bands.

Some limitations are associated with the quantification of proteins by immunodetection. These include incomplete protein transfer from the gel to membrane, and nonspecific binding of some antibodies. Staining of the polyacrylamide gel after transformation resolves this problem.

Chapter 3

3 Quantification of neuroligin-1, neuroligin-2 and β-neurexin-1 proteins

3.1 Aims of the research

1. To quantify the expression of the synaptic proteins neuroligin-1, neuroligin-2 and β-neurexin-1 in human post-mortem brain tissues from AD cases and controls.
2. To evaluate differences in expression in three different regions of the brain (hippocampus, occipital cortex and inferior temporal cortex) in AD cases and controls.
3. To assess the impact of age and gender on expression.
4. To investigate expression according to the pathological severity of the disease.

3.2 Introduction

Synaptic transmission is crucial for nervous system function, and its disruption is considered an important cause for many neurobiological diseases, including AD. The progressive loss of synaptic proteins and hence neurological function in dementia has been a topic of interest since the relationship between synaptic loss and AD was first reported (Davies et al., 1987). Further studies have shown that synapse and synaptic protein loss have substantial effects on function in AD (DeKosky and Scheff, 1990, Scheff et al., 1990, Terry et al., 1991). Synapse loss is the major correlate of cognitive impairment. Synaptic weakening is considered to be a general component in the pathological alterations linked to dementia, and is the best correlate with dementia ante mortem (DeKosky and Scheff, 1990). An approximate 30% decrease in synapse number per cortical neuron has been observed in AD brain (Walch-Solimena et al., 1993). Synaptic pathology occurs early in AD progression and it is more strongly correlated with dementia than are senile plaques and NFT (Terry et al., 1991). Synaptic alterations in AD have been verified by electron microscopy as well as by proteomic approaches (Zhou et al., 2013, Masliah et al., 2001, Davies et al., 1987, Chang et al., 2013). Gene expression assays using brain autopsy tissues from AD cases and controls have shown lower levels of different gene transcripts involved in synaptic vesicle trafficking (Liang et al., 2008). The mechanisms of synaptic pathology in AD are not totally clear, although several synaptic proteins

such as synaptophysin and gephyrin have been related to synaptic disruption in the disease (Agarwal et al., 2008, Tannenberg et al., 2006). It is not clear whether other synaptic proteins are involved in synaptic dysfunction in AD. Moreover, it remains unclear how synaptic organization, involving presynaptic, postsynaptic, and synaptic membrane proteins, is changed in AD.

3.2.1 Fluctuations of synaptic proteins in AD

Different studies have been conducted to quantify synaptic protein levels in human autopsy brain tissues from AD cases. For example, synaptophysin concentrations are lower in specific brain areas (Reddy et al., 2005, Lassmann et al., 1992, Honer et al., 1992, Hamos et al., 1989). However, different studies have shown contradictory results. Reduced synaptophysin levels were only detected at advanced stages of AD by Davidsson and Blennow (1998). The discrepancies between different studies may be due to differences in the region of brain tissue tested.

Dynamin I is a presynaptic terminal protein and functions in synaptic vesicle recycling (Liu et al., 1996). Quantification studies have revealed lower dynamin I mRNA and protein levels in the superior frontal gyrus of AD cases than in controls (Yao et al., 2003). A major component of the postsynaptic density (PSD) is the α-subunit of calcium/calmodulin-dependent protein kinase II (αCaMKII), which comprises 2% of total protein in rodent hippocampus and 1% of total protein in the forebrain (Ziff, 1997). No difference in αCaMKII level was observed in the hippocampi of AD cases and controls (Simonian et al., 1994). N-cadherin is a member of the cell-adhesion molecules that has important functions in neurite outgrowth, synaptic junctional complex formation, and synaptic stability (Shapiro and Colman, 1999, Tang et al., 1998). It is located with synaptophysin, synapsin I, PSD95, and GluR1 at the synapse both in the pre-synaptic membrane and on the PSD (Benson and Tanaka, 1998, Tanaka et al., 2000, Tang et al., 1998). Tannenberg et al. (2006) found that the level of N-cadherin protein was higher in all brain areas of 15 AD cases than in 15 controls. This might be explained by the increase in synaptic apposition length that occurs in AD (Scheff et al., 1990).

Complexin I is synaptic protein that controls inhibitory neurotransmitter release, while complexin II regulates excitatory neurotransmitter release. Both are membrane proteins that have roles in synaptic vesicle docking to the presynaptic membrane, which in turn mediates neurotransmitter release (Ono et al., 1998, Yamada et al., 1999). The expression of both complexins was significantly lower in all AD brain areas than in controls, but the ratio of complexin II to complexin I was not altered. These data show a loss of regulation of neurotransmitter release in AD in preserved presynaptic terminals. Quantitative immunohistochemistry in the entorhinal cortex from AD brain cf age-matched controls showed significantly higher levels of PSD-95 that positively correlated with □-amyloid and phosphorylated tau proteins (Leuba et al., 2008b). Quantifying these different types of synaptic proteins has proved fruitful in measuring the degree of synapse loss in AD. Further study of the roles of these and related molecules could illuminate mechanisms behind the synaptic loss and dysfunction that are characteristics of the disease.

3.2.2 Measurement of synapses and synaptic proteins

Electron microscopy was the first method used to quantify synapses, which were detected by thickening of the synaptic membrane, in a brain with cognitive decline, (Davies et al., 1987). One limitation of this approach is the ability to quantify only small areas of tissue. It also requires the use of preserved and rapidly fixed material, which limits its use with much autopsy tissue.

Antigen-specific immunochemical methods detect synapse loss in AD through the quantification of different synaptic proteins involved in the synaptic cycle. The immunochemical techniques utilized in the research of AD brain autopsies have linked synaptic loss with Aβ oligomer proteins as well as recognized synapse loss as the best correlate to AD.

Reliable and accurate techniques are able to precisely quantify proteins specific to different phases of the synaptic cycle. They can be correlated to disease stage as well as the region where the protein is expressed by using immunohistochemistry, enzyme-linked immunosorbent assay (ELISA) and immunoblotting methods. Immunohistochemistry measures synaptic protein levels by labelling synaptic proteins linked to presynaptic terminals or synaptic vesicles (Hamos et al., 1989). The

relative quantification of synaptic proteins can be measured via optical density of immunoreactive regions of the cortex. Utilizing immunoblotting to quantify synaptic density and synaptic proteins in neurological disease gives reproducible and specific results (Masliah et al., 1991). Acurate quantifications for neuroligin-1, neuroligin-2 and β-neurexin were performedby using internal standard higher and lower than the unknown protein concentration in each gel in this chapter.

3.3 Materials and Methods

3.3.1 Tissue collection

All brain tissues were obtained from the Queensland Brain Bank, which is located at the School of Chemistry and Molecular Bioscience at The University of Queensland. It is a part of the Australian Brain Bank Network, and offers services for Australian and international clinicians and researchers to study neurological diseases. Autopsies for this study were obtained with informed written consent from the next of kin. Diagnosis of AD was validated by examination of the tissue by qualified neuropathologists (Halliday et al., 2002). Tissues were dissected from specific areas of AD and control brains and stored in 0.32 M sucrose at –80°C (Dodd et al., 1986).

3.3.2 Case selection and neuropathological severity score

Fifteen cases and 15 controls were selected with an average age of 77 years for the AD cases and 76 years for the controls (Table 3.1). The average post mortem delay for the AD cases was approximately 27 hours while for the controls it was 25 hours. Tissue from three different areas — hippocampus (Hipp), occipital cortex (OC) and inferior temporal cortex (ITC) — was obtained from each brain.

These cases were all collected between 1993 and 2003. During this time, Alzheimer's disease was classified using the CERAD neuropathologic assessment based on Mirra et al. (1993). The Braak & Braak system was not used by the neuropathologists who did the Brain Bank examinations during that time. The CERAD assessment is a combination of 1. A gross examination to determine if cerebrovascular disease was present. 2. Semi-quantitative analysis of the degree of cortical atrophy and ventricle enlargement. 3. Visual examination of the hippocampus and entorhinal cortex for

atrophy. 4. Examination of the pallor of the substantia nigra and locus ceruleus. 5. Examination of the blood vessels for atherosclerosis or obstruction, ischemic events or other anomalies. 6. Semi-quantitative assessment of the presence and number of neocortical senile plaques (silver-positive neurites). 7. Evaluation of the substantia nigra for Lewy bodies, neuronal loss, gliosis and NFTs to rule out Parkinson's disease. 8. Evaluation of clinical presence of dementia. The combination of these assessments result in a level of certainty of the diagnosis of AD: Definite (A), Probable (B), Possible (C). To determine the Braak & Braak level of these cases we used The National Institute for Aging and Ronald and Nancy Reagan Institute of the Alzheimer's Association (NIA-Reagan Institute) combined criteria, which suggests that the two effectively correlate to one another in broad categories. Since further examination of these pathological samples is not possible due to the time that has elapsed since their collection, the exact Braak & Braak staging level cannot be determined. However, each area of each brain was given a neuropathological severity score from 0 to 3 according to the abundance of AD hallmarks NFT and Aβ, and the extent of neuronal loss (Tannenberg et al., 2006; Table 3.2). This allowed us to rate disease severity in each of three areas from each case, effectively tripling the number of samples available for determining the influence of pathology on expression, and also eliminating the averaging of pathology across tissue regions that is inherent in the Braak staging approach (Tannenberg et al., 2006; Table 3.2). Pathological score is a composite of three measures; in occipital cortex, Aβ plaques are generally quite common, whereas neither tangles nor cell loss usually occur in this area except at very late disease stages. The pH of samples was not measured as it has no effect on the protein quality. Trabzuni et al. (2011) found that pH has no great effect on RNA or protein levels, and so is not a factor. That study assessed the influence of post-mortem delay and tissue pH as predictors of gene expression measured on 1266 Affymetrix Exon Arrays. The study found that post-mortem delay and brain pH had negligible effects on array performance.

Table 3.1. Details of AD cases and controls.

Subject#	**Age, y**	**PMD(h)**	**Gender**	***APOE***
AD1	65	34.83	M	ε3,ε4
AD2	82	54.92	M	ε3,ε4
AD3	72	25.00	M	ε3,ε3
AD4	79	26.33	M	ε4,ε4
AD5	92	48.00	F	ε3,ε3
AD6	61	12.00	F	ε3,ε3
AD7	84	18.42	M	ε3,ε4
AD8	70	16.00	F	ε3,ε4
AD9	87	35.50	F	ε3,ε3
AD10	81	1.67	F	ε3,ε3
AD11	82	41.25	F	ε3,ε4
AD12	75	4.00	M	ε4,ε4
AD13	73	48.00	M	ε4,ε4
AD14	82	15.38	F	ε3,ε3
AD15	66	18.83	M	ε3,ε4
Average	77 ± 8.4	26.7 ± 15.9	8M, 7F	
NC1	78	4.00	F	ε3,ε4
NC2	87	21.50	F	ε2,ε3
NC3	57	9.75	F	ε3,ε3
NC4	82	46.83	M	ε3,ε3
NC5	85	24.50	M	ε2,ε3
NC6	81	21.43	F	ε3,ε3
NC7	74	85.25	M	ε3,ε3
NC8	68	43.67	F	ε3,ε4
NC9	72	15.42	F	ε3,ε3
NC10	74	24.00	F	ε3,ε3
NC11	71	7.75	F	ε3,ε4
NC12	78	16.25	M	ε3,ε3
NC13	68	28.17	M	ε2,ε2
NC14	84	16.53	M	ε3,ε4
NC15	76	24.00	F	ε3,ε3
Average	76 ± 7.6	25.9 ± 11.3	6M, 9F	

AD, Alzheimer’s disease case; NC, normal control; M, male; F, female

Each area of each brain was given a neuropathological severity score from 0 to 3 according to the abundance of AD hallmarks NFT and Aβ, and the extent of neuronal loss (Tannenberg et al., 2006; Table 3.2).

Table 3.2. Neuropathological score

Subject#	**Hipp**	**ITC**	**Occ**
AD1	3	3	1
AD2	3	3	1
AD3	2	2	1
AD4	3	3	1
AD5	3	3	1
AD6	3	3	2
AD7	3	3	3
AD8	2	3	2
AD9	2	2	1
AD10	1	2	1
AD11	3	3	3
AD12	3	3	1
AD13	1	3	3
AD14	2	1	1
AD15	3	3	1
NC1	0	0	0
NC2	1	0	0
NC3	0	0	0
NC4	0	0	0
NC5	0	0	0
NC6	0	0	0
NC7	0	0	0
NC8	0	0	0
NC9	1	0	0
NC10	0	0	0
NC11	0	0	0
NC12	0	0	0
NC13	0	0	0
NC14	0	1	0
NC15	0	0	0

3.3.3 Membrane preparations

Tissues were homogenized in 10× (w/v) of 0.32 M sucrose at 4°C, and centrifuged for 10 min at 500 × *g* in a Beckman JA20 at 4°C. The supernatant of the homogenate was centrifuged again for about 20 min at 12 000 × *g* at 4°C. The final pellet was resuspended in 10 ml of 50 mM Tris-HCL, pH 7.4. Total protein concentrations were estimated by the Lowry et al. (1951) method. Samples were frozen at –80°C for long-term storage.

3.3.4 Quantification of neuroligin-1, neuroligin-2 and β-neurexin-1 proteins

Different amounts of neuroligin-1, neuroligin-2 and β-neurexin-1 recombinant protein ranging from 10 ng to 100 ng were mixed with each of the membrane protein samples (~30 µg). Only one replicate was performed for each sample due to tissue limitations for some of the cases used in the current study. All samples were diluted 2:3 with SDS buffer (1.7% SDS, 5% glycerol, 1.55% DTT, 58 mM Tris-HCl, pH 6.8, with 0.002% bromophenol blue). The samples were heated for 5 min to 95°C, loaded onto 8% SDS-PAGE, and run for 35 min at 200V in running buffer (150 mM glycine, 20 mM Tris, 0.1% SDS). Recombinant β-neurexin-1 protein was purchased from Abnova (Walnut, CA, U.S.A). The truncated proteins neuroligin-1 (38kDa), neuroligin-2 (40Kda) and β-neurexin-1 (36kDa) separated clearly from the target protein (110 kDa, 95 KDa and 46 kDa, respectively) as sharp bands. A standard curve was created by plotting the intensity of the truncated band against its concentration using Odyssey software.

Proteins were then transferred from the gel to the PVDF membrane (Immobilon®-FL, Millipore, Billerica, MA, USA) in transfer buffer (10 mM $NaHCO_3$, 3 mM Na_2CO_3, pH 9.9, with 20% methanol). After transfer, the membrane was blocked in 1% skim milk in phosphate-buffered saline (PBST; 137 mM NaCl, 2.7 mM KCl, 10 mM Na_2HPO_4, 2 mM KH_2PO_4, 0.1% Tween-20, pH 7.4) with agitation for 1h at room temperature. A 1:10,000 dilution (2 µl/20,000 µl of blocking solution) of neuroligin-1, neuroligin-2 and β-neurexin-1 primary antibodies was added to the corresponding membrane and all membranes were incubated overnight at 4°C with agitation. The membranes were washed with PBST three times for 10 min each. A 1:2, 0000 dilution of secondary

antibody (Alexa Fluor 680, goat anti-mouse IgG, Molecular Probes, Invitrogen) in 1% skim milk/PBST was added to neuroligin-1 membrane. A 1:2, 0000 dilution of secondary antibody (Alexa Fluor 680 of rabbit anti-goat IgG, Molecular Probes, Invitrogen) in 1% skim milk/PBST was added to both neuroligin-2 and β-neurexin-1. All membranes were agitated for 1h at room temperature in the dark. Membranes were then washed with PBST three times for 10 min each followed by phosphate-buffered saline (PBS) twice for 10 min each. The intensities of the recombinant and target proteins bands were assessed using the LI-COR Odyssey scanner at 700 nm.

3.3.5 Data analysis

The intensities of the unknown bands fell within the intensity values of the lowest and highest concentrations of the recombinant proteins standards. Normal probability plots of each set of protein concentrations indicated that the data distribution was positively skewed. Box-Cox transformations performed with the Statistica software package (Tulsa, OK, USA) stabilized the variances and gave linear normal probability plots. Multiple comparisons were evaluated by ANOVA with appropriate post-hoc tests. Differences were considered statistically significant at $P < 0.05$. Mean and S.E.M. values were converted back to the original scale of measurement for presentation in text and figures.

3.4 Results

To quantify neuroligin-1, neuroligin-2 and β-neurexin-1 in autopsy tissues, the immunodetection protocol with recombinant truncated neuroligin-1, neuroligin-2 and β-neurexin-1 proteins as standards was optimized as outlined in Chapter 2. This minimized error from gel to gel variations and allowed precise quantification. Membrane preparations from all samples gave sharp bands with the anti-neuroligin-1 antibody at ~110 kDa, anti-neuroligin-2 antibody at 95 kDa and anti-β-neurexin-1 antibody at 46 kDa (Figs 3.1, 3.2 and 3.3). The molecular masses of the bands were confirmed by measuring their migrations against those of the markers. Normal probability plots of the levels of each protein in each brain areas indicated that the data distributions were positively skewed (Fig. 3.4). Box-Cox transformations stabilized the variances and gave linear normal probability plots for neuroligin-1 (Fig. 3.5A), neuroligin-2 (Fig. 3.5B) and β-neurexin-1 (Fig. 3.5C).

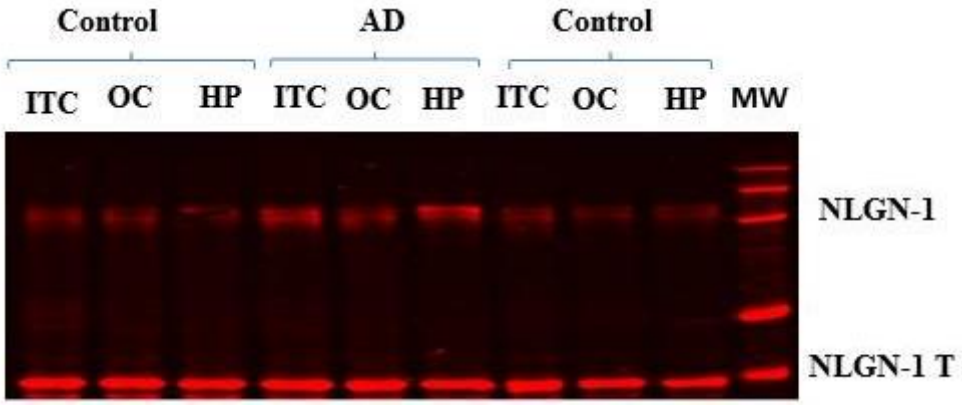

Fig. 3.1. Representative immunoblot of neuroligin-1 in hippocampus and inferior temporal and occipital cortices from two controls and one AD case selected at random. Neuroligin-1 recombinant truncated protein was detected at 38 kDa MW. Endogenous neuroligin-1 ran at 110 kDa and was quantified as described in the text.

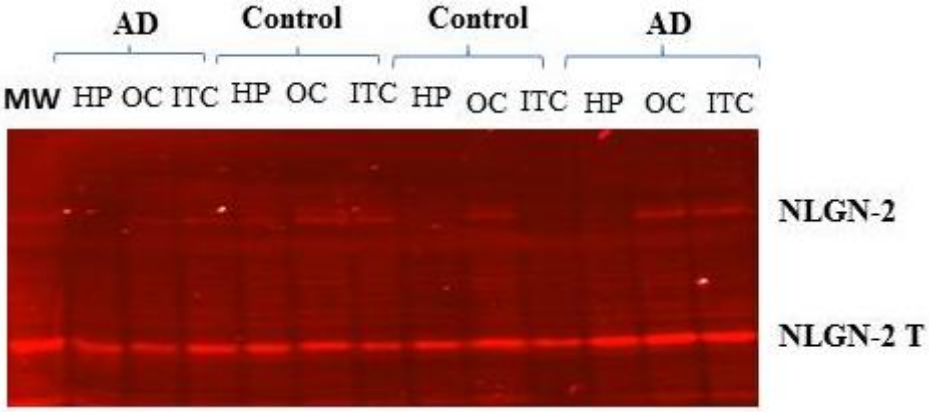

Fig. 3.2. Representative immunoblot of neuroligin-2 in the three brain areas from two controls and two AD cases selected at random. Neuroligin-2 recombinant truncated protein was detected at 40 kDa MW. Endogenous neuroligin-2 protein ran at 95 kDa and was quantified as described in the text.

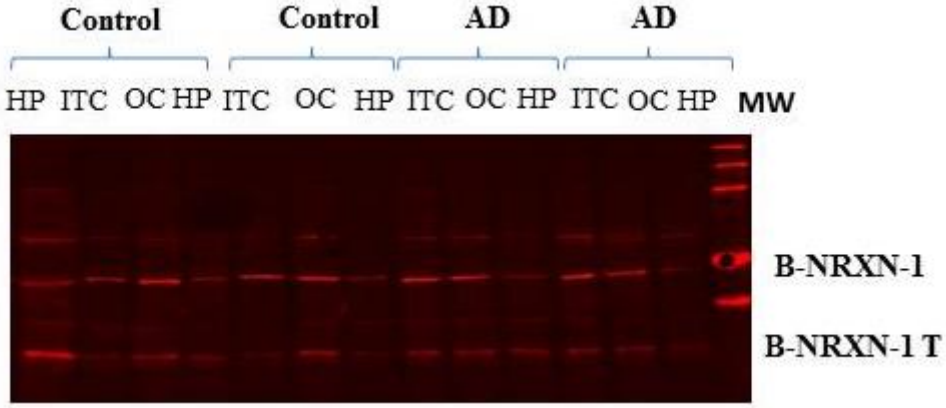

Fig. 3.3. Representative immunoblots of β-neurexin-1 in the three brain areas from

two controls and two AD cases selected at random. β-Neurexin-1 recombinant truncated protein was detected at 36 kDa MW. Endogenous β-neurexin-1 protein was detected at 46 kDa and was quantified as described in the text.

(A) Neuroligin-1

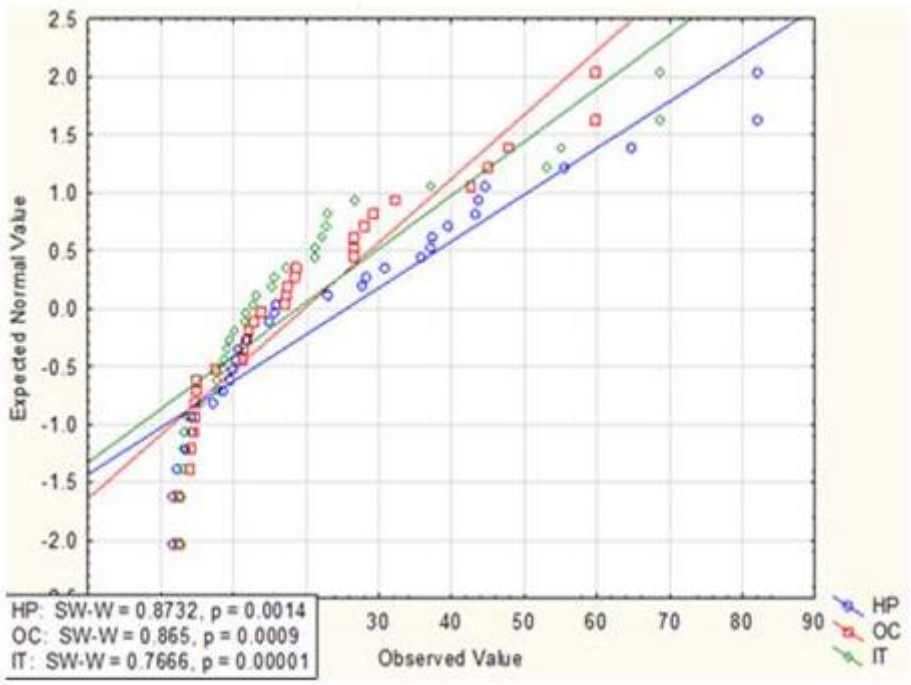

(B) Neuroligin-2

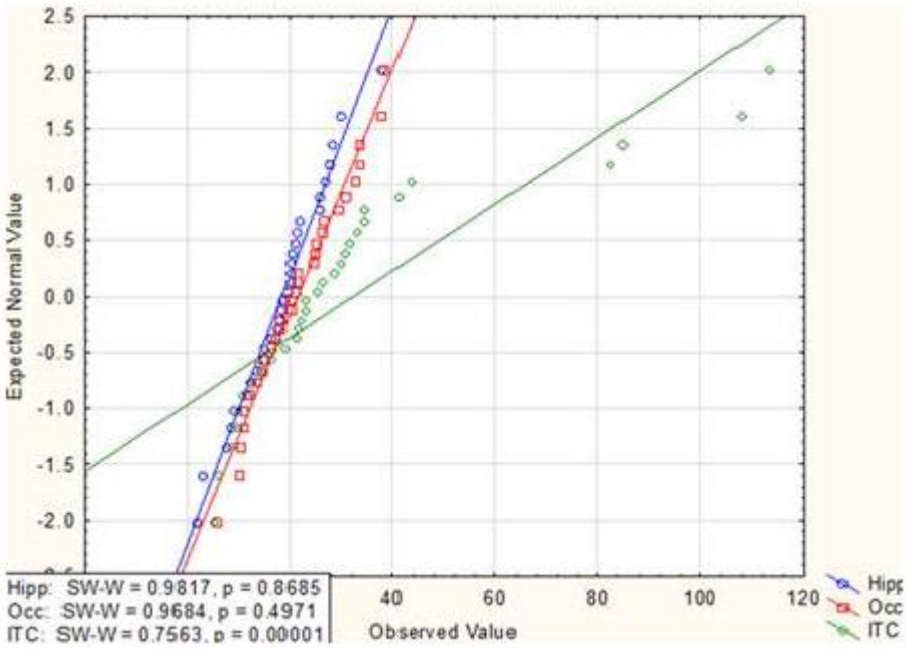

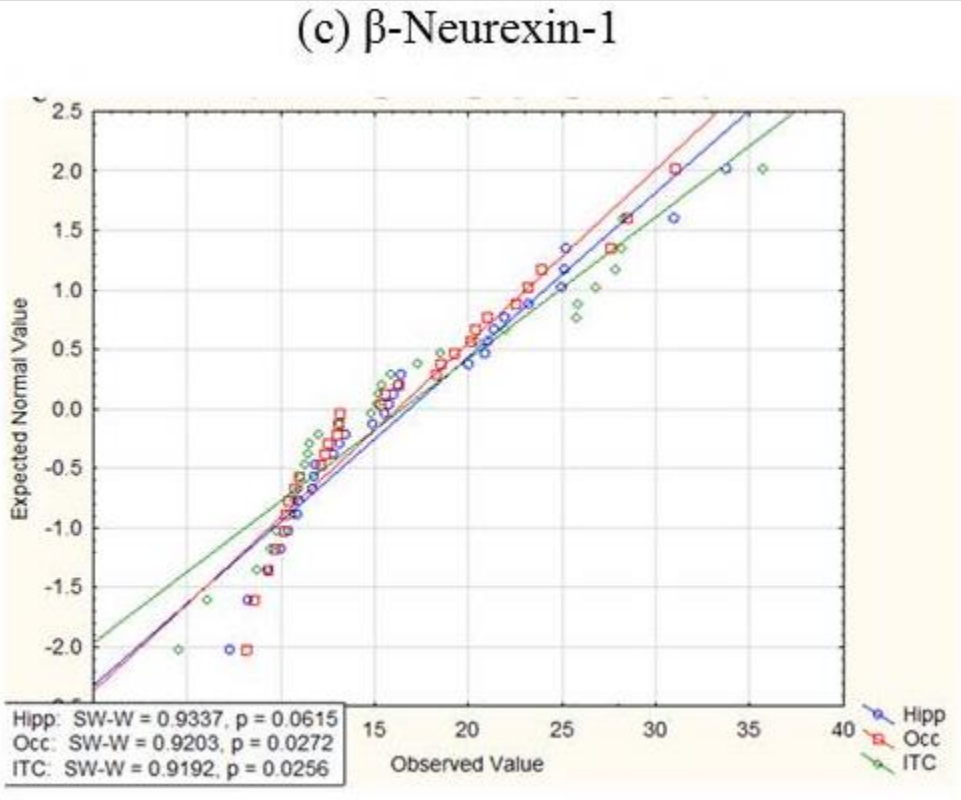

Fig. 3.4. Normal probability plots for **A,** neuroligin-1, **B,** neuroligin-2 and **C,** β-neurexin-1 concentrations in unadjusted values. Shapiro-Wilks testing showed that most untransformed data distributions deviated significantly ($P < 0.01$) from normal as shown in the in-graph boxes.

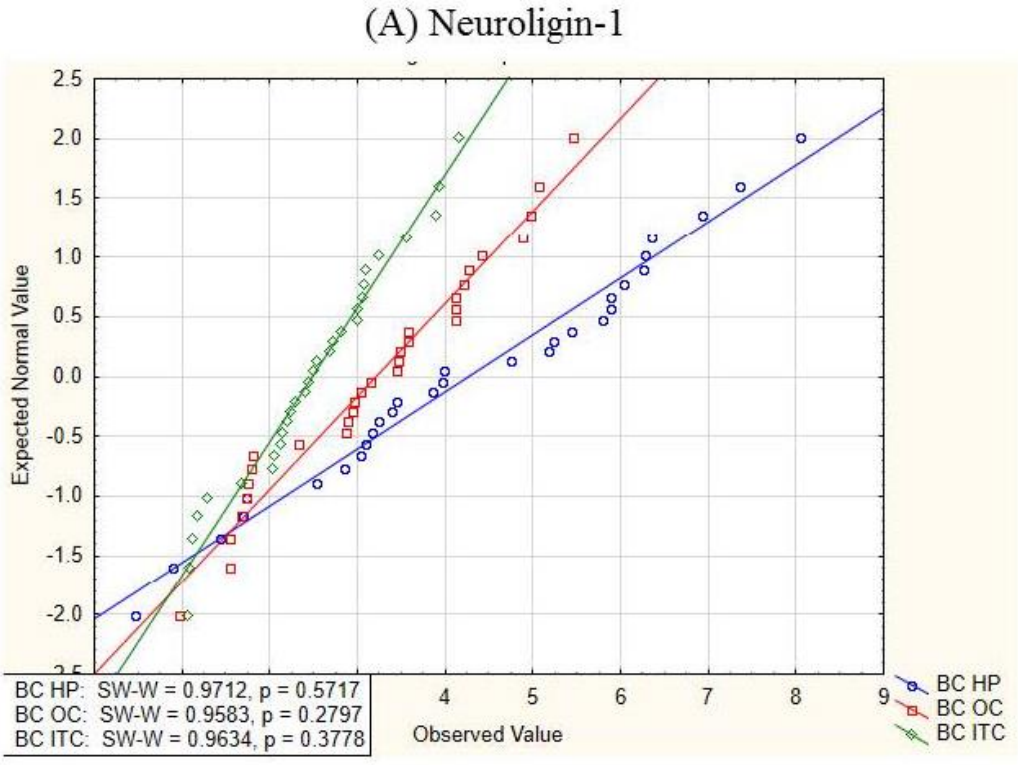

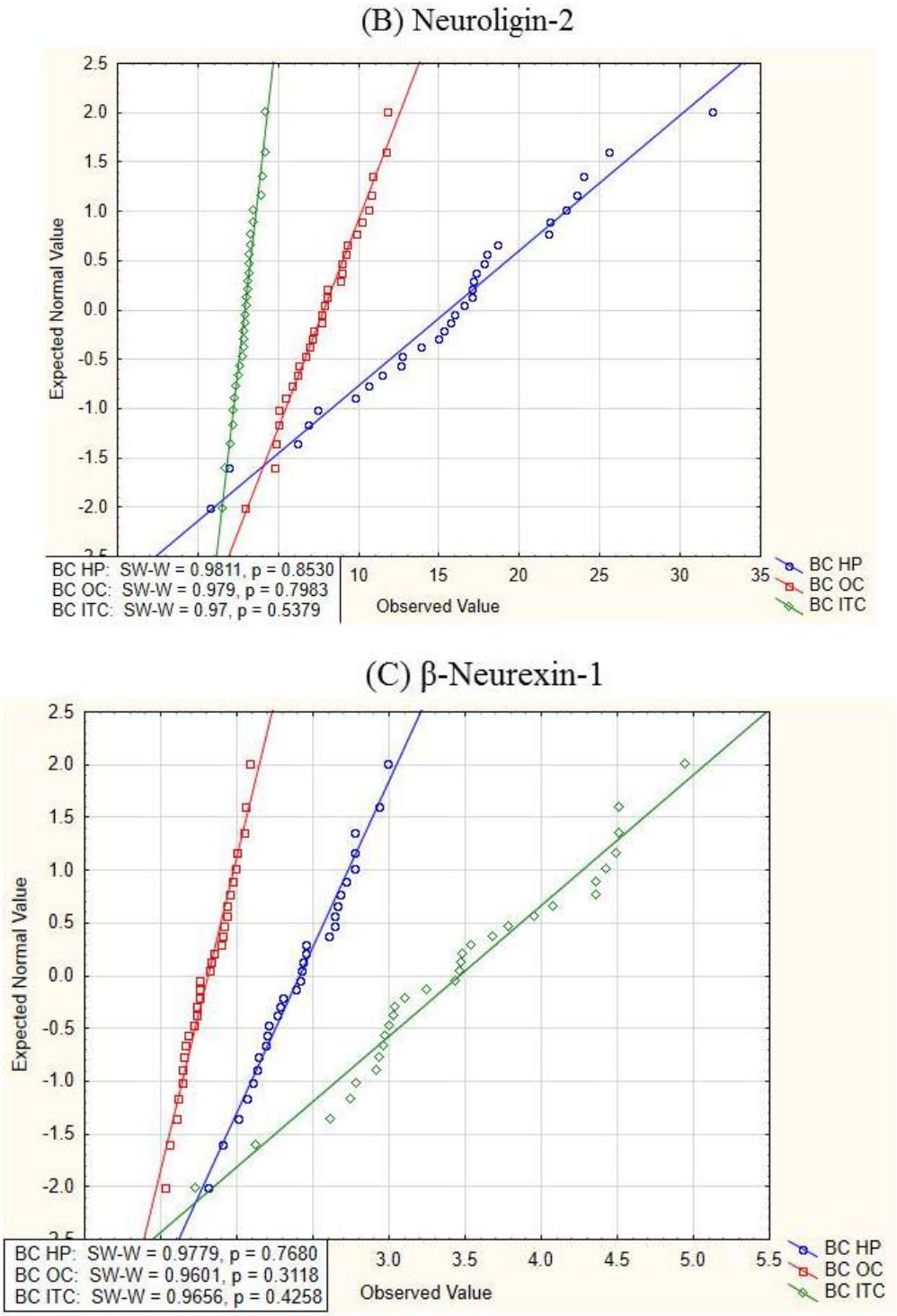

Fig. 3.5. Normal probability plots for Box Cox transformations of **A**, neuroligin-1, **B**, neuroligin-2 and **C**, β-neurexin-1 concentrations. Shapiro-Wilks testing showed the transformed data distributions did not deviate significantly ($P > 0.25$) from normal as shown in the in-graph boxes.

3.4.1 Post-mortem delay and age at death

In order to obtain accurate results in the current study, post-mortem delay (PMD) and age at death were matched as closely as possible between the two groups. Some neurochemical research has shown that the quality of some proteins is not affected by PMD, while others have found that PMD and age can impact protein degradation. Furthermore, the levels of some proteins vary with age due to processes such as neuronal homeostasis, protein regulatory mechanisms, degradation pathways and increased oxidative stress. In the current study, regression analyses were performed to assess the effect of PMD and age on the expression of the three proteins; these were non-significant. To ensure there were no subtle influences of these potential confounds, a series analyses of covariance on neuroligin-1 and neuroligin-2 proteins showed there was no significant effect of either factor, alone or in combination, on expression values in combined subjects and areas, and that ANCOVA did not significantly reduce error variances. There was no significant effect of PMD or age on neuroligin-1 concentration ($F_{1,88}$ = 0.356, P = 0.85 and $F_{1,88}$ =1.457, P = 0.23; Figs 3.6A and 3.6B), nor was there a significant effect of either PMD or age on neuroligin-2 concentration ($F_{1,88}$ = 0.651, P = 0.42 and $F_{1,88}$ =1.036, P = 0.31 respectively; Figs 3.6C and 3.6D). This allowed the expression values to be assessed by analyses of variance without further normalization. For β-neurexin-1, significant associations were observed between protein expression and both age and PMD ($F_{1,88}$ =13.619, P < 0.001 and $F_{1,88}$ = 5.480, P = 0.021 respectively; Figs 3.6E and 3.6F). To maintain consistency with the analyses of the other two proteins, and because AD cases and controls were reasonably well matched, ANOVA was also used for statistical testing of β-neurexin-1, but this issue needs to be revisited with a larger data set.

3.4.2 Neuroligin-1 expression by case-group

ANOVA showed that the overall neuroligin-1 protein concentration was significantly higher in AD cases than in controls ($F_{1,26}$ = 4.646, P = 0.041; Fig. 3.7). Expression differed significantly according to brain region ($F_{2,52}$ = 14.100, P < 0.001; Fig. 3.8), being highest in hippocampus and lowest in inferior temporal cortex across all subjects, and each area differing significantly from both others (P < 0.05 in all instances, Newman-Keuls).

A

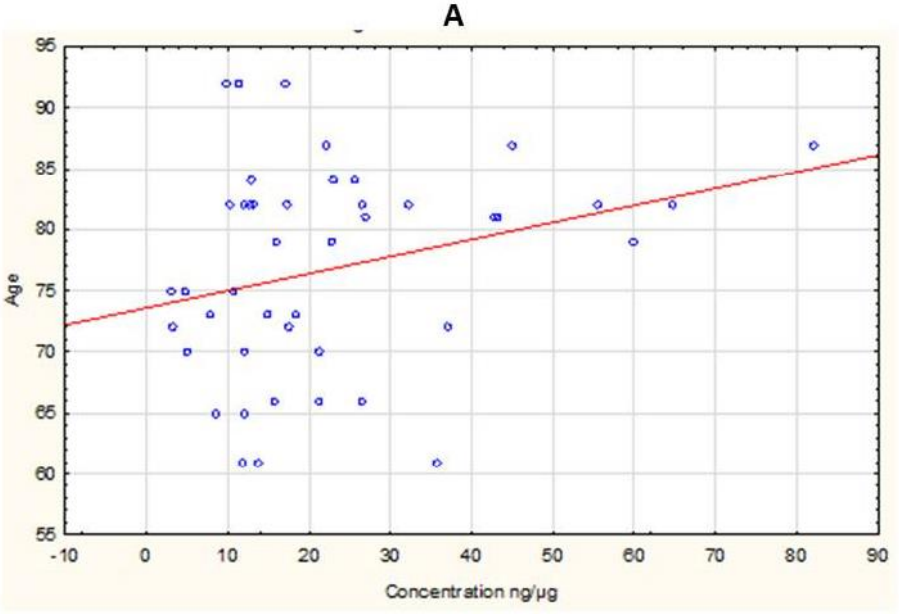
Age
Concentration ng/µg
95
90
85
80
75
70
65
60
55
-10
0
10
20
30
40
50
60
70
80
90

B

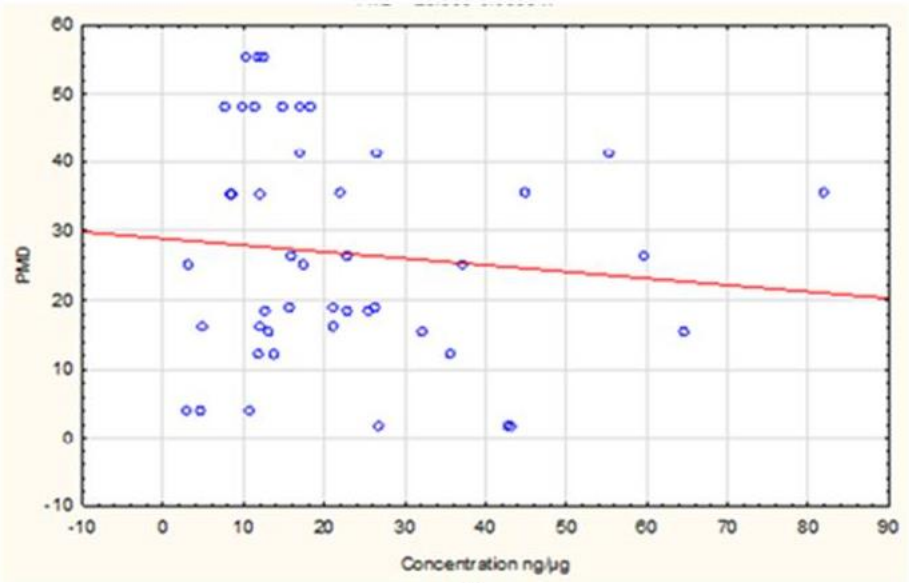
PMD
Concentration ng/µg
60
50
40
30
20
10
0
-10
-10
0
10
20
30
40
50
60
70
80
90

C

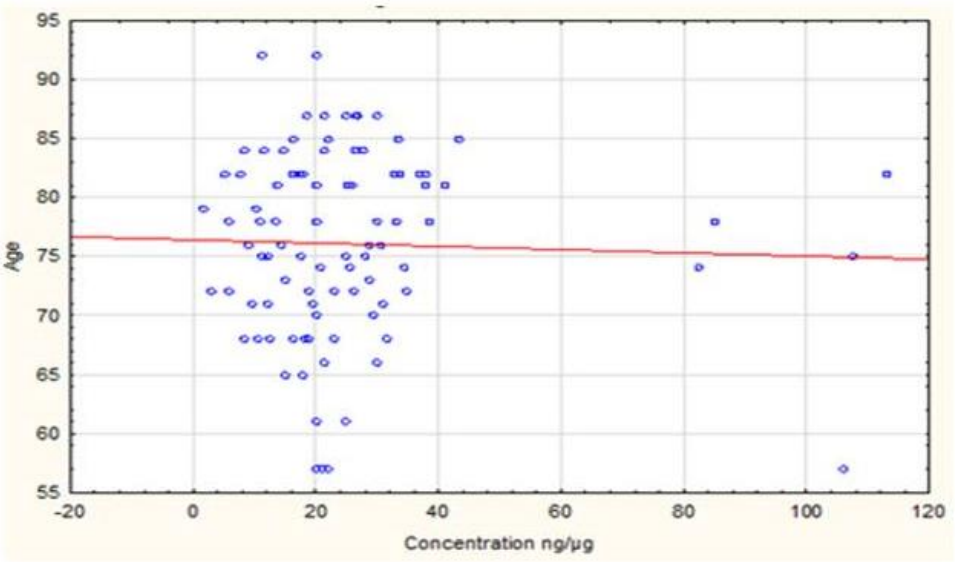
Age
Concentration ng/µg
95
90
85
80
75
70
65
60
55
-20
0
20
40
60
80
100
120

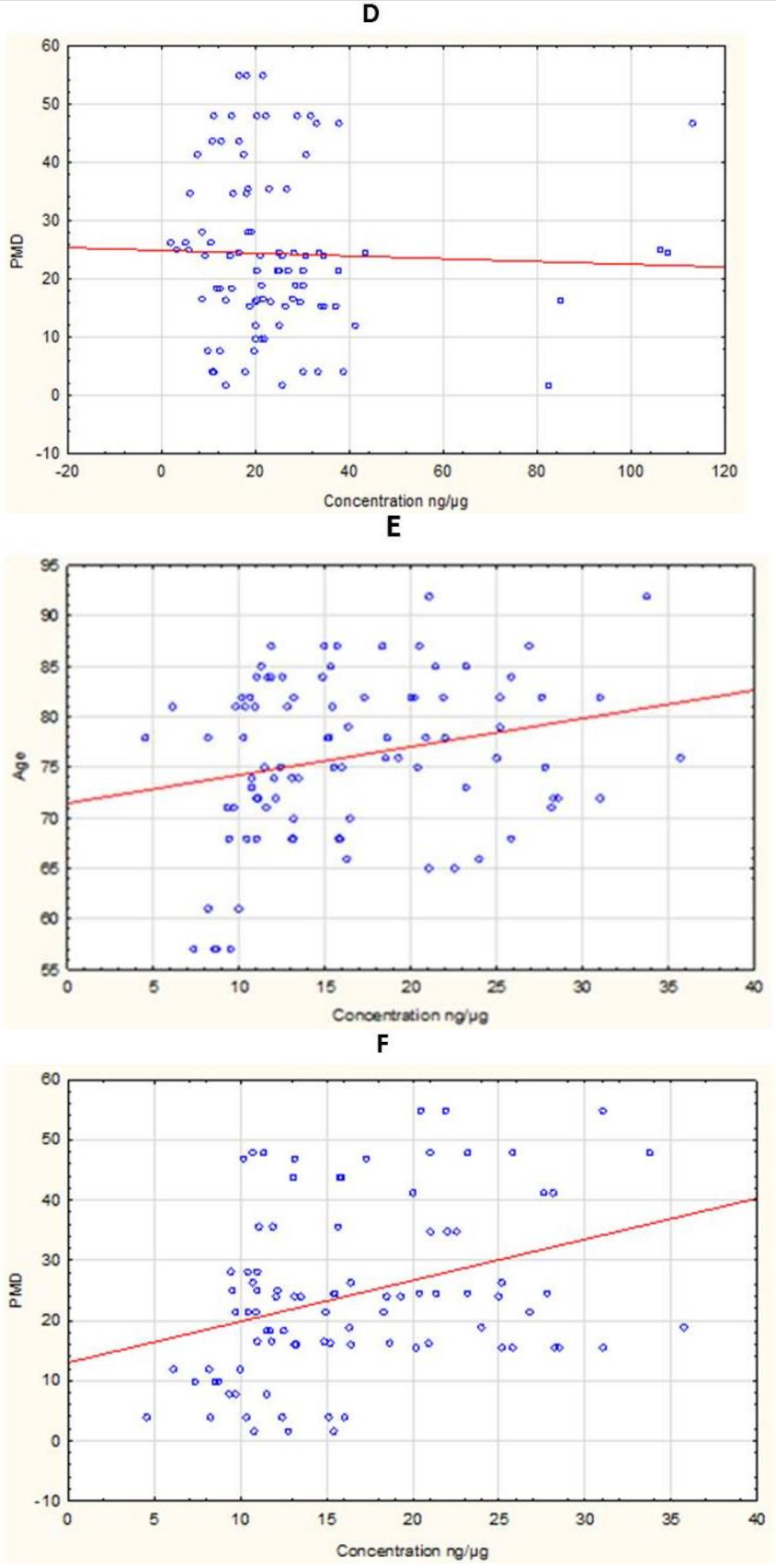

Fig. 3.6. Regression analyses of protein concentrations against age and PMD. **A**, neuroligin-1 expression on age and **B**, PMD; **C**, neuroligin-2 expression on age and **D**, PMD; **E**, β-neurexin-1 expression on age and **F**, PMD.

Although the Group × Area interaction was not significant, *post-hoc* testing showed that expression in AD hippocampus was significantly higher than in both AD occipital cortex ($P = 0.027$) and AD inferior temporal cortex ($P < 0.001$), and also higher than in normal control hippocampus ($P = 0.021$; Fig. 3.8). *Post-hoc* analysis showed that the neuroligin-1 level was significantly higher in AD cases than in controls in both hippocampus ($P = 0.036$) and occipital cortex ($P = 0.04$). Values in inferior temporal cortex did not differ significantly (P = 0.09, Fig. 3.8).

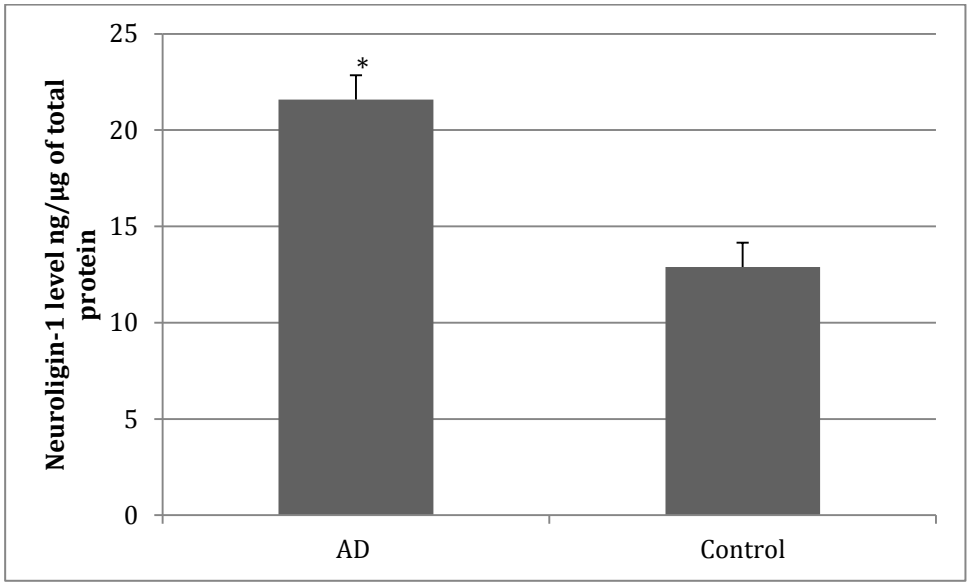

Fig. 3.7. Overall neuroligin-1 expression by case-group. Protein levels were averaged across the three areas studied (hippocampus, inferior temporal cortex and occipital cortex) in each group; *, significantly higher than in controls (n = 15, both groups). Error bars represent S.E.M.

3.4.3 Neuroligin-1 level by gender

No significant differences were observed in males between AD cases and controls. The level of neuroligin-1 in AD females was higher than in control females, but this was not statistically significant (Fig. 3.9). Regionally, *post-hoc* testing showed that the level of neuroligin-1 in the hippocampus was significantly higher in AD females than in AD males and significantly higher in AD females than in control females. There were no gender differences in either the occipital cortex or the inferior temporal cortex between cases and controls (Fig. 3.10).

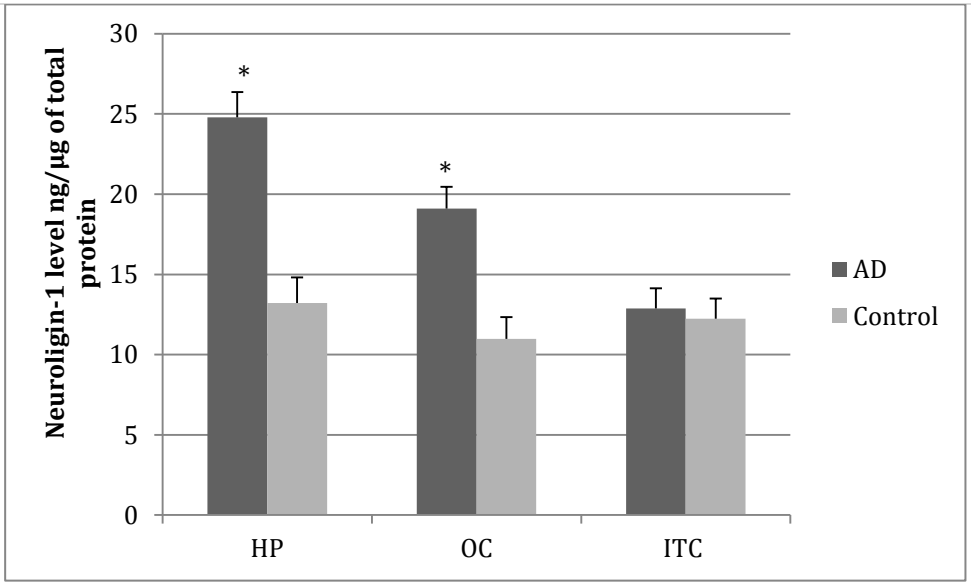

Fig. 3.8. Neuroligin-1 protein by case-group and area. HP, hippocampus; OC, occipital cortex; ITC, inferior temporal cortex; *, significantly different from the level in the corresponding control sample, $P < 0.05$ by *post-hoc* Newman-Keuls test.

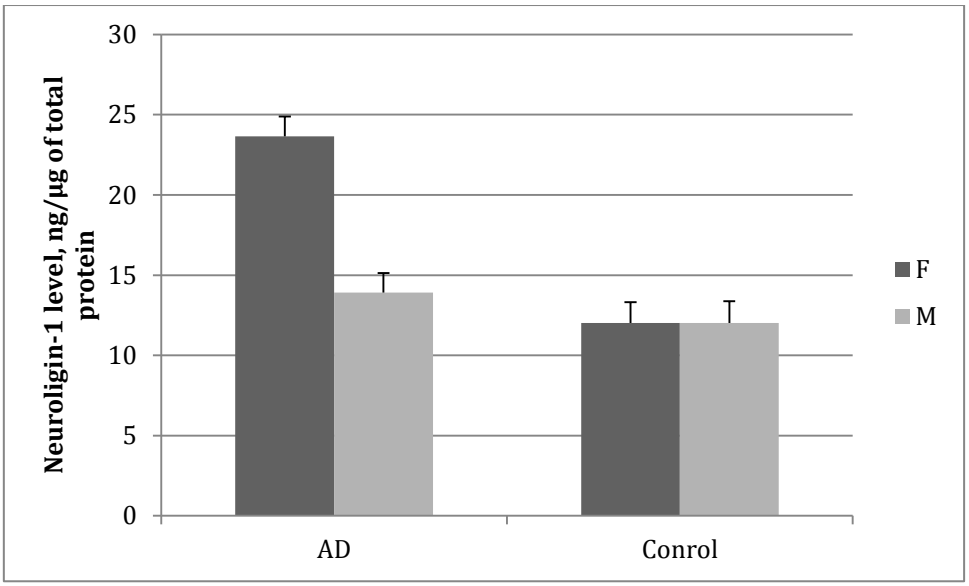

Fig. 3.9. Overall neuroligin-1 expression by gender. Neuroligin-1 protein concentrations were averaged across the three brain regions in AD cases and controls partitioned by gender.

3.4.4 Neuroligin-1 level and APOE genotype

The most common genotype among the population is *APOE* ε3; seven of the 15 normal controls in this study were ε3,ε3 homozygotes and all but two had at least one ε3 allele; the latter were ε2,ε4 and ε2,ε2, at no increased risk of AD. The AD cases included six ε3,ε3 homozygotes; six

had one ε3 allele, and non had an ε2 allele. About 50% of AD cases carry at least one copy of the risk-factor ε4 allele: this was true of 9/15 AD cases here, three of whom were ε4,ε4 homozygotes; four normal controls had one ε4 (three with one ε3) allele, none was an ε4,ε4 homozygote. The lowest frequency *APOE* allele is ε2, found in 2–8% of the population (Schellenberg, 1995). This allele was only found in normal controls here, two of whom were ε2,ε3, another ε2,ε2: all three of these subjects would have been at reduced risk of AD.

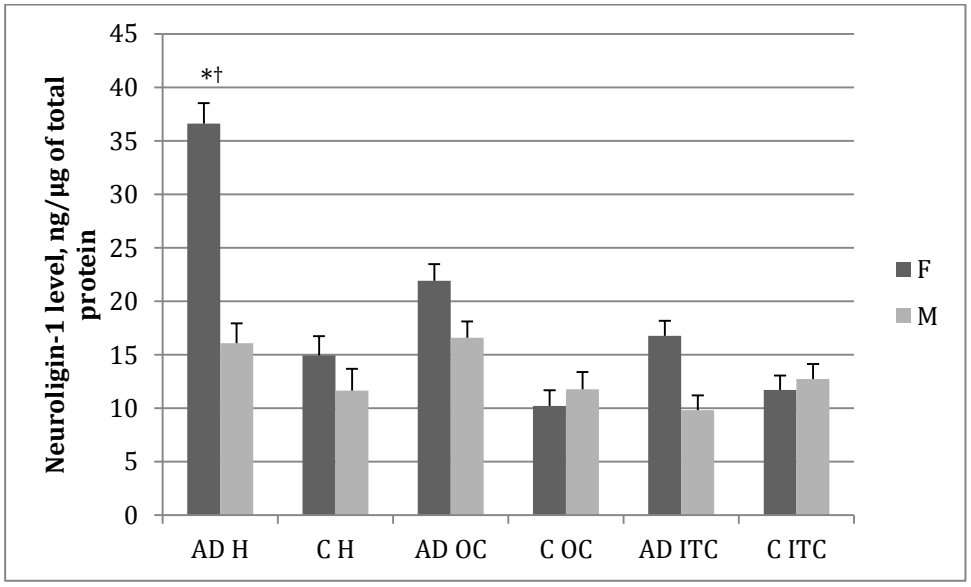

Fig. 3.10. Neuroligin-1 expression by group, gender, and and area. Details as Fig. 3.9; *, significantly higher than in female controls and †, significantly higher than in AD males, $P < 0.05$ by Newman-Keuls test.

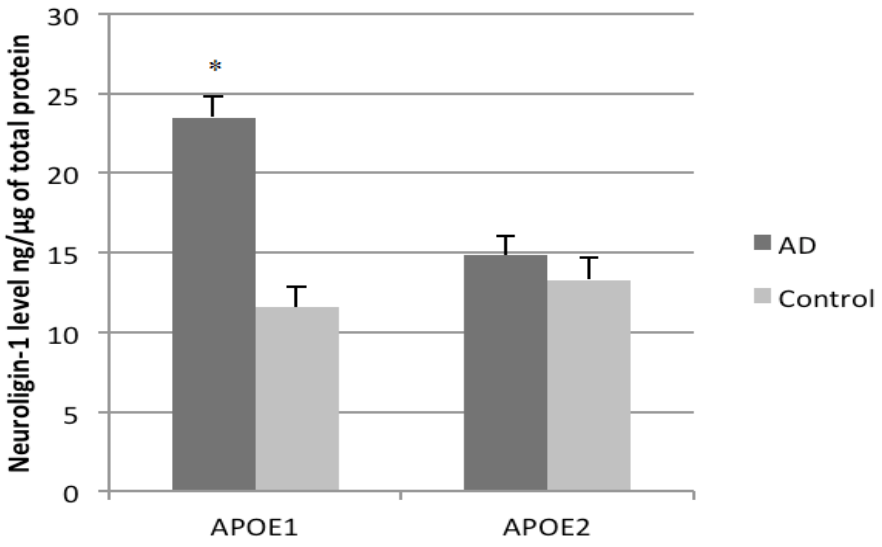

Fig. 3.11. *APOE* genotype and neuroligin-1expression in AD. AD cases were divided by whether they did (APOE2) or did not (APOE1) carry an *APOE* ε4 allele.

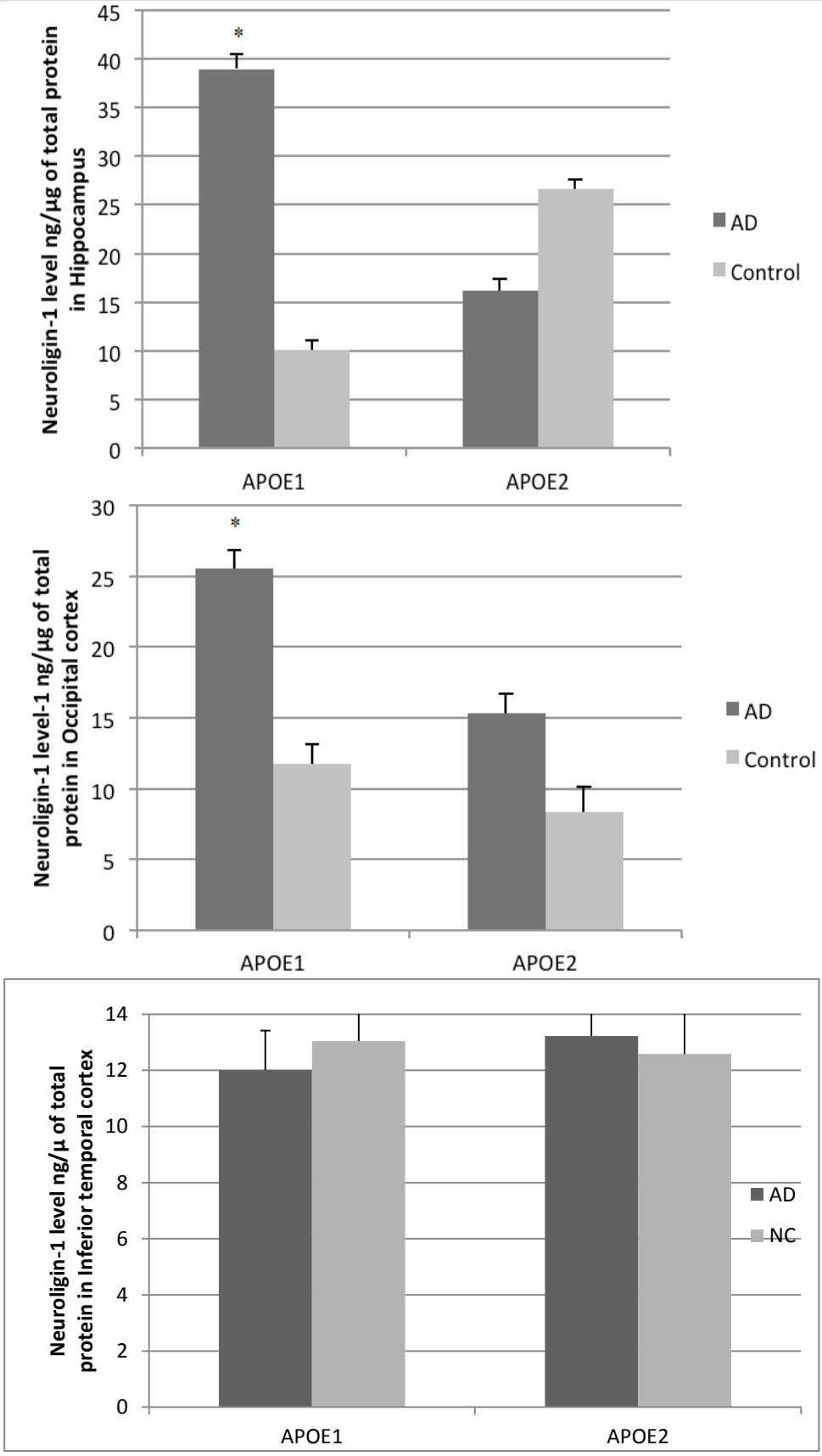

Fig. 3.12. Neuroligin-1 expression by *APOE* genotype, group, and area. Key as for Fig. 3.11; *, significantly different from matched controls, $P < 0.05$, Newman-Keuls.

As the full range of six *APOE* genotypes was not represented in both groups we classified the subjects according to the number of ε4 alleles they possessed to study genotype–phenotype interactions. Although the Group × Nº of ε4 alleles interaction was significant ($F_{1,25}$ = 5.608; P = 0.026), in essence because AD cases with no ε4 alleles differed from all other subjects ($P \leq 0.01$, Newman-Keuls), this result must be treated with caution because these few AD cases were confounded by gender: all were female (Fig. 3.11). Similarly, the Area × Group × Nº of ε4 alleles interaction was significant ($F_{2,52}$ = 3.281, P = 0.045), and a significantly higher neuroligin-1 level was found in AD cases with no ε4 than in comparable controls in both hippocampus and occipital cortex (Fig. 3.12), but again, these effects are not statistically reliable. No significant differences were found in neuroligin-1 level between cases and controls in inferior temporal cortex (Fig. 3.12).

3.4.5 Neuroligin-1 expression and severity of disease

The impact of the severity of the disease on neuroligin-1 protein was studied. Tissue samples were divided according to the extent of Aβ and *tau* deposition and the degree of neuronal loss, and given a score from 0 to 3 by an experienced neuropathologist blinded to diagnosis (Tannenberg et al., 2006). In the AD cases, no sample had a score of zero; and because almost all control tissue samples gave scores of zero it was not possible to make an across-group comparison: so the analysis was confined solely to samples from AD cases. A slightly higher level of neuroligin-1 was found at pathological score 2 in all three areas, but this was not significant. The concentration of neuroligin-1 was lower at pathological score 3 in all areas, but p*ost-hoc* testing showed no significant difference in neuroligin-1 level between tissue samples with differing pathological scores (Fig. 3.13). Regional expression did not vary significantly with pathological score ($F_{2,42}$ = 1.142, P = 0.33; Fig. 3.14).

3.4.6 Neuroligin-2 expression in AD cases and controls

Overall expression of neuroligin-2 protein was significantly lower in AD cases than in controls ($F_{1,28}$ = 4.690, P = 0.039; Fig. 3.15). Newman-Keuls *post-hoc* testing showed a significantly lower neuroligin-2 level in inferior temporal cortex in AD cases than in controls (P = 0.021). Levels in the other two areas were also lower in AD cases than in controls, but not statistically significant

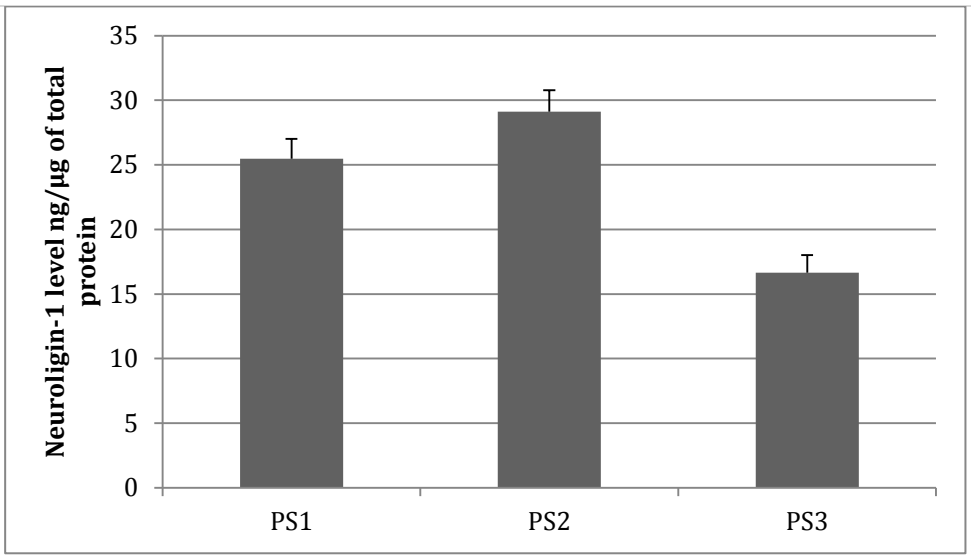

Fig. 3.13. Overall expression of neuroligin-1 and pathological severity. AD tissue samples undifferentiated by region were divided according to pathological severity (PS) score between 1 and 3. No difference was statistically significant.

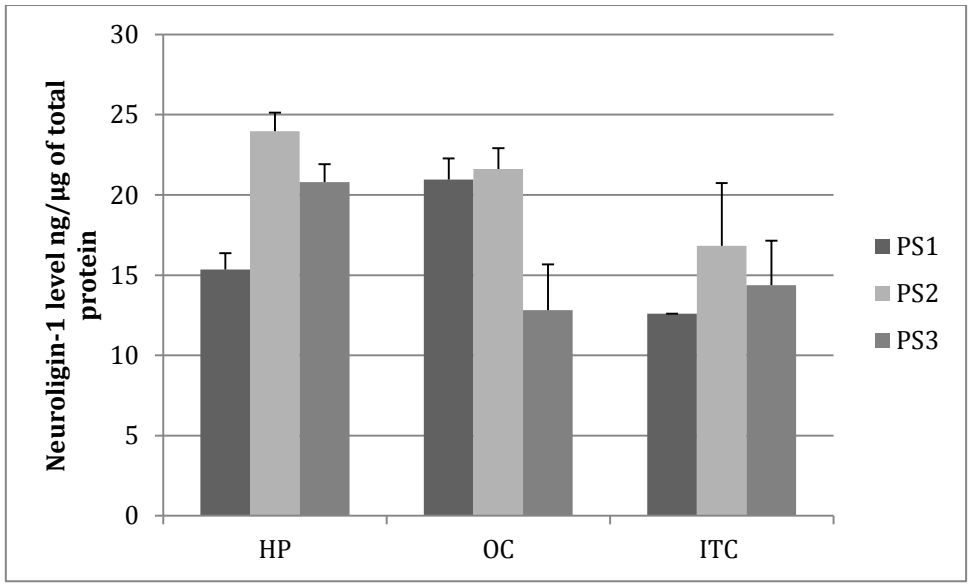

Fig. 3.14. Pathological severity and regional neuroligin-1 protein expression. There were no differences in expression with pathological severity in any area by Newman-Keuls *post-hoc* testing.

(Fig. 3.16). When AD cases and controls were combined, the inferior temporal cortex showed the highest expression level of neroligin-2 compared to the occipital cortex and the hippocampus (see Fig. 3.16; graph not explicitly shown).

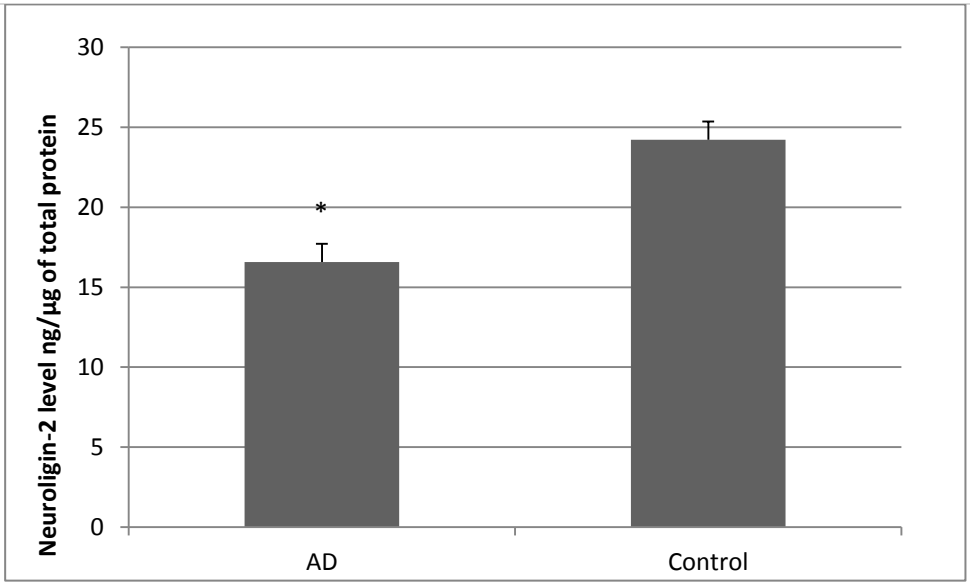

Fig. 3.15. Total neuroligin-2 protein concentrations averaged across the three areas studied; *, significantly lower than in controls, $P < 0.05$.

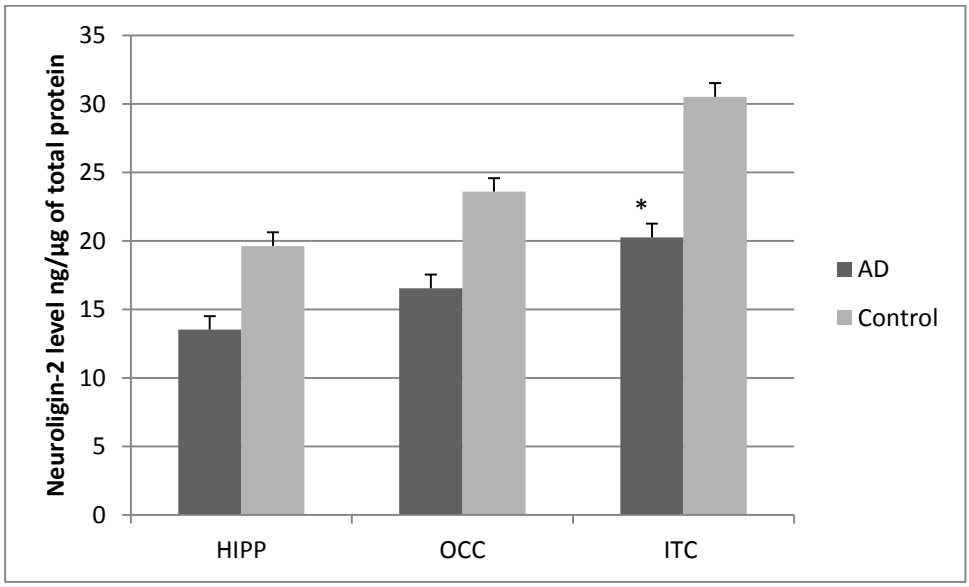

Fig. 3.16. Neuroligin-2 protein expression by area. Key as for Fig. 3.8; *, significantly lower than in the same area in controls, $P < 0.05$ by Newman-Keuls *post-hoc* test.

3.4.7 Neuroligin-2 level and gender

The influence of gender on neurolign-2 protein expression was significant by ANOVA ($F_{1,86} = 13.461$, $P < 0.001$; Fig. 3.17). No significant differences were found between AD cases and controls in hippocampus or occipital cortex in either sex. Neuroligin-2 protein level was lower in AD males than in control males in inferior temporal cortex, whereas the reverse was true for females in this area (Fig. 3.18).

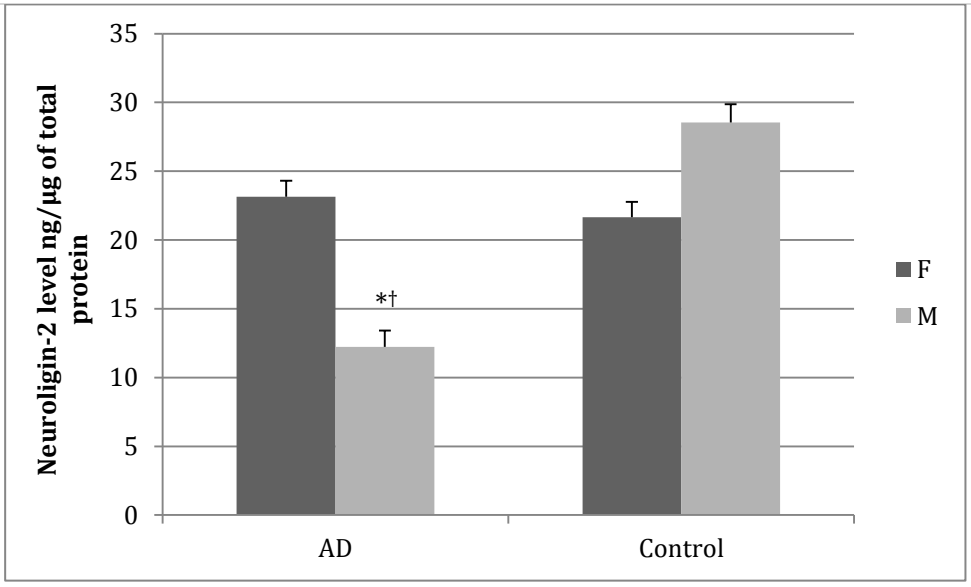

Fig. 3.17. Neuroligin-2 expression by case-group and gender. Neuroligin-2 concentrations were averaged across all areas studied in AD cases and controls. Newman-Keuls *post hoc* test showed that expression was significantly lower in male AD cases than in male controls (*; $P < 0.001$) or female AD cases (†; $P = 0.002$).

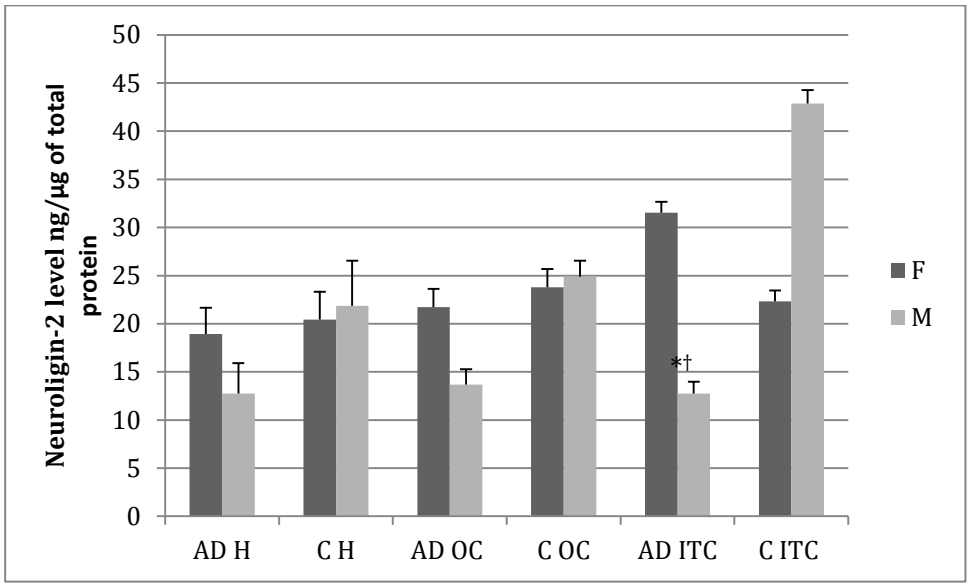

Fig. 3.18. Gender effects on neuroligin-2 protein expression. In inferior temporal cortex: *, significantly lower than in male controls; †, significantly lower than in AD females; both $P < 0.001$, Newman-Keuls *post-hoc* tests.

3.4.8 Neuroligin-2 level and APOE genotype

Neuroligin-2 protein expression was significantly lower in AD *APOE* ε4 carriers than in AD non-cariers ($F_{1,88}$ =10.574, $P = 0.002$; Fig. 3.19). The Group × APOE interaction was not significant

($F_{1,86}$ =0.212, P = 0.64; Fig. 3.20). Although the Group × Area × *APOE* interaction was not significant ($F_{2,52}$ =1.316, P = 0.27), some differences were detected by *post-hoc* testing (Fig. 3.21).

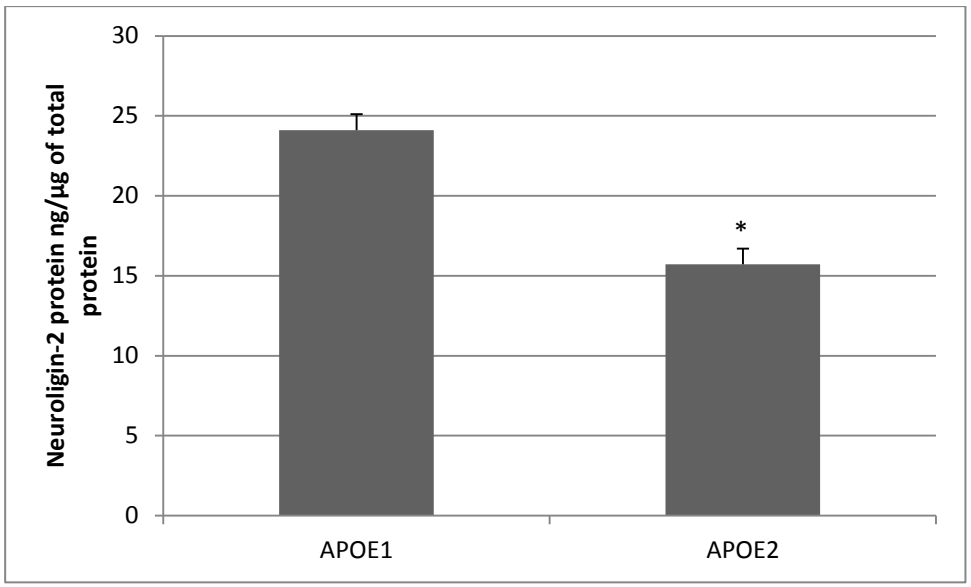

Fig. 3.19. Expression of neuroligin-2 by Nº of *APOE* ε4 alleles in AD cases. Key as for Fig. 3.10; *, significantly different from cases without at least one e4 allele, see text for details.

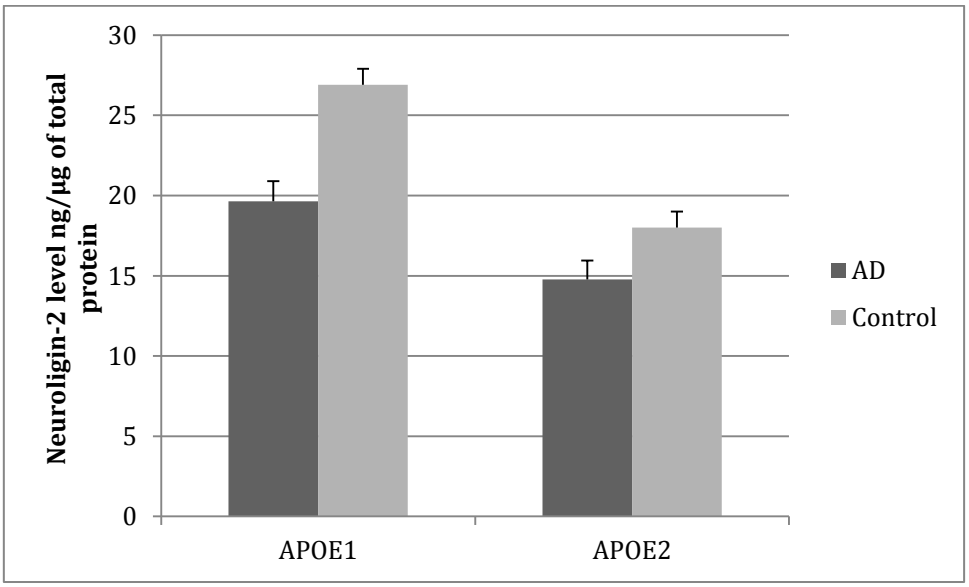

Fig. 3.20. *APOE* ε4 genotype, neuroligin-2 expression and group. Key as for Fig. 3.10. No comparison was significant by Newman-Keuls *post-hoc* test.

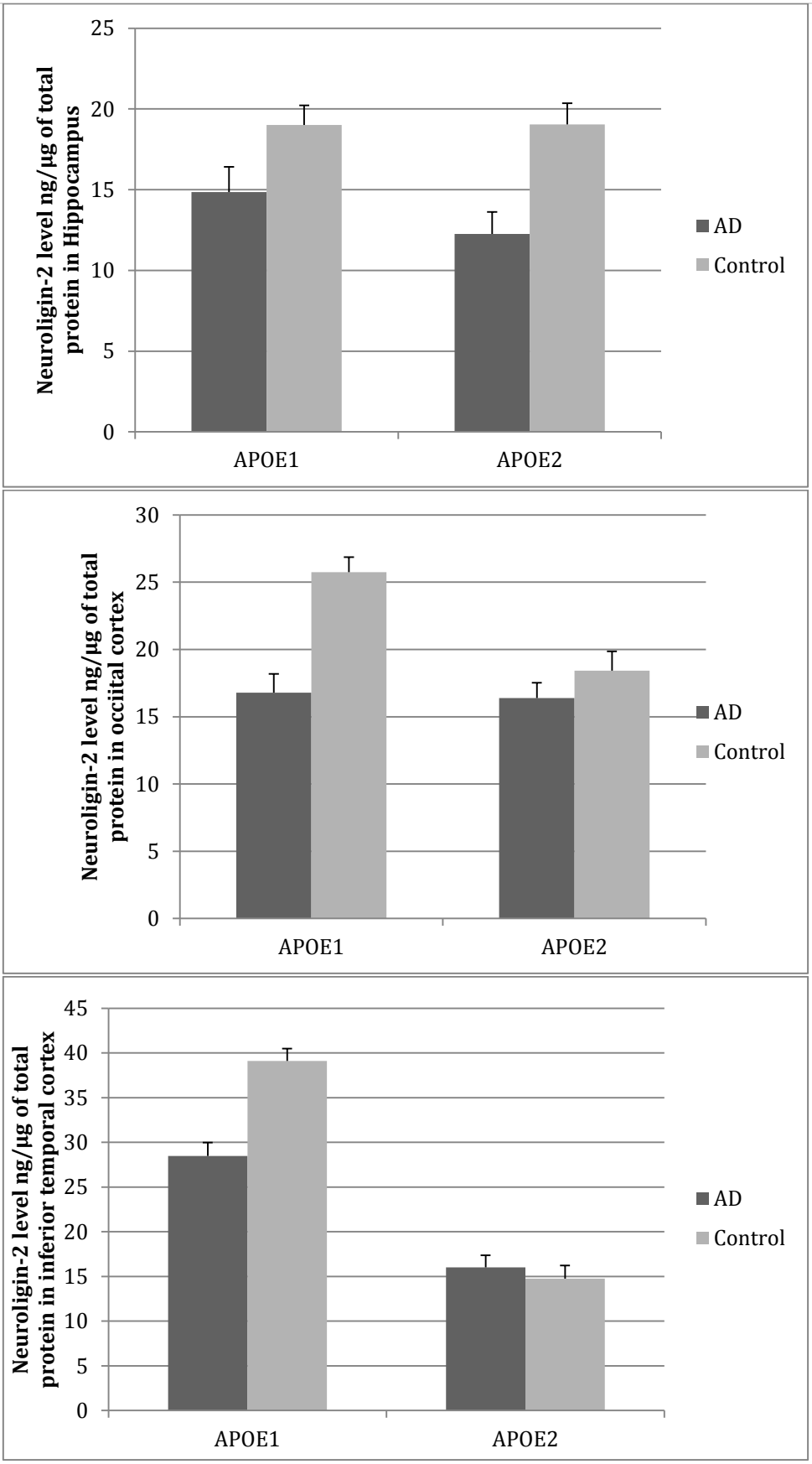

Fig. 3.21. Neuroligin-2 expression by group, *APOE*, and area. Key as for Fig. 3.10.

Newman-Keuls *post hoc* test showed significantly lower neuroligin-2 expression in

AD *APOE* ε4 carriers than in matched controls in hippocampus ($P = 0.046$). A trend was seen in AD *APOE* ε4 non-carriers *cf* controls in occipital cortex ($P = 0.071$).

3.4.9 Neuroligin-2 expression and severity of disease

Overall neuroligin-2 protein expression was highest at the moderate stage, and lowest at the severe stage, but not statistically significant ($F_{2,42} = 0.389$, $P = 0.68$; Fig.3.20); neither was the PS × Area interaction ($F_{4,36} = 0.696$, $P = 0.59$; Fig 3.21), although some *post-hoc* tests were.

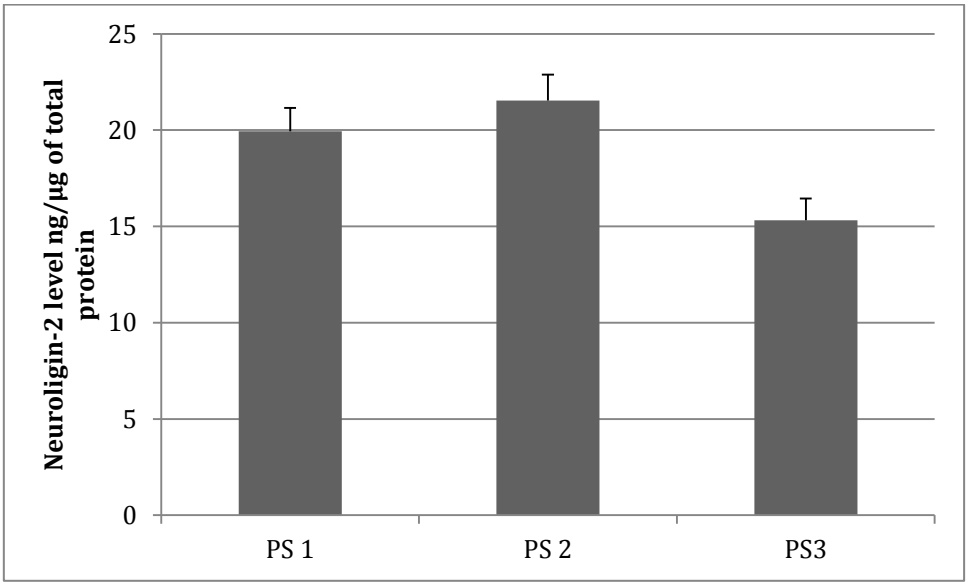

Fig. 3.22. Neuroligin-2 protein expression and disease severity. Key as for Fig. 3.12.

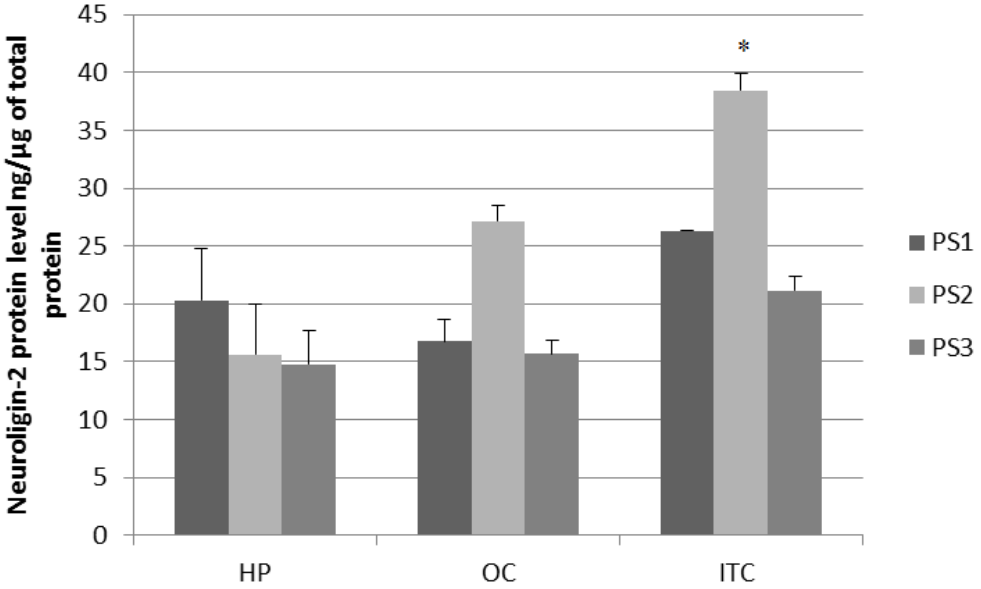

Fig. 3.23. Neuroligin-2 expression by area and disease severity. Key as for Fig. 3.12.

There was no variation in expression with pathological severity in either hippocampus or occipital cortex. Newman-Keuls *post-hoc* testing in inferior temporal cortex

showed that neuroligin-2 level at the moderate stage of AD was significantly higher than at the mild and severe stages, $P < 0.05$.

3.4.10 β-neurexin-1 by case-group and brain region

Even though the level of β-neurexin-1 was slightly higher in AD cases than in controls, the case-groups did not differ significantly ($F_{1,86} = 0.157$, $P = 0.91$; Fig. 3.24). Expression did not differ significantly by brain region between case-groups ($F_{2,52} = 0.125$ $P = 0.88$; Fig. 3.25).

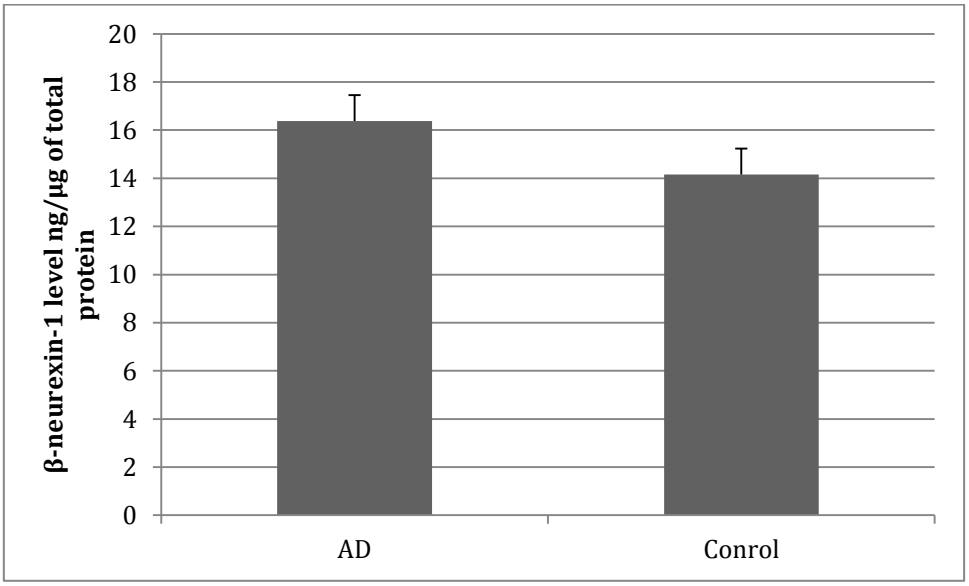

Fig. 3.24. Overall β-neurexin-1 expression by case-group. Values were averaged across areas as described under Fig. 3.7.

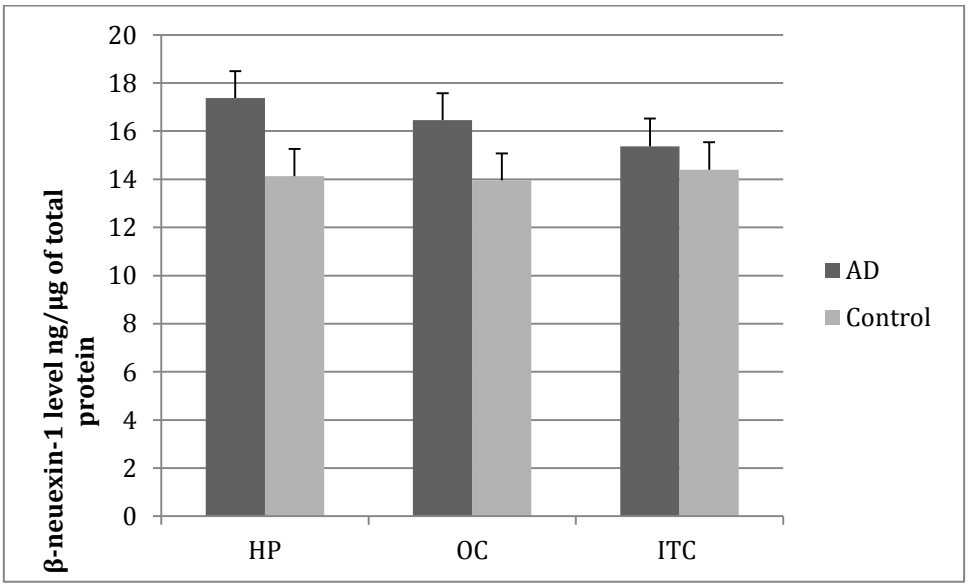

Fig. 3.25. Expression of β-neurexin-1 protein by case-group and area. No difference between or within areas was significant, see text.

3.4.11 β-neurexin-1 level and gender

The effect of gender on β-neurexin-1 expression was analysed. The Group × Gender interaction was not significant ($F_{1,86}$ = 0.662, P = 0.42; Fig. 3.26), nor was the Group × Gender × Area interaction ($F_{2,52}$ = 0.059, P = 0.942; Fig. 3.27).

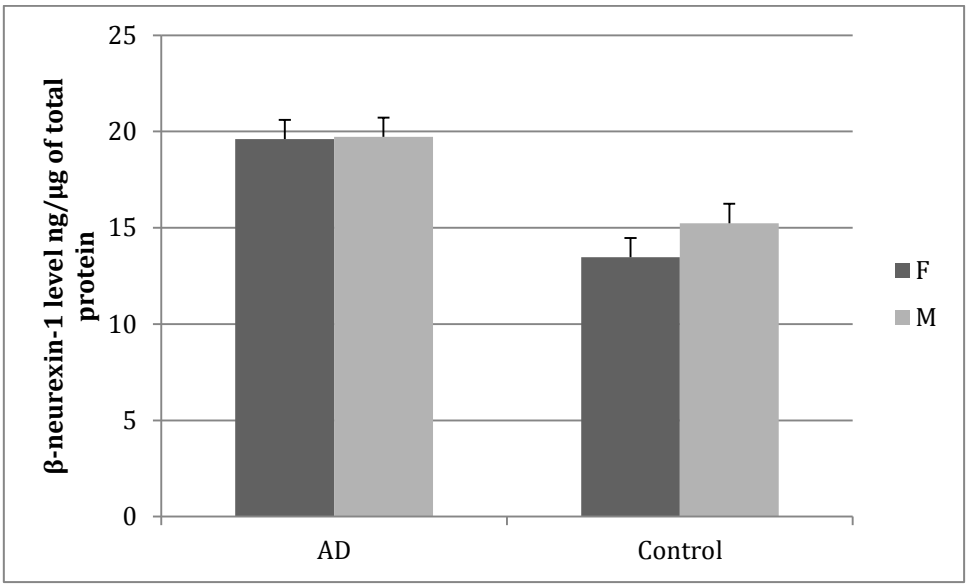

Fig. 3.26. β-neurexin-1 expression by case-group and gender. Details as for Fig. 3.16.

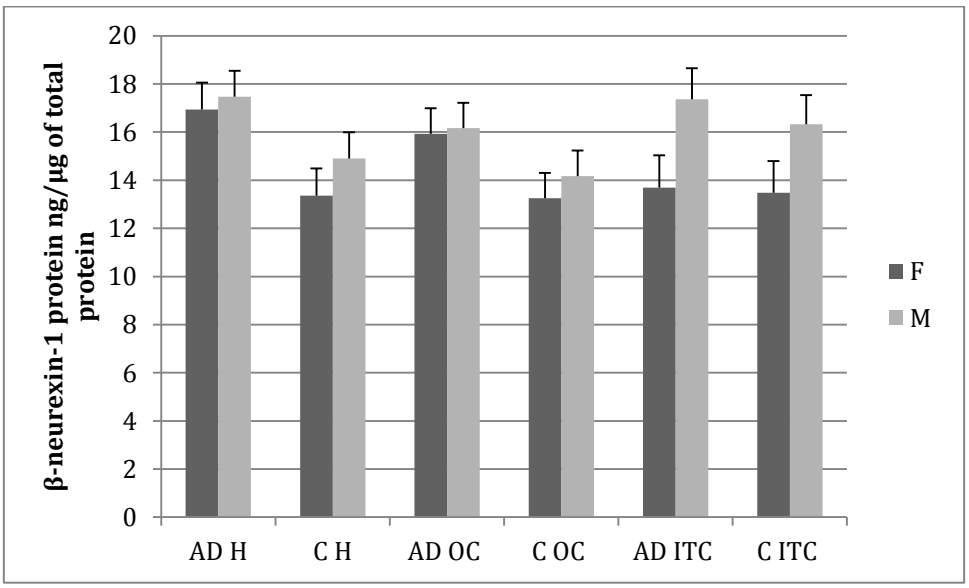

Fig. 3.27. β-neurexin-1 protein expression by goup, sex and area. See text for details.

3.4.12 β-Neurexin-1 level and APOE genotype

The Group × Nº of *APOE* ε4 alleles was significant ($F_{1,26}$ = 6.431, P = 0.017), due to higher β-neurexin-1 expression in AD *APOE* ε4 carriers than in control ε4 carriers (Fig. 3.28).

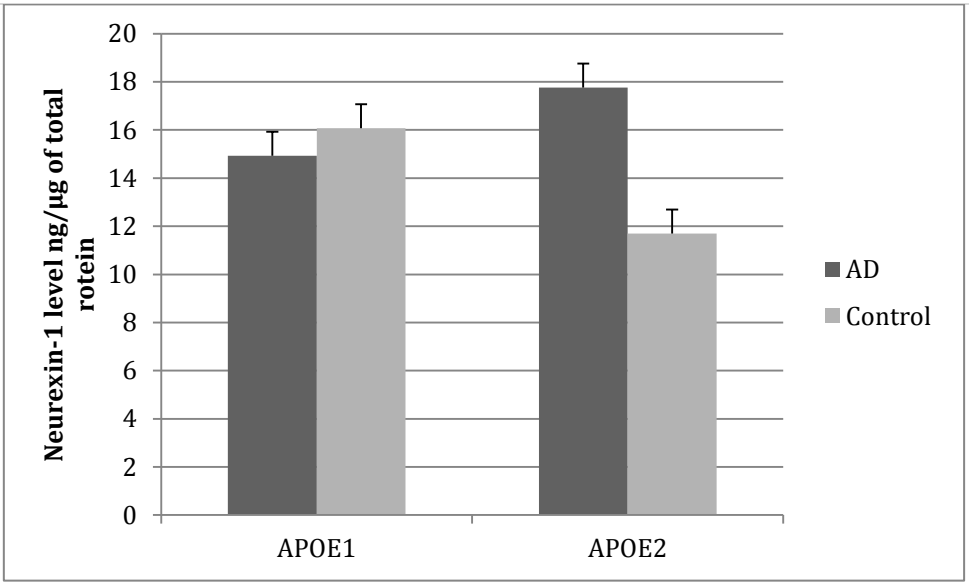

Fig. 3.28. *APOE* genotype and β-neurexin-1 by case-group. Key as for Fig. 3.10. Newman-Keuls *post*-hoc testing showed that expression was significantly higher in AD *APOE* ε4 carriers than in control ε4 carriers (APOE2), $P < 0.001$.

The brain region by group and ε4 interaction was also significant ($F_{2,52} = 5.376$, $P = 0.0075$), most notably in inferior temporal cortex (Fig. 3.29). However, these and the statistics on overall expression by *APOE* genotype are not reliable, for the reasons outlined in Sections 3.4.4 and 3.4.8.

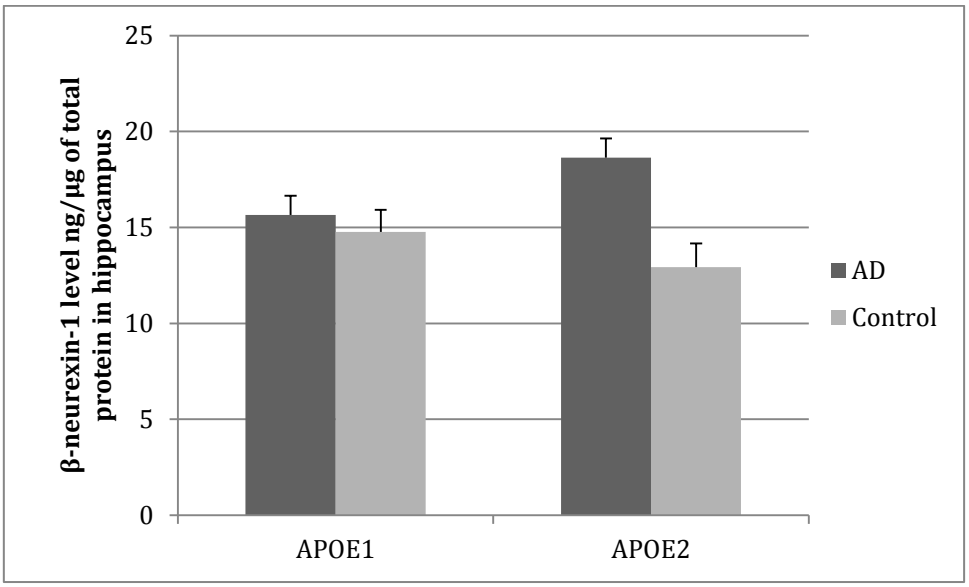

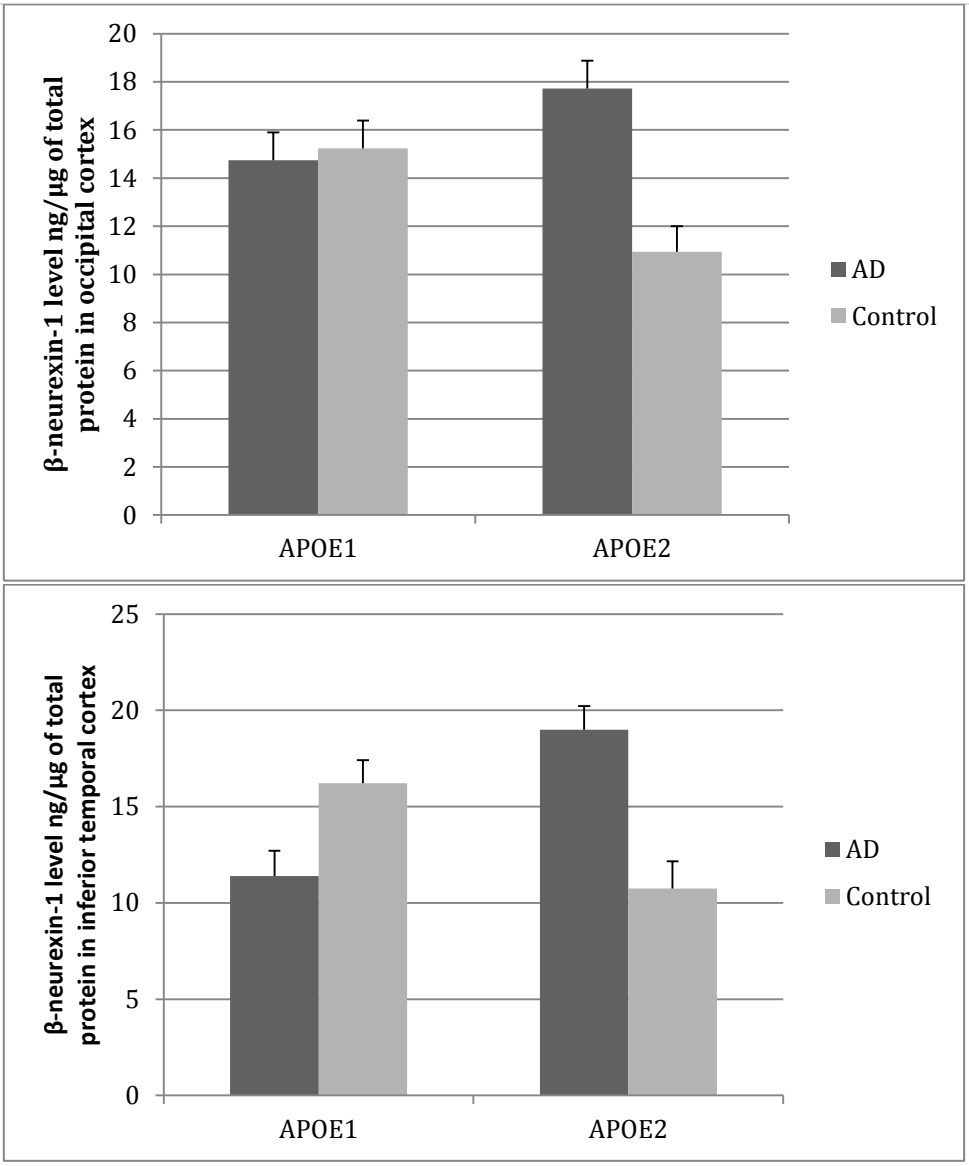

Fig. 3.29. *APOE4* genotype effects on regional β-neurexin-1 expression by case-group. Key as for Fig. 3.10. Newman-Keuls *post hoc* test showed significantly higher expression in AD cases carrying at least one *APOE* ε4 allele (APOE2) than in the equivalent controls in inferior temporal cortex, $P = 0.004$. Expression in AD cases carrying at least one *APOE* ε4 allele (APOE2) was significantly higher ($P = 0.006$) than in AD cases without an *APOE* ε4 allele (APOE1) in inferior temporal cortex.

3.4.13 β-neurexin-1 expression and severity of disease

When AD tissue samples were divided by pathological score without regard to brain region there was no significant variation in β-neurexin-1 expression ($F_{2,40} = 2.481$, $P = 0.10$; Fig. 3.30). Further examination showed that this was in part due to a regional confound; although the Group ×

Pathological × Score Area interaction was not significant ($F_{4,36}$ = 0.528, P = 0.71), *post-hoc* testing revealed some regional differences (Fig. 3.31).

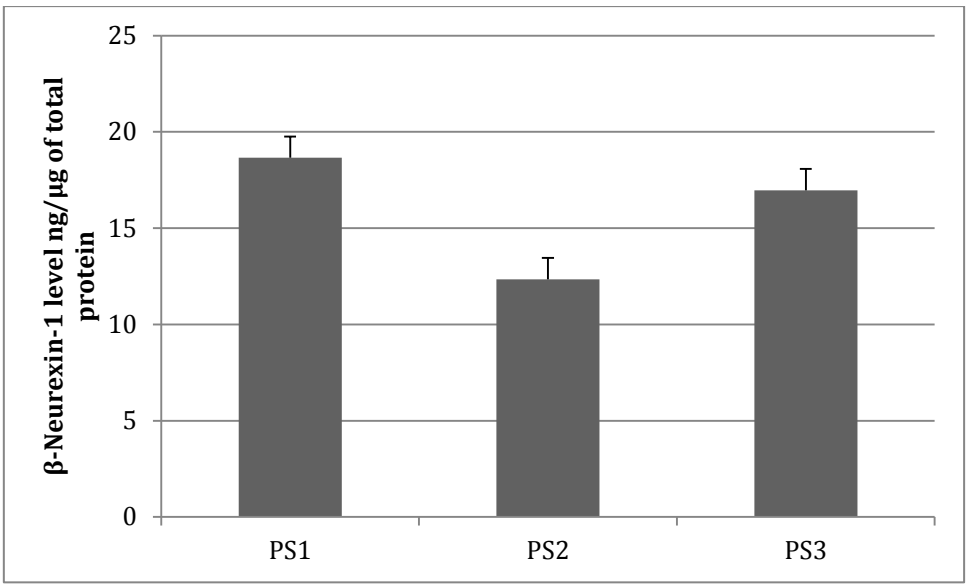

Fig. 3.30. β–neurexin-1 protein expression by pathological severity of disease. Key as for Fig. 3.12.

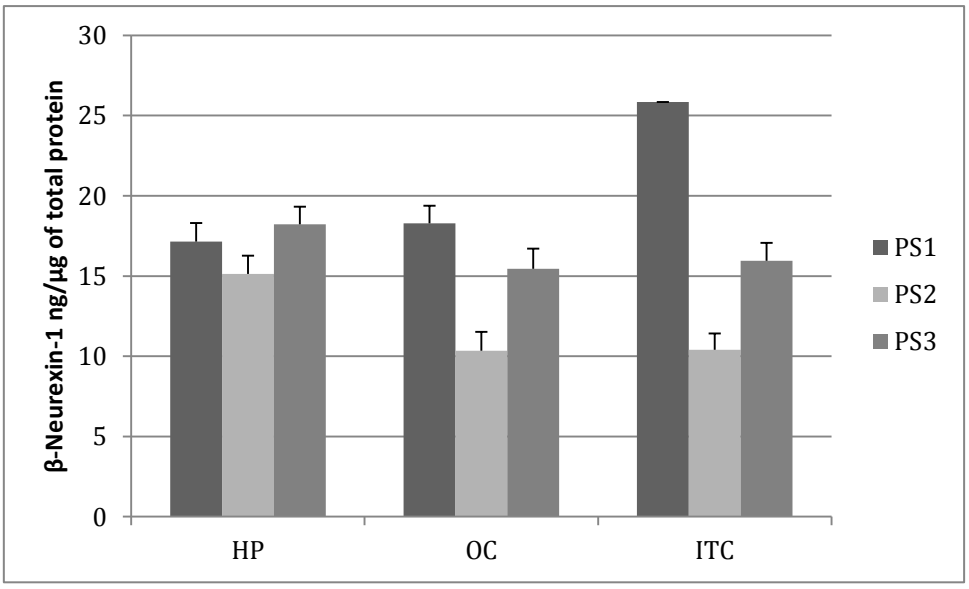

Fig. 3.31. Pathological severity and β-neurexin-1 protein expression by region. Key as for Fig. 3.12. There were no variations in expression with pathological severity in hippocampus. Newman-Keuls *post-hoc* testing showed significantly lower expression in samples with pathological score 2 than in those with scores of 1 or 3 in both occipital cortex and inferior temporal cortex, $P < 0.05$.

3.5 Discussion

3.5.1 Neuroligin-1 expression in AD

There is much evidence that alterations in synaptic protein expression could have an impact on synaptic loss (Masliah et al., 2001, Arendt, 2009). Various brain autopsy studies have found synaptic protein differences between AD cases and controls (Agarwal et al., 2008, Proctor et al., 2010, Tannenberg et al., 2006). Data from this chapter showed that the overall level of neuroligin-1 was significantly higher in AD tissue samples than in age- and sex-matched controls, which suggests there might be post-synaptic excitatory dysfunction. The level of neuroligin-1 in AD cases was significantly higher than in the relevant controls in both hippocampus and occipital cortex, which might indicate synaptic toxicity in these two areas. It was surprising not to see significantly higher levels in AD inferior temporal cortex, because it is one of the most affected areas in AD.

Neuroligin-1 levels did not vary with pathological score significantly in any of the three areas. However, levels were slightly higher in PS2 samples than in PS1 samples in all three areas, and lower in PS3 samples that exhibit the final stage of the disease. The low level in PS3 samples could be due to the marked loss of synapses at this stage. Taken together, these results show that neuroligin-1 differences in AD vary with both brain region and disease progression, which is consistent with documented asynchronous changes in synaptic protein levels in AD (Agarwal et al., 2008, Kirvell et al., 2006).

We found that neuroligin-1 level varied regionally. The highest concentration was found in control inferior temporal cortex, which is consistent with previous reports of the levels of other synaptic proteins such as synaptophysin, dynamin I, N-cadherin, and αCaMKII in this area (Tannenberg et al., 2006). A higher neuroligin-1 level was observed in female cases than in female controls, and levels in AD females were higher than those in AD males. This result suggests that the higher expression level of neuroligin-1 could be gender specific. It is noteworthy that the age-adjusted incidence of AD is higher in females (Schmidt et al., 2008).

The overall higher level of neuroligin-1 in AD cases compared with age- and sex-matched controls could indicate a role for this protein in excitotoxicity. The β-neurexin-1–neuroligin-1 complex is a powerful inducer of post-synaptic differentiation of glutamatergic synapses *in vitro*. It induces accumulation of, and can bind to, two crucial components of the PSD — PSD-95 and NMDAR — at mature synapses. The NMDAR has a critical function in neural circuit development and synaptic plasticity (Barria and Malinow, 2002), and selective neuronal death in AD may depend primarily on NMDAR activation (Greenamyre and Young, 1989). The function of neuroligin-1 in maintaining NMDAR-mediated excitatory post-synaptic currents (EPSCs) could be due to the modification of post-synaptic NMDARs rather than alterations in pre-synaptic transmitter release, because neuroligin-1 is located at post-synaptic sites (Song et al., 1999). The higher neuroligin-1 levels in AD cases shown in this study could lead to increased numbers of NMDARs at post-synaptic sites, which has been reported recently (Leuba et al., 2014). The higher levels of neuroligin-1 in AD cases than in controls, found here in some regions, may reflect higher PSD-95 concentrations in AD cases (Leuba et al., 2008a, 2008b, Rubenstein and Merzenich, 2003).

The higher neuroligin-1 level in AD cases might reflect a reduced rate of proteolytic cleavage in the synapse. Most γ-secretase substrates such as amyloid precursor protein (APP), Notch, ErbB4, E-cadherin and ephrinB2 shed their extracellular domains to yield a membrane-tethered C-terminal fragment (CTF) and a soluble ectodomain (Beel and Sanders, 2008, De Strooper et al., 1999, Wolfe, 2008). In addition, ADAM10 cleaves a number of γ-secretase substrates such as APP, cadherin, and Notch (Jorissen et al., 2010, Kuhn et al., 2010, Reiss et al., 2005). Both γ-secretase and ADAM10 metalloproteinase regulate neural stem cell numbers by changing Notch signalling in the mature synapse (Jorissen et al., 2010). They also mediate the cleavage of several substrates in neurons to control synaptic function (Restituito et al., 2011, Rivera et al., 2010). Neuroligin-1 undergoes proteolytic processing in rat brain and mouse primary cortical neuronal cultures (Suzuki et al., 2012). ADAM10 removes the extracellular domain of neuroligin-1 and γ-secretase removes the intracellular domain from the remaining membrane-tethered fragment of the protein. Incubating cultures with NMDA or β-neurexin-1 increases N-terminal fragment (NTF)-neuroligin-1 levels. Thus, neuroligin-

1 cleavage can be controlled by neuronal activity or by binding with β-neurexin-1, which offers a mechanism for the regulation of neuroligin-1 levels on the neuronal membrane (Peixoto et al., 2012, Suzuki et al., 2012).

Acute neuroligin-1 cleavage destabilizes β-neurexin-1 and depresses excitatory neurotransmission by reducing the probability of neurotransmitter release. Consequently, inhibiting neuroligin-1 cleavage may increase the probability of pre-synaptic release. Neuroligin-1 cleavage can alter glutamate transmission and have an impact on post-synaptic dendritic spines (Sindi et al., 2014). Changes in proteolytic processing of neuroligin-1 might enhance pathophysiology and provide a link between neuroligin-1 levels and the PSD in AD cases (Welberg, 2012). In conclusion, this study suggests a possible role of neuroligin-1 in the pathogenesis of AD. Its increased level could contribute to the dysfunction of excitatory synapses in AD.

Treatment of cultured cortical neuron with neuroligin-1 increases the number of excitatory synapses on GABAergic interneurons. These data suggest that neuroligin-1 enhances the formation of new synapse in developing neurons only (Ting et al., 2011). Neuroligin-1 also increases the size of excitatory synapse on GABAergic interneurons, which suggest it can strengthen existing synapses. Neuronal excitability depends on the balance of excitatory and inhibitory input signals, which is regulated by excitatory and inhibitory synaptic contacts. As a result, promoting the effect of neuroligin-1 on excitatory synapses can be essential to the role of GABAergic interneurons. The overall increase of neuroligin-1 protein observed in the current study could lead to increasing the number of excitatory synapses on GABAergic interneurons.

Synaptophysin was measured in an earlier study from the lab (Tannenberg et al., 2006) and we have now compared neuroligin-1 and synaptophysin in the cases that are in common between the two studies. We aim to publish this new data soon. We found no difference in synaptophysin between AD cases and normal controls in any of the three brain areas studied. The concentration of neuroligin and synaptophysin is expressed in ng/µg of total synaptosomal protein in the nerve-

endings that remain in the preparation. That is, it is a measure of the concentration of each protein *per synaptosome,* and thus should not be affected by atrophy or synapse loss.

3.5.2 Neuroligin-2 expression in AD

Neuroligin-2 is a synaptic cell adhesion protein specific for inhibitory synapses. In the current study, neuroligin-2 levels were significantly lower in AD cases than in matched controls, signifying either a decrease in the number of inhibitory synapses in total or in the density of neuroligin-2 clusters within such synapses. Neuroligin-2 levels varied with brain region. The highest concentration was found in control inferior temporal cortex samples, which is consistent with previous reports that higher levels of synaptic proteins such as synaptophysin, dynamin I, N-cadherin, and αCaMKII are found in this region than in other brain regions (Tannenberg et al., 2006). The level of neuroligin-2 in both the hippocampus and occipital cortex did not differ significantly between AD cases and controls. One the other hand, neuroligin-2 in the inferior temporal cortex, which is one of the most-affected areas in the AD brain, was significantly lower in AD cases than in controls. In occipital cortex and inferior temporal cortex, neuroligin-2 was higher at a moderate pathological severity, which indicates it is prone to AD damage. At the severe disease stage the level of neuroligin-2 protein in these areas was again lower, which is consistent with the marked synaptic loss seen at the final stage of the disease.

It was very surprising to find no significant differences in neuroligin-2 protein expression in the highly affected hippocampus when a significant reduction in neuroligin-2 proteins was observed in the AD inferior temporal cortex. Neurodegeneration in AD progresses through the brain in a predictable, region-specific manner (Braak and Braak, 1991a). Given that the hippocampus is one of the first areas affected in AD and one of the most degenerated, and that the inferior temporal cortex is affected after the hippocampus, it would be expected that the inferior temporal cortex would not be as degenerated as the hippocampus. The finding reported here could be explained by a specific decline of neuroligin-2 protein in the inferior temporal cortex that does not occur in hippocampus. More study on the associations between excitatory and inhibitory synaptic proteins in AD may provide an explanation of this conundrum with respect to excitotoxicity in AD.

The AD-specific paucity of neuroligin-2 was more noticeable in male than in female cases, and this underpinned the overall lower neuroligin-2 level in AD cases. Because AD has a higher incidence in females than males, the greater lack of neuroligin-2 in male cases appears contradictory. It could be explained by the younger average age at death in males than in females in this study, and hence the earlier age of disease onset, which would suggest a greater disease severity. Females died at a higher mean age, and may have had less-severe disease on average. However, the case numbers were limited in this study and it will be better to study more cases to obtain a more conclusive result.

Neuroligin-2 is crucial for post-synaptic inhibitory function. Data from the current study is consistent with a report that deletion of neuroligin-2 impairs inhibitory synapse function as measured by evoked synaptic transmission (Chubykin et al., 2007). The paucity of neuroligin-2 in AD cases may portray a dysfunction in GABAergic transmission, and is in conformity to a previous report that *NLGN2* knockout mice have decreased GABAergic transmission (Blundell et al., 2009). The role of neuroligin-2 in regulating GABAergic function is further illustrated by a loss-of-function mutation of this protein in patients with schizophrenia (Sun et al., 2011).

3.5.3 β-Neurexin-1 expression in AD

β-Neurexin-1 has not been previously quantified in AD cases and controls, and it was surprising to find that the level of β-neurexin-1 was higher, although not significantly, in AD cases than in controls in all three brain regions. This higher level of β-neurexin-1 is compatible with a previous study that quantified another pre-synaptic cell adhesion molecule, N-Cadherin, in AD cases and controls (Tannenberg et al., 2006). The higher levels of β-neurexin-1 in AD cases derive from the increase in synaptic apposition length that occurs in AD (Scheff et al., 1990). Further work with a larger number of cases and controls is required to confirm this.

The highest level of β-neurexin-1 was observed in the inferior temporal cortex, which is compatible with previous findings of high synaptic protein abundance in this area. The lowest level of β-neurexin-1 was observed in the occipital cortex. β-Neurexin-1 protein level was found to be modulated by the pathology severity of disease. It was lower in all three regions at the moderate

severity stage and higher again at the severe stage. This increase in the final stage of AD may be triggered by a compensatory mechanism to offset some of the excitotoxic damage.

This study was the first to examine neuroligin-1, neuroligin-2 and β-neurexin-1 in subjects with AD. Overall, the data presented suggest a selective synaptic dysfunction in AD. The quantities of these synaptic proteins differed in AD in a regionally selective manner.

The neuropathology of the AD cases used showed a contrasting result in the levels of neuroligin-1 and neuroligin-2 proteins, which are specific for glutamatergic and GABAergic synapses respectively. Both neuroligin-1 and β-neurexin-1 levels were higher in AD cases than in controls. Variations in the levels of neuroligins and neurexins could sway the balance between excitatory and inhibitory neurotransmissions in the brain, and could lead to damage of synapses and dendrites and ultimately to the neuronal death seen in AD.

3.5.4 APOE genotype and protein expression

It was surprising to find a significant enhancement of neuroligin-1 levels in cases without an *APOE* ε4 allele in the current study. The level of neuroligin-2 did not significantly differ between in AD *APOE* ε4 carriers and AD cases without an *APOE* ε4 allele. On the other hand, β-neurexin-1 was higher in *APOE* ε4 carriers than in AD ε4 non-carriers. It must be emphasized that this analysis was badly underpowered because there were so few AD cases without an *APOE* ε4 allele and because of the overall lack of representation of sufficient numbers of subjects in each allelic category; further work on this issue will require a much larger data set. *APOE* has an important function in synaptogenesis, and both *APOE* ε2 and *APOE* ε3 alleles, particularly the former, are protective against AD (Rebeck et al., 2002), while *APOE* ε4 increases the risk of AD (Liu et al., 2013). Hemizygous and homozygous *APOE* ε3 transgenic mice are protected against neurodegeneration compared with homozygous *APOE* ε4 littermates (Buttini et al., 2000). As a consequence, AD cases with at least one ε4 allele are likely to be more vulnerable to neurodegeneration than AD cases with ε2 or ε3 alleles. There were no AD cases with an ε2 allele in this study, and very few in the Queensland Brain Bank.

3.5.5 Limitations of the study

Neuroligin-1, neuroligin-2 and β-neurexin-1 proteins were quantified in AD cases and controls matched as closely as possible for age, gender, and post-mortem delay. Nevertheless, some data, such as medical history, environmental context, and family history, were missing for some AD cases and controls. Environmental factors such as smoking and alcohol dependence can have an impact on protein expression in the central nervous system. A meta-analysis of 43 studies showed that cigarette smoking significantly increases the risks dementia and cognitive decline (Anstey et al., 2007). Another study showed a significant association of the *NRXN1* gene with nicotine dependence in European- and African-American smokers, and indicated that smoking has an impact on neurexin levels (Nussbaum et al., 2008). Alcohol use reportedly increases the risk of AD (Piazza-Gardner et al., 2013) and influences synaptic protein expression in human subjects (Matsuda-Matsumoto et al., 2007). Neurexin-3 polymorphisms are reportedly associated with alcohol dependence and altered expression of specific isoforms of the protein (Hishimoto et al., 2007).

A limitation of the current study was the small number of samples with varying degrees of pathological severity in the three brain regions. Increasing the number of cases and controls can strengthen the study and enhance statistical power. Additional time and effort to extend the study would help in replicating the work for validation purposes.

Some limitations are associated with the quantification of proteins by immunodetection. These include incomplete protein transfer from the gel to the membrane; different post-translational modifications might alter the efficiency of transfer. Non-specific binding of some antibodies can vary between the standard and the endogenous protein. Quantification of proteins by mass spectrometer-based assays will aid validation and help determine whether different post-translational modifications occur in the neuroligins and neurexins. Therefore, more time and effort should be put into the quantification of these molecules by the multiple reaction monitoring and SWATH techniques described in chapter 4.

Advanced imaging techniques such as FDG-PET can hopefully give new insights into disease progression in living subjects, based on the current study. However, at present, PET ligands are not available for the neuroligins and neurexins, and it is hard to get resolution down to the level of the nerve ending with current clinical scanner technology, but the data presented in this thesis may suggest that higher numbers of excitatory synapses will be found in pathologically affected areas of the AD brain when the new 7T instruments become available for clinical use.

The approach to quantification used here is expensive, low-throughput, and time-consuming, and required the generation of critical recombinant reagents. The three proteins were identified in human brain membrane preparations at ~110 kDa for neuroligin-1, ~95 kDa for neuroligin-2 and ~46 kDa for β-neurexin-1. These predicted molecular weights were obtained from UniProt and it was assumed that each antibody used was specific only for the protein of interest and did not cross-react with any other protein. This should be verified independently, for example by the techniques set out in Chapter 4. The need for high-throughput techniques to explore several of the interesting preliminary results outlined in this Chapter was another motivation that led to the Chapter 4 study.

Chapter 4

4 Quantification of neuroligin and neurexin proteins by MRM and SWATH

4.1 Aims of the research

1. To identify synaptic proteins in human autopsy brain tissues by mass spectrometry.
2. To search for neuroligin-1, neuroligin-2, neuroligin-3, neuroligin-4 and neuroligin-4Y proteins in human autopsy brain tissue by mass spectrometry.
3. To search for neurexin-1α and neurexin-1β in human autopsy brain tissue by mass spectrometry.
4. To quantify neuroligins and neurexins with multiple reaction monitoring (MRM) and SWATH techniques.

4.2 Introduction

A range of experimental approaches is required to assess synaptic processes and their adaptive alterations, which are highly ordered and complex (Bard and Groc, 2011, Coba et al., 2009). Neuropathological diseases show characteristic molecular changes, with diverse ætiologies, that are mainly located at the synapse (Dosemeci et al., 2007, Fernandez et al., 2009, Husi et al., 2000). Studying the protein configuration of the synapse in autopsy brain tissues may provide useful insights into various diseases (Keller et al., 2007). Molecular and cellular studies of these processes have until recently been restricted to techniques that can study one molecule at a time within a network. Research into proteins in autopsy tissue is limited by the lack of good paradigms; it is essential to develop methods to quantify proteins and their post-translational modifications at the synapse as well as to develop strategies to validate the quantification of these entities.

During the last decade, mass spectrometry (MS)-based proteomic techniques, and biochemical fractionation techniques, has allowed researchers to begin investigating the proteomes underlying synaptic signalling (Bayes et al., 2011, Cheng et al., 2006, Hahn, 2010, Peng et al., 2004).

Many proteins and post-translational modifications can be studied simultaneously, which allows investigation of signalling pathways in the context of various other intracellular molecular events.

4.2.1 Mass spectrometry based techniques

Protein analysis using MS first requires separating the proteins into fractions using methods such as electrophoresis and chromatography (Woods et al., 2012). After fractionation, each protein is analysed by MS. The initial fractionation before analysis is important to enhance sensitivity and to identify and characterise low-abundance proteins that may be masked in complex mixtures. However, some samples can be run in MS without fractionation.

There are three main parts in a mass spectrometer: the ionization source, the mass analyser, and the detector. An ionization source ionizes the peptides in the sample, which then travel through the analyser according to their mass:charge (*m/z*) ratios. The ionized sample then hits the detector and spectra are recorded: the spectra are used to identify the proteins (Fig. 4.1)

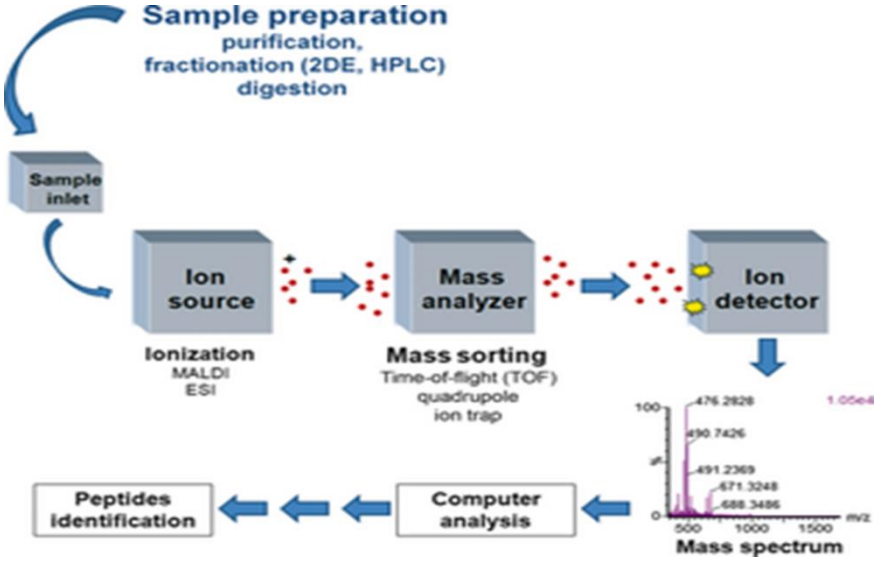

Fig. 4.1 Example of basic mass spectrometer experiment. The sample is fractionated by electrophoresis or HPLC and then digested by an enzyme such as trypsin. The digest is ionized in a MALDI-MS or ESI-MS. The ions fly and are sorted through different types of mass analysers. The ions are detected and then recorded and a mass spectrum is produced.

4.2.1.1 Ionization techniques

Ionization techniques convert uncharged molecules into ions that can then be manipulated in electric or magnetic fields. The most important issue with biological molecules like peptides and proteins is to convert polar, zwitterionic molecules into gas-phase ions without degradation. The most common ionization methods for biological samples are electrospray ionization (ESI) and matrix-assisted laser desorption/ionization (MALDI).

4.2.1.1.1 Electrospray ionization

ESI generates ions by spraying an electrically generated fine mist of ions into the inlet of a mass spectrometer at atmospheric pressure (Fenn et al., 1989). Ionization is generated from the potential difference between the capillary inlets to the mass spectrometer in which the liquid flows and small droplets of liquid are formed. The liquid is translocated to a heating device that causes evaporation of the solvent. When the droplets reach the point at which charge repulsion exceeds the surface tension, ions are desorbed from the droplet to create bare ions, which are then transferred to the ion optics of the mass spectrometer. ESI transforms solution-phase molecules into gas-phase ions; the ions are created with different charges, which complicates the calculation of molecular weight due to a one-to-one association between the *m/z* value and molecular weight. Multiple charging has the advantage of lowering the *m/z* value detected in the spectrometer, which allows the use of less-sophisticated mass analysers.

4.2.1.1.2 MALDI

The second ionisation technique, MALDI, uses laser energy to alter molecules into gas-phase ions. A matrix is mixed with the sample that absorbs the energy of the laser and is used to support thermal desorption.

4.2.1.2 Mass analyser

The different types of analysers include quadruple (Q), time-of-flight (TOF), and ion trap (IT), which have different applications. They differ in their physical principles and analytical

performance. MALDI sources are generally coupled with TOF or TOF/TOF mass analysers because of their pulse mode of action. Shotgun proteomics liquid chromatography (LC) is associated with mass spectrometry for the identification of proteins. The main advantage of LC-MALDI-MS over LC-ESI-MS is the robustness of the former in resisting very harsh LC conditions and the high *m/z* range of the TOF mass analyser (Ngounou Wetie et al., 2013, Sokolowska et al., 2013). The limitations of LC-MALDI-MS include the difficulty in spotting directly from the LC apparatus. In MS, proteins can be recognized by measuring the *m/z* of gas-phase ions. In general, LC-MS methods are valued for their capability to examine complex samples and difficult proteins, such as those embedded in membranes, and as a result offer better proteome coverage in comparison to other proteomic techniques.

4.2.1.3 Sample preparation, fractionation, and tags

Protein quantification is ideally carried out with internal standards that are added to the sample before preparation to eliminate differences resulting from the preparation itself. Both label-based and label-free methods can be used (Gant-Branum et al., 2009). Label-based methods tag peptides or proteins before LC separation utilizing one of the three following techniques: 1, *i*sobaric *t*ags for *r*elative or *a*bsolute *q*uantification, iTRAQ (Applied Biosystems, AB Sciex, Foster City, CA, USA; Ross et al., 2004); 2, *i*sotope-*c*oded *a*ffinity *t*ags, ICAT (Gygi et al., 1999); and 3, *s*table *i*sotope *l*abelling of *a*mino acids in *c*ell culture, SILAC (Darie et al., 2011, Mann, 2006, Spellman et al., 2008). The isotopic labelling approach has some disadvantages due to their elaborate chemistry. However, there are several label-free methods, such as *m*ultiple *r*eaction *m*onitoring, MRM, and *s*equential *w*indow *a*cquisition of all *th*eoretical fragment-ion spectra, SWATH, which have various advantages and will be discussed in detail in this chapter.

4.2.1.4 Proteomic bioinformatics

Computer processing of MS data allows large-scale and high-throughput analysis that has enabled proteomic studies. Different strategies have been established to find unique tandem mass spectra of amino acid sequences in publically available databases. All database methods are based on matching the theoretical fragmentation pattern of the target peptide with the fragmentation pattern in

the tandem mass spectrum. Each match peptide is given a score based on fragment ion frequencies, and cross-correlation (Eng et al., 1994, Perkins et al., 1999). Intensity models are used in correlation analyses to increase the matches between sequence and spectra, while probability-based methods offer a statistical measure for the fit between sequence and spectra (MacCoss et al., 2002, Perkins et al., 1999, Sadygov and Yates, 2003). Most of these programs are also appropriate for the study of protein modifications. There are various software packages for the analysis of LC/LC/MS/MS data, such as Mascot, PEAKS DP, ProteinPilot, and others. Proteomic studies can produce huge amounts of data; hence, a high level of automation of data analysis is required.

4.2.2 Multiple reaction monitoring (MRM)

MRM is an MS-based quantification method that is commonly used in triple-quadruple MS instruments. It is a robust multiplexed assay for the precise and sensitive detection of protein expression levels and post-translational protein modifications (Lange et al., 2008). It is used to identify and quantify from ten to a few hundred peptides, but can in principle be used for multiple peptides in a single assay. MRM assays can detect and quantify proteins present at low ng per ml concentrations, such as has been shown for serum (Keshishian et al., 2007, 2009). MRM also has the advantage of high reproducibility (Addona et al., 2009), which makes it a first choice for biomarker validation. It exploits the unique capabilities of triple-quadrupole (QQQ) MS for quantitative analysis. It is a selective workflow for mass spectrometry that can only identify a predefined combination of precursor and fragment ions. In MRM, the first and the third quadruples act as filters to specifically select predefined *m/z* values corresponding to the target peptide ion and a specific fragment ion of the precursor peptide (Fig. 4.2). In the second quadruple, which serves as a collision cell, the pre-defined peptides in Q1 are selected and fragmented. In quadruple three, transitions (precursor/fragment ion pairs) are monitored over time to produce a set of chromatographic traces with the retention time and signal intensity for each specific transition. Two types of mass selection with narrow mass windows lead to high selectivity and the successful filtering out of co-eluting background ions. Compared to other MS-based proteomic techniques, no full mass spectra are recorded in QQQ-based MRM analysis. The non-scanning property of this mode of operation

translates into an enlarged sensitivity by one or two orders of magnitude compared with-full scan techniques. Furthermore, it gives a linear response over a wide dynamic range of up to five orders of magnitude, which allows the detection of scarce proteins in highly complex mixtures: this is vital for systematic quantitative studies.

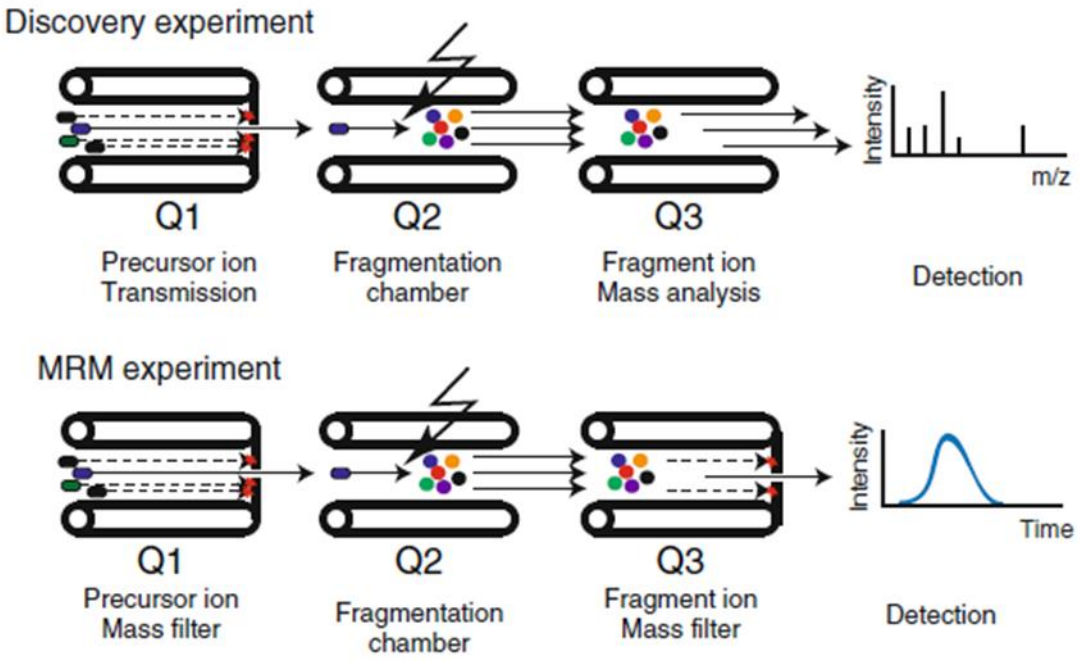

Fig. 4.2. Diagram of information-dependent analysis (IDA) mass spectrometry and MRM mass spectrometry. In IDA, quadruple 1 (Q1) is used to select the most abundant precursor ion, which is then fragmented in Q2. Subsequent analysis of all fragment ions takes place in Q3. The resulting MS/MS spectrum is used to identify the fragmented precursor ions. In MRM, only pre-defined peptides in Q1 are chosen for fragmentation in Q2. Pre-selected fragment ions are selectively passed through Q3 and identified.

4.2.2.1 Selection of a target protein in MRM

The first step in an MRM assay involves choosing the proteins of interest. MRM can target different proteins in one LC-MS analysis after the transitions have been optimized. Choosing the protein of interest may depend on previous experiments or relevant information from the literature. Different information resources on the Web can be used for this purpose, such as gene expression and protein expression data, protein–protein interaction data or the Kyoto Encyclopædia of Genes

and Genomes (KEGG) database. Network expansion can be used to enhance an initial set of proteins that have been revealed in quantitative screens (Table.4.1). Ideally, internal standards are chosen as an invariant reference set to minimize experimental error, such as variable protein amounts per sample.

Table 4.1. Online information resources relevant to the selection of a set of proteins of interest.

Gene Expression	GEO	http://www.ncbi.nlm.nih.gov/geo/	(Barrett et al., 2007)
Protein expression	ProteinAtlas	http://www.proteinatlas.org/	(Uhlén and Pontén, 2005)
Gene ontology group	GO	http://www.geneontology.org/	(Karp, 2000)
Functional group	KEGG	http://www.genome.jp/kegg/	(Kanehisa and Goto, 2000)
Protein-protein interactions	IntAct	http://www.ebi.ac.uk/intact/	(Kerrien et al., 2007)
Protein-protein interactions	MINT	http://mint.bio.uniroma2.it/	(Ferrari et al., 2011)

4.2.2.2 Selection of the peptide

After tryptic digestion, each protein produces tens to hundreds of peptides (Picotti et al., 2007). However, only a few representative peptides for each protein are targeted to identify and quantify it in a sample. The right choice of peptides is crucial for the success of MRM. Different factors have an impact in choosing the right peptide, such as uniqueness and post-translational modification.

4.2.2.3 Uniqueness

Choosing peptides for targeted MS analysis is crucial. It is important to select unique peptides that are specific for the targeted protein or one of its isoforms. Thus, it is critical to choose peptides that differentiate between different splice isoforms. Information about splice variants can be obtained from Ensembl (www.ensembl.org/), NCBI (www.ncbi.nlm.nih.gov/sites/entrez, www.ncbi.nlm.nih.gov/projects/SNP/), and UniProt (http://www.uniprot.org/) databases. Peptide Atlas (www.Peptide Atlas.org/) can differentiate between several splice isoforms and different genes by reporting the number of genome locations for observed peptides and visualizing the peptide–

protein relationship by cytoscape, an open source bioinformatics software platform for visualizing molecular interaction networks and integrating them with gene expression profiles (Shannon et al., 2003).

4.2.2.4 Post-translational modifications

In the MRM assay, modified peptides cannot be identified without being specifically targeted due to mass differences caused by post-translation modifications (PTMs). Observed differences in the quantity of a peptide may portray alterations in the abundance of the protein across samples, or modification of the target peptide. For accurate quantification, at least two peptides should be monitored for each protein. It is essential to first consult sites such as Uniprot (http://www.uniprot.org/) to check that the targeted peptides are not known to be modified, and to avoid peptides with cysteine or methionine residues. Post-translation modification may lead to two peptides from the same protein displaying different relative abundances across samples. However, MRM can be used to quantify peptides with post-translational modifications if the PTM is known and transitions for those peptides can be established. Examples of different types of PTM that have been targeted by MRM in other studies include phosphorylation (Unwin et al., 2005, Williamson et al., 2006), ubiquitination (Mollah et al., 2007) and acetylation (Griffiths et al., 2007).

4.2.2.5 Selection of MRM transitions

In MRM, quantification of a peptide needs specific choices of *m/z* settings for the first and third quadruple to provide highly sensitive and selective detection of the peptide. The mass and predominant charge state of the peptide determines the *m/z* value used in the first quadrupole, while a specific fragment ion of the peptide is selected in the third quadrupole. The intensities of individual fragment ions resulting from one precursor ion can differ significantly. To attain very sensitive results it is best to choose transitions specific for the most intense fragments. Usually the best 2–4 transitions for each peptide are chosen for quantitative assays. These choices may be based on data from shotgun experiments, which can be obtained from SRMAtlas or Peptide Atlas, or experimentally detected on the QQQ instrument. The condition of ionization can have an impact on

the charge state distribution as well as the intensity of the ion, which is dependent on the type of instrument used and the operating parameters.

The fragment ion masses of the peptide of interest can be calculated and experimentally verified by MRM assay on a QQQ instrument that produces high-performing transitions. If two precursor charge states and multiple ions are considered, more than 30 transitions for each peptide could be measured. As a result, the number of peptides that can be examined in one LC-MS analysis is restricted due to the time required to acquire the data representing each transition. The number of transitions monitored can be increased by using scheduled MRM (Stahl-Zeng et al., 2007). The principle of this approach is to acquire the transitions of a specific peptide during a narrow time window around its expected elution time, rather than monitoring it across the entire LC-MS run. During this time more transitions can be examined so as to obtain the best-performing ones. To conduct this type of experiment, the instrument must have a scheduling functionality and the retention times of the peptides of interest must be known. The retention times of specific transitions can be obtained from previous experiments or predicted by tools such as SSRCalc (http://hs2.proteome.ca/SSRCalc/SSRCalc.html; Krokhin et al., 2004), although in most cases RT are empirically determined. Another approach is to first study a small number of transitions that are chosen based on available MS/MS data. Choosing 2–4 fragment ions from both doubly and triply charged precursor ions will produce at least one transition with reasonable performance from which to derive retention-time data for subsequent experiments. Restricting the final assay to 2–4 transitions for each peptide allows the study of many hundred peptides in one LC-MS analysis.

4.2.2.6 Validation of transitions

The QQQ MRM assay is a very specific approach using two consecutive mass filtering steps. However, an individual precursor/fragment ion combination may not be specific for a peptide targeted in a complex sample. An example of this problem is explained in Fig. 4.3. Incorrect signals can develop from other peptides with precursor/fragment ion pairs of identical masses. Peptides with the same precursor mass and fragment ion could have closely related sequences and as a result part of the transitions may be identical. Distinct sequences could by chance produce mass pairs that are

very hard to filter out in the quadrupoles; this nonspecific signal may be of lower intensity than the optimized transitions. When MRM is used to study peptides that are an order of magnitude of less abundant than the most abundant peptides, non-specific signals can be higher than the detection limit and sometimes more intense than the signal for the peptide of interest. Because there are no full-range mass spectra in MRM, signals could be easily mistaken; these would give rise to mis-quantification errors. In consequence, it is essential to validate the primary set of transitions to confirm that the quantified signals produced are from the peptide of interest. Two ways to validate the transition are 1, scanning the full MS/MS of the precursor ion to sequence the peptide: the scan can be manually checked to confirm that the fragment ions that were selected are the most abundant following *c*ollision-*i*nduced *d*issociation, CID; 2, parallel acquisition of multiple transitions for a targeted peptide. The latter is based on the elution time of peptide: The transitions produce a perfect set of 'co-eluting' intensity peaks if they are produced from the same peptide. By producing more transitions, the capability for a random match is markedly reduced if perfect co-elution is observed. Many non-target peptides with similar precursor *m/z* could produce a plethora of low-intensity non-canonical fragment ions, which might generate transitions and lead to false quantification. It is strongly recommended that parallel acquisition of multiple transitions be checked by another kind of validation. The best approach to validate transitions is to acquire MS/MS spectra and sequence it from database searching to assure that the derived signals produced are from the peptide of interest. This process uses the QQQ tool for the MRM experiment under a protocol known as MRM-triggered MS/MS scanning (Unwin et al., 2005). In this procedure, the QQQ instrument is programmed to obtain a full fragmentation spectrum whenever a signal for a particular transition is identified. The MS/MS spectra produced can be compared with the predicted peptide fragments to confirm that the major MS/MS peaks are matched (Figure 4.3). This method provides assurance that the MRM signals are derived from the target peptide.

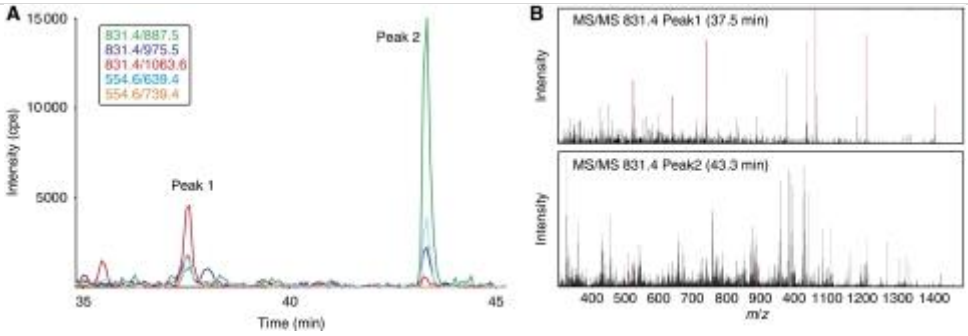

Fig. 4.3. Validation of transitions for the peptide VFAQFSSFVDSVIAK, which belongs to a protein of interest. **A,** MRM traces of five transitions. Two peaks with co-eluting transitions are apparent at 37.5 and 43.3 min. **B,** MS/MS spectra of peaks 1, top panel and 2, lower panel. Peaks corresponding to the y ions are in red. Although MRM transition intensities are higher at 43.3 min, the MS/MS spectrum that corresponds to the targeted peptide elutes at 37.5min. If transition intensities at 43.3 min were used without validation the quantification of the peptide would be in error.

4.2.2.7 MRM software

There are differences between MRM assays and shotgun proteomic experiments. In shotgun experiments, proteins are identified in samples without targeting, based on matching MS/MS spectra to databases, while in MRM experiments a software system allows MRM assays to be set up and supports the following: 1, choosing the target protein; 2, choosing the peptide signifying the protein of interest; 3, choosing the best transitions; and (4) validating the transitions by MS/MS spectra.

An example of MRM software is Targeted Identification for Quantitative Analysis of MRM (TIQAM; Lange et al., 2008), which can integrate proteomic data from local experiments and the Peptide Atlas database to produce peptides in the best order. It can also generate MRM transition lists and detect the best performing transitions from previous MRM experiments. All the peptide and transition data is kept in a database to permit recovery of the validated transitions for quantitative purpose. There are several other software programs that can help set up MRM experiments, such as MRMPilot (Applied Biosystems), SRM Workflow Software (Thermo Scientific), Verify E (Waters), Optimizer (Agilent Technologies) and Skyline (MacCoss lab software).

4.2.3 MS/MS^{ALL} with SWATH^{TM} Acquisition assay

MS/MS^{ALL} with SWATH^{TM} is a novel MS-based proteomics technique to quantify peptides and proteins in a sample by a single analysis. It utilizes a data-independent MS/MS acquisition to produce complete, high-specificity fragment ion maps that can be queried for the existence and quantity of any protein of interest using a targeted data analysis strategy. It utilizes an advanced hybrid quadrupole-time of flight mass spectrometer, the TripleTOF 5600® (AB SCIEX, Framingham, MA, USA).

SWATH produces fragment ion information for all precursors in the monitored range. It differs from the traditional acquisition assay, which does not depend on precursor ion mass detection to trigger MS/MS acquisition. Rather, SWATH systematically fragments all components of a sample *via* a rapidly moving selection window (Fig. 4.4).

SWATH can produce high-resolution fragment ion chromatograms for each target peptide that can be interrogated to detect the peptide of interest, similar to MRM. Using public libraries for ion data such as MRMAtlas, or database search software such as ProteinPilot^{TM}, the ouput can be searched for quantitative data on the target peptides or proteins. SWATH delivers a complete qualitative and quantitative archive of the sample that can be interrogated *in silico* and post-acquisition as new hypotheses are established.

MRM and SWATH have become important techniques to study synaptic trafficking events in autopsy brain tissue and thereby to explore the ætiology of neural diseases (Craft et al., 2013). Neuropsychiatric diseases may result from aberrant synaptic signalling involving different proteins that are arrayed in a microdomain-specific manner. Studying the proteomes of synapses in autopsy brain will provide an understanding of disorders such as autism, depression, schizophrenia, and AD. It will help define targets for novel therapeutics for these disorders. It will allow the assessment of protein expression and trafficking with high precision using accurate techniques such as MRM and SWATH. Previous studies have successfully utilized MRM to quantify synaptic proteins in subcellular fractions prepared from autopsy human brain (Chang et al., 2014a, 2014b). A

bioinformatics search showed that these assays can quantify thousands of additional synaptic proteins in different model systems.

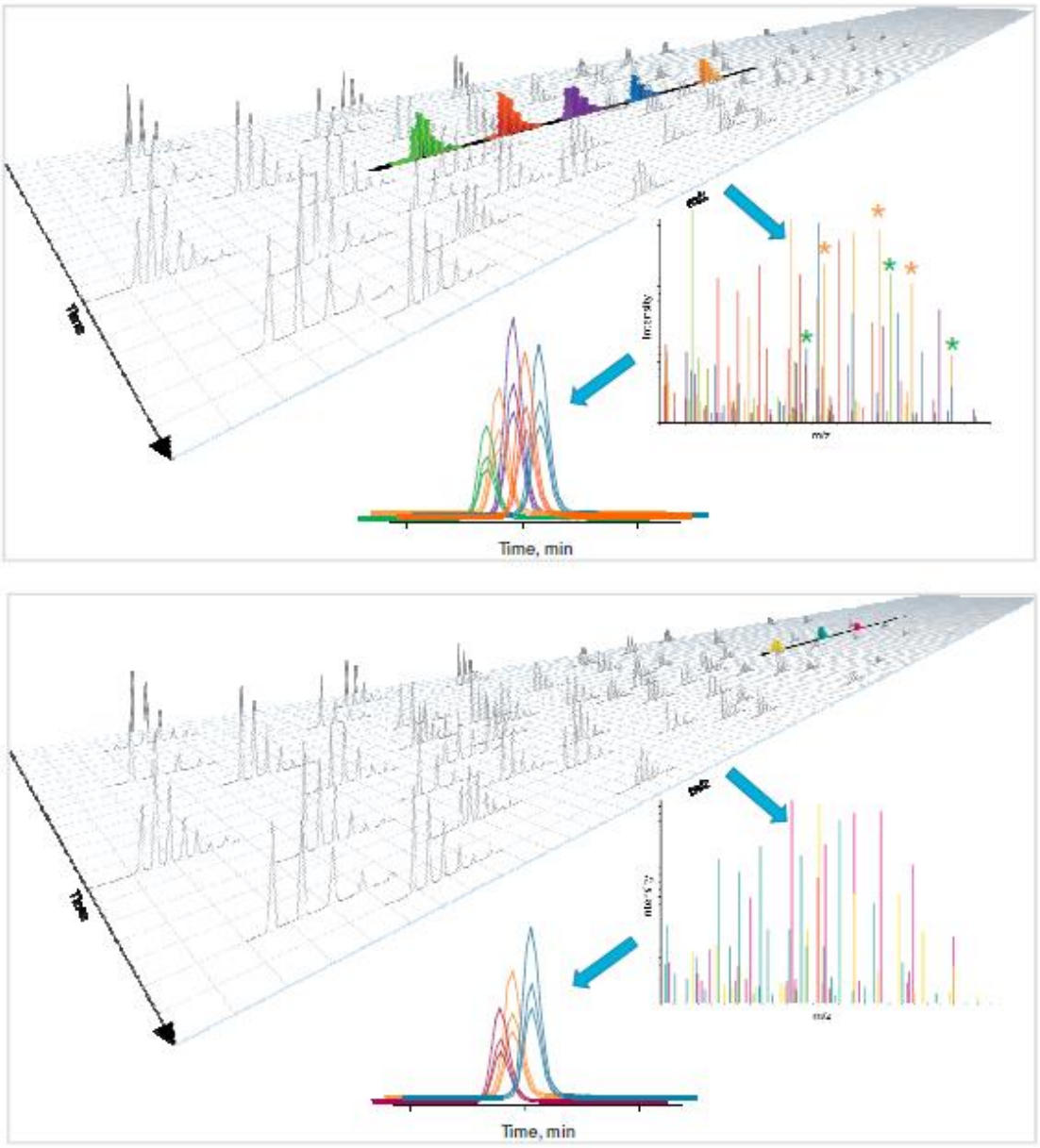

Fig. 4.4. MS/MS ALL with SWATH Acquisition. The method depends on passing a wider window of analytes to the collision cell. More-complex MS/MS spectra are produced, which comprise all the analytes within the Q1 *m/z* window selected. As the fragment ions are high resolution, high quality XICs are produce post-acquisition to generate data similar to MRM. The Q1 window can be stepped across the mass range, collecting full-scan composite MS/MS spectra at each step, with an LC-compatible cycle time. This approach allows a data-independent LC workflow.

In this chapter, the development of a LC-MRM/MS-based methodology for validation of neuroligin-1, neuroligin-2 and β-neurexin-1 protein quantification in human autopsy brain tissues from AD cases and controls is described. Various optimizations were performed for SWATH to obtain the most accurate quantification protocols.

4.3 Materials and Methods

4.3.1 Reagents used

Deoxycholate, trichloroacetic acid, sucrose, acetonitrile, acetone, urea, thiourea, ammonium bicarbonate, dithiothreitol, iodoacetamide, trypsin, and formic acid were obtained from standard suppliers and were of the highest grades available. The 2-D Quant kit was purchased from GE Healthcare Life Sciences, Rydalmere, NSW, Australia.

4.3.2 Autopsy brain tissue preparation

The Queensland Brain Bank at the School of Chemistry and Molecular Biosciences, The University of Queensland, a node of the Australian Brain Bank Network, provided autopsy brain tissue. Donors and the next of kin provided informed written consent for the research. Tissues were stored in ice-cold 0.32M sucrose at –80°C. The Medical Research Ethics Committee of The University of Queensland approved the project (Certificate #2010000105).

Sectioning of the tissue was done on dry ice and preparation of the synaptosomes was performed as per Etheridge et al. (2009). To prepare the synaptosomes, 0.5 g tissue samples were homogenized with ice-cold 0.32 M sucrose (10× w/v) in a motor-driven Teflon-glass homogenizer using 8–10 pestle strokes. The mixture was transferred to a 15 ml polypropylene tube and centrifuged at 750 × *g* for 10 min at 4°C in a Beckman JA 20 centrifuge (Beckman Coulter P/L, Lane Cove, NSW, Australia). The pellet was resuspended in the original volume of 0.32 M sucrose and centrifuged at 19,000 × *g* for 20 min at 4°C. The pellet, which contained the crude synaptosomal fraction, was resuspended in a 5 ml 0.32 M sucrose, layered onto a gradient of 5 ml of 0.8 M sucrose overlying 5 ml of 1.2 M sucrose, and centrifuged at 82,500 × *g* in a swinging bucket rotor (SW41 Ti, Beckman L8-60M ultracentrifuge) for 120 min at 4°C. Both myelin (at the 0.32/0.8 M interface) and

synaptosome (at the 0.8/1.2M interface) fractions were obtained by aspiration with a Pasteur pipette in minimal volumes. Mitochondria formed a pellet that was also retained for future studies.

4.3.3 Trichloroacetic acid/deoxycholate/acetone precipitation

Deoxycholate (DOC; 0.4 µg/µl, 20 µl) was added to each synaptosomal fraction (200 µl) to give a final concentration of ~0.04 µg/µl. The sample was incubated on ice for 30 min, then 25 µl of 6.4 M trichloroacetic acid (TCA; 0.65 M final) was added and the sample incubated on ice for 60 min. Samples were centrifuged at 10,000 × *g* at room temperature for 10 min. The supernatants were removed and 1 ml of 90% ice-cold acetone was added to each tube. Samples were vortexed for 3–4s, left at –20°C overnight, then centrifuged at 10,000 × *g* at 4°C for 20 min and supernatants removed. A second 1 ml of 90% ice-cold acetone was added to each tube, the procedure repeated, and the supernatants discarded. The pellets were dried for 5 min and 30 µl of rehydration buffer (8M urea and 2M thiourea in 50 mM NH_4HCO_3) was added. The tubes were incubated for 3h at room temperature, then stored overnight at –20°C. Samples were sonicated 3× briefly in an ice bath for 20s and frozen overnight at –20°C. This step was repeated three times to allow ice crystals to break up the pellets.

4.3.4 Quantification of samples using the 2-D Quant Kit

To determine the protein concentration of the samples, a 2-D Quant Kit (GE Healthcare Life Science) was used. Colour reagent A (5.15 ml) was mixed with colour reagent B (51.5 µl). A BSA standard was prepared between 0 and 4 µg. Each protein sample (2 µl) was placed in a separate tube and 100 µl of precipitant was added, including to the BSA standard samples. Tubes were vortexed and incubated for 2–3 min at room temperature. Co-precipitant (100 µl) was added and the samples mixed by inversion, then centrifuged at 10,000 × *g* for 5 min and the supernatant discarded. Copper solution (20 µl) and of Milli QH_2O (80 µl) were added and the tube vortexed briefly. Samples were aliquoted into a 96-well plate and 200 µl of assay mix (colour reagents A+B) added to each well. The plate was incubated for 20 min at room temperature. The absorbance of each sample and standard was read at 480 nm and a standard curve created to determine the sample protein concentrations.

4.3.5 Reduction and alkylation

d,l-Dithiothreitol (30 µl of 10 mM; 5 mM final) was added to each sample (30 µl) and the mixture incubated at room temperature for 2h. Iodoacetamide (3 µl of 0.5 M; 25 mM final) was added and the incubation continued in the dark for 30 min. Finally, an additional 30 µl of 10 mM *d,l*-dithiothreitol was added to each sample.

4.3.6 Trypsin digestion

Samples were diluted to 2 M in urea with 50 mM NH_4HCO_3 (26.8 µl). Each sample (76 µg; 0.63 µg/µl) was then digested with trypsin (15µl, 20 ng/µl) by incubation for 6h at room temperature. The same amount of trypsin was added and the incubation continued overnight at 37°C.

4.3.7 ZipTip sample cleanup

Samples (10 µl) were aliquoted into Eppendorf tubes and subjected to ZipTip purification (Merck Millipore, Kilsyth, VIC, Australia) for sample binding. The ZipTip was washed with 100% acetonitrile twice, then equilibrated with 1% trifluoroacetic acid (TFA) twice. Samples (10 µg) of peptide digests were bound to the tip by fully depressing the pipette, then aspirated and dispensed through 10 cycles for maximum binding of the mixture. The Zip Tips samples were washed with 1% TFA twice, then 4 µl of 0.1%TFA in 80% acetonitrile was used to elute the peptides from the tips. Buffer B (0.1% formic acid in acetonitrile; 96 µl) was added and the samples placed in mass spectrometer tubes.

4.3.8 Preparation of HPLC-QTRAP 5500 mass spectrometer for MRM analysis

Chromatography was performed using an 1100/1200 capillary LC (Agilent Technologies, Mulgrave, Vic, Australia) with the following buffers: Buffer A (5% acetonitrile, 0.1 % formic acid) and Buffer B (0.1% formic acid in acetonitrile). Samples (20 µl) were loaded onto the column trap (ZORBAX 300SB-C_{18}, 5 × 0.3 mm, 5 µm; Agilent Technologies) and washed for 5 min with Buffer A delivered at a flow rate of 20 µl/min. A QTRAP 5500 mass spectrometer (AB SCIEX) with a TurboSpray ion source in positive ion mode was used to detect the peptides. The settings for the ion source were: declustering potential 80V, entrance potential 10V, collision cell exit potential 35V,

curtain gas 20 psi, collision gas 'high', ionspray voltage 4kV, temperature 150°C, with first and second ion source gases set at 20 psi.

4.3.8.1 Choosing the protein of interest, peptide and transitions

Targeted protein accession numbers were input to the MRMPilot software, which were: neuroligin-1, NP_055747, neuroligin-2, AAM46111) and β-neurexin-1, BAA87821.1. Multiple tryptic peptides were obtained and the best peptide sequences that had lengths of 4–22 amino acids and were free of any known chemical and/or post-translational modifications were chosen. Peptides with methionine or cysteine residues were deselected because they are prone to modification (oxidation and alkylation, respectively). The best peptides were utilized for automated MRM selection and method building. For each peptide at least four MRM transitions were selected.

4.3.8.2 Verification of peptide selections and development of transitions

The digested peptides were subjected to analysis with the QTRAP 5500 mass spectrometer in MRM-initiated detection and sequencing (MIDAS) mode to produce MS/MS spectra of targeted transitions. MIDAS involves MRM-based high-sensitivity product-ion scans and triggers a full MS/MS scan for sequence confirmation. All transitions that had peak intensities below 800 cps, as well as nonspecific multiple peaks, were excluded. IDA files were exported to MASCOT (generic format) for a database search against the UniProt database (MASCOT: http://www.matrixscience.com) for human entries with carbamidomethylation as fixed and methionine oxidation as variable modifications. The following setting was used for the search: Peptide tolerance 0.4Da, MS/MS tolerance 0.4Da, peptide charge 2+, 3+ and 4+. Because none of the peptides were matched to the target protein MASCOT search, manual sequencing of the MS/MS spectra using PeakView software (AB SCIEX) was performed.

4.3.9 MS/MS^{ALL} with SWATH^{TM} Acquisition

4.3.9.1 Membrane sample preparation for SWATH

Brain tissues were slowly frozen and stored in 0.32 M sucrose at –80°C (Dodd et al., 1986). Thawed tissues were homogenized in 10× (w/v) of 0.32M sucrose at 4°C in a motor-driven Teflon-

glass homogenizer at 500 rpm and the suspension centrifuged for 10 min at 756 × *g*. The supernatant was centrifuged at 13,700 × *g* at 4°C for 20 min. The supernatant was discarded and the pellet resuspended in 50 mM Tris-HCl, pH 7.

4.3.9.2 Protein extraction, quantification, digestion and ZipTip

Refer to methods section 4.2.3, 4.2.4, 4.2.5, 4.2.6 and 4.2.7.

4.3.9.3 Strong cation exchange (SCX) with the LC Agilent fractionator

The system was equipped with a 4.6 × 50 mm SCX column (ZORBAX Bio-SCX Series II). The following buffers were used for washing and column preparation: Buffer A (0.5% acetic acid, 2% acetonitrile), Buffer B (0.5% acetic acid, 2% acetonitrile 250 mM ammonium acetate). A sample (50 µg) of the reduced and alkylated protein was loaded into the injector port at 0.4 ml/min.

Proteins were eluted with buffers A and B in 96-well plates according to charge and salt gradient. Flow-through fractions (47 in total) were collected in a 96-well plate over 45 min. Adjacent fractions were combined to obtain 6 pooled fractions that were subjected to ZipTip clean-up (Section 4.3.7) for desalting before MS analysis.

4.3.9.4 In-gel digestion

Protein concentration was measured with the 2-D Quant protein assay kit (Section 4.3.4). Samples (40 µg of protein) were loaded onto a 1 mm 10-well 8% SDS-PAGE gel and separated for 1h at 120V. The gel was stained with Coomassie Brilliant Blue (Sigma) in 50% methanol and 10% glacial acetic acid for 1h then destained overnight with 45% methanol, 5% acetic acid at room temperature. Neuroligin-1 and neuroligin-2 proteins bands, which separated at 110 and 95 kDa respectively, were manually excised from the gel, destained and dehydrated with acetonitrile, reduced and alkylated with 10 mM dithiothreitol at 60°C for 30 min and 50 mM iodoacetamide at room temperature for 30 min in the dark. Prior to enzymatic digestion, excess reagents were removed and the gel pieces washed twice with 50 mM NH_4HCO_3 and dehydrated with 100% acetonitrile. For protein digestion, gel samples were incubated with 10 µl of trypsin (10 ng/µl in 50 mM NH_4HCO_3)

for 15 min at 4°C. An additional 15 µl of 50 mM NH_4HCO buffer was added and the incubation overnight at 37°C. Peptides were extracted from the gel by sonication twice for 10 min with 50 µl of 50% acetonitrile/0.1% trifluoracetic acid. Samples were vacuum centrifuged to remove acetonitrile and ZipTipped before MS was performed.

4.3.9.5 Sample analysis by mass spectrometry and chromatography

Samples were analysed using an HPLC system connected to a TripleTof 5600 mass spectrometer (AB SCIEX). Samples were acquired in data dependent mode to obtain MS/MS spectra for the most abundant ions.

4.3.9.6 Bioinformatics database search

Mass spectrometer data were searched using the MASCOT server v2.3.02. Peak lists for MASCOT searches were produced by AB SCIEX MGF converter. MS/MS datasets were also analysed using ProteinPilot™ software v4.5 (AB SCIEX), which uses the Paragon algorithm (Shilov et al., 2007) to search the SwissProt database. The settings for the search were as follows: cysteine alkylation, iodoacetamide; digestion, trypsin; fixed modification, carbamidomethylation; variable modification, methionine oxidation; detected protein *P*-value threshold 0.05.

4.4 Results

Three proteins were targeted for this study: neuroligin-1, neuroligin-2 and β-neurexin-1. Proteotypic peptides (that uniquely represent these proteins) were chosen using MRM Pilot software (Fig. 4.5) and the best peptides with the highest mean intensity and best CV value were added from the peptide selection view (Fig. 4.6). Lists of all possible trypsin-digested peptides were produced for the three target proteins. To determine the true total protein abundance in the samples, peptides with methionine, cysteine, or amino acids with known chemical and/or post-translational modifications were excluded. Due to the susceptibility of methionine to oxidation and cysteine to alkylation, quantitative data attained from target peptides with these amino acids could produce errors. To produce a reliable MRM and to evaluate which is the most sensitive and reproducible, replicate samples are required. Fig. 4.7 is an example of results from running several replicates.

Different transitions were produced for these proteins. Several transitions were produced for each peptide (Table 4.2), and after MIDAS analysis on the QTRAP 5500, transitions that gave peak intensities below 700 cps, or different indistinct peaks, were removed from the list. To prevent false characterizations, MS/MS data produced from MIDAS analysis were searched against MASCOT to confirm protein identity. The MASCOT search failed to identify any peptides from neuroligin-1, neuroligin-2 or β-neurexin-1. As none of the peptides matched the MASCOT search, manual sequencing of the MS/MS spectra from the MIDAS analysis were conducted to confirm their sequence using the fragment ion table for each peptide. B-, y- and a-ions between 100 and 999 *m/z* were searched within the spectra for all peptides. None of the peptides from the three proteins could be sequenced correctly (Figs 4.8, 4.9). The incorrect matching might result from highly abundant peptide/s with similar *m/z* values co-eluting with the peptides of interest and producing an error to the targeted transitions signal.

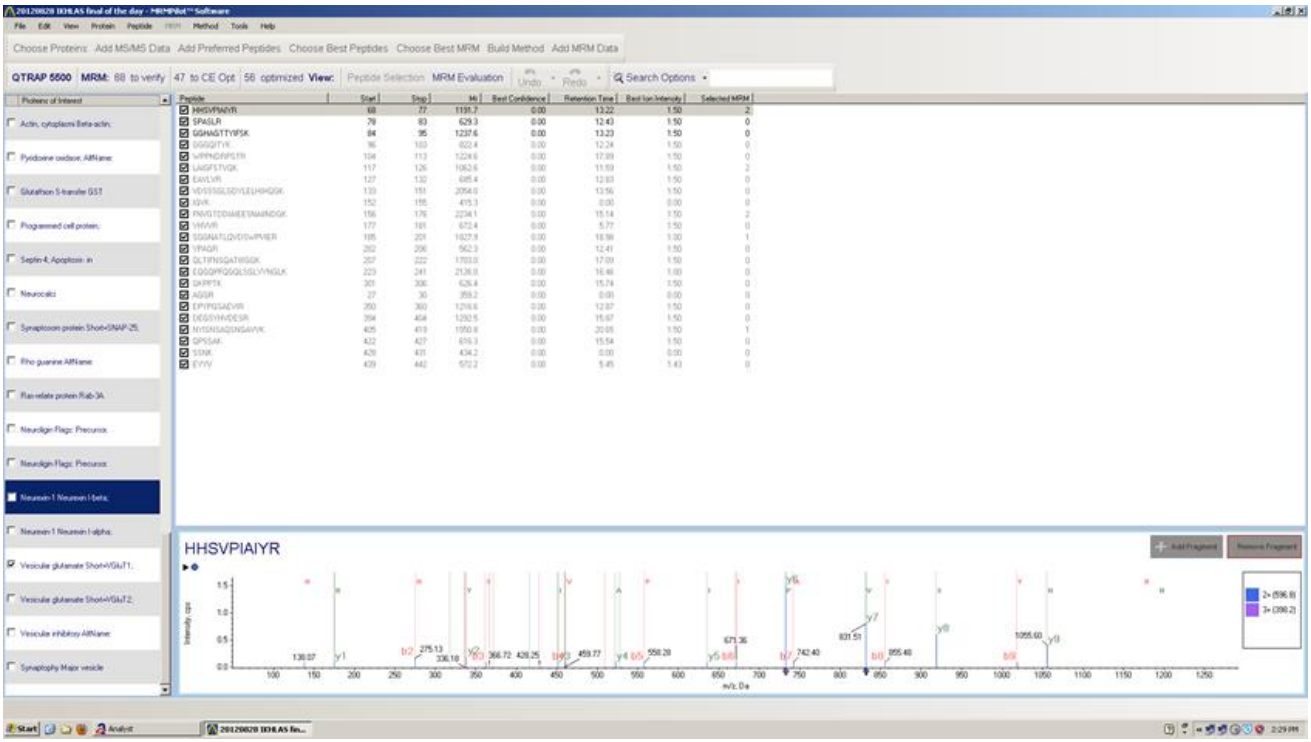

Fig. 4.5. MRM peptide selection view. After importing proteins into MRM Pilot Software, MRM transitions are created. The best transitions for the best peptides for each protein were selected. The peptide fragment data is shown in the bottom pane for the selected peptide from neuroligin-1protein.

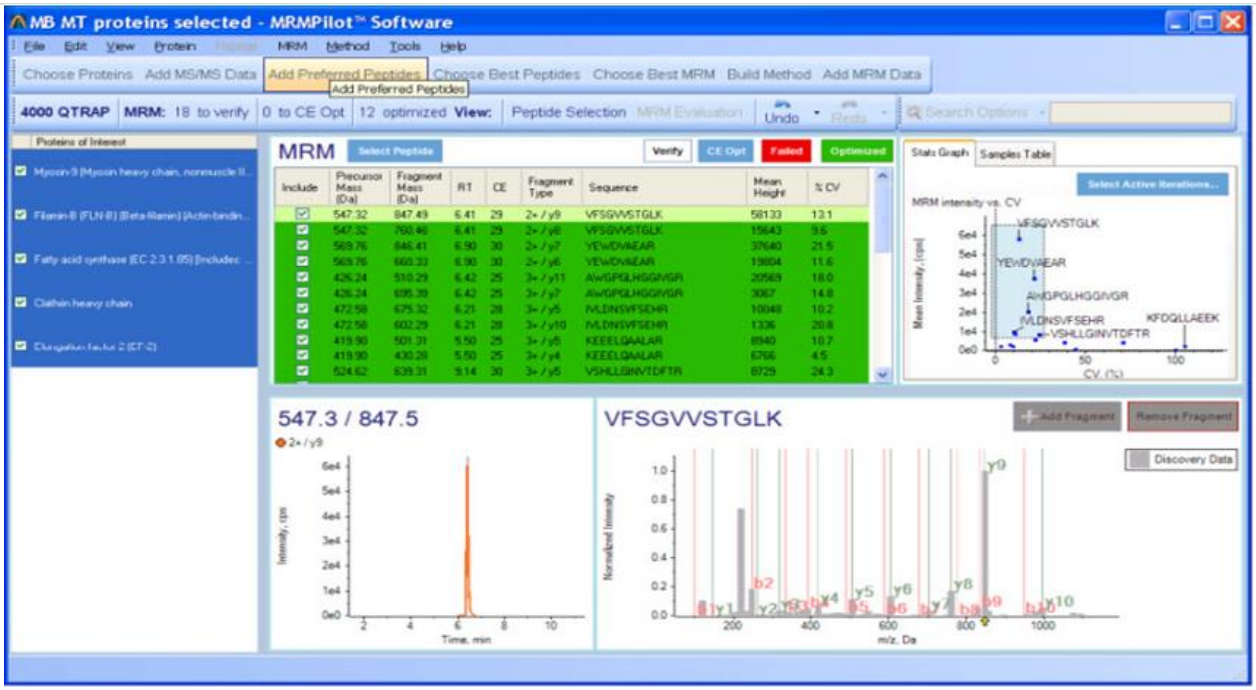

Fig. 4.6. MRM Table view. The table displays panes of data related to MRM for the selected protein. A table of all peptide MRM transitions is shown in the top pane for the selected protein. The top right pane displays a graph of MRM intensity *vs* variation (% CV) used to study the quality of the MRM transitions. This graph allows easy visualization of peptides with the highest intensity and reproducibility for quantitative purpose. The bottom pane has overlays of all extracted ion chromatograms (XIC) for the chosen MRM, spectra for the selected MRM, and full-scan MS/MS data acquired using the MIDAS™ Workflow for confirmatory purposes.

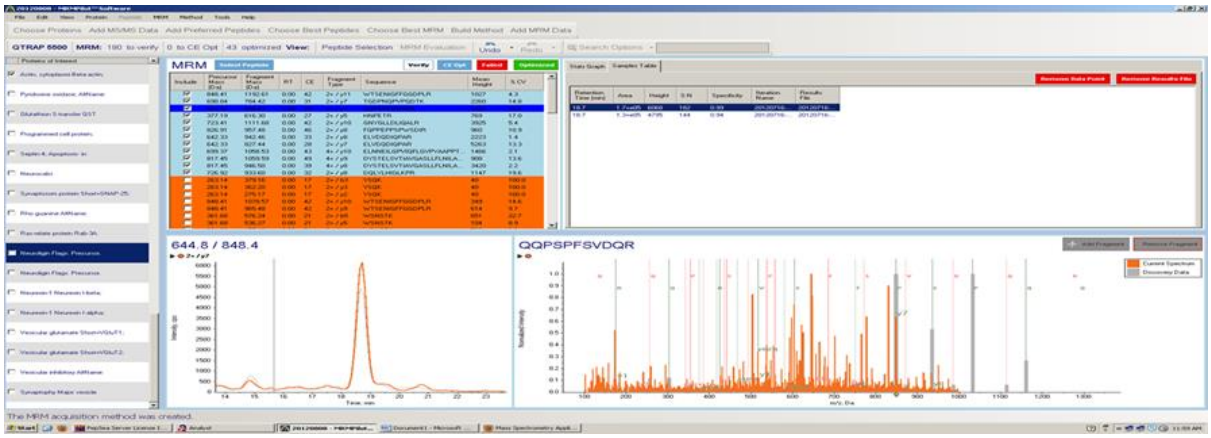

Fig. 4.7. MRM validation of the transitions. The summary graph in the top right of the MRM Table view shows the best MRM selected for optimization highlighted in blue and the remaining poor/failed MRM transitions highlighted in orange.

Table 4.2. MRM transitions and parameters for proteins of interest from MRMpilot software.

Accession Nº Protein name	Precursor mass, Da	Fragment mass, Da	RT[1]	CE[2]	Fragment type	Sequence	Mean height	CV %
NP_055747 Neuroligin-1	644.82	848.43	17.45	33	2+ / y7	QQPSPFSVDQR	5432	16.6
	642.33	827.44	14.03	33	2+ / y7	ELVDQDIQPAR	5263	13.3
	723.41	1111.68	15.61	37	2+ / y10	GNYGLLDLIQALR	3925	5.4
	817.45	946.5	20.3	44	4+ / y8	DYSTELSVTIAVGASLLFLNILAFAALYYK	3420	2.2
	698.84	784.42	16.59	36	2+ / y7	TGDPNQPVPQDTK	2260	14.8
	642.33	942.46	14.03	33	2+ / y8	ELVDQDIQPAR	2223	1.4
	699.37	1058.53	17.59	38	4+ / y10	ELNNEILGPVIQFLGVPYAAPPTGER	1466	2.1
	726.92	933.6	16.96	37	2+ / y8	DQLYLHIGLKPR	1147	19.6
	848.41	1192.61	20.21	42	2+ / y11	WTSENIGFFGGDPLR	1027	4.3
	826.91	957.48	16.27	41	2+ / y8	FQPPEPPSPWSDIR	960	10.9
	817.45	1059.59	20.3	44	4+ / y9	DYSTELSVTIAVGASLLFLNILAFAALYYK	908	13.6
	377.19	616.3	13.21	22	2+ / y5	HNPETR	769	17
AAM46111 Neuroligin-2	981.98	1087.57	18.65	48	2+ / y11	GGGGPGGGAPGGPGLGLGSLGEER	30807	1.9
	707.7	1134.59	13.99	39	3+ / y9	AIAQSGTAISSWSVNYQPLK	2390	6.6
	718.4	1141.64	14.29	40	3+ / y11	TLLALFTDHQWVAPAVATAK	1061	12.2
	707.7	948.51	13.99	39	3+ / y8	AIAQSGTAISSWSVNYQPLK	1020	12.1
	769.89	1166.6	17.03	39	2+ / y11	FQPPEAPASWPGVR	729	8.4
	654.99	1184.63	18.65	37	3+ / y12	GGGGPGGGAPGGPGLGLGSLGEER	248	24.3
NP_620072.1 β-Neurexin-1	745.7	931.48	14.72	41	3+ / y9	FNVGTDDIAIEESNAIINDGK	996	2.6
	532.31	766.41	12.69	28	2+ / y7	LAIGFSTVQK	905	5.1
	532.31	709.39	12.69	28	2+ / y6	LAIGFSTVQK	762	23.9
	776.39	873.48	21.3	39	2+ / y9	NYISNSAQSNGAVVK	725	15.8
	914.96	1228.63	19.51	45	2+ / y10	SGGNATLQVDSWPVIER	675	30.5
	596.83	831.51	13.32	31	2+ / y7	HHSVPIAIYR	637	9.5
	745.7	1189.57	14.72	41	3+ / y11	FNVGTDDIAIEESNAIINDGK	583	0.6
	596.83	732.44	13.32	31	2+ / y6	HHSVPIAIYR	488	4.6

	532.31	879.49	12.69	28	2+ / y8	LAIGFSTVQK	456	6.4
	745.7	1060.53	14.72	41	3+ / y10	FNVGTDDIAIEESNAIINDGK	411	7.2
	613.31	845.42	16.37	32	2+ / y7	WPPNDRPSTR	342	1.4
	609.31	991.52	15.09	32	2+ / y9	EPYPGSAEVIR	313	6.6
	776.39	1074.55	21.3	39	2+ / y11	NYISNSAQSNGAVVK	227	29.9
	647.27	1049.46	17.37	33	2+ / y9	DEGSYHVDESR	203	39
	412.22	766.41	11.68	23	2+ / y7	GGGQITYK	195	60.9
	343.71	557.38	11.89	20	2+ / y5	EAVLVR	98	17.3
	282.15	332.16	9.82	17	2+ / b3	YPAGR	52	32.6
	309.17	471.22	17.94	19	2+ / b5	QPSSAK	35	30.7
	412.22	652.37	11.68	23	2+ / y5	GGGQITYK	34	87.3
	314.19	570.36	18.08	19	2+ / y5	GKPPTK	27	100
	315.68	456.25	10	19	2+ / b5	SPASLR	27	100
	282.15	400.23	9.82	17	2+ / y4	YPAGR	27	100
	287.13	444.21	4.91	18	2+ / y3	EYYV	20	49.5
	315.68	543.32	10	19	2+ / y5	SPASLR	20	49.5
BAA87821.1	515.25	784.4	12.72	28	2+ / y6	TGSISFDFR	5168	14.5
α-Neurexin-1	516.3	918.5	15.67	28	2+ / y9	ITTQITAGAR	4064	10.1
	559.32	777.41	18.44	30	2+ / y7	NIIADPVTFK	2396	6.7
	380.24	545.34	12.36	22	2+ / y5	LTLASVR	1647	10.7
	623.29	869.43	15.58	32	2+ / y7	FNDNAWHDVK	1137	2.7
	500.75	742.41	17.76	27	2+ / y6	EEYIATFK	1062	20.1
	547.3	820.49	15.3	29	2+ / y7	SADYVNLALK	976	2.6
	547.3	935.52	15.3	29	2+ / y8	SADYVNLALK	777	15.4
	435.76	563.36	14.11	24	2+ / y5	IHGVVAFK	679	2.8
	559.32	706.38	18.44	30	2+ / y6	NIIADPVTFK	662	17.9
	516.3	716.4	15.67	28	2+ / y7	ITTQITAGAR	611	15.2
	507.76	899.49	14.75	27	2+ / y8	DTSNLHTVK	585	1.9
	511.76	794.4	13.18	28	2+ / y7	DLFIDGQSK	550	15.8
	387.21	660.33	12.58	22	2+ / y6	LELDAGR	516	1.5
	524.29	689.39	16.29	28	2+ / y6	SGTISVNTLR	457	12.4
	511.78	707.41	13.06	28	2+ / y7	SDLYIGGVAK	440	55
	778.37	1056.49	16.5	43	3+ / y8	GPETLFAGYNLNDNEWHTVR	438	5.7
	524.29	802.48	16.29	28	2+ / y7	SGTISVNTLR	431	0.8
	689.86	949.5	16.98	35	2+ / y8	NTTLFIDQVEAK	401	5.5
	387.21	599.3	12.58	22	2+ / b6	LELDAGR	344	1
	524.29	903.53	16.29	28	2+ / y8	SGTISVNTLR	294	11.8

500.75	871.46	17.76	27	2+ / y7	EEYIATFK	280	6.6
263.64	379.21	20.13	17	2+ / y3	FGFR	273	32.6
632	1161.63	17.82	36	3+ / y11	GYLHYVFDLGNGANLIK	204	1.4
260.64	391.23	17.38	16	2+ / y3	EPFK	123	48.3
272.64	416.21	17.73	17	2+ / y4	QGDPK	80	100
260.64	374.17	17.38	16	2+ / b3	EPFK	55	97.7
263.64	352.17	20.13	17	2+ / b3	FGFR	40	100
309.18	504.28	9.87	19	2+ / y4	LELSR	40	100
259.16	343.2	7.23	16	2+ / b3	TLQR	40	100
324.15	532.26	8.19	19	2+ / y4	DGWNR	27	100
270.64	310.18	10.1	17	2+ / y2	ETYK	27	100
266.16	474.28	7.46	17	2+ / y3	GWIR	13	100

Notes: [1], RT, retention time detected for a peak matching the transitions listed that subsequently was found to not match the specific protein of interest; [2], CE, collision energy, V.

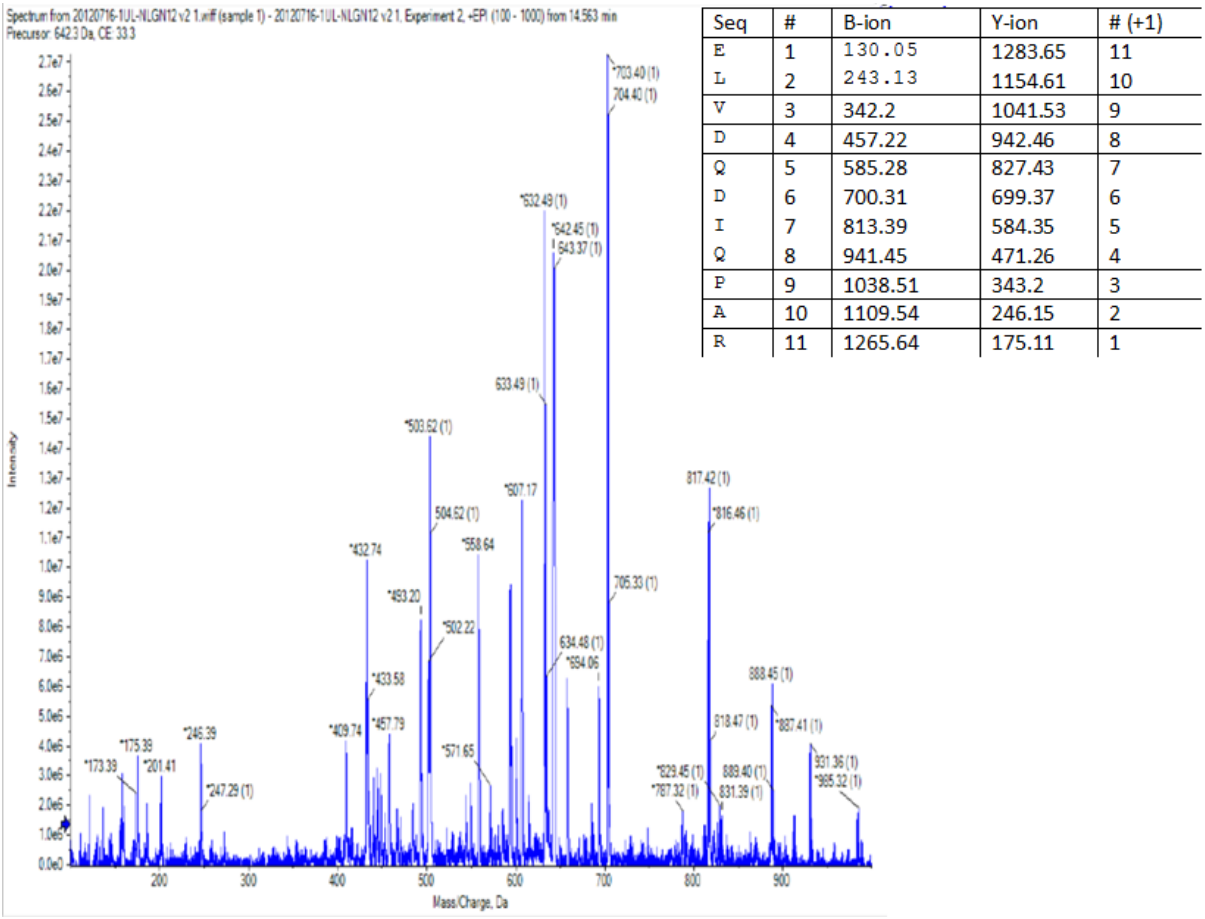

Fig. 4.8. Validation of transitions by examination of the full MS/MS spectrum during MRM set-up. Example of manual sequencing for a peptide (ELVDQDIQPAR) that

could not be identified by MASCOT search. The fragment ion for the peptide was determined using the web-base fragment ion calculator http://db.systemsbiology.net:8080/proteomicsToolkit/FragIonServlet.html. The table at the top right shows the b/y ions obtained from the fragment ion calculator for the peptide. A peak that matched the calculated b- and y-ion masses was searched on a MS/MS spectrum.

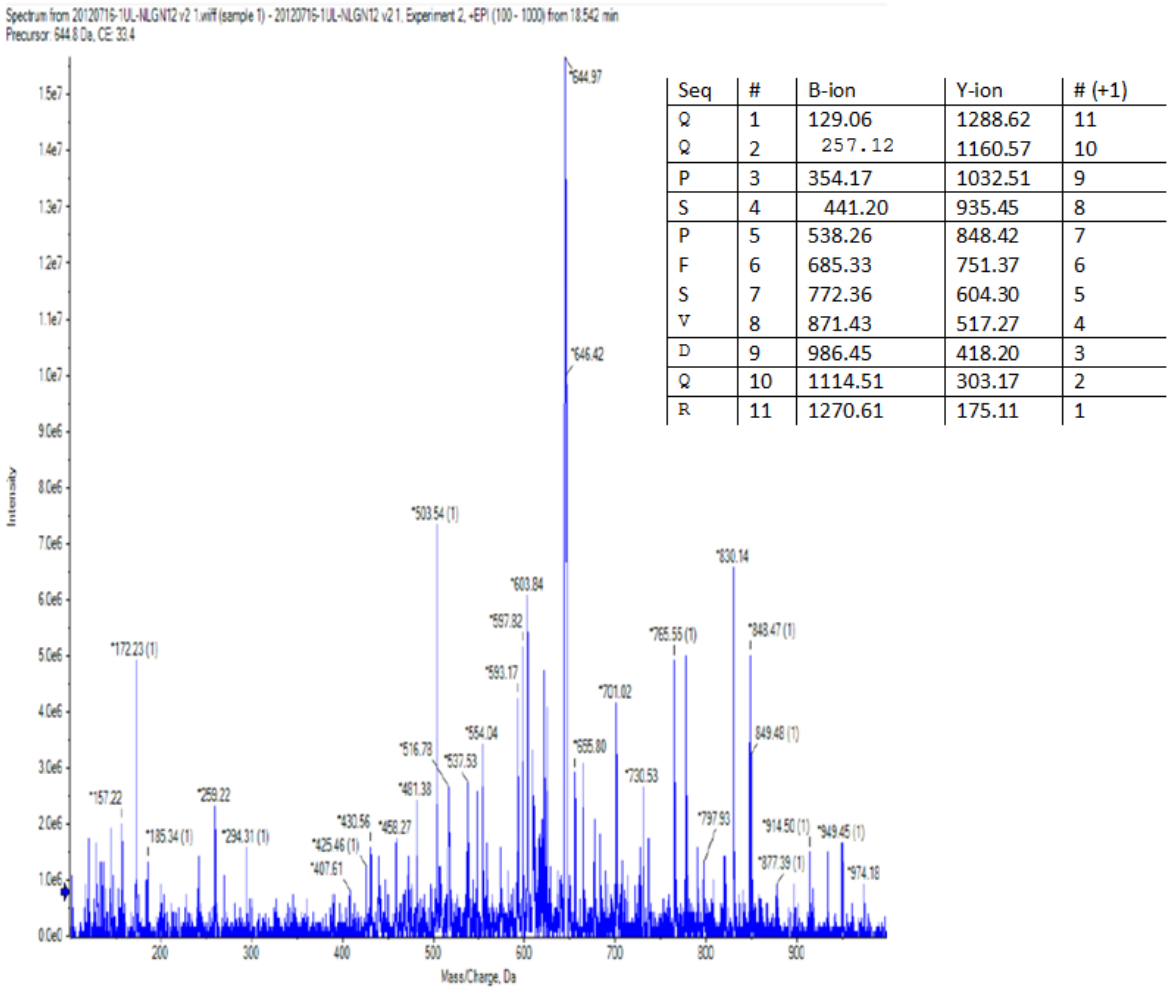

Seq	#	B-ion	Y-ion	# (+1)
Q	1	129.06	1288.62	11
Q	2	257.12	1160.57	10
P	3	354.17	1032.51	9
S	4	441.20	935.45	8
P	5	538.26	848.42	7
F	6	685.33	751.37	6
S	7	772.36	604.30	5
V	8	871.43	517.27	4
D	9	986.45	418.20	3
Q	10	1114.51	303.17	2
R	11	1270.61	175.11	1

Fig. 4.9. Validation of the transitions by examination of the full MS/MS spectrum in the MRM set-up. Example of manual sequencing for a peptide (QQPSPFSVDQR) peptide that could not be identified using MASCOT search. Detail as for Fig. 4.8.

The IDA results from in-solution samples were searched using both MASCOT and Protein Pilot software. This approach detected several hundred proteins that are listed in Supplementary Table 4.3 in the Appendix for this chapter. However, none of the proteins of interest (neuroligin-1, neuroligin-2 or β-neurexin) was found in the search lists. This could be due to the complexity of the

sample or to the low abundance of these proteins. Hence, SCX fractionation was used prior to mass spectrometry. Data obtained were searched using both MASCOT and Protein Pilot. Again, more than 200 proteins were identified that did not include the proteins of interest (Supplementary Table 4.4 in the Appendix for this chapter).

A final approach used to find these proteins was SDS-PAGE separation and in-gel digestion. Sections of gel representing proteins around 100 kDa in size was excised and the protein extracted. MASCOT search identified all five neuroligin proteins (neuroligin-1, -2, -3, -4 and -4Y). However, each protein identification was based on only one or two peptides, with one peptide in common to all five proteins. This meant that no unique peptide was detected for any individual protein. Some of the scores of peptides matching to neuroligin proteins were very low, such as 6, 1 and 2 for neuroligin-1, neuroligin-2 and neuroligin-3 respectively, which is not reliable data for quantification (Table 4.5).

Table 4.5. Neuroligin peptides obtained from in-gel digestion.

Query	Observed	Mr(expt)	Mr(calc)	ppm	Miss	Score	Expect	Rank	Unique	Peptide
NLGN1_HUMAN: Mass: 94574 Score: 74 Matches: 4(2) Sequences: 2(1) emPAI: 0.03										
6676	723.4040	1444.7934	1444.8038	–7.16	0	6	19	1	U	K.GNYGLLDLIQALR.W
6934	738.9209	1475.8272	1475.7984	19.5	0	49	0.00064	1	–	R.LGVLGFLSTGDQAAK.G
NLGN2_HUMAN: Mass: 91333 Score: 218 Matches: 7(5) Sequences: 3(2) emPAI: 0.07										
2802	562.3078	1122.6010	1122.5822	16.8	0	1	96	8	U	R.FPVVNTAYGR.V
6790	730.9128	1459.8110	1459.7783	22.4	0	90	5.1×10^{-8}	1	–	K.GNYGLLDQIQALR
6934	738.9209	1475.8272	1475.7984	19.5	0	49	0.00064	1	–	R.LGVLGFLSTGDQAAK
NLGN3_HUMAN: Mass: 94463 Score: 168 Matches: 5(3) Sequences: 3(1) emPAI: 0.03										
6790	730.9128	1459.8110	1459.7783	22.4	0	90	5.1×10^{-8}	1	–	K.GNYGLLDQIQALR
7434	766.9205	1531.8264	1531.8722	–29.87	1	20	0.59	2	U	R.LTALPDYTLTLRR
8480	846.9831	1691.9516	1691.9433	4.95	0	2	23	8	U	R.SLCLTLWFLSLALR
NLGN4_HUMAN Mass: 92427 Score: 213 Matches: 6(5) Sequences: 2(2) emPAI: 0.07										
6790	730.9128	1459.8110	1459.7783	22.4	0	90	5.1×10^{-8}	1	–	K.GNYGLLDQIQALR.W
7090	745.9289	1489.8432	1489.8140	19.6	0	54	0.00016	1	U	R.LGILGFLSTGDQAAK.G

4.4.1 Identification of other synaptic proteins by these methods

Several hundred membrane proteins as well as synaptic proteins were identified using quadrupole Triple TOF 5600 mass spectrometry and MASCOT search with the different approaches

utilized. Examples of these were synapsin-1, Vesicle-associated membrane protein 2, excitatory amino acid transporter 1 and 2, synapsin-2, synaptosomal-associated protein 25, septin-5 and -9, synaptic vesicle membrane protein, synaptic vesicle glycoprotein, synaptophysin, neural cell adhesion molecule, cadherin and vesicular glutamate transporter 3. These proteins were detected with sufficient number of unique peptides and a high score of identity. An example is shown below:

Protein View: EAA2_HUMAN; Excitatory amino acid transporter 2 OS=Homo sapiens GN=SLC1A2 PE=1 SV=2; Database: SwissProt; Score: 58; Nominal mass (Mr): 62577; Calculated pI: 6.09; Taxonomy: *Homo sapiens*; Protein sequence coverage: 6%

Matched peptides are shown in bold.

1	**MASTEGANNM**	**PKQVEVR**MHD	SHLGSEEPKH	RHLGLRLCDK	LGKNLLLTLT
51	VFGVILGAVC	GGLLRLASPI	HPDVVMLIAF	PGDILMRMLK	MLILPLIISS
101	LITGLSGLDA	KASGRLGTRA	MVYYMSTTII	AAVLGVILVL	AIHPGNPKLK
151	KQLGPGKKND	EVSSLDAFLD	LIRNLFPENL	VQACFQQIQT	VTKKVLVAPP
201	PDEEANATSA	VVSLLNETVT	EVPEETKMVI	KKGLEFKDGM	NVLGLIGFFI
251	AFGIAMGKMG	DQAKLMVDFF	NILNEIVMKL	VIMIMWYSPL	GIACLICGKI
301	IAIKDLEVVA	RQLGMYMVTV	IIGLIIHGGI	FLPLIYFVVT	RKNPFSFFAG
351	IFQAWITALG	TASSAGTLPV	TFRCLEENLG	IDKRVTRFVL	PVGATINMDG
401	TALYEAVAAI	FIAQMNGVVL	DGGQIVTVSL	TATLASVGAA	SIPSAGLVTM
451	LLILTAVGLP	TEDISLLVAV	DWLLDRMRTS	VNVVGDSFGA	GIVYHLSK**SE**
501	**LDTIDSQHRV**	**HEDIEMTK**TQ	SIYDDMKNHR	ESNSNQCVYA	AHNSVIVDEC
551	KVTLAANGKS	ADCSVEEEPW	KREK		

4.5 Discussion

The purpose of the study in this chapter was to validate the quantifications of neuroligin, and neurexin proteins in human autopsy brain tissues from AD cases and controls performed in chapter 3. It is essential to use more accurate and sensitive techniques to validate the immunoblotting approach, due to the possibility of off-target antibody binding. The study aimed to demonstrate the feasibility of isolating the neurexin-neuroligin complex from autopsy specimens for quantitative mass spectrometric proteomic analysis. MRM was chosen for its advantages of capacity for high

throughput in quantification and ability to detect up to 100 proteins in complex mixtures (Picotti et al., 2009), and its good reproducibility across laboratories (Addona et al., 2009).

Autopsy brain whole-membrane samples from hippocampus, occipital cortex and inferior temporal cortex were and trypsin-digested for mass spectrometry for MRM quantification of the proteins. Samples were run on the QTRAP 5600 for MIDAS analysis and various transitions from each protein were obtained. Due to the possibility of incorrect signals derived from other peptides with precursor/fragment ion pairs of similar *m/z* values for the specific transitions, validation of the transitions obtained were performed both by the parallel acquisition of multiple transitions approach and by scanning the full MS/MS spectra manually. Unfortunately, neither approach matched the transitions to the proteins of interest, which may suggest that these proteins are of very low abundance in brain samples. In consequence I could not use MRM for quantification.

Although MRM is very powerful for proteomics and can detect scarce proteins, it has some limitations. For each protein, at least two peptides are required to confirm the identity of the protein of interest and determine its quantity. It is necessary to differentiate between correctly identified peptides and false positives: digested peptides can share considerable homology. MRM results can be degenerate if there are sequence similarities between the target peptide and any other peptide in the sample. In the current study, I could not obtain any transitions matching the protein of interests due to variations in the elution time of the same transitions. This was confirmed by full MS/MS spectra manual sequencing. As a result the technique could not be used.

Alternatively, I attempted to use SWATH, which is a new technique introduced for targeted protein quantification to provide MRM-like reproducibility but with higher multiplexing. Samples of hippocampus, occipital cortex and inferior cortex from AD cases and controls were prepared in solution form (The preparation of these samples resemble that for MRM). To perform SWATH to quantify proteins of interest, samples should be run on an HPLC system connected to a quadrupole triple TOF mass spectrometer to obtain data using an information dependent acquisition mode to generate MS/MS spectra based on the precursor ions detected in the sample. These data were

subsequently analysed using Protein Pilot software and the MASCOT search algorithm to identify the proteins. Unfortunately, none of the proteins of interest was found in any of the samples run on the mass spectrometer. Nevertheless, several hundred proteins were identified in the sample mixture.

Proteomics based on mass spectrometry can to detect and identify very small amounts of proteins in the femtomole to attomole range, but sample complexity can result in difficulties in detecting and quantifying proteins present at two to three orders of magnitude lower than the most abundant ones. Hence, extensive fractionation is crucial to reduce the concentration range and improve the coverage of the proteins in the sample mixture. SCX fractionation was used in the current study to overcome this problem. After fractionation the peptides were run on an HPLC system connected to a Triple TOF mass spectrometer. Data were analysed using both MASCOT search and Protein Pilot software. Many proteins were identified using this approach, but none of them was a protein of interest.

Finally, an alternative approach was used to fractionate the sample mixture, in-gel digestion. This is a popular sample preparation method that offers a simple way of protein pre-fractionation based on size. Subsequent gel excision of the approximate range of the protein of interest means the removal of low- and high-molecular weight proteins irrelevant to the project. In-gel digestion was combined with a gel-staining protocol that does not interfere with protein digestion (Vasilj et al., 2012, Piersma et al., 2013). After the extraction of proteins at the expected molecular weight from the gel, samples were run on an HPLC system connected to a Triple TOF mass spectrometer. Data were analysed using both MASCOT search and Protein Pilot software. This approach gave fewer proteins, but all neuroligin isoforms were found in Mascot search but not in ProteinPilot software. On closer inspection, only two peptides were obtained for neuroligin-1 and neuroligin-4 and three peptides for neuroligin-2 and neuroligin-3. As mentioned above, uniqueness of the peptides to the protein of interest is crucial to the assay. I found one peptide in common to all four proteins (GNYGLLDLIQALR), which left neuroligin-1 and neuroligin-4 with only one peptide and neuroligin-2 and neuroligin-3 with 2 peptides in total. The confidence in the identification scores for the remaining peptides was very low, and did not allow me to confirm that these peptides belong to

the proteins of interest. In consequence, I could not use SWATH to quantify neuroligins and neurexins in AD cases and controls.

The inability to detect a sufficient number of peptides in neuroligin-1, neuroligin-2 and β-neurexin-1 could reflect their relatively low abundance in the synaptic membrane. It is also possible that some of these proteins migrate with more-abundant proteins and are thus difficult to detect by mass spectrometry. It is noteworthy that the low abundance of a protein in a membrane preparation does not necessarily indicate that it is absent from the synaptic terminal *in vivo*. It is more likely that the association of some proteins with other synaptic proteins is disrupted by extraction with the reagents used in the methodology. The inability to detect neurexins and neuroligins in the current study conforms to a previous report on the identification of proteins in the postsynaptic density fraction by mass spectrometry (Walikonis et al., 2000). Multiple synaptic proteins located at the post synaptic density could not be identified, such as SHANK, GKAP, PSD-95 and SAP102 (Müller et al., 1996), even though they have been reported to be enriched in PSD. This is interesting because neuroligin binds to PSD-95 *via* its PDZ domains, and PSD-95 in turn, interacts with GKAP and SHANK, which lie deep in the PSD. GKAP and SHANK also bind through their PDZ domain to the C terminus of PSD-95. All these proteins are located in the PSD and attached to each other, and their strong association to the synaptic membrane could prevent their extraction by the protocols used here. Additional methods, such as high-resolution immunolocalization, will be needed to ascertain the full protein composition of the synaptic proteome. Increasing the amount of starting material or modifying the fractionation strategy, such as immunoprecipitation followed by mass spectrometry, might be worth pursuing in the future.

4.6 Supplementary material for Chapter 4 Appendix

Table 4.3. Membrane proteins identified using in-solution detection.

Table 4.4. Proteins identified by MASCOT search using SCX fractionation.

Chapter 5

5 Quantification of neuroligin-1, neuroligin-2 and β-neurexin-1 mRNA

5.1 Aim of the research

1. To assay *NLGN-1*, *NLGN-2* and *β-NRXN-1* messenger RNA (mRNA) transcript expression in human autopsy brain tissue in AD cases and matched controls.
2. To compare transcript expression across the three brain regions studied.
3. To evaluate the impact of age, gender, and post-mortem delay on transcript expression
4. To assess transcript expression according to severity of AD pathology and *APOE* genotype.

5.2 Introduction

To understand the biological machinery involved in neuronal survival and death, it is important to study gene expression to gain information about cellular pathways. Neuronal functions and behavioural alterations in an organism are modified by gene expression and the resulting functional consequences. The death of a neuron can be mediated by disorders in processes that are derived from altered gene expression, which can lead to functional changes. Cellular pathways in the brain are highly regulated, and minor alterations in mRNA expression can have strong effects. To understand AD ætiology and disease progression, and to aid the development of new therapeutics, the characterization of changes in cellular and molecular pathways responsible for neuronal survival will provide relevant information. Small changes in gene expression can have large impacts on cellular pathways. Alterations of many synaptic proteins involved in mechanisms of plasticity, memory, and learning have been studied at the level of gene transcription. These changes could play roles in synaptic damage. Nerve-endings require mRNA to express the proteins required for synaptic activity. Impairment of LTP occurs prior to neuronal loss in hippocampal neurons harvested from transgenic AD animal models; by analogy, altered gene expression could be implicated in cognitive impairment in AD. Comparisons of confirmed AD cases and controls using autopsy brain tissue have shown differences in the expression of genes involved in memory processing and learning. Most of these studies report down-regulation of these genes in the AD cases.

The structure of the human brain is complicated and heterogeneous. Advanced technologies can be used to quantify transcript expression, including high-throughput gene expression assays (microarrays). Microarray techniques allow researchers to analyse thousands of mRNA transcripts and portray patterns of differentially regulated genes in the disease state. The techniques produce a huge amount of information that highlights pathogenic pathways. A limitation of the microarray approach is the inability to distinguish between gene variants that arise by alternate RNA splicing. Techniques that can be used to validate high-throughput assays include Northern blot, quantitative real time reverse-transcription (RT)-PCR (Gutala and Reddy, 2004, Reddy et al., 2004, Therianos et al., 2004) and *in situ* hybridization (Mirnics et al., 2000, Yang et al., 1999). Each technique has advantages and limitations. Northern blotting, for example, uses electrophoresis to separate RNA transcripts by size, and the transcripts of interest are detected by probe hybridization. This technique can determine minor changes that RNA microarrays cannot, and can yield data about the size of the transcript, but has low sensitivity, is time consuming, and needs large amounts of RNA. The last-mentioned is an issue with the limited amounts of starting material available from autopsy tissues. *In situ* hybridization can be used to determine the location and distribution of mRNA transcripts across tissues, but its facility for quantifying the transcript is low. End-point relative RT-PCR quantifies the transcript at the final stage of a PCR reaction on a DNA acrylamide gel. This technique has some limitations such as limited dynamic range and resolution, poor precision, and it requires post-PCR processing.

Real time RT-PCR is considered the most sensitive quantitative gene transcription assay. It has a broad (10^7) dynamic range and allows the measurement of both abundant and scarce transcripts (Higuchi et al., 1992). There are two RT-PCR chemistry strategies available: fluorescent probes such as TaqMan®, Molecular Beacons, or Scorpions®, and the SYBR® Green method. The SYBR® Green I method utilizes a DNA binding dye that intercalates into the minor groove of double-stranded DNA as the fluorescent reporter. During amplification of the target sequence by PCR, SYBR® Green I attaches to the amplified sequence and then fluoresces, so that as the amplicon concentration increases following each PCR cycle, the fluorescence increases proportionally and can

be quantified. Although this method is cost effective it has the disadvantage that the probe binds to all double-stranded DNA, including primer-dimers and any non-specific products present, some of which cannot be effectively removed from the assay.

RT-PCR quantification by the gene-specific TaqMan® probe and primer method has advantages for quantitative gene expression studies. The assay comprises an 6-carboxyfluorescein (FAM™) dye-labelled TaqMan® minor groove binder (MGB) probe and two PCR primers combined in one tube. As the specific target is amplified the probe gets cleaved, decoupling the fluorescent and quencher moiety and preventing fluorescence resonant energy transfer, so the total reaction fluorescence increases with each amplification cycle. The fluorescence increase takes place in proportion to the original concentration of target mRNA present, which can be accurately quantified. The assay is optimized to run under universal thermal cycling conditions with a final reaction concentration of 250 nM for the probe and 900 nM for each primer. The technique has several advantages over the SYBR Green method in that it is customized, fast, and easy to set up. It is specific and sensitive as well as cost effective compared with microarrays. The TaqMan® probe and primer RT-PCR assay was chosen for the study.

RT-PCR quantification can be either relative or absolute. In relative qRT-PCR the level of the target gene is normalized to a housekeeper reference gene that is uniformly expressed across all samples. Unfortunately, the levels of many commonly used housekeeper genes, which are involved in energy metabolism, cell cycling, communication, and cytoarchitecture, differ between AD cases and controls (Gebhardt et al., 2010). Absolute qRT-PCR is more accurate because it utilizes a standard curve of known concentrations of either RNA or DNA to quantify the target gene. Most absolute quantification methods use known concentrations of recombinant plasmids that contain the transcript of interest to calculate the copy number of the transcript in each unknown sample. In the current study I chose this approach. An absolute TaqMan qRT-PCR assay was developed to quantify the levels of neuroligin-1, neuroligin-2 and β-neurexin mRNA transcript in autopsy brain tissue from AD cases and controls.

5.3 Methods

5.3.1 Tissue collection and storage

See Chapter 3, Section 3.2.1.

Table 5.1. Details of AD cases and controls.

#	Age, y	PMD, h	Gender	ApoE	Pathological score		
					Hipp	ITC	OCC
AD cases							
AD1	65	34.83	M	ε3,ε4	3	3	1
AD2	82	54.92	M	ε3,ε4	3	3	1
AD3	79	26.33	M	ε4,ε4	3	3	1
AD4	91	48.00	F	ε3,ε3	3	3	1
AD5	86	35.50	F	ε3,ε3	2	2	1
AD6	81	1.67	F	ε3,ε3	1	2	1
AD7	82	41.25	F	ε3,ε4	3	3	3
AD8	75	4.00	M	ε4,ε4	3	3	1
AD9	82	15.38	F	ε3,ε3	2	1	1
AD10	66	18.83	M	ε3,ε4	3	3	1
AD11	78	7.50	F	ε2,ε3	3	3	0
AD12	77	19.50	M	ε2,ε3	3	3	2
AD13	84	25.40	M	ε4,ε4	3	2	3
AD14	72	80.00	M	ε4,ε4	3	3	2
Average	78.7 ± 7.1	29.67 ±21	8M, 6F				
Normal controls							
NC1	78	4.00	F	ε3,ε4	0	0	0
NC2	87	21.50	F	ε2,ε3	1	0	0
NC3	82	46.83	M	ε3,ε3	0	0	0
NC4	85	24.50	M	ε2,ε3	0	0	0
NC5	75	24.43	F	ε3,ε3	0	0	0
NC6	68	43.66	F	ε3,ε4	0	0	0
NC7	72	15.41	F	ε3,ε3	1	0	0
NC8	71	7.75	F	ε3,ε4	0	0	0
NC9	78	16.25	M	ε3,ε3	0	0	0
NC10	68	28.16	M	ε2,ε2	0	0	0
NC11	76	24.00	F	ε3,ε3	0	0	0
NC12	73	85.15	M	ε2,ε3	1	0	0
NC13	77	18.00	F	ε3,ε4	0	0	0
NC14	80	47.15	M	ε3,ε3	0	0	0
Average	76.6 ± 5.5	24.8 ± 12.8	6M, 8F				

5.3.2 Case selection and neuropathological classification

Fourteen AD cases and 14 controls were selected and matched as closely as possible for age, PMD and gender. The average age at death for AD cases was 78.7 years, for controls 76.6 years. The average post-mortem delay for the AD cases was 29.7h, for controls 24.8h. Tissue from the three different areas used in other Chapters was obtained from each brain, although some AD cases were replaced because of a lack of available tissue. Each area of each brain was given a neuropathological severity score from 0-3 based on AD hallmarks, which are the severity of neuronal loss and the abundance NFTs and Aβ (Table 5.1).

5.3.3 RNA extraction

RNA was extracted from frozen tissue that had been stored in 0.32 M sucrose at –80°C. The TRIzol® (Invitrogen) extraction protocol was used according to the manufacturer's instructions. Tissue pieces were rapidly thawed and homogenized on ice in 10× (w/v) of TRIzol® using a Polytron® homogenizer (Kinematica). The homogenate was incubated for 5 min at room temp., 0.2× (v/v) of chloroform was added, the mixture incubated at room temp. for 2–3 min with shaking, then centrifuged for 20 min at 10 000 × *g* at 4°C and the aqueous phase transferred to a new tube. A one-tenth volume of isopropanol was added and the mixture incubated at room temp. for 10 min. To deposit the RNA, samples were centrifuged at 10 000 × *g* for 15 min at 4°C. The pellet was resuspended in 1 ml of 75% ethanol and the mixture centrifuged at 10 000 × *g* for 20 min at 4°C. The pellet was dried, resuspended in 50 µl of nuclease-free MilliQ H_2O, and incubated for 10 min at 60°C.

5.3.4 RNA integrity

The quality of the RNA was tested by electrophoresis on a 1.5% agarose/2.2 M formaldehyde gel. The integrity of the RNA was checked using an Agilent RNA 6000 Nano kit as per the manufacturer's instructions. The Agilent software gives an RNA integrity number (RIN) between 1 and 10, where 1 is the poorest quality and 10 is the best (Imbeaud et al., 2005). RNA samples with a

RIN below 2 were discarded. The quantity of RNA was measured by UV spectrometry at the absorbance wavelengths (λ) 240, 280 and 320 nm.

5.3.5 Reverse transcriptase

To remove contaminating genomic DNA, DNase was added (1 µl of 10× DNase I reaction buffer, Fermentas) was added to each 3 µg of RNA and the mixture incubated with 40 U of RNase OUT (Fermentas) and 1 U of RNase-free DNase (Fermentas) for 30 min at –37°C. EDTA was added to a final concentration of 2.27 mM and the incubation continued for 5 min at 75°C.

The synthesis of cDNA was conducted by adding 0.82 µg of DNase and 300 µM dNTPs (Promega), 1 µg of Oligo (dT) 12–18 primers (Promega) and 0.5 µg of random hexamers (Promega) to the RNA. The volume adjusted to 12 µl with nuclease-free MilliQ H_2O and the mixture incubated for 5 min at 65°C. 5× first-strand buffer, 4.8 mM DTT, 40 U of RNaseOUT and 400 U of Superscript III Reverse Transcriptase® (Invitrogen) were added and the mixture incubated for 5 min at 25°C, then for 60 min at 50°C, then for 15 min at 70°C. To remove contamination 2 U of DNase-free ribonuclease H (Invitrogen) was added and the incubation continued for 20 min at 37°C. The cDNA was stored in –80°C.

5.3.6 Standard preparation and dilution

NLGN-1 and *NLGN-2* standards were prepared by the method outlined in Chapter 2, Section 2.2.1. QIAprep Spin Miniprep kits (QIAGEN) were used to purify high-copy plasmid DNA. The concentrations of the plasmids were measured by nanodrop and aliquots of the dilutions were kept at –80°C to prevent degradation and avoid experimental variation between RT-PCR assays (Dhanasekaran et al., 2010). A fresh aliquot of each standard was used for each RT-PCR assay.

β-NRXN-1 plasmid was obtained from GeneArt® Gene Synthesis (Life Technologies). The following is the sequence of the *β-NRXN-1* standard used:

```
1 CCCCGCCATG TACCAGAGGA TGCTCCGGTG CGGCGCCGAG CTGGGCTCGC CCGGGGGCGG
61 CGGCGGCGGC GGCGGCGGCG GCGGCGCAGG GGGGCGCCTG GCCCTGCTTT GGATAGTCCC
121 GCTCACCCTC AGCGGCCTCC TAGGAGTGGC GTGGGGGGCA TCCAGTTTGG GAGCGCACCA
```

```
181 CATCCACCAT TTCCATGGCA GCAGCAAGCA TCATTCAGTG CCTATTGCAA TCTACAGGTC

241 ACCGGCATCC TTGCGAGGCG GACACGCTGG GACGACATAT ATCTTTAGCA AAGGTGGTGG

301 ACAAATCACG TATAAGTGGC CTCCTAATGA CCGACCCAGT ACACGAGCAG ACAGACTGGC

361 CATAGGTTTT AGCACTGTTC AGAAAGAAGC CGTATTGGTG CGAGTGGACA GTTCTTCAGG

421 CTTGGGTGAC TACCTAGAAC TGCATATACA CCAGGGAAAA ATTGGAGTTA AGTTTAATGT

481 TGGGACAGAT GACATCGCCA TTGAAGAATC CAATGCAATC ATTAATGATG GGAAATACCA

541 TGTAGTTCGT TTCACGAGGA GTGGTGGCAA TGCCACGTTG CAGGTGGACA GCTGGCCAGT

601 GATCGAGCGC TACCCTGCAG GGCGTCAGCT CACAATCTTC AATAGCCAAG CAACCATAAT

661 AATTGGCGGG AAAGAGCAGG GCCAGCCCTT CCAGGGCCAG CTCTCTGGGC TGTACTACAA

721 TGGCTTGAAA GTTCTGAATA TGGCAGCCGA AAACGATGCC AACATCGCCA TAGTGGGAAA

781 TGTGAGACTG GTTGGTGAAG TGCCTTCCTC TATGACAACT GAGTCAACAG CCACTGCCAT

841 GCAATCAGAG ATGTCCACAT CAATTATGGA GACTACCACG ACCCTGGCTA CTAGCACAGC

901 CAGAAGAGGA AAGCCCCCGA CAAAAGAACC CATTAGCCAG ACCACAGATG ACATCCTTGT

961 GGCCTCAGCA GAGTGTCCCA GCGATGATGA GGACATTGAC CCCTGTGAGC CGAGCTCAGG

1021TGGGTTAGCC AACCCAACCC GAGCAGGCGG CAGAGAGCCG TATCCAGGCT CAGCAGAAGT

1081 GATCCGGGAG TCCAGCAGCA CCACGGGTAT GGTCGTTGGG ATAGTAGCCG CTGCCGCCCT

1141 GTGC
```

5.3.7 Taqman PCR assay

Assays were carried out in duplicate on MicroAmp® optical 384-well reaction plates (Applied Biosystems) on an ABI Prism® 7900HT Sequence Detection System. cDNA was diluted 1:8; 2 µl was added to each 10 µl reaction mix containing 5 µl PCR universal master mix (Applied Biosystems), 0.5 µl of primer probes (*NLGN1:* Hs00208784_m1; *NLGN2:* Hs00395803_ml; *βNRXN1:* Hs00373346_m1; and *RPL13*; Life Technologies). An EpMotion 5075 robotics system (Eppendorf South Pacific P/L, North Ryde, NSW, Australia) was used to ensure accurate pipetting.

5.3.8 Data Analysis

Multiple comparisons were evaluated by ANCOVA and ANOVA using the SPSS (Chicago, IL, USA) and Statistica (Tulsa, OK, USA) software packages with appropriate *post-hoc* tests. Differences were considered statistically significant at $P < 0.05$.

5.4 Results

RT-PCR assays were utilized to measure the absolute expression of *NLGN1*, *NLGN1* and *βNRXN1* transcxripts in RNA extracted from samples of hippocampus, inferior temporal cortex and occipital cortex from AD and control subjects. The absolute quantities of the three trancripts were calculated by interpolation from their respective known plasmid copy-number standard curves based on their observed Ct value (Fig. 5.1).

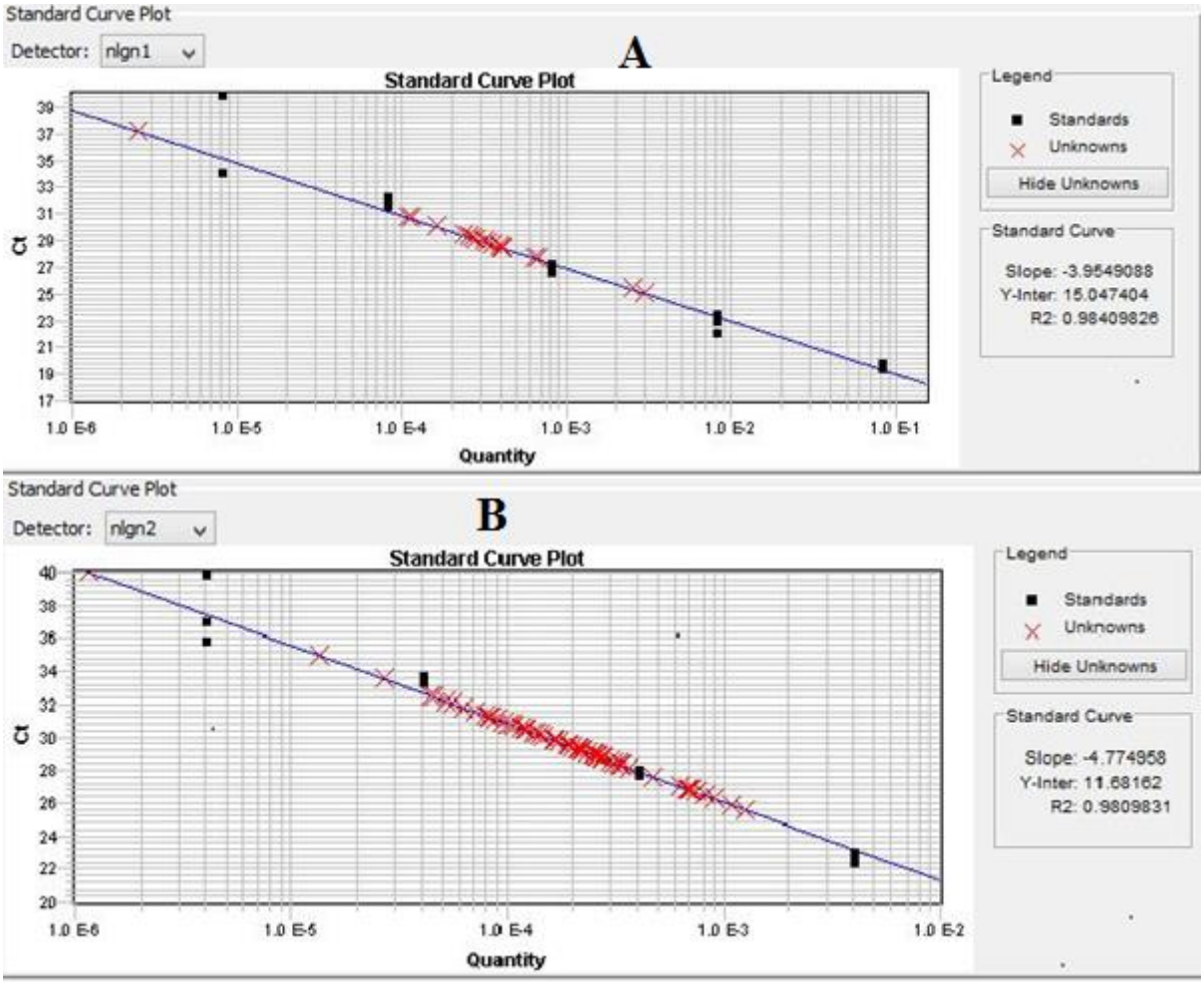

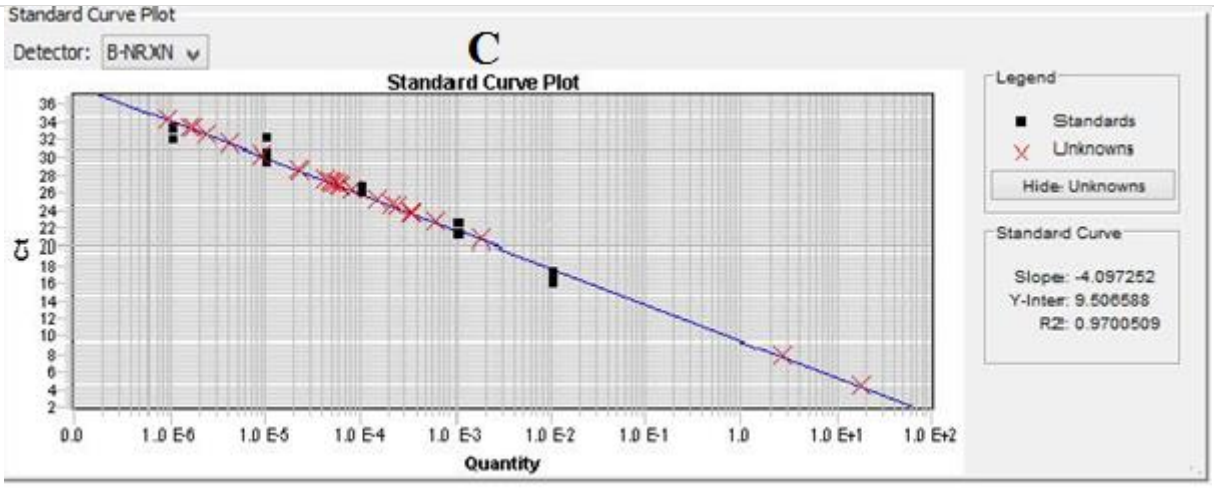

Fig. 5.1. Standard curves for absolute quantification. Standards, black squares, unknowns, red crosses; **A,** *neuroligin-1*, **B,** *neuroligin-2*, **C,** *β-neurexin-1*.

5.4.1 Data distribution

Normal probability plots of non-adjusted levels of *NLGN1*, *NLGN2* and *βNRXN1* showed positively skewed distributions that deviated significantly from normal (Fig. 5.2).

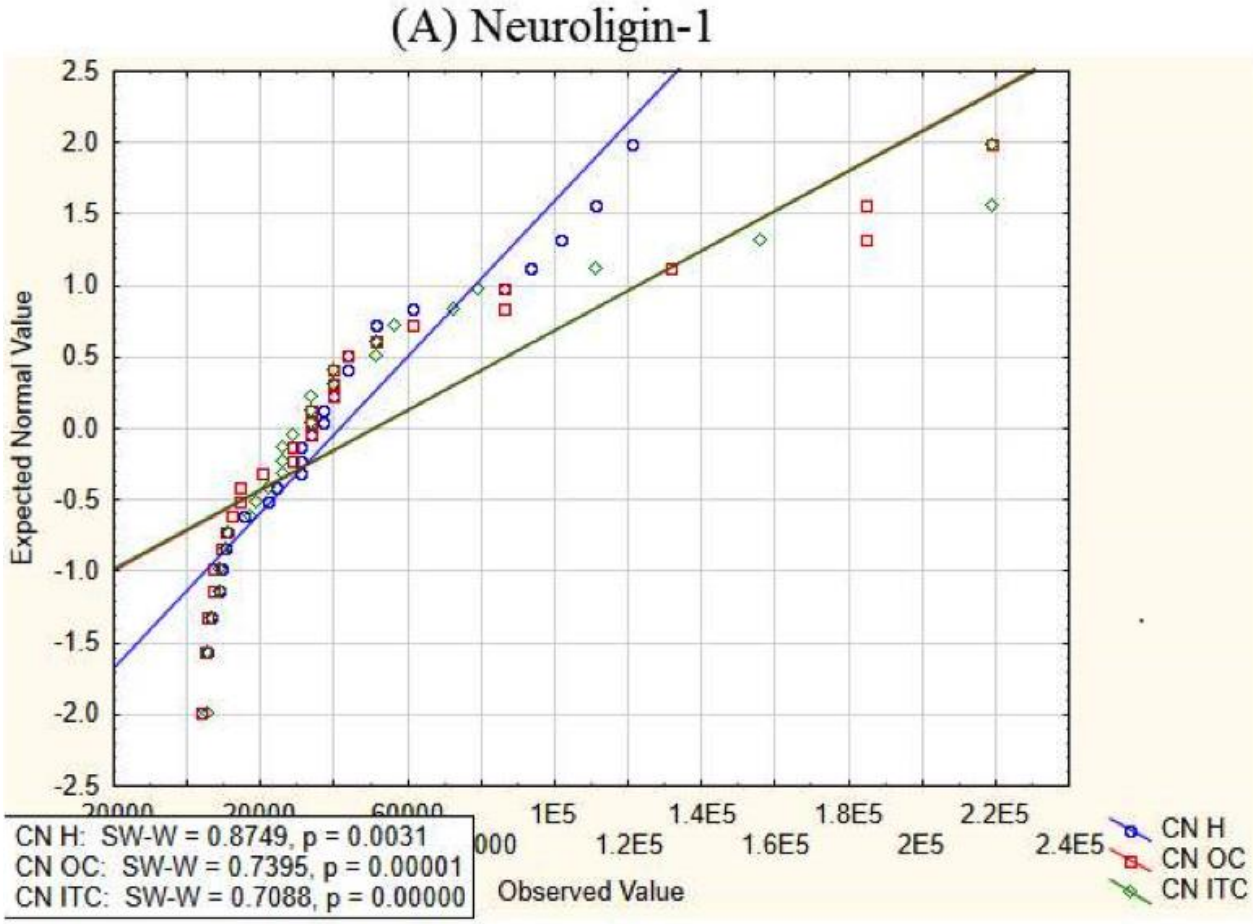

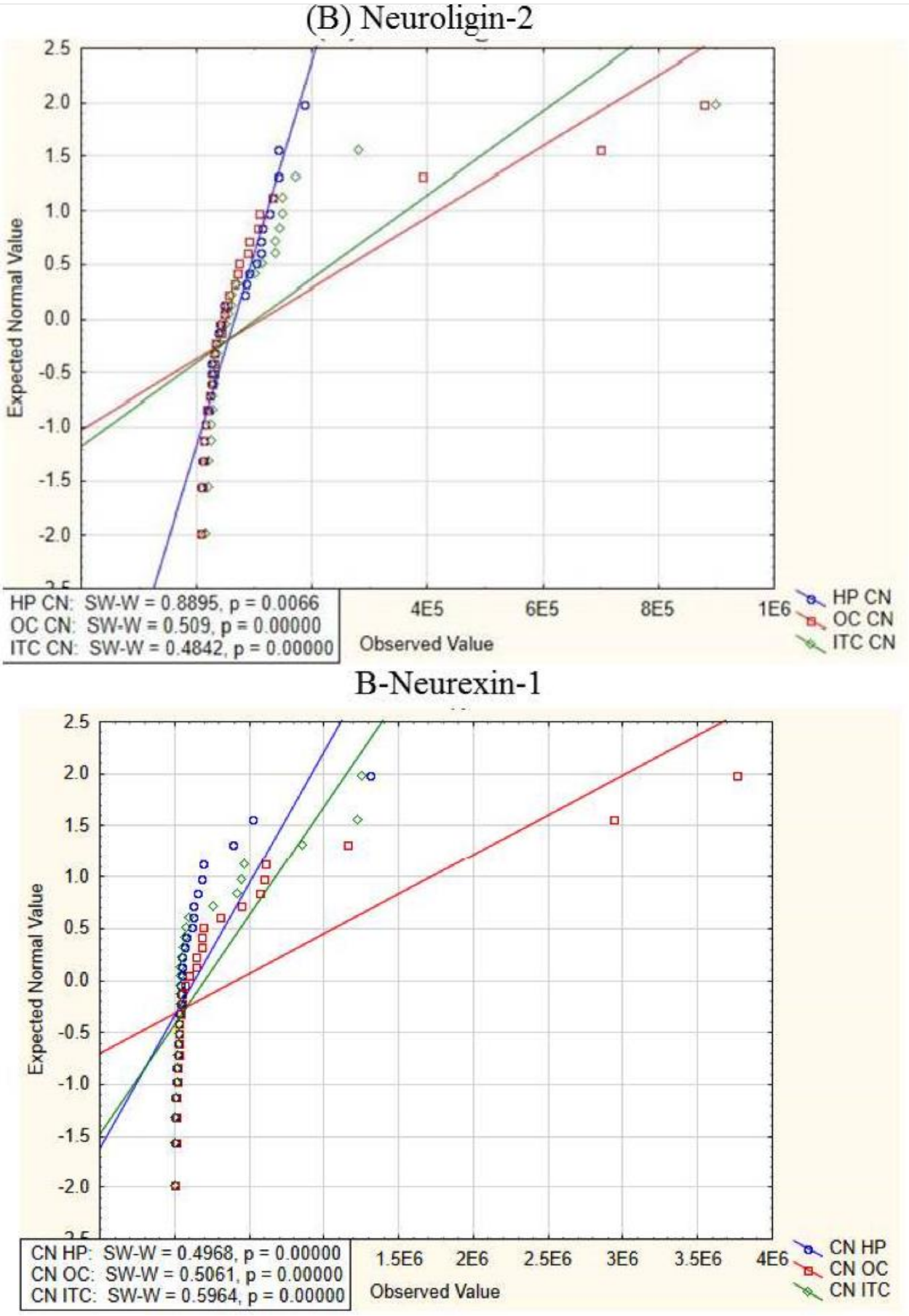

Fig. 5.2. Normal probability plots of transcript expression. **A,** *NLGN1*, **B,** *NLGN2*, **C,**

βNRXN1 across the three areas. Shapiro-Wilks testing showed that all traces deviated significantly from the normal distribution, as shown in the in-graph boxes.

Transforming the values using the Box-Cox algorithm, available in the Statistica package, stabilized the variances and corrected the distributions (Fig. 5.3). This permitted parametric statistics to be used for the rest of the analyses, which was critical because the aim of the study was to undertake a quantitatve assessment of expression in AD cases and controls.

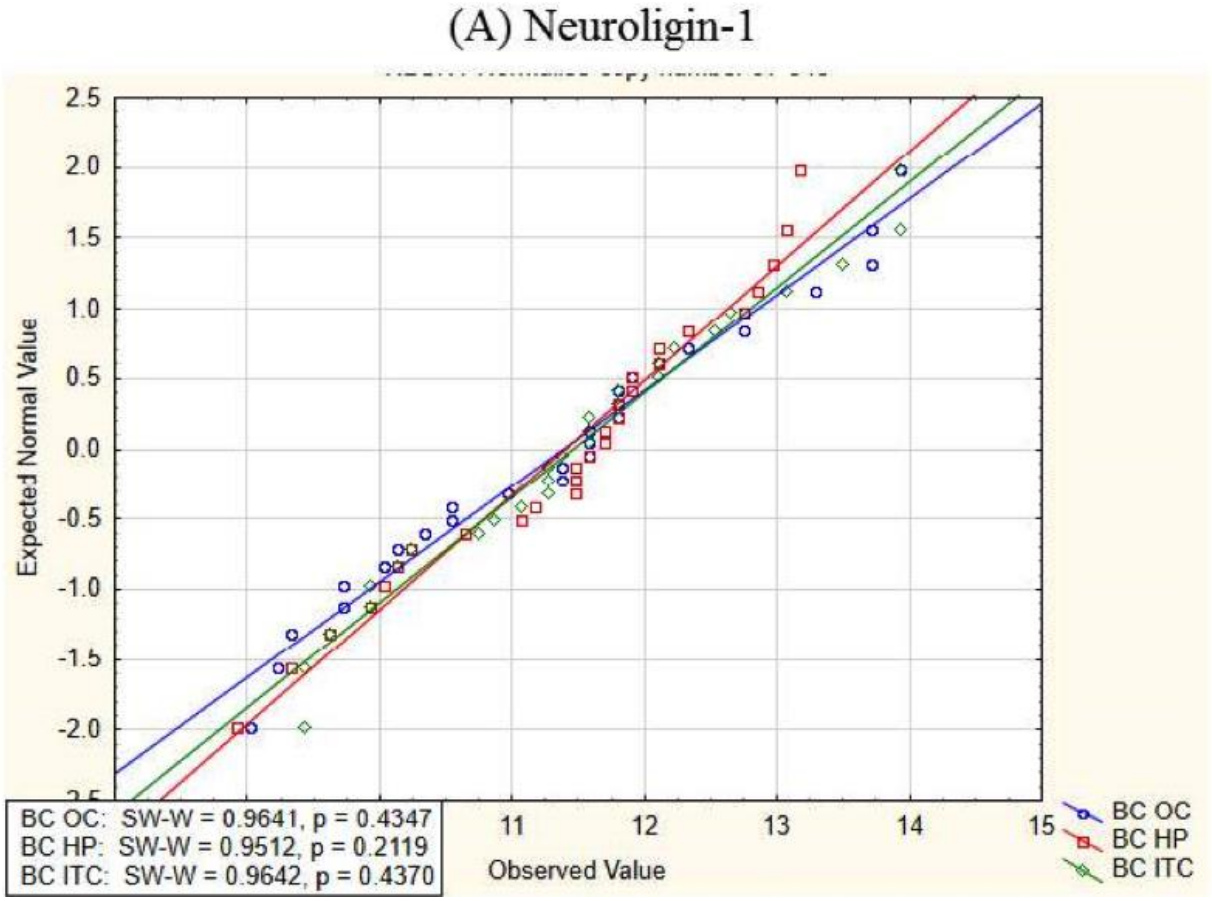

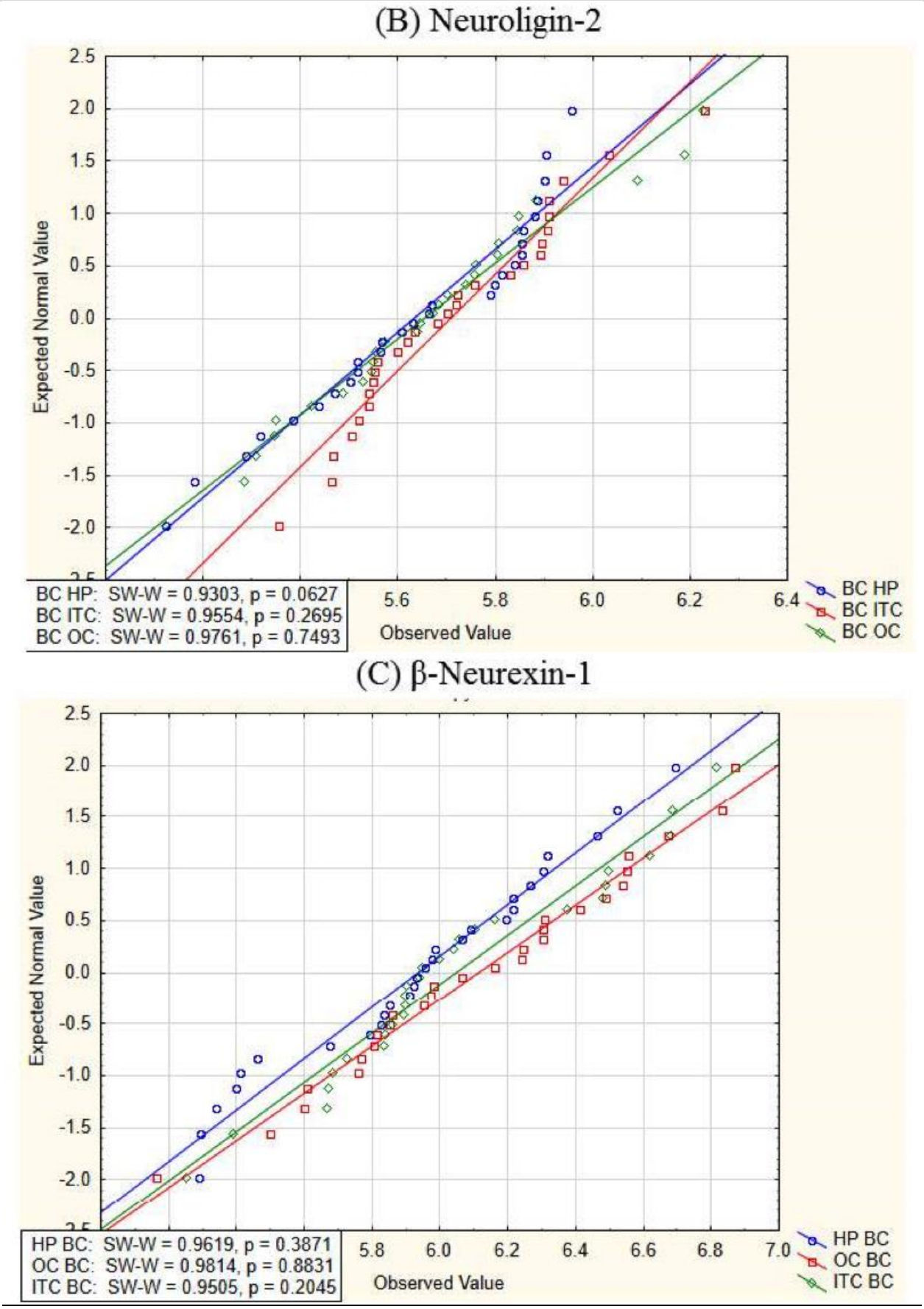

Fig. 5.3. Normal probability plots of Box-Cox transformed data. **A,** *NLGN1*, **B,** *NLGN2*, **C,** *βNRXN1*. Details as for Fig. 5.1. Shapiro-Wilks tests showed that no trace

deviated significantly from the normal distribution, as shown in the in-graph boxes.

Table 5.2. RNA integrity number

	AD Cases				Controls		
	HP	OC	ITC		HP	OC	ITC
AD1	3.3	4.8	4.5	NC1	6.3	6.4	7
AD2	4.7	5	4.8	NC2	4.8	2.3	4.8
AD3	4.7	5.3	4.6	NC3	6	5.9	6.6
AD4	4.9	5	5.3	NC4	3.4	5.1	4.1
AD5	5	5.9	5	NC5	6.1	6.8	7
AD6	5.3	4.8	5	NC6	3.9	3.4	4.5
AD7	5	5	3.2	NC7	6.2	7	5.8
AD8	4.7	3.6	4.8	NC8	2.2	3.8	3.2
AD9	5.1	5.5	5.7	NC9	5.1	4.6	5.4
AD10	3.2	2.5	2.7	NC10	4.4	3	4.3
AD11	2.9	2.6	3.4	NC11	5.9	6.8	6.2
AD12	2.6	3.8	2.7	NC12	4.9	3	4
AD13	3.5	3.3	2.9	NC13	5.3	4.6	5.3
AD14	4.3	4.2	3.5	NC14	5.5	4.8	4.5

5.4.2 RNA integrity

RNA integrity was estimated in each sample to check whether the quality of the RNA would impact the concentration of transcripts measured (Table 5.2). A number of studies have reported on the impact of age at death and PMD on the quality of the mRNA, and shown that neither has a marked effect (Chevyreva et al., 2008, Harrison et al., 1991). RNA in autopsy tissue is stable for up to 120h post-mortem (Hynd et al., 2003). In this study regression analyses showed that post-mortem delay had no effect on the integrity of RNA ($F_{1,82} = 0.146$, $P = 0.70$), while age showed a just-significant effect on RIN ($F_{1,82} = 3.757$, $P = 0.056$; Fig. 5.4). RIN was normally distributed (Fig. 5.5)

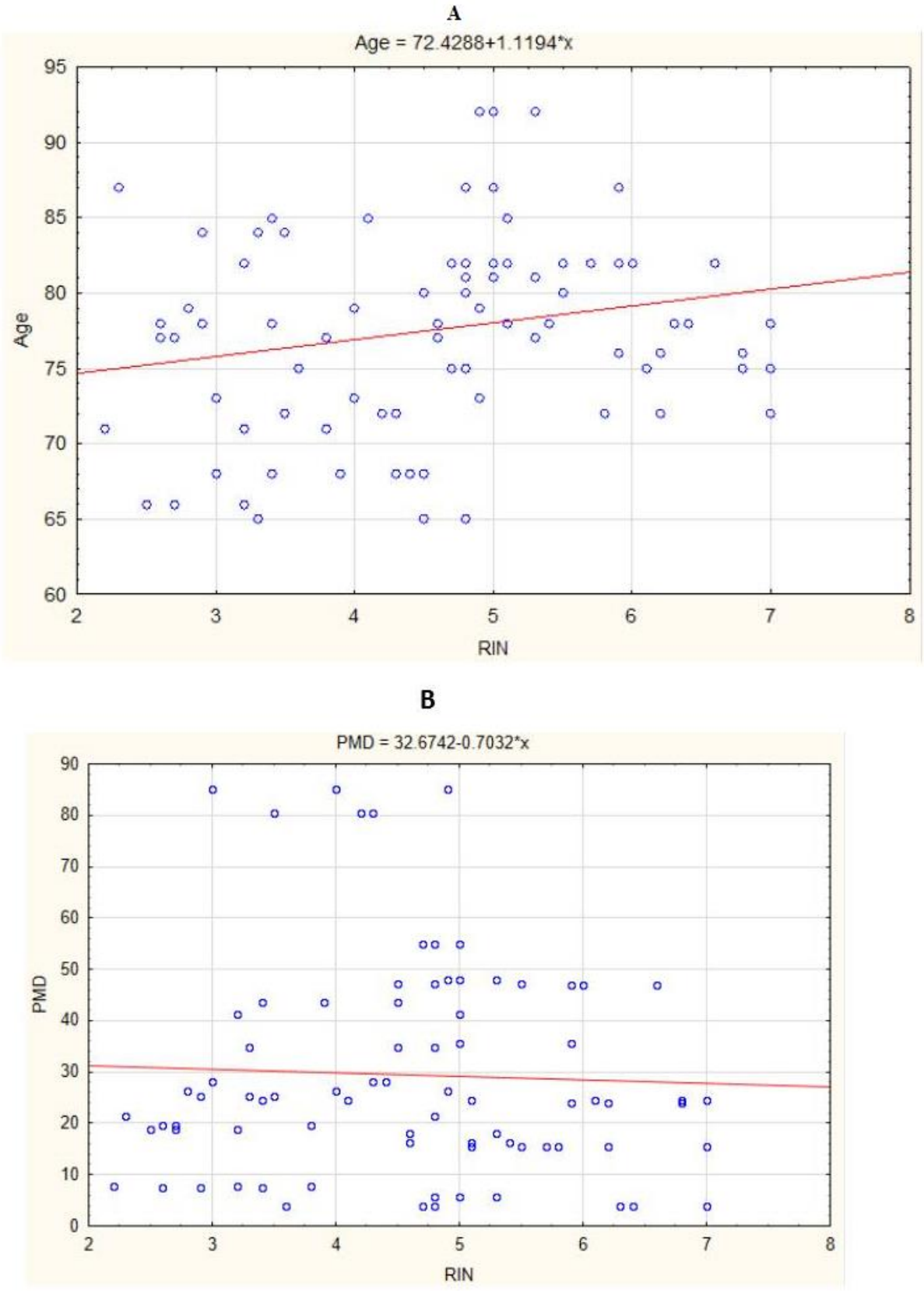

Fig. 5.4. Scatterplots of RIN against **A,** age, **B,** PMD.

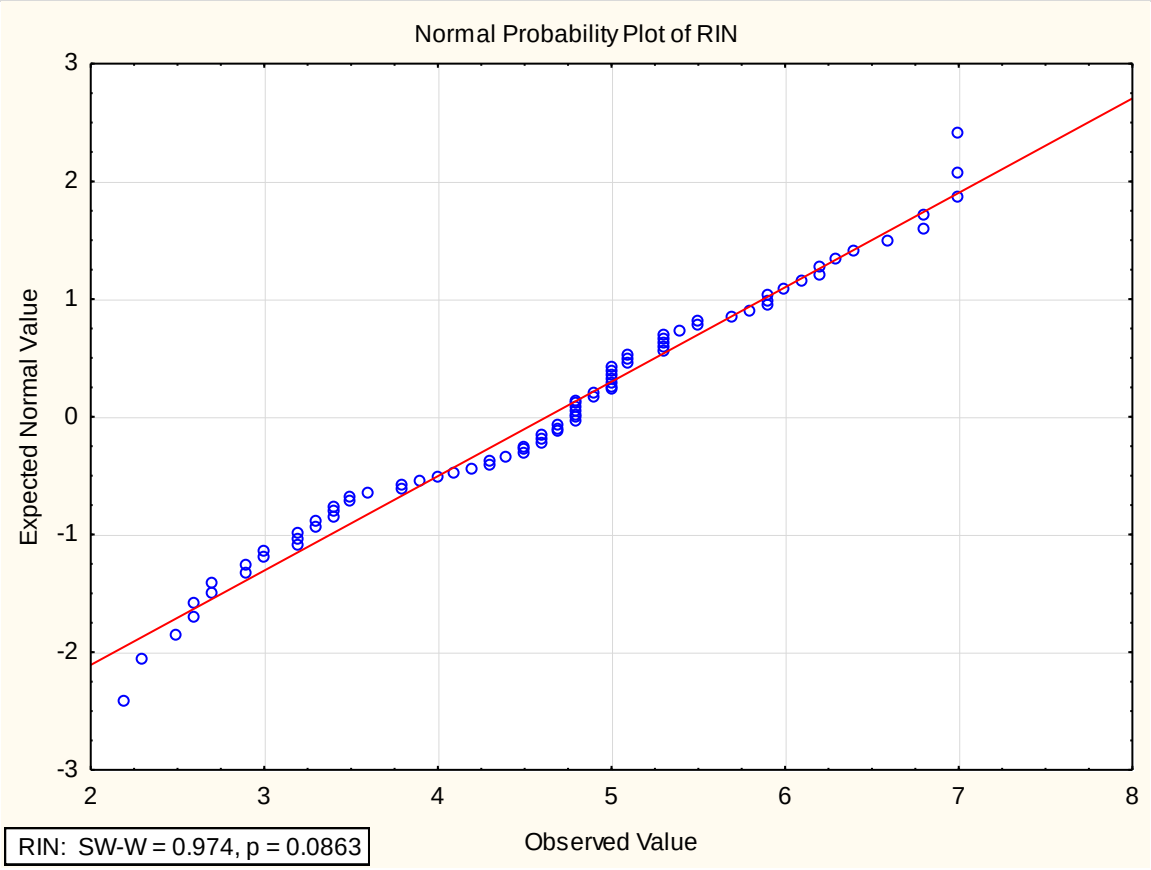

Fig. 5.5. Normal probability plot of RIN. Data did not deviate significantly from the normal distribution by Shapiro-Wilks testing as shown in the in-graph box.

5.4.3 Reference gene (RPL13 expression)

There are several housekeeper genes that are uniformly expressed across many tissue and cell types, such as glyceraldehyde-3-phosphate dehydrogenase (*GAPDH), HSP90, CYC1, EIF4A2* and β-actin. However, the expression of these genes may vary depending on experimental and pathological conditions. In the RT-PCR assay, there is no universal reference gene suitable for all experimental conditions. Careful validation of housekeepers should be performed to choose the most appropriate. Differences in the expression of the reference gene between study samples and controls can profoundly compromise interpretation. Most RT-PCR studies in the literature use *GAPDH* (NM_002046.3) as the reference gene for normalization. In AD, reduced synthesis of *GAPDH* mRNA, abnormal aggregation of GAPDH protein in the nucleus of, and increased activity of the enzyme cells have been observed in diseased tissues, suggesting a direct or indirect relationship of GAPDH with the neurodegenerative process. This makes *GAPDH* unsuitable as a reference gene in

this study. The housekeeping gene that showed the most constant expression in AD cases and controls in autopsy tissues was *RPL13*, which is a component of the 60S ribosomal subunit (Gebhardt et al., 2010). In this study *RPL13* was used as a housekeeper. Its expression across samples showed no overall difference between AD cases and controls ($F_{1,80}$ = 0.078, P = 0.78; Fig. 5.6). No variation in *RPL13* expression was observed between cases and controls in any brain area ($F_{2,50}$ = 0.092, P = 0.91; Fig. 5.7).

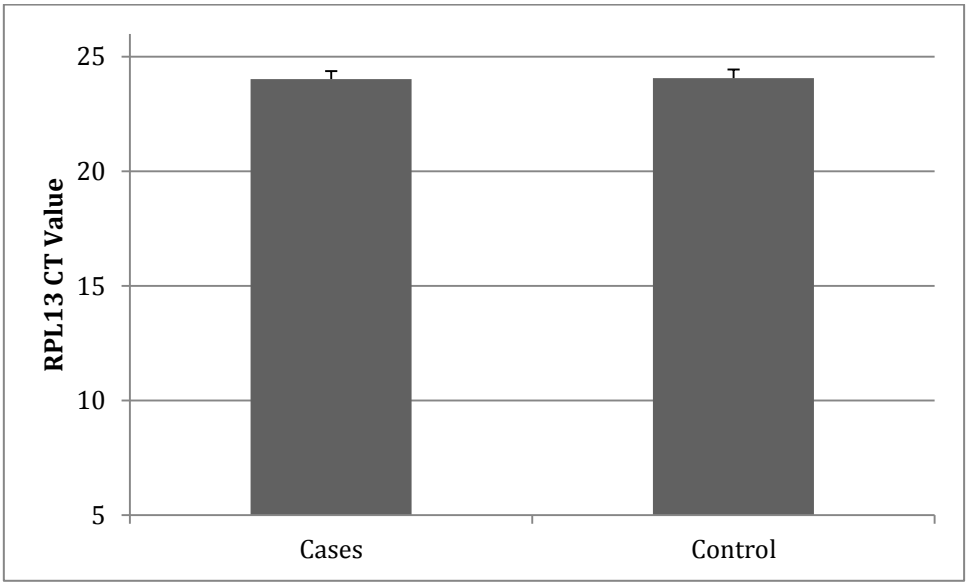

Fig. 5.6. *RPL13* expression by case-group.

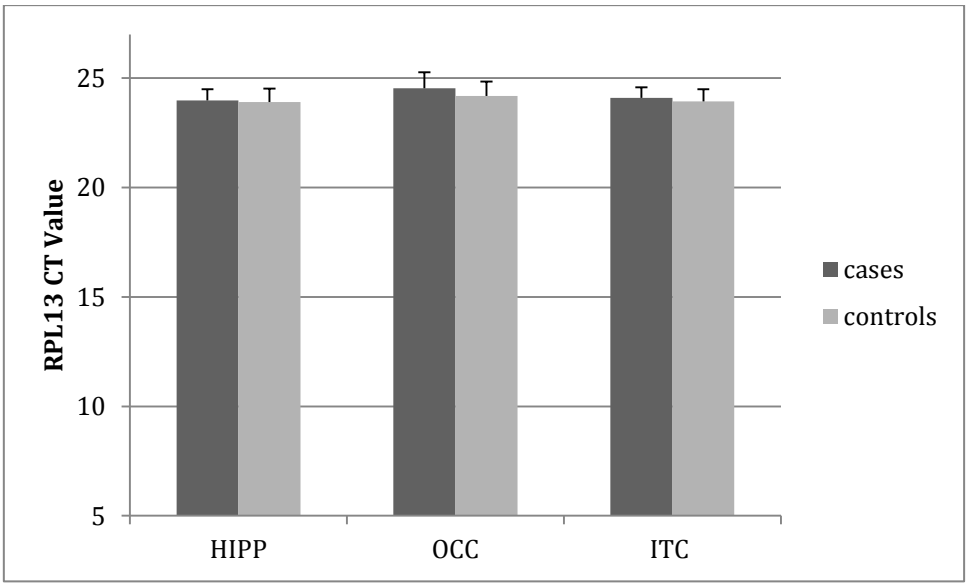

Fig. 5.7. RPL13 by case-group across brain regions.

5.4.4 Age at death and post-mortem delay with RPL13 transcript expression

Regression analyses showed no relationship between either PMD or age and RPL13 CT value

($F_{1,82}$ = 0.010, P = 0.92; $F_{1,82}$ = 3.921, P = 0.051 respectively; Fig. 5.8).

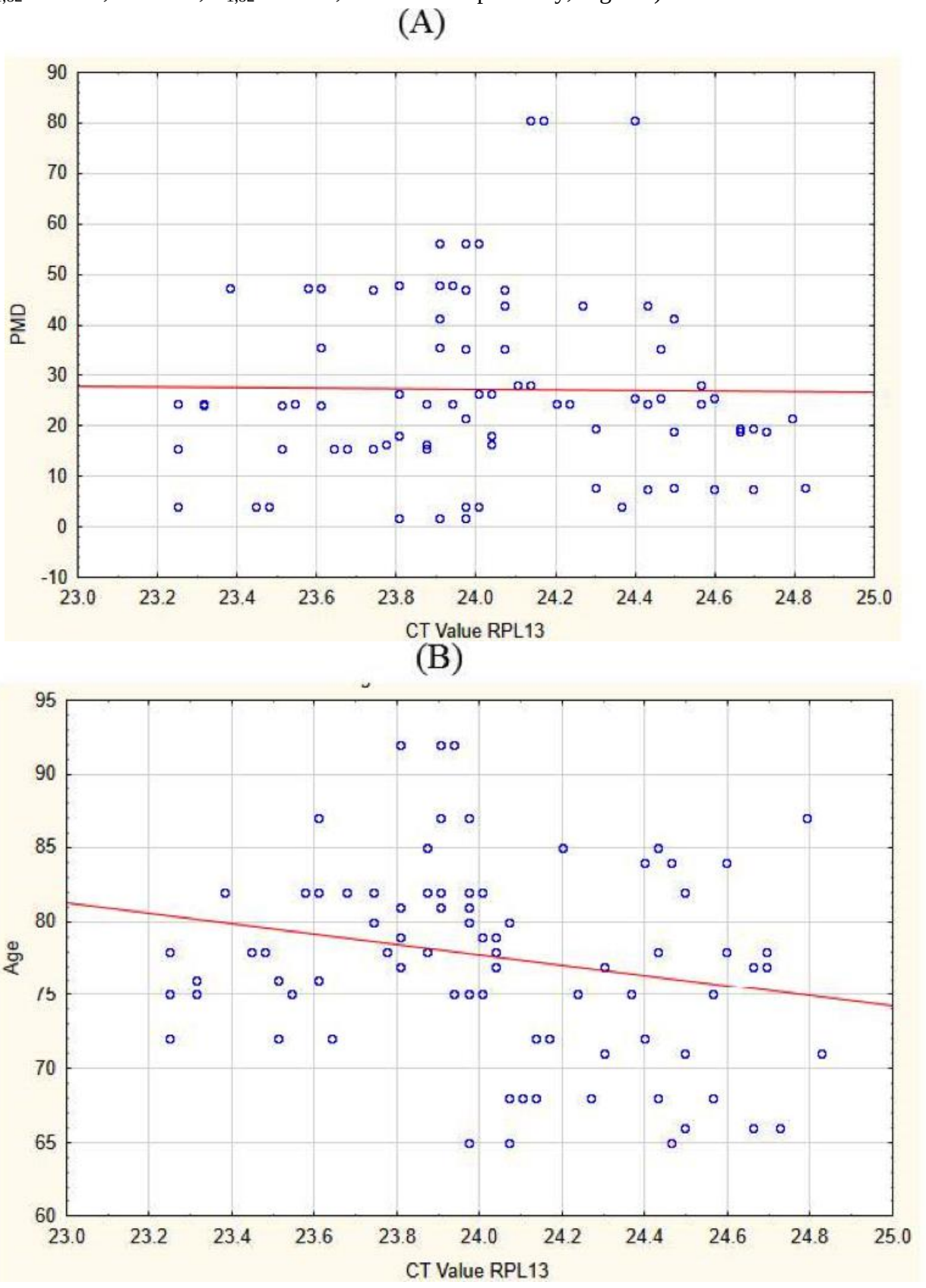

Fig. 5.8. Regression of *RPL13* CT value on **A,** PMD and **B,** Age.

No significant association was observed between PMD and the expression of *NLGN1* ($F_{1,82}$ = 0.004, P = 0.94), *NLGN2* ($F_{1,82}$ = 0.261, P = 0.61) or *βNRXN1* ($F_{1,82}$ = 0.011, P = 0.91). *NLGN1* showed a near-significant relation with age ($F_{1,82}$ = 3.836, P = 0.053), although *NLGN2* ($F_{1,82}$ = 0.042, P = 0.83) and *βNRXN1* ($F_{1,82}$ = 1.375, P = 0.24) did not (Fig. 5.9). As a result age was used as a covariant in subsequent analyses for all transcripts.

5.4.5 Neuroligin-1 transcript expression between cases and controls

The copy number of *NLGN1* transcript was quantified by RT-PCR assay using a standard curve with known copy numbers of recombinant plasmid and adjusted for RIN. There was significant difference in expression levels averaged across all areas between AD cases and controls ($F_{1,82}$ = 8.978, P = 0.004). The transcript copy number of neuroligin-1 mRNA was lower in AD cases and controls (Fig. 5.10). The Group × Area interaction was significant ($F_{2,52}$ = 4.780, P = 0.012), and was probed further by *post-hoc* testing (Fig. 5.11). The level of neuroligin-1 transcripts measured was lowest in the occipital cortex and highest in inferior temporal cortex.

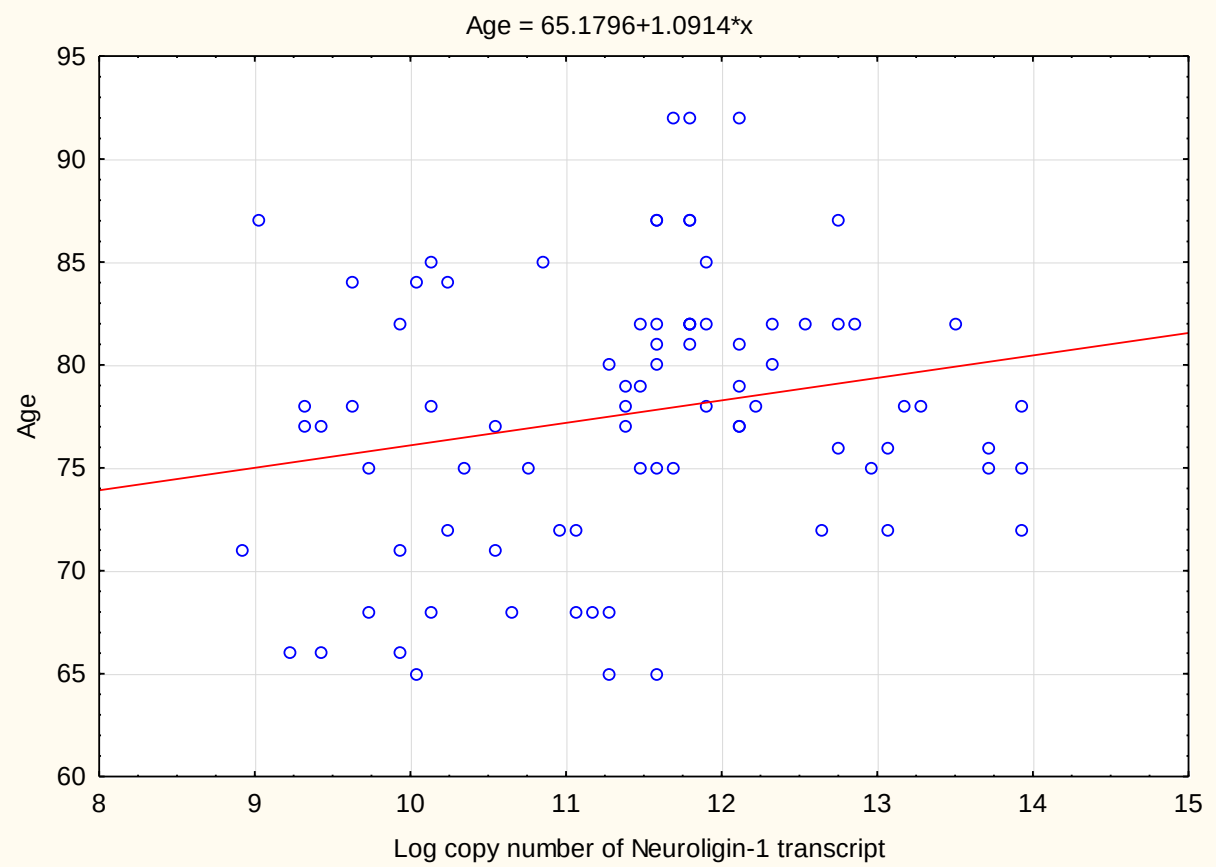

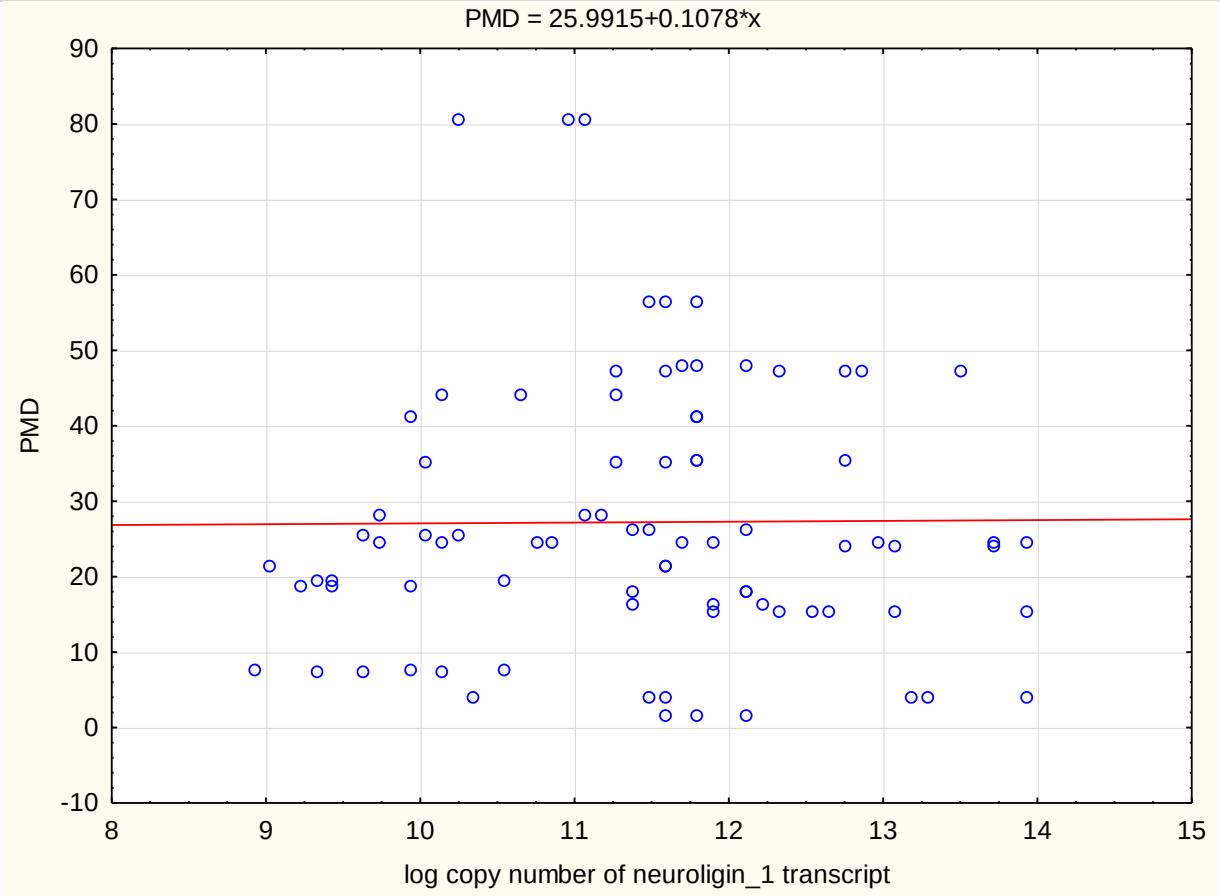
PMD = 25.9915+0.1078*x
PMD
log copy number of neuroligin_1 transcript

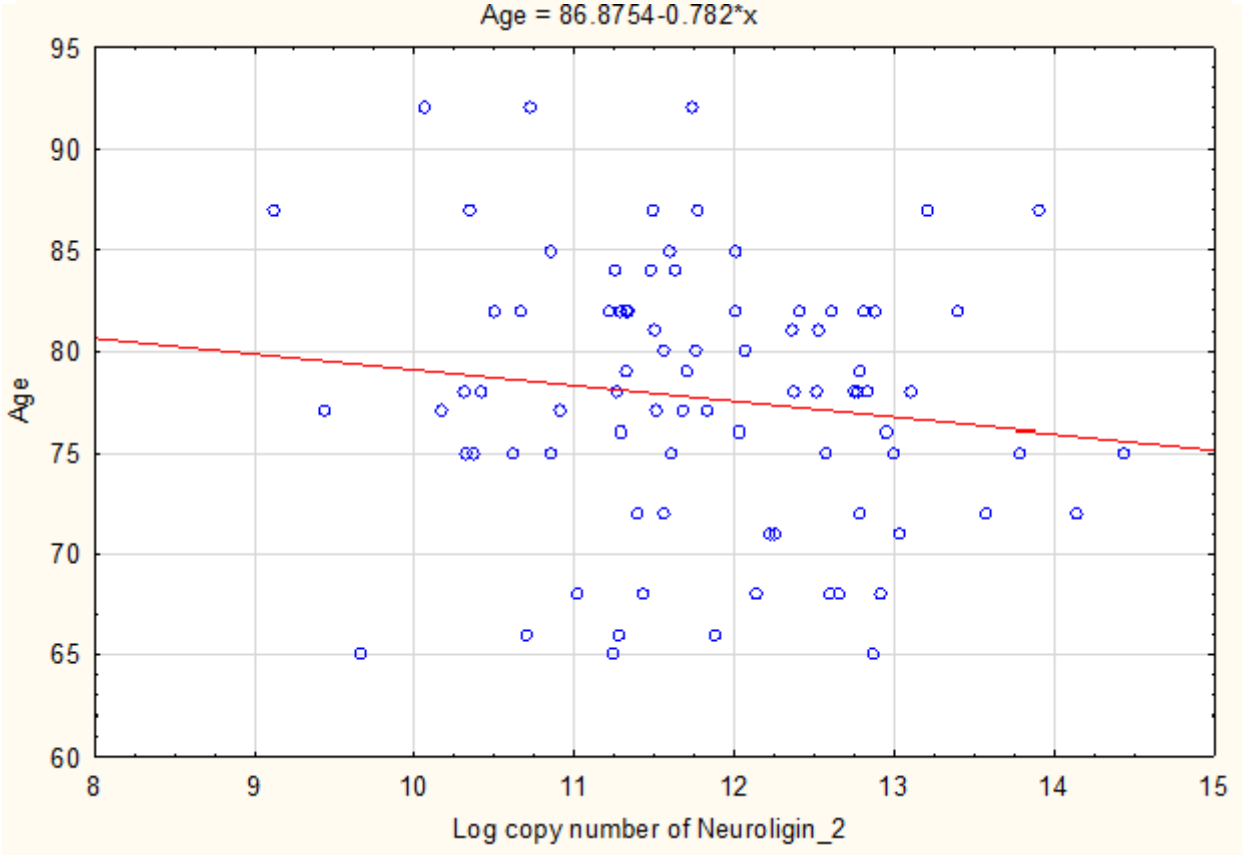
Age = 86.8754-0.782*x
Age
Log copy number of Neuroligin_2

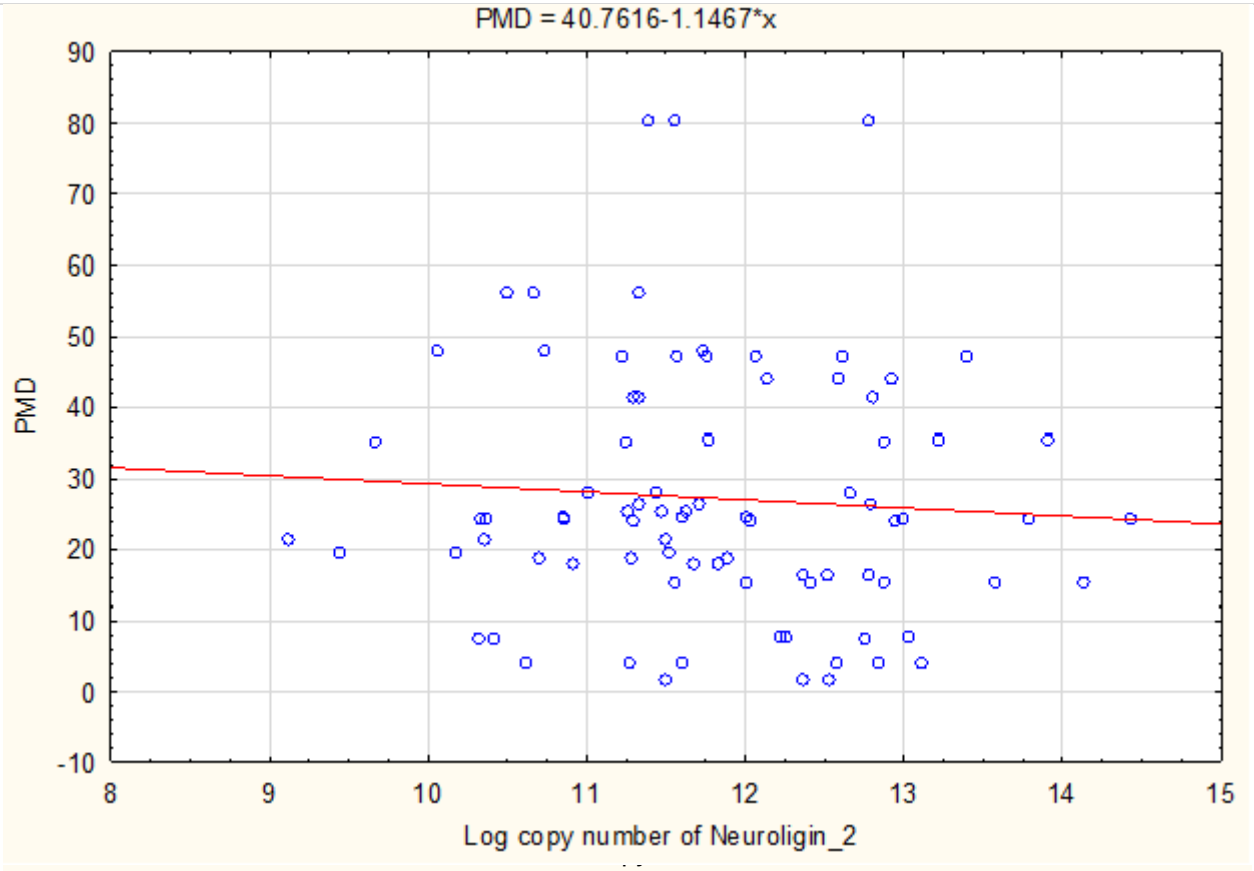
PMD = 40.7616-1.1467*x
PMD
Log copy number of Neuroligin_2

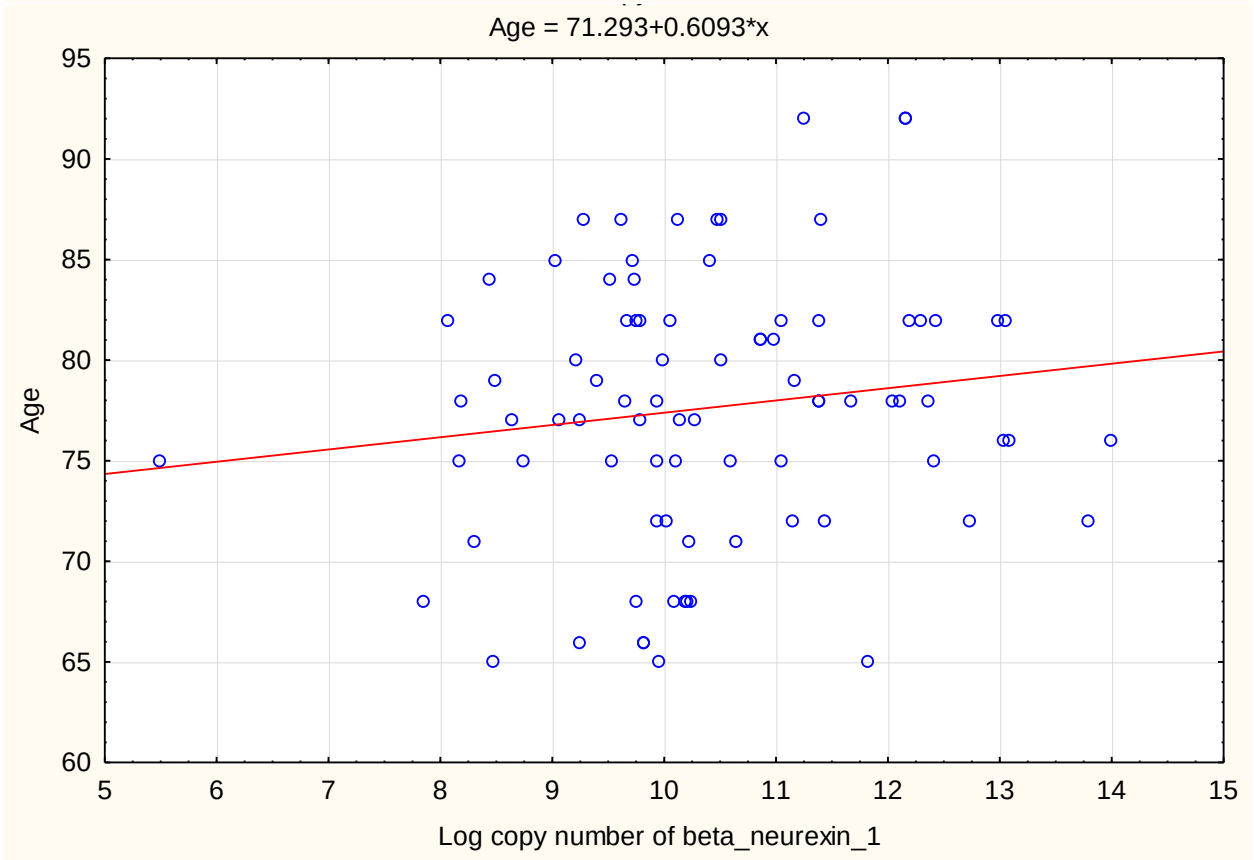
Age = 71.293+0.6093*x
Age
Log copy number of beta_neurexin_1

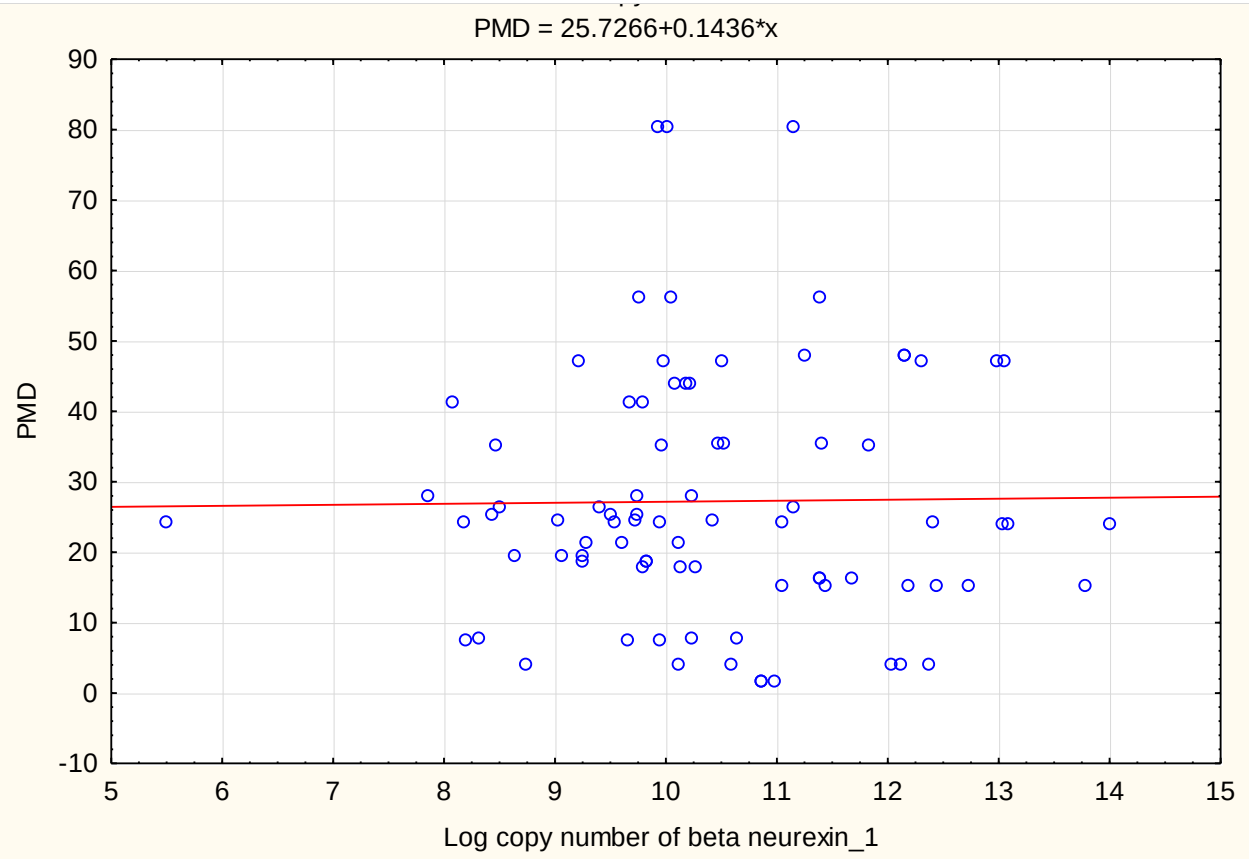

Fig. 5.9. Regression of *NLGN1*, *NLGN2* and *βNRXN1* transforms on age at death and PMD. See text for details.

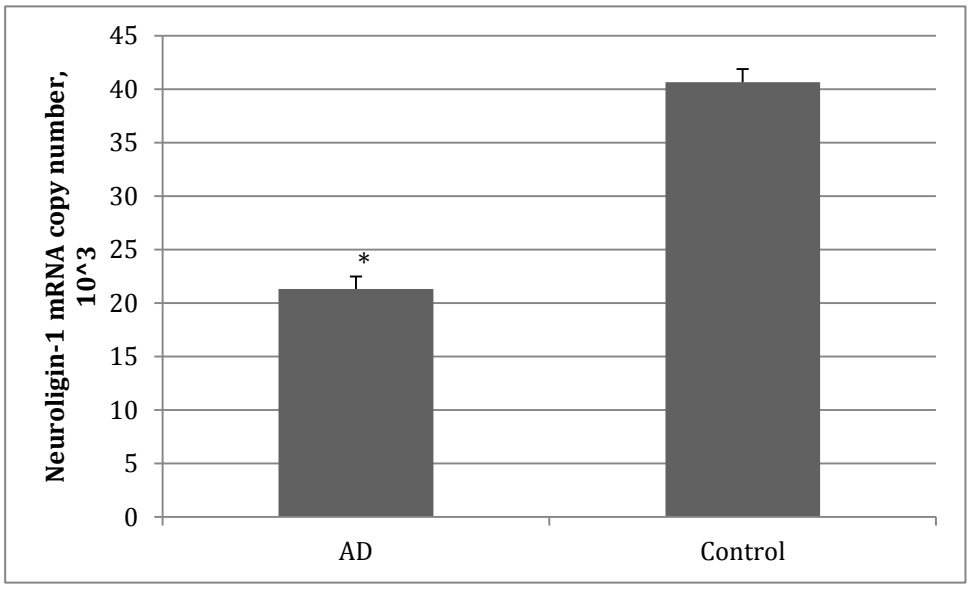

Fig. 5.10. *NLGN1* transcript level by case-group averaged across the three areas. *, Significantly different from controls, see text. Bars show mean copy number × 10^3 per µg of total RNA ± S.E.M.

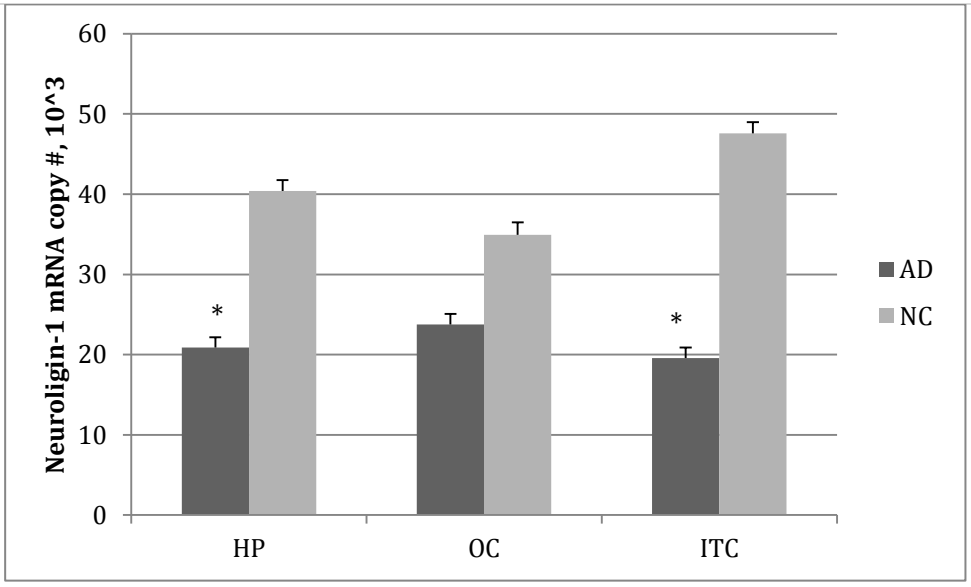

Fig. 5.11. *NLGN1* mRNA copy numbers by case-group and area. Details as for Fig. 5.10; *, significantly different from controls in the same area, $P < 0.05$ by Newman-Keuls *post-hoc* test.

5.4.6 Neuroligin-1 transcript expression and gender

Gender is a significant factor in disease progression, and medications targeting proteins that are differentially expressed between males and females may significantly impact treatment (Vina and Lloret, 2010). Some genes that shown similar expression levels in both sexes in normal healthy controls could be differentially expressed between genders in disease (Vawter et al., 2004). Gender may be important in disease progression (Hynd et al., 2003). In this study the main effect for Gender was significant ($F_{1,82} = 8.909$, $P = 0.003$) because *NLGN1* expression was expression was lower overall in males than in females. This pattern was similar in both case-groups: the Group × Sex interaction on *NLGN1* was not significant ($F_{1,80} = 0.024$, $P = 0.87$), in essence because expression was higher in females in both groups, as revealed by *post-hoc* testing (Fig. 5.12). When samples were further divided by area, the *NLGN1* copy number was higher in females than in males in all three areas and in both groups. This resulted in a non-significant Group × Gender × Area interaction ($F_{2,48} = 0.692$, $P = 0.50$), but *post-hoc* testing showed that regional differences reached significance in both hippocampus and inferior temporal cortex (Fig. 5.13).

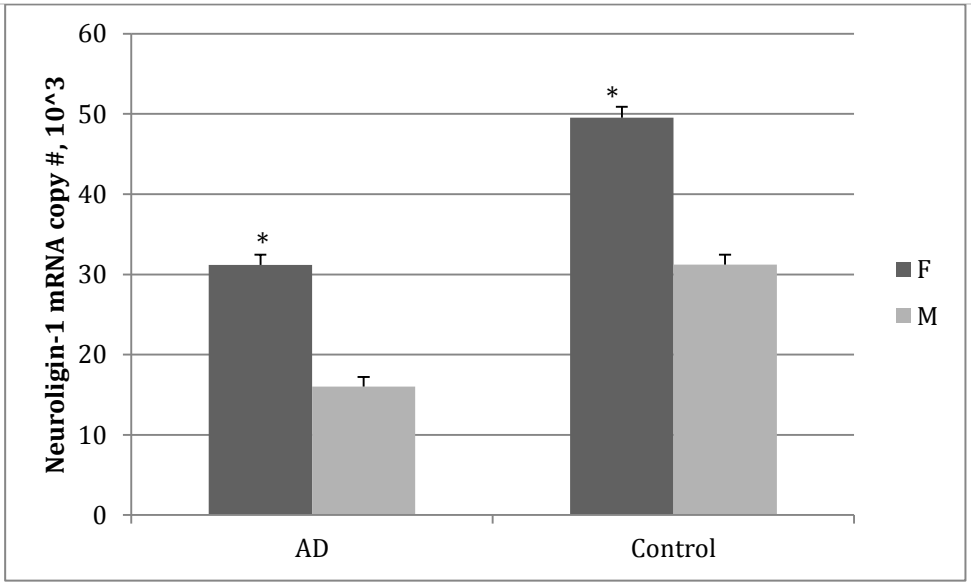

Fig. 5.12. *NLGN1* mRNA expression by case-group and sex. Details as for Fig. 5.11; *, significantly higher than expression in males in the same case-group, $P < 0.05$ by Newman-Keuls *post-hoc* test.

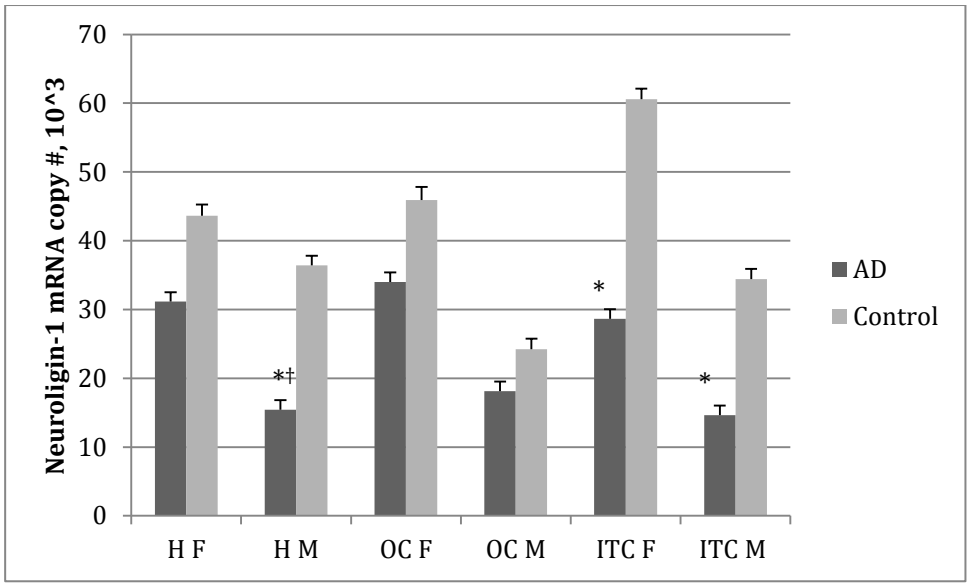

Fig. 5.13. *NLGN1* expression by case-group, sex, and area. Details as for Fig. 5.11; *, significantly different from same-sex controls, and †, opposite-sex AD cases, in the same area, $P < 0.01$ by Newman-Keuls *post-hoc* testing.

5.4.7 NLGN1 transcript expression and APOE genotype

As noted in Chapter 3, not all *APOE* genotypes were present in the dataset. For statistical analysis subjects were divided into two groups: ε4 allele carriers and ε4 non-carriers. These two groups were obtained by dividing cases into three groups: cases with ε4 allele, cases with one copy

of the ε4 allele and finally cases with two copies of the ε4 allele. Because ε2 allele is known to be neuroprotective, it was decided that ε2,ε4 carriers resembled ε3,ε3 cases, and as a result these two genotypes were combined in the same class.

NLGN1 expression was significantly lower overall in *APOE* ε4 carriers than in those without an ε4 allele ($F_{1,82}$ = 6.203, P = 0.014; Fig. 5.14). The patterns were parallel in AD cases and controls, hence the Group × Nº of ε4 alleles interaction was not significant ($F_{1,80}$ = 0.767, P = 0.384) but the differences remained significant in AD cases under *post-hoc* testing (Fig. 5.15). There was no significant regional variation in *NLGN1* expression pattern ($F_{2,52}$ = 0.149, P = 0.86; Fig. 5.16), and the statistics had insufficient power to find differences between the genotypes within case-groups at this level by *post-hoc* testing. However, there were differences in *NLGN1* expression between AD cases and matched controls in both hippocampus and inferior temporal cortex in subjects that did not carry any ε4 allele.

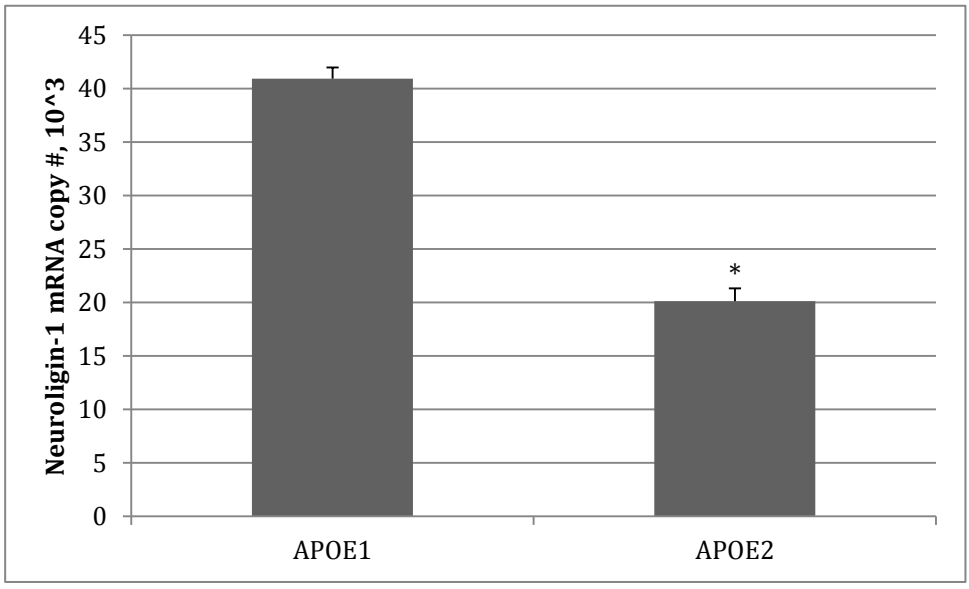

Fig. 5.14. *NLGN1* transcript expression by *APOE* genotype. Display details as for Fig. 5.10. Subjects were combined across case-groups and divided into those who had no (APOE1) or at least one (APOE2) *APOE* ε4 allele; *, significantly different from subjects with no ε4 allele, $P < 0.02$, see text.

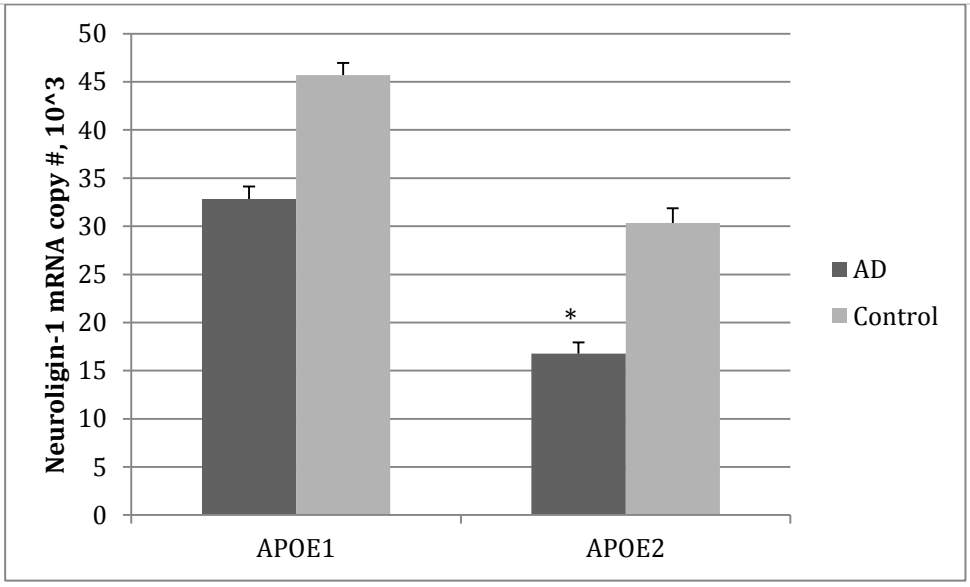

Fig. 5.15. *NLGN1* expression by case-group and Nº of *APOE* ε4 alleles. Details as for Fig. 5.14; *, significantly different from AD cases with no ε4 allele, $P < 0.05$ by Newman-Keuls *post-hoc* test.

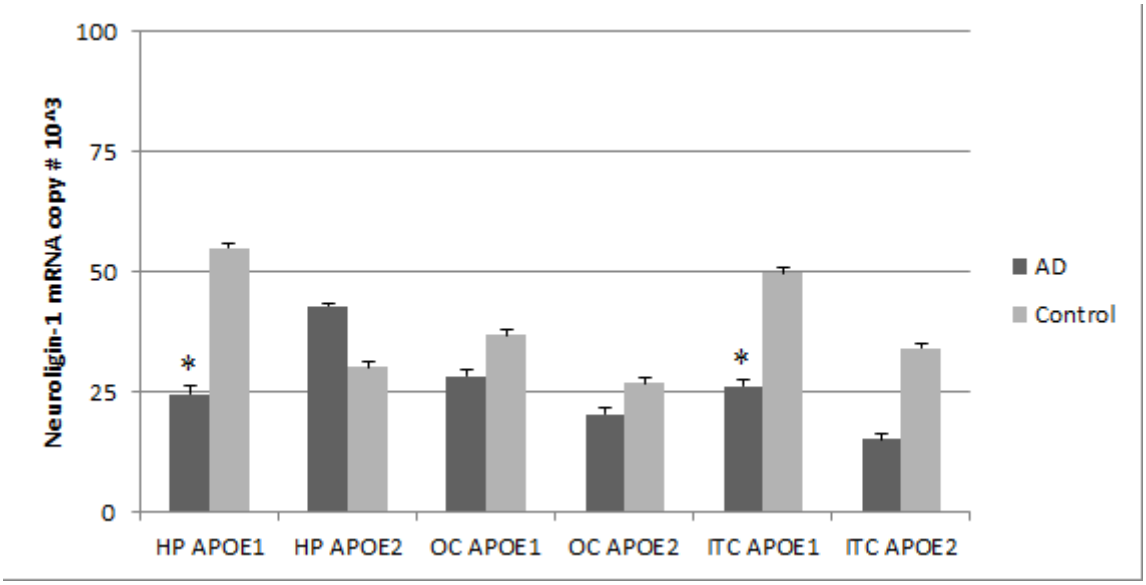

Fig. 5.16. *NLGN1* expression by case-group, area, and Nº of *APOE* ε4 alleles. Details as for Fig. 5.14; *, significantly different from controls with the same genotype, $P < 0.02$ by Newman-Keuls *post-hoc* tests.

5.4.8 NLGN1 expression and disease severity

AS explained in Chapter 3, only AD cases were analysed by pathological score. Overall, the effect of disease severity on *NLGN1* expression only trended toward significance ($F_{2,39}$ =2.973, P = 0.062), in part because the generally spared occipital cortex showed a different pattern from the

other two areas (Fig. 5.17). In conformity with this regional difference in patter, the PS × Area interaction was significant ($F_{4,33}$ = 3.016, P = 0.031).The level of *NLGN1* transcript in inferior temporal cortex samples from AD cases at a moderate stage of disease were significantly lower than from those with mild disease, and significantly lower again in cases that showed severe disease features. Only the latter comparison reached significance in hippocampus (Fig. 5.17).

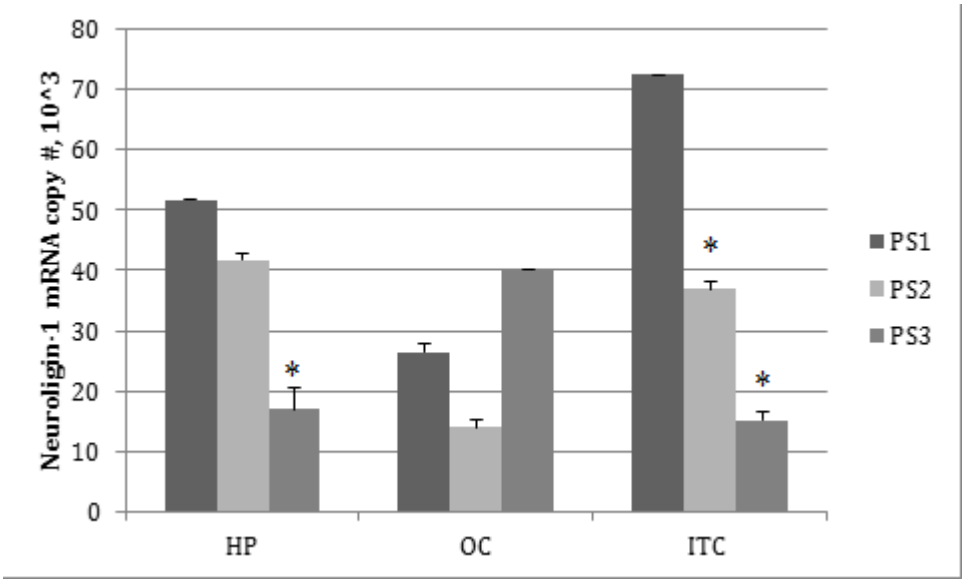

Fig. 5.17. *NLGN1* transcript expression by disease severity. Tissue samples from AD cases were divided according to the index of pathological severity as described in the text. Newman-Keuls *post-hoc* testing showed that expression in hippocampus at the severe stage was significantly lower than at the moderate stage (P = 0.006). In inferior temporal cortex expression was significantly lower at the moderate stage than at the mild stage (P = 0.001) and significantly lower again at the severe stage (P = 0.013). Expression did not vary significantly with disease severity in AD occipital cortex.

5.4.9 Neuroligin-2 transcript expression by case-group

The copy number of neuroligin-2 transcript was quantified by RT-PCR assay as described in Methods. Statistical tests were performed on Box-Cox transforms of the values as outlined in Section 5.4.1 and the means converted to the original scale for presentation. The transcript copy number of neuroligin-2 was averaged and quantified across all three areas. Overall, *NLGN2* expression was significantly lower in AD cases than in controls ($F_{1,82}$ =23.515, P < 0.001; Fig. 5.18). The Group ×

Area interaction also reached significance ($F_{2,52}$ =4.345, P =017); although expression was lower in AD cases than controls in all areas, it was more marked, and significant, in the two areas most affected by disease pathology (Fig. 5.19).

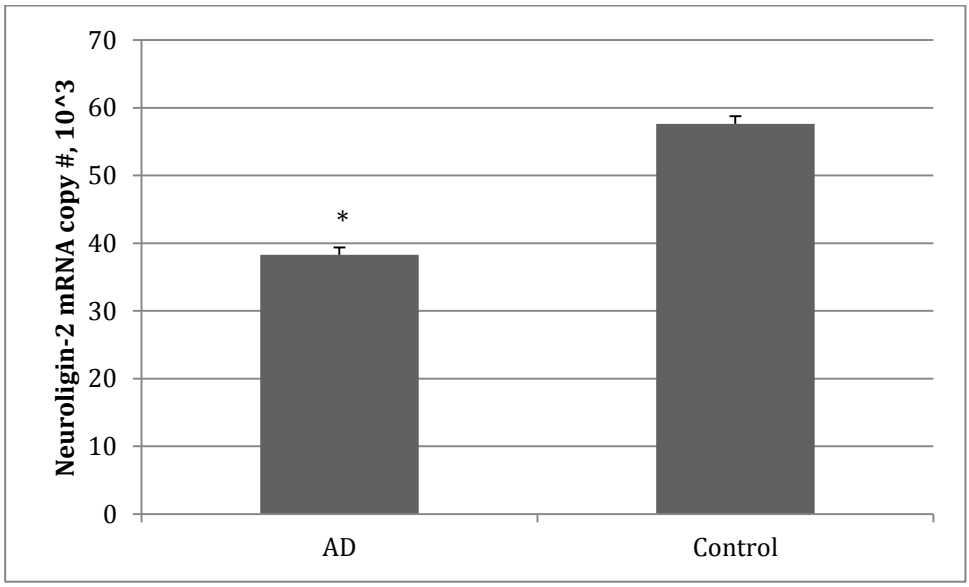

Fig. 5.18. *NLGN2* transcript expression by case-group averaged across the three areas. Details as for Fig. 5.10; *, significantly different from controls, see text.

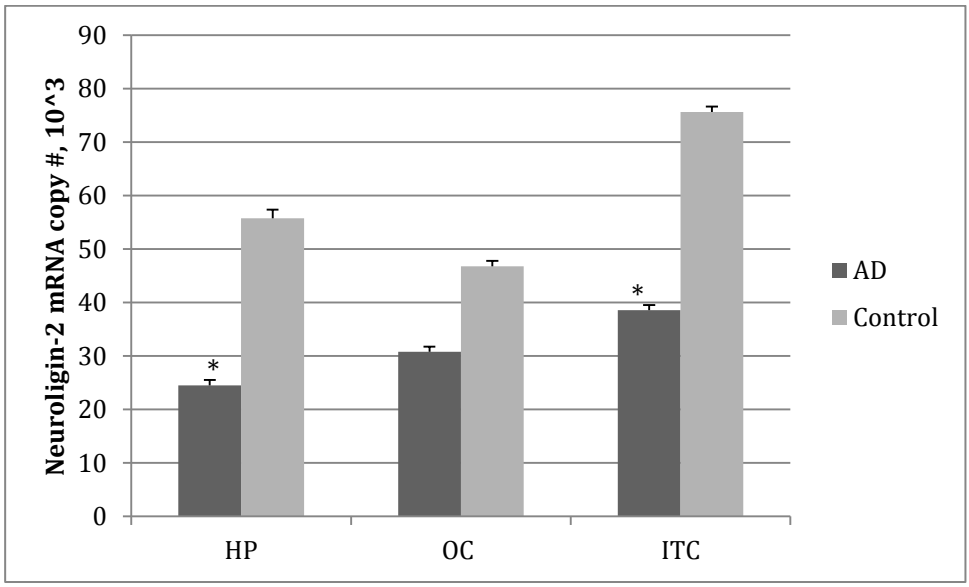

Fig. 5.19. *NLGN2* mRNA copy numbers by case-group and area. Details as for Fig. 5.11; *, significantly different from controls in the same area. *Post-hoc* Newman-Keuls testing showed significantly lower expression in AD cases than controls in hippocampus (P = 0.002) and inferior temporal cortex (P = 0.001). No significant difference was found in occipital cortex.

5.4.10 Neuroligin-2 transcript expression and gender

The influence of gender on the expression of *NLGN2* transcripts was studied no significant difference was found ($F_{1,80}$ = 0.175, P =0.67). *Post-hoc* testing showed there were significantly lower *NLGN2* mRNA levels in in both male and female AD cases than in same-sex controls (Fig. 5.20). The Group × Gender × Area interaction was not significant ($F_{2,48}$ =0.015, P = 0.98) because patterns were similar in the three regions, as portrayed by *post-hoc* testing (Fig. 5.21).

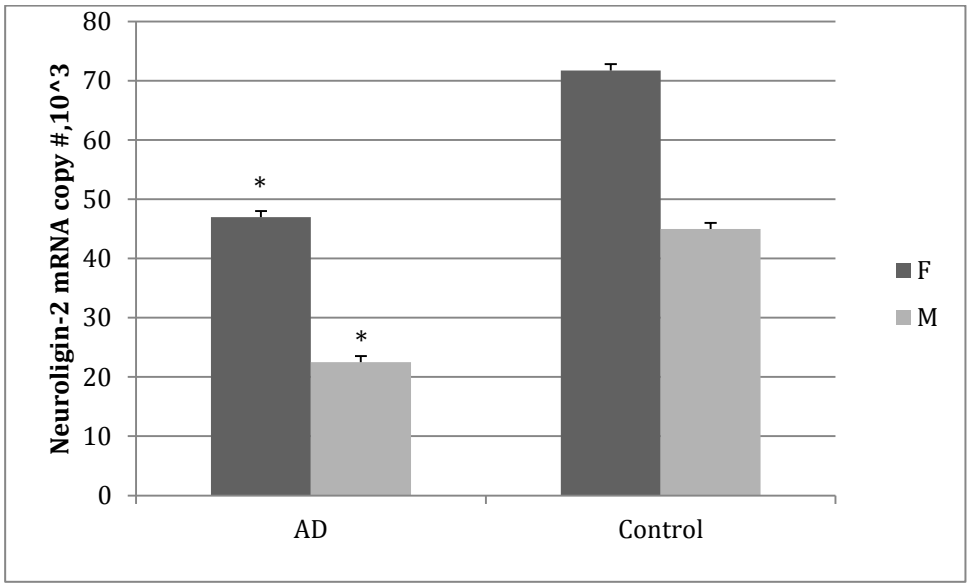

Fig. 5.20. *NLGN2* copy numbers by case-group and sex. Details as for Fig. 5.11; *, significantly lower than expression in same-sex controls, $P < 0.05$ by Newman-Keuls *post-hoc* test.

5.4.11 Neuroligin-2 transcript expression and APOE genotype

Expression trended lower in AD cases carrying the *APOE* ε4 allele than in non-carrier AD cases, but did not reach significance ($F_{1,82}$ = 3.028, P = 0.08; Fig. 5.22). The Group × Nº of *APOE* alleles interaction was not significant ($F_{1,80}$ = 0.160, P = 0.68), in essence because the same pattern was seen in subjects with the same genotype (Fig. 5.23). The further interaction with area was also not significant, for a similar reason (Fig. 5.24).

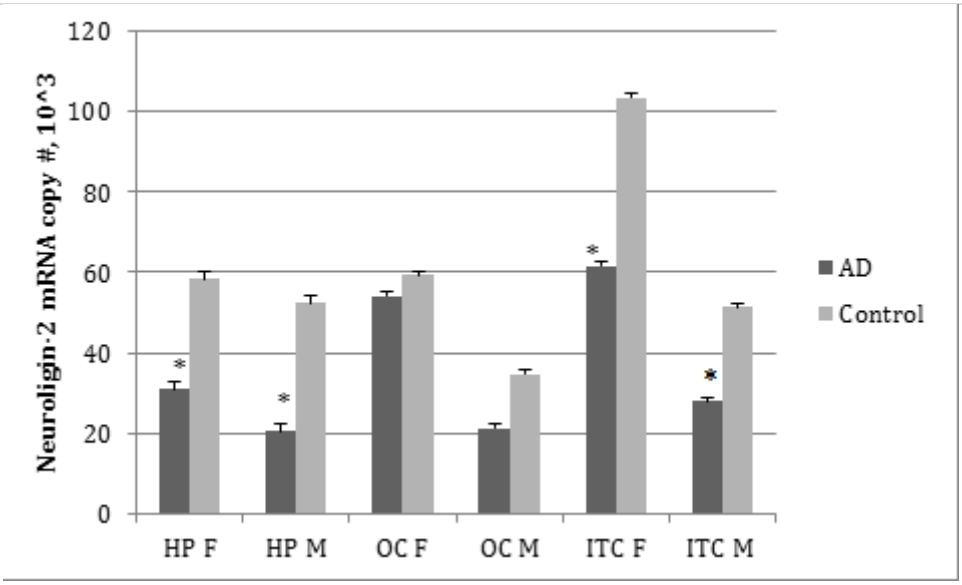

Fig. 5.21. *NLGN2* copy numbers by case-group, area, and sex. Details as for Fig. 5.11; *, significantly lower in AD cases than in same-sex controls by Newman-Keuls *post-hoc* testing, $P < 0.001$. No other comparison was statistically significant.

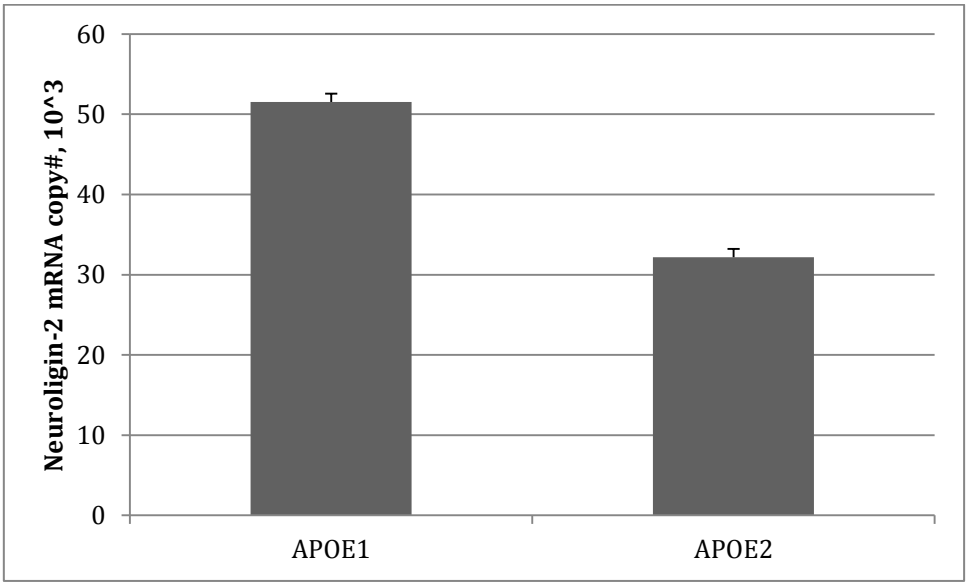

Fig. 5.22. *NLGN2* transcript expression by *APOE* genotype. Details as for Fig. 5.14.

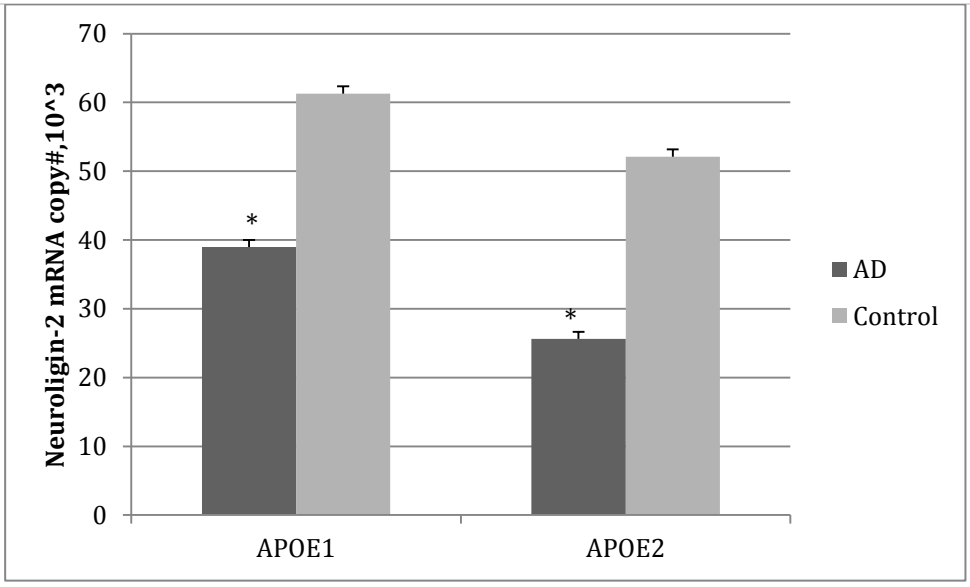

Fig. 5.23. *NLGN2* transcript expression by case-group and the Nº of *APOE* ε4 alleles. AD cases and controls were separated by APOE genotype as set out in Fig. 5.14 legend; *, there was significantly lower expression in AD cases than controls both in subjects without an ε4 allele ($P = 0.014$) and those with at least one ($P = 0.002$) by Newman-Keuls *post-hoc* test.

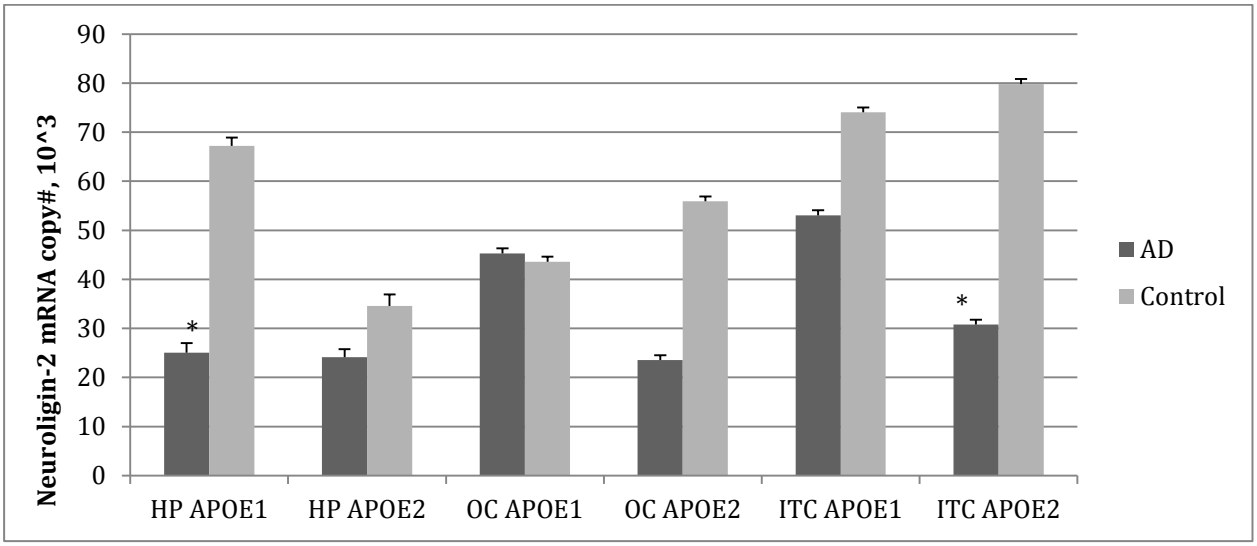

Fig. 5.24. *NLGN2* mRNA copy numbers by case-group, *APOE* genotype and area. Details as for Fig. 5.14; *, in hippocampus, expression was significantly lower in AD cases with no ε4 alleles than in matched controls, while in inferior temporal cortex AD cases with at least one ε4 allele showed lower expression than the corresponding controls, $P < 0.001$ by Newman-Keuls *post-hoc* testing.

5.4.12 Neuroligin-2 transcript expression and pathological score

The PS main effect on *NLGN2* expression was not significant ($F_{2,39}$ = 1.858, P = 0.16), but the PS × Area interaction was ($F_{4,33}$ = 3.097, P = 0.02). There was a graded reduction in *NLGN2* copy number with disease stage in hippocampus. In occipital cortex the copy number did not vary. In inferior temporal cortex, there was no significant difference between mild and moderate stages but expression was markedly attenuated at the severe stage of the disease (Fig. 5.25).

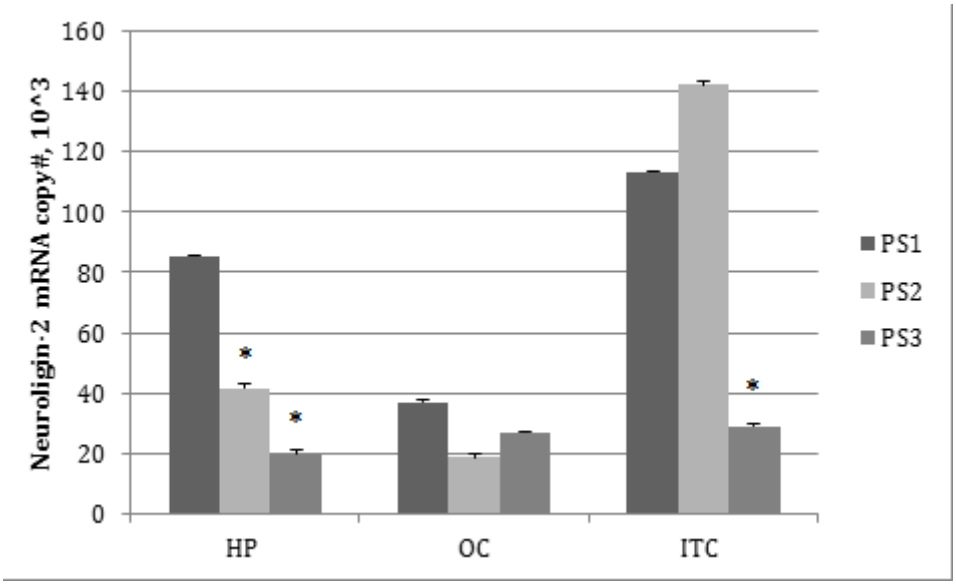

Fig. 5.25. *NLGN2* copy number and pathological score. Details as for Fig. 5.17. Expression was significantly lower in hippocampus at the moderate stage than the mild stage ($P < 0.001$) and lower again at the severe stage ($P < 0.001$). Inferior temporal cortex showed significantly lower expression at the severe stage than at either earlier stage ($P < 0.001$). Newman-Keuls *post-hoc* tests.

5.4.13 β-Neurexin-1 transcript expression by case-group

The copy number of *βNRXN1* transcripts was quantified as described in Methods, Section 5.3. *βNRXN1* mRNA expression was significantly lower overall in AD cases than in controls ($F_{1,82}$ = 5.303, P = 0.02; Fig. 5.26). The Group × Area interaction was not significant ($F_{2,52}$ =0.777, P = 0.46), in essence because the same general pattern was seen in all three areas (Fig. 5.27). None of the within-area differences between cases and controls reached significance on *post-hoc* testing, but

within AD cases the expression in hippocampus was significantly lower than in the other two areas (Fig. 5.27).

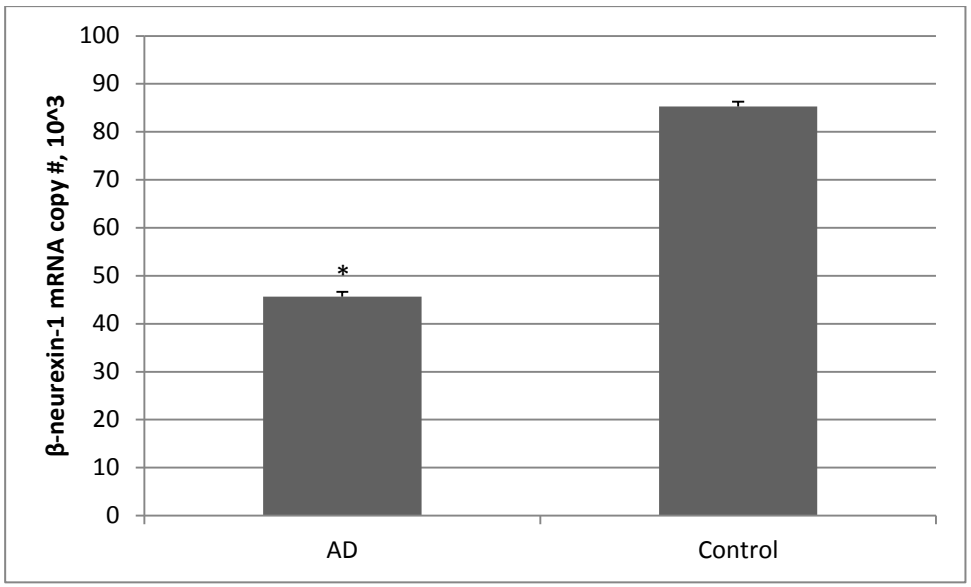

Fig. 5.26. *βNRXN1* transcript level by case-group averaged across the three areas. Details as for Fig. 5.10; *, significantly different from controls, see text.

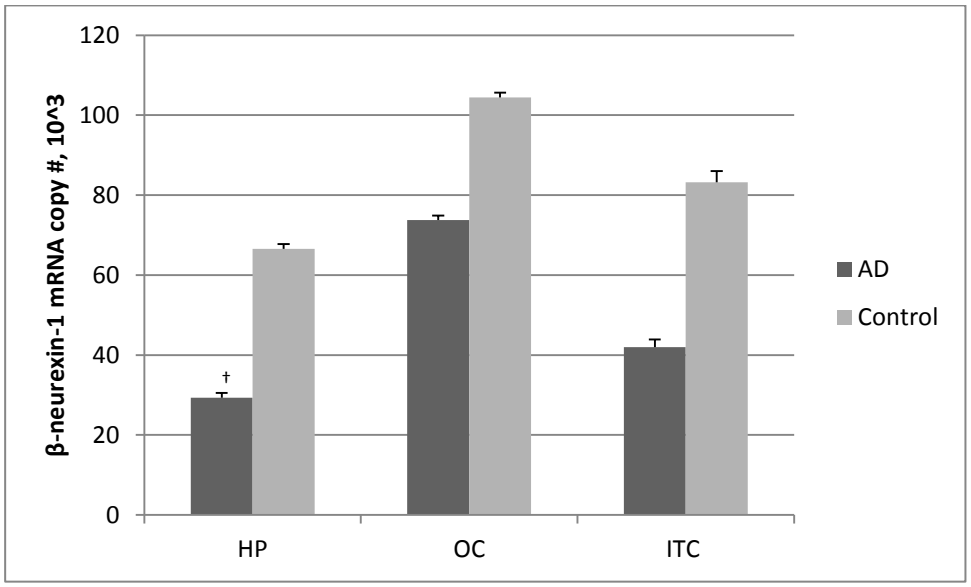

Fig. 5.27. *βNRXN1* mRNA copy numbers by case-group and area. Details as for Fig. 5.11; †, significantly different from occipital cortex and inferior temporal cortex in the same cases, $P < 0.001$ by Newman-Keuls *post-hoc* test. The differences between AD cases and controls showed a strong trend in inferior temporal cortex ($P = 0.06$), and a weak trend in hippocampus ($P = 0.13$), by Newman-Keuls test.

5.4.14 β-Neurexin-1 transcript expression by gender

Overall *βNRXN1* expression was significantly lower in males than in females ($F_{1, 40}$ = 6.192, P = 0.017, and because the same pattern was seen in both case-groups the Group × Sex interaction was not significant ($F_{1,80}$ = 1.457, P =0.23). Post-hoc testing confirmed the differences between cases and controls in each sex/between sexes in each case-group (Fig. 5.28).

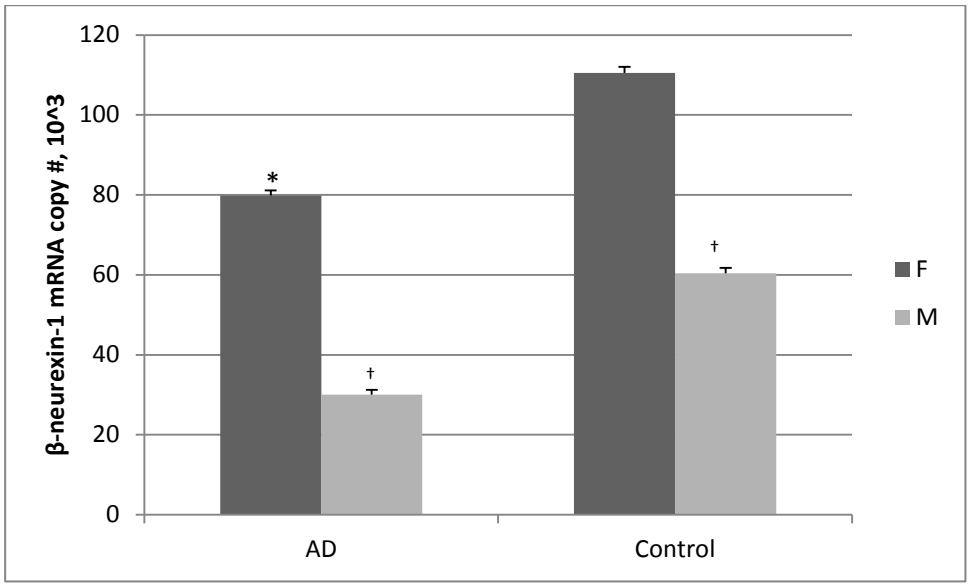

Fig. 5.28. *βNRXN1* copy numbers by case-group and sex. Details as for Fig. 5.11; *, significantly lower than expression in same-sex controls, and †, significantly different from opposite-sex subjects in the same case-group, $P < 0.05$ by Newman-Keuls *post-hoc* test.

The Group × Sex × Area interaction was not significant ($F_{2,48}$ = 0.839, P = 0.43), in part because the pattern seen in Fig. 5.28 was repeated across the three areas (Fig. 5.29), and in part because the statistics for such a deep-level interaction were underpowered. *Post-hoc* testing revealed that the between-group difference only reached significance in occipital cortex in females, though there was a trend in inferior temporal cortex (Fig. 5.29). Within-subject expression was significantly lower in occipital cortex, a pathologically spared area, than in inferior temporal cortex, a strongly affected area, in female AD cases (Fig. 5.29).

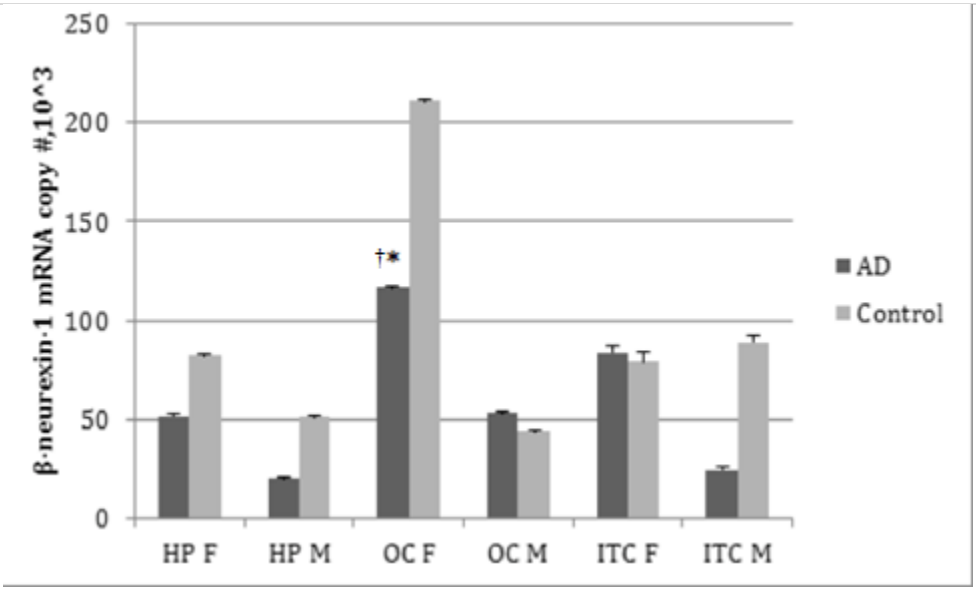

Fig. 5.29. *βNRXN1* copy numbers by case-group, area, and sex. Details as for Fig. 5.11; *, significantly lower in female AD cases than in female controls, $P < 0.001$, and †, significantly higher than in occipital cortex in AD males, $P = 0.013$, by Newman-Keuls *post-hoc* testing. No other comparison was statistically significant.

5.4.15 β-Neurexin-1 transcript expression by APOE genotype

When not divided by diagnosis, the overall level of *βNRXN1* transcript was lower in subjects with at least one ε4 allele ($F_{1,82}$ =6.612, P = 0.01; Fig. 5.30). The level of *βNRXN1*transcript trended lower for both genotypes in AD cases than in matched controls, but the Group × Nº of ε4 alleles was not significant ($F_{1,80}$ =0.430, P =0.51; Fig. 5.31). There was a trend toward significance in the Group × Area × Nº of ε4 alleles interaction but it was not significant ($F_{1,80}$ = 1.770, P = 0.181). *Post-hoc* testing showed no significant difference in expression between AD cases and controls matched for *APOE* genotype in any area of the brain (Fig. 5.32).

5.4.16 β-Neurexin-1 transcript expression and pathological score

There was a graded reduction in β-neurexin-1 copy number with pathological score in all three areas of the AD cases, and the Area × Disease severity interaction was significant ($F_{2,39}$ =8.255, P = 0.001). The pattern varied from region to region, and was most pronounced in inferior temporal cortex (Fig. 5.33), but all area showed markedly lower *βNLGN1* mRNA levels by the severe stage of the disease.

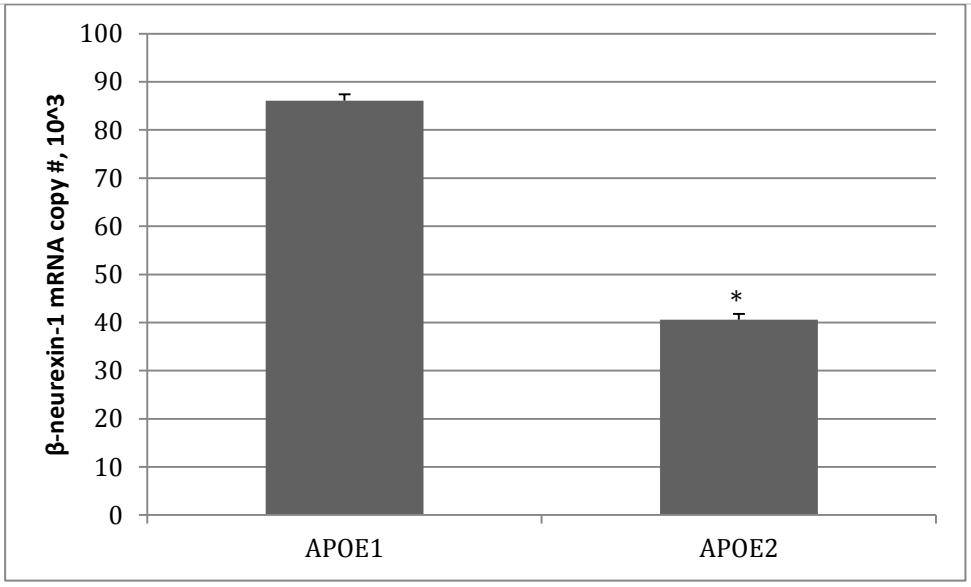

Fig. 5.30. *βNRXN1* transcript expression by *APOE* genotype. Details as for Fig. 5.14; *, significantly lower in subjects with at least one *APOE* ε4 allele, see text.

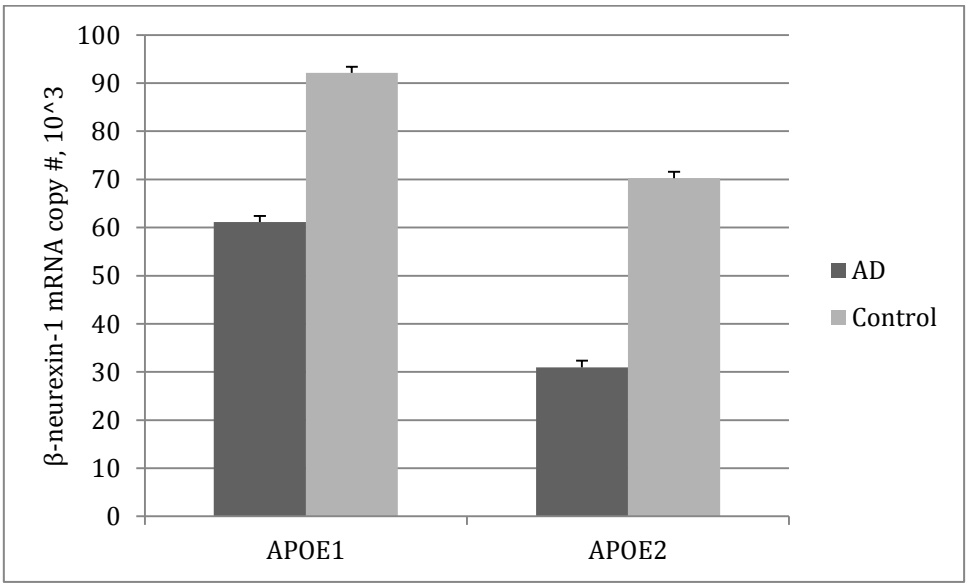

Fig. 5.31. *βNRXN1* transcript expression by case-group and the Nº of *APOE* ε4 alleles. Subjects were separated by *APOE* genotype as set out in Fig. 5.14 legend; there was a trend toward significantly lower expression in AD cases with at least one ε4 allele than in matched controls, $P = 0.09$ by Newman-Keuls *post-hoc* test.

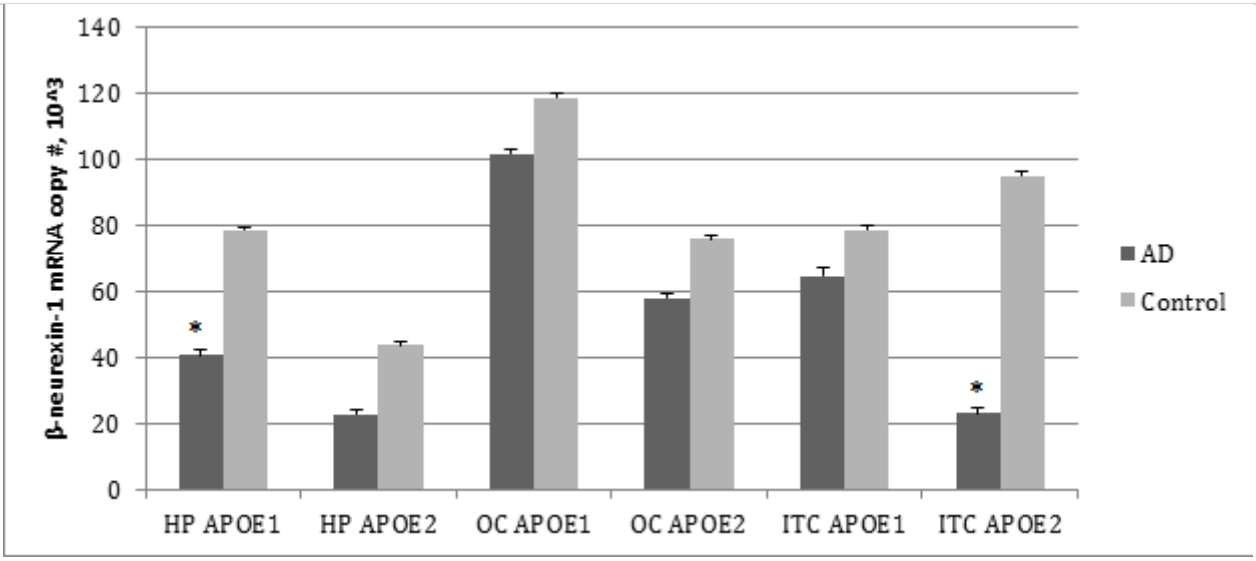

Fig. 5.32. *βNRXN1* mRNA copy numbers by case-group, *APOE* genotype and area. Details as for Fig. 5.14; *, in hippocampus, expression was significantly lower in AD cases with no ε4 alleles than in matched controls, while in inferior temporal cortex AD cases with at least one ε4 allele showed lower expression than the corresponding controls, $P = 0.001$ by Newman-Keuls *post-hoc* testing.

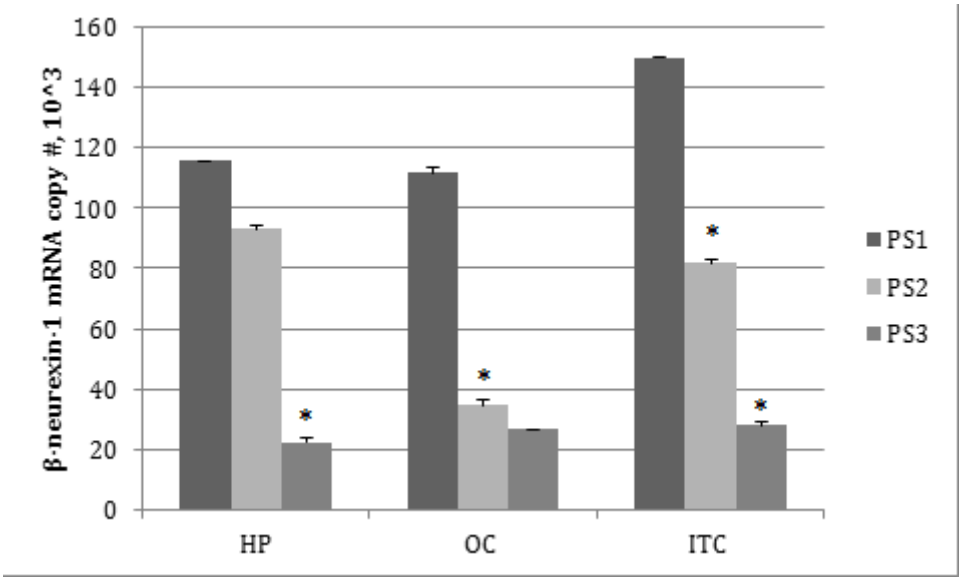

Fig. 5.33. *βNRXN1* copy number and pathological score. Details as for Fig. 5.17. Expression was significantly lower in hippocampus at the severe stage than at either earlier stage ($P = 0.01$ and $P = 0.001$). In occipital cortex, expression was lower at both moderate ($P = 0.03$) and severe ($P = 0.001$) stages than at the mild stage. Expression trended lower in inferior temporal cortex at the moderate stage than at the

mild stage, ($P = 0.063$) and was significantly lower at the severe stage than at the mild stage ($P < 0.001$). Newman-Keuls *post-hoc* tests.

5.5 Discussion

Loss of memory and cognitive dysfunction are associated with the regional impairment of specific synapses, which precedes neuron loss, in the AD brain. Synaptic impairment occurs at early in AD stages and may result from a loss in the amounts and activities of key synaptic proteins, enzymes and receptors. Alterations in the quantities of synaptic proteins that mediate memory, learning, synaptic strength, and plasticity have been reported in the early stages of AD, and underpin the changes in LTP and LTD in animal cell culture models of AD and other diseases. Most changes in synaptic protein expression in many neurological diseases take place at the level of transcription. In the current study, methods were developed to quantify the mRNA levels of the post-synaptic proteins neuroligin-1 and -2 and the pre-synaptic protein β-neurexin-1 by absolute qRT-PCR assays. Expression of the three transcripts was assessed using human autopsy brain tissue from AD cases and gender- and age-matched controls. Two of the areas studied are the most affected areas in AD: hippocampus and inferior temporal cortex, while the relatively spread occipital cortex was used as a regional control. Expression of the three transcripts was also evaluated with respect to gender, *APOE* genotype and pathological severity.

5.5.1 Neuroligin-1 mRNA expression

Neuroligin-1 is a post-synaptic protein located in the excitatory synapse that has been primarily implicated in autism spectrum disorders (ASD) as mutations in gene encoding neuroligin-1 has been linked with some rare cases of inherited ASD (Jamain et al., 2003, 2008, Hines et al., 2008, Lawson-Yuen et al., 2008, Talebizadeh et al., 2005, Yan et al., 2005, Ylisaukko-Oja et al., 2005b). The involvement of neuroligins in synapse formation has been addressed in several studies (Lisé and El-Husseini, 2006, Craig and Kang, 2007). The role of neuroligin-1 in LTP in the amygdala and the development of associative fear memory in adult animals has been established (Kim et al., 2008). Neuroinflammation activated by amyloid deposition results in epigenetic suppression of neuroligin-1

expression and consequent damage of synaptic function and memory (Malkki, 2014). These data help to explain the pathogenic effects of amyloid deposition at the molecular level. The reduction of neuroligin-1 expression lowers synaptic efficacy, impairs synaptic plasticity, and disrupts memory. In line with these findings, the data presented here showed that *NLGN1* mRNA copy numbers were lower in AD cases than in controls. This finding was surprising because it conflicts with data on neuroligin-1 protein level presented in Chapter 3, which were high in AD cases than in controls. Significant differences were observed in *NLGN1* transcript level between AD cases and controls in both hippocampus and inferior temporal cortex.

The highest level of *NLGN1* transcript expression was found in occipital cortex, which is relatively spared in AD. Both hippocampus and inferior temporal cortex showed lower transcript levels. Also noteworthy was the significant, graded decrease in *NLGN1* transcript levels with increasing severity of disease in both hippocampus and inferior temporal cortex. In occipital cortex, *NLGN1* transcript copy number was lower at the moderate stage of disease than at the mild stage, but higher again at the severe stage. The latter could portray attempts by neurons to form new contacts in this region that is resistant to AD pathology, as neuroligin is critical in this process. *NLGN1* transcript copy number was significantly lower in AD males than in AD females, especially in hippocampus and inferior temporal cortex, and lower in AD males than in male controls.

5.5.2 Neuroligin-2 mRNA expression

Neuroligin-2 and its presynaptic binding partner, neurexin, form a complex in the synapse that has an important role in synaptogenesis (Huang and Scheiffele, 2008, Südhof, 2008). *NLGN2* gene knockout *in vivo* and acute *NLGN2* transcript knockdown by shRNAs *in vitro* both generate significant deficits in synaptic transmission (Varoqueaux et al., 2006, Chih et al., 2005). Overexpression of *NLGN2* with $GABA_A$ receptors in HEK cells can induce functional GABAergic innervation from surrounding neurons (Dong et al., 2007), whereas knockdown of *NLGN2* markedly reduces GABAergic synaptogenesis (Sun et al., 2013, Poulopoulos et al., 2009). Transgenic mice overexpressing *NLGN2* display improved GABAergic transmission (Hines et al., 2008), which is impaired in *NLGN2* knockout mice (Blundell et al., 2009).

In the current study, the expression of *NLGN2* transcripts was significantly lower in AD cases than in age- and gender-matched controls. Regionally, *NLGN2* expression in both AD cases and controls was lowest in occipital cortex and highest in inferior temporal cortex and hippocampus. The high level in hippocampus could relate to the critical function of this molecule in regulating contextually appropriate emotional behaviour (Jackson et al., 2012, Belichenko et al., 2009).

The level of *NLGN2* transcript varied with pathological score in AD cases. In hippocampus, *NLGN2* expression decreased with increasing severity of disease. For occipital cortex and inferior temporal cortex, the transcript level was higher at moderate stages but lower again at late stages of the disease. However, dividing the data by transcript, area and pathological score gave a limited number of data points with some of the pathological scores in this higher-order analysis, and adding more cases to the study would help detect trends. *NLGN2* transcript expression was lower in male AD cases than in male controls. The variations in *NLGN2* transcript levels in AD cases and controls were compatible with neuroligin-2 protein expression, which showed the same trends.

5.5.3 β-Neurexin-1 transcript expression

In the current study, *βNRXN1* mRNA copy number was significantly lower in AD cases than in age- and gender-matched controls. The highest transcript expression was found the occipital cortex area, which is the area least affected by AD of the three studied, while the lowest expression was observed in the hippocampus, which is the most-affected area in the AD brain. *βNRXN1* expression was lower in male AD cases than in male controls. The variations in *βNRXN1* level in males were compatible with *NLGN1* and *NLGN2* transcript levels in AD cases and controls. This may indicate that the male cases included in the current study had more-severe Alzheimer's disease than the females. From Table 5.1 it may be seen that the males were on average younger (75 ± 2.5y) than the females (83 ± 2y), and this was statistically significant ($t_{12} = 2.367$, $P = 0.036$); earlier age at death can been argued to be an inverse index of severity (Hynd et al., 2001).

βNRXN1 mRNA copy number was lower in AD cases carrying *APOE* ε4 alleles than in non-carriers. Note, however, that most AD cases in the current study carried at least on *APOE* ε4 allele

(9/14), so this finding must be treated with caution. *βNRXN1* transcript expression decreased with increasing pathological severity of disease, both overall and in all three areas, which may stem from the reduction in total synaptic number. However, additional cases are needed to validate this.

5.5.4 APOE genotype and transcript expression

APOE genotype adds more complexity to the pathophysiology of AD. The *APOE* ε4 allele influences the prevalence of AD and lowers the age of onset in sporadic cases (Ashford, 2004). It is noteworthy that in this study, two of the AD cases possessed a copy of the "protective" ε2 allele, and, as in the Chapter 3 study, several of the controls had the "deleterious" ε4 allele, clearly demonstrating that these factors influence *risk* rather than exhibiting classical Mendelian genetics.

It was predicted that the ε4 allele might impact the pathological severity of brain samples from AD cases. In this study, the quality of RNA was poorer in AD cases than in controls, as assessed by RIN. Nevertheless, no differences were observed in the expression of any of the three transcripts with respect to *APOE* ε4 genotype by group. The current study used AD cases and controls in whom both diagnoses were pathologically confirmed by detailed examination at autopsy. The brain tissue was mostly from late-onset patients, and the transcripts detected reflect the impact of end-stage AD. The conclusions from these mRNA studies give a range of insights and add new data to assist in understanding AD progression and pathology.

5.5.5 Limitations of the study

Overall, the data presented here on *NLGN1*, *NLGN2* and *βNRXN1* transcript expression by qRT-PCR in AD cases and controls show complex variations in gene expression patterns that suggest the involvement of multiple cellular pathways in AD progression. Studies of expression in human autopsy brain are restricted by various factors such as mRNA variability between patient–patient and control–control groups, which can occur due to differences in genetic makeup and lifestyle. These may make gene expression patterns complex in ways are not faced in animal studies (Mirnics and Pevsner, 2004). The most important lifestyle factors to be considered include smoking, alcohol consumption, physical exercise, and diet, which have significant effect on gene expression in the

brain (Dodd et al., 2006, Cotman and Berchtold, 2002). Additional factors like education and exposure to environmental contaminants could also have impacts (Thiriet et al., 2008, Miller et al., 2009, Andin et al., 2007).

The medical history of the subjects is an important potential confound for consideration, because medication can change mRNA expression, but in the current study medical histories were not available. To fully explore AD pathogenesis, it would be ideal to examine brain tissues from unmedicated subjects, but this is unlikely for both AD cases and controls in this age-group. The results from this study might be aided by comparisons with mRNA expression in AD *post-mortem* brains by conventional methods such as Northern blots and microarrays, but the methodology used is currently considered to be the gold standard for quantification. An important consideration is th the in AD that neuropathology of AD does not affect all brain regions to the same extent; this was exploited here by comparing several regions from each brain, such the subjects acted as their own controls. This is particularly important to help reduce the impacts of some of the factors discussed above.

Correlating synaptic protein transcript levels at autopsy with clinical changes observed ante-mortem an important goal for future work, to obtain a more complete picture of the cases included in the study. Clinical data such as the Mini-Mental State Examination (MMSE) and ADAScog for each subject was not available for most cases used here, which come mainly from community donors. Thus, clinical correlates could not be studied. For autopsies that have been in the brain bank for a long time, there are legal aspects of privacy and ethics which made it difficult to recover data, if permission was not explicitly gained from the next of kin at the time of autopsy. Many subjects now being collected have a much higher level of clinical and other data available.

The method used to determine the pathological score of disease severity is not the same as Braak staging, which is based on measuring the spread of NFTs and Aβ across all areas in a brain and gives an accurate representation of actual AD severity. The method used to check the severity of the disease in separate tissue samples here was based on the Aβ plaque and NFT load, neuronal loss

and gliosis. This gave a score from 0 to 3 corresponding to the stages of none, mild, moderate and severe AD in the particular tissues from different brain areas. Both methods have the disadvantage of being semi-quantitative observations of histology markers, and require experienced pathologists who are blinded to diagnosis.

Giving a pathological severity score for each area used can overcome problems related to determining the significance of more-complex, localized interactions, but in the current study it was difficult to obtain sufficiently large numbers of samples with some scores. For instance, there were relatively few samples with pathology scores of 1 or 2 available for hippocampus and inferior temporal cortex, while the opposite was true for occipital cortex. Therefore, it was difficult to obtain statistically significant differences with the number of AD cases available. This problem impacts the transcript level by area, *APOE*, and pathological score interactions.

It has been widely noted that transcript expression often does not relate to protein expression for the products of the same gene, but it can predict overall protein expression. That can be due to different post-translational factors that might impact overall protein isoforms, trafficking, recycling and degradation. These processes may be badly disrupted in neurodegenerative disease. As a result, some differences were not detected in the expression of neuroligin and neurexin transcripts between AD cases and controls, even though marked differences were found at the level of protein expression of these synaptic adhesion molecules.

It's hard to correlate the RNA and protein data because the scales are so different. We applied different Box-Cox transforms to the protein and RNA data, which makes regression analysis very problematic. In preparing the protein-RNA comparison data for publication we will seek the advice of a professional statistician on this point. It is noteworthy that all possible variations can be found in the literature: RNA concentrations can show differences between disease cases and controls that are not reflected in protein levels; or the two moieties can be congruent; or protein levels can differ where no differences in RNA concentrations can be found. The present work is based on a single time-point in the subject's life – i.e., death – and the abundance of transcripts and proteins measured

reflect the difference in the synthesis and degradation of each as well as possible differences in location, compartmentalization, and trafficking.

Chapter 6

6 Genetic association of neuroligins and neurexins with AD

6.1 Aim of the research

The aim of this chapter was to use a case-control association approach in an Australian Caucasian population to confirm the association between AD and the single nucleotide polymorphism (SNP) rs17757879 in *βNRXN3*, previously reported in a Spanish cohort. A meta-analysis of genome-wide association studies (GWAS) had shown that this SNP had a consistent protective effect.

6.2 Introduction

AD genetics can be divided into two types. The first leads to early appearance of the disease, at around 50 to 65 years, and has a strong familial clustering and dominant Mendelian transmission linked to one of three genes, *APP*, *PSEN1* and *PSEN2*. Mutations in any of these lead to modifications in the production of Aβ (Tanzi and Bertram, 2005). However, only 5% of AD cases appear have these familial forms of the disease (Janssen et al., 2003). The second type is by far the more common; cases show later-onset, around 65 years of age, and there is no significant familial aggregation. The genetic underpinning of this form comprises a number of low-penetrance, common risk alleles at different genomic loci that may have impact on various pathways in the production and accumulation of Aβ. Several lines of evidences suggest that combinations of these risk-factor genes have significant effects on disease susceptibility and age of onset (Bertram and Tanzi, 2008). Over the last three decades several very large candidate-gene association studies have been conducted on 500 genes identified as a possible risk factors for late-onset AD (Bertram et al., 2007). Recently, new markers, which are found near or within the following genes: *CLU, PICALM, CR1, BIN1, MS4A, CD2AP, ABCA7, EPHA1,* and *CD33*, have been linked with AD in GWAS (Seshadri et al., 2010, Lambert et al., 2009). However, the ε4 allele of *APOE* still shows the strongest association with late-onset AD (Saunders et al., 1993).

AD is considered to be a polygenic disorder (Pedersen, 2010) and its complex genetic architecture makes genetic analysis difficult. A pathway-based method has been applied to the available GWAS datasets to explore biological mechanisms underlying AD susceptibility. Significant pathways related to the immune system have been identified using KEGG analysis (Hong et al., 2010, Jones et al., 2010, Lambert et al., 2010). (Lambert et al., 2009) performed a GenGen pathway-based analysis of a French AD GWAS dataset and found several significant pathways related to autophagy and the immune system. These pathway-based approaches complement standard single-marker analysis by extracting more biological information from the GWAS datasets. Another recent study consistently found an association between the CAM pathway and AD susceptibility in two GWAS datasets (Liu et al., 2012).

The role of CAM in cognitive decline in AD and the involvement of genes such as *PS1* in regulating the processing of neuroligins and neurexins, as set out in Section 1.4.4.1, have led to the suggestion that mutations in *NLGN* or *NRXN* genes might have roles in sporadic AD. Five GWAS included 1,256 SNPs in the *NRXN1*, *NRXN2*, *NRXN3*, and *NLGN1* genes (3,009 AD cases and 3,006 controls). Meta-analysis identified one SNP in the *NRXN3* gene (rs17757879) that showed a consistent protective effect in all the GWAS, although the differences between AD cases and controls did not reach statistical significance (Martinez-Mir et al., 2013). Dividing the cases by gender showed that the protective effect was limited to males. A replication study conducted in a Spanish cohort of 1,785 AD cases and 1,634 controls confirmed the protective effect in males. These data suggest a possible role for *NRXN* in AD. I undertook to validate the results in this chapter by genotyping the *NRXN3* marker in genomic DNA (gDNA) from Queensland Brian Bank.

6.3 Methods

6.3.1 gDNA preparation from autopsy brain tissue

Autopsy brain tissue samples stored at –80°C in 0.32M sucrose according to the Dodd et al. (1986) protocol were obtained from Queensland Brain Bank. The phenol-chloroform method was used for gDNA extraction. Small pieces from each brain were thawed and incubated overnight in

1 ml lysis buffer (2% SDS, 200 mM NaCl, 50 mM EDTA, 50 mM Tris-HCl, pH 8) and 0.4 mg protease K at 37°C. Next day, 1 ml of phenol:chloroform:isoamyl alcohol (Sigma-Aldrich) was added and the mixture vortexed and centrifuged at 13,000 × *g* for 15 min at room temperature. The top aqueous layer was transferred to a new tube, 1 ml of phenol:chloroform:isoamyl alcohol was again added, and mixture vortexed and centrifuged at 3,000 × *g* for 10 min. The top layer was transferred to new tube, 100 µl of 3 M sodium acetate and 2 ml ethanol were added and the mixture centrifuged at 3,000 × *g* for 10 min at 4°C. The supernatant was discarded, 1 ml of 70% cold ethanol was added to the pellet and the mixture centrifuged at 3,000 × *g* for 10 min at 4°C. The pellet was dried and resuspended in 0.5 ml TE buffer (10 mM Tris-HCl, 1 mM EDTA, pH 8.0).

6.3.2 DNA quantification and quality Control

DNA was quantified on a NanoDrop 1000 Spectrophotometer (Thermo Scientific, Scoresby, Vic, Australia). Samples with higher concentrations were diluted to 10 ng/µl and stored at –20°C until genotyped.

6.3.3 DNA genotyping

Genotypes for 162 AD cases and 119 controls for rs17757879 gene were obtained using Taqman SNP Genotyping Assay (Life Technologies; assay Nº C__34498830_10). This technique was performed in the ABI-ViiA7 RT-PCR facility located at the School of Chemistry and Molecular Biosciences. Assays were prepared by mixing 2.5 µl of 2× TaqMan® Genotyping Master Mix (Applied Biosystems; AmpliTaq Gold® DNA Polymerase ultrapure, buffer, dNTPs, ROX™ dye) with 0.25 µl of TaqMan® SNP Genotyping Assay containing sequence-specific forward and reverse primers and two TaqMan® MGB probes labelled with VIC and 6-carboxy-fluorescein (FAM; Applied Biosystems). 0.25 µl of MilliQ H_20 was added and 2.5 µl of 10 ng/µl gDNA. Total reaction was 5 µl, performed in 384-well plates. PCR conditions were as follows: an initial denaturation step of 95°C for 10 min, followed by 40 cycles of 95°C for 15s and 60°C for 1 min and a final extension step of 60°C for 30s.

6.3.4 Genotyping quality control and validation

Chosen samples were sequenced as a positive control to validate genotyping methods. To confirm the reproducibility of the genotyping results, about 30% of samples were randomly chosen for re-genotyping. The consensus rate ranged from 97% to 100%.

6.3.5 Data quality control

Before performing genetic association analysis, data quality control was applied to check samples and gene polymorphisms with high rates of missing data, which could be caused by poor DNA quality and assay inefficiency. A Hardy-Weinberg equilibrium (HWE) test was performed to detect bias in dominant/recessive models of tri-allelic genotype for both AD cases and controls.

6.3.6 Genetic association

Genetic association of tri-allelic polymorphisms were detected by the χ^2 test of association for allelic (D vs d), genotypic (DD vs Dd vs dd), dominant (DD+Dd vs dd) and recessive (DD vs Dd+dd) models.

6.3.7 Sample size and power

Statistical power estimated by the Genetic Power Calculator (Purcell et al., 2003) showed that 96 cases and 115 controls were required to attain 80% power at $\alpha = 0.05$ for allelic comparison (relative risk increases by 2 in the presence of one copy of the risk allele). The prevalence of AD is 13% according to Thies and Bleiler (2013).

6.4 Results

Genotyping missing data rates were less than 3% for all polymorphisms. The sample size was 162 AD cases and 119 controls. The genotype distribution did not deviate significantly from HWE in cases or controls (Table 6.1). Data were re-classified as a bi-allelic model before analysis. Genotype distributions were analysed separately in SPSS v.17.

6.4.1 Genotypic and allelic associations

No significant difference was observed between AD cases and controls in general (χ^2 = 2.069, df = 2, *P* = 0.36). To check if there is any significant association with gender SNP, a χ^2 test was performed between AD cases and control for each gender separately. No significant differences were observed in females, but males trended toward significance in CC allele frequency (Table 6.2). To maximize the statistical power and to make a valid summary, CT and TT alleles combined were against the CC allele. This gave near-significant association in males but not in females (Table 6.3).

Table 6.1. Genotype and allele distributions of rs17757879.

	Alleles	AD Cases	HWE χ^2	Controls	HWE χ^2	*P*
β-NRXN-3	CC	116	1.14	77	0.45	0.355
rs17757879	CT	40		38		
	TT	6		3		

Table 6.2. Genotyping allele distribution of rs17757879 SNP between genders.

	Males			Females		
	AD Cases	Controls	χ^2	AD Cases	Controls	χ^2
β-NRXN-3	n = 83	n = 79	3.872;	n = 79	n = 39	0.142;
rs17757879			*P* = 0.144			*P* = 0.931
CC/CT/TT	63/17/3	50/27/2		53/23/3	27/11/1	

6.5 Discussion

GWAS in AD was performed by Harold et al. (2009) and two SNPs in NRXN-3 were listed as possibly associated with AD. However, the same group perform larger follow-up work and the association with these two SNPs disappeared (Hollingworth et al., 2011).

Considering the recent studies about the molecular interaction between γ-secretase and the neurexins and neuroligins (Suzuki et al., 2012, Saura et al., 2011, Martinez-Mir et al., 2013, Bot et

al., 2011) and the physical interaction of neurexin-neuroligin complex (Chih et al., 2006, Boucard et al., 2005), attention was given to these molecules and their genetic association with AD. A meta-analysis utilizing five GWAS datasets was performed by including previous work conducted by the same group (Antunez et al., 2011). Antunez et al. (2011) found no association of *NRXN* or *NLGN* with sporadic AD; these data were similar to the result obtained from previous GWAS. By limiting the study to localized regions of the selected genes, an interesting and consistent association was observed — although not statistically significant — with the rs17757879 SNP within the *NRXN3* gene across the five GWAS analysed (Martinez-Mir et al., 2013). Remarkably, the effect observed with *β-NRXN-3* SNP was found only in males but not in females.

Table 6.3. Distribution of rs17757879 SNP between sexes for combined alleles, CT + TT *vs* CC

	Males			Females		
	AD Cases	Controls	χ^2	AD Cases	Controls	χ^2
β-NRXN-3	n = 83	n = 79	3.052;	n = 79	n = 39	0.55;
rs17757879			*P* = 0.057			*P* = 0.49
CC+CT/TT	63/20	50/29		53/26	27/12	

In this chapter I performed a genotyping study on the rs17757879 SNP with the available population from the Queensland Brain Bank. Tissue samples were taken from 162 AD cases and 119 controls. The genotyping showed no significant association overall between the SNP and the disease. However, by divinding the subjects by gender, I found a trend toward significance between rs17757879 and AD. The most interesting finding was obtained by comparing subjects with at least one T allele (CT and TT) against CC homozygotes. This gave a near-significant result, which indicated that the T allele was protective against AD in males. Since the study was based on a prediction from earlier work, it may be justified to use 1-tailed statistics, in which case the *P* value would be significant, at 0.028. The data indicate that the effect size for the *NRXN*-3 SNP in AD is quite small, which would be consistent with it not being associated to AD in previous GWAS, although it should be noted that the sample was quite small for genetic work. A repetition with a

larger sample is clearly necessary. Considering the dimorphism observed in the current and previous studies will be important to elucidate the role of *NRXN*-3 in AD susceptibility.

Various studies have shown differential expression of genes in the brain according to sex (Cahill, 2006). Previous evidence of morphological and functional brain dimorphisms have raised the awareness of the importance of sex in molecular neuroscience. Differences between males and females are ultimately controlled by the gonadal sex determination systems (Carruth et al., 2002). Due to factors controlled by the sex chromosomes, the impact of hormones is central, especially the gonadal hormones and their actions in the CNS (Flerko, 1971). The main male hormone testosterone is produced by the testes during late gestational and neonatal periods, where it mediates brain sexual dimorphism. Sexual dimorphism could mediate male-female differences in the ætiology, incidence, and development course of different neurological disorders, including AD.

Several lines of evidences support the hypothesis of sexual dimorphism in AD, such as the higher incidence of AD in females than in males (Mielke et al., 2014). There are differences in the expression of synaptic proteins in between female and male AD cases (Proctor et al., 2010, Agarwal et al., 2008). Differential expression of protein and mRNA transcripts of the neuroligin–neurexin complex between male and females was also observed in the current study (Chapters 3 and 5). Sexual dimorphism for ESR1and APOE in AD was also observed in some studies (Monastero et al., 2006). These data indicate that stratification by sex in GWAS analysis could be a strategy to detect novel genetic alterations linked to AD susceptibility. *NRXN-3* has not previously been reported to show sexual dimorphism in human subjects. However, in *α-NRXN-1* heterozygous KO mice only male and show increased locomotor activity in a new environment and improved habituation upon subsequent exposures to this environment (Laarakker et al., 2012).

The results from the current chapter indicate that the *β-NRXN*-3 gene could mediate AD susceptibility in males, and that the differences between genders observed could explain the lack of association of *β-NRXN3* with AD in published GWAS. Additional replication studies in bigger samples are required to confirm these results.

6.5.1 Limitation of the study

Some DNA samples for both cases and controls were obtained from different sources that produce characteristic that should be considered. The geographical origin, and as a result the ethnicity, of the subjects, was not 100% confirmed as Caucasian. As noted, the sample size was very small, and must it be considered to be a pilot. Increasing the number of subjects will provide more reliable results.

The choice of the technique use for genotyping here was based on many factors, including accuracy of the assay, sensitivity, robustness, reproducibility, cost, and reliability. A SNP detection assay is capable of detecting mixed alleles and it is crucial to note that the TaqMan genotyping assay is a PCR-based protocol that discriminates the presence of either allele based on the affinity of one probe to the SNP sequences of the allele present as opposed to the one not present. Allele detection relies on the chemistry of each set of probes, which should provide accurate results so long as the samples are subjected to a low number of freeze-thaw cycles (ideally, none) and are stored at the right temperature. Care was taken here to only thaw samples once, at the time of homogenization; as noted, they had been stored at –80°C since autopsy.

Chapter 7

7 Final discussion, conclusions and future direction

7.1 General findings and implications of the project

Alzheimer's disease was first described in 1906, but no cure has been found nor any drug with significant impact developed. The characterization and sequencing of the main constituents of Aβ and NFTs has helped established links between these pathological markers and AD. Although this was an important advance in knowledge of the basic roles of these proteins and their critical function in neurotoxic pathways in AD, it has not led to significant attenuation of the disease. Most researchers agree that Aβ and NFTs have a significant function in the overall pathophysiology of AD; these deposits are pathological alterations that take place quite early in the disease timeline. Much evidence supports the idea that synaptic loss and dysfunction are better correlates with early cognitive decline in AD. A significant outcome of synaptic failure is the disruption of plasticity and LTP at early stages in AD animal models (Rowan et al., 2003). These functionalities are major mediators of memory and learning processes, so it is likely that such alterations play roles in the early in cognitive problems experienced by AD sufferers as the disease develops. The mechanisms that underlie synaptic dysfunction and neuronal loss are still unknown. Nevertheless, results from different studies have detected common changes in systems and pathways, which provide indications of the proteins or receptors that are most likely altered in the disease. The aim to detect these synaptic protein alterations was the basis of the studies in this thesis.

7.2 The expression of neuroligin and neurexins proteins and transcripts in AD

Presented here is the first study to quantify neurexins and neuroligins at both the transcript and protein level in AD. In Chapter 2, a quantitative immnodetection method was developed. First, recombinant truncate neuroligin-1 and neuroligin-2 proteins were cloned, expressed, and purified. These were used as standards to precisely quantify endogenous neuroligin-1 and neuroligin-2 in two of the most affected area in the brain, hippocampus and inferior temporal cortex, and the relatively

spared occipital cortex. β-Neurexin-1 protein level was quantified in the same area by the same approach, using a commercial sample of neurexin recombinant protein. A major novel finding was the differing regional patterns of these proteins in AD cases and controls. Notably, the level of neuroligin-1 protein was significantly higher in AD cases than in controls. This difference was restricted to hippocampus and occipital cortex; the lack of difference in inferior temporal cortex was unexpected, since it is one of the most affected areas in the AD brain. In contrast, the opposite pattern was found for neuroligin-2 in the same AD cases and controls. Neuroligin-2 protein expression was lower in AD cases than control in all areas, but the most marked reduction was in inferior temporal cortex. The contrasting patterns of neuroligin-1 and neuroligin-2 expression in AD may reflect the complementary functions of these proteins at the synapse. Both molecules are localized to the post-synaptic density, but neuroligin-1 is specific for excitatory synapses while neuroligin-2 is specific for inhibitory synapses. It has been reported, in studies conducted *in vitro* using biochemical and physicochemical techniques, that neuroligin-1 binds to Aβ oligomers and that this binding takes place *via* the extracellular domain of neuroligin-1. This signifies that neuroligin-1 is a putative target for Aβ oligomers at excitatory synapses. On the other hand, Aβ reportedly does not bind to neuroligin-2, which is specific for inhibitory synapses. Aβ binding may explain the higher level of neuroligin-1 in AD cases found here. Aβ facilitates glutamate-mediated synaptic transmission in animal models, which could lead to alterations in the homeostasis of neuronal networks, a phenomenon that has been widely documented in AD (Palop et al., 2007, Cuevas et al., 2011). Neuroligin-1 performs a significant function as an adhesion protein on the post- synaptic membrane, where it stabilizes and maintains synaptic transmission; the binding of Aβ oligomers in AD would thus have a significant impact (Dinamarca et al., 2011).

In the current study the level of β-neurexin-1 was higher in AD cases than in controls, but this difference was not significant. This slight increase could reflect neurotoxicity arising from the binding of Aβ to neuroligin-1, given that β-neurexin-1 is located on pre-synaptic terminals. At these synapses it binds to neuroligin-1 and forms heterophilic adhesion complexes. Any disturbance of this binding could have an impact on the integrity of excitatory synaptic contacts in AD.

To further understand the roles of these molecules in AD, the levels of neuroligin-1, neuroligin-2 and β-neurexin-1 transcripts in hippocampus, occipital cortex and inferior temporal cortex in AD cases and controls were measured using absolute quantification RT-PCR TaqMan assays (Chapter 5). The data obtained were in contradistinction to the protein data in Chapter 3. The expression of all three transcripts was significantly lower in AD cases than in controls. It was found that the mRNA copy number for all transcripts was negatively correlated with increasing the severity of disease. That is, the observed down-regulation of the transcripts could follow the progression of disease. The contrary results obtained for protein levels for neuroligin-1 and β-neurexin-1 may suggest that the higher protein levels arise from the binding of these proteins to Aβ which induce the neurotoxicity at the protein level.

7.3 Conclusion and Future directions

No specific, single molecule is essential for synaptic assembly or function. Nevertheless, the neuroligin–neurexin complex is a major organizer of synaptic connections and a stabilizer of the networks of pre- and post-synaptic proteins across the synaptic junction. The ability of neuroligins and neurexins to determine and maintain excitatory and inhibitory synapses provides a basis for their potential roles in neurological disorders such as AD. Changes in groups of synapses in a neural circuit, as opposed to a general impairment of all synapses in all circuits, makes it very difficult to compare single-protein complexes across brain disorders. Identical molecular changes could lead to varying neurological outcomes in different brain diseases.

Data presented in this thesis indicate that neuroligins and neurexins are implicated, at least in part, in synaptic loss in AD. Further understanding of the association between fluctuations in the levels of neuroligin–neurexin complexes could open up a new understanding of synaptic pathogenesis in AD.

The proteolytic regulation of neuroligins and neurexins may be a key pathophysiological mechanism in AD, as well as playing a general role in trans-synaptic signalling in diverse neural circuits. Therapeutic strategies for preventing or ameliorating synaptic dysfunction in AD might

fruitfully explore whether, and how, this process can be modified. The pathological disturbance of synapses through disruption of the metalloprotease and γ-secretase cleavage pathways may be critical to synaptic deficits in mild cognitive impairment and early-stage AD, which then lead to cognitive dysfunction and neurotoxicity in late-stage AD. Impairments in the processing of the neuroligin–neurexin complex due to a loss of PS1/γ-secretase activity could contribute to neuronal disruption. Neurexins have the LNS domain responsible for interaction with the CLD of neuroligin across the synaptic cleft. The transmembrane domain and C-terminal cytoplasmic tail of neuroligins comprise a PDZ II binding motif crucial for targeting presynaptic proteins such as CASK, VELI and MINT that play roles in vesicle clustering (Tabuchi and Südhof, 2002). The physical interactions of neurexins with neuroligins on the extracellular side of the membrane, and with scaffolding proteins on the cytoplasmic side, underpin the assembly of synapses. Impaired processing of full-length β-neurexin-3 by α- and γ-secretases could alter the activity of synapses in AD. As discussed earlier in the thesis, mutations in the catalytic core of γ-secretase that lead to early-onset forms of AD also impair the processing of β-neurexin-3.

Studies on the relationship between this complex and AD should attempt to answer the following questions: 1. Do neurexins and neuroligins function only by binding to each other, or through binding with other molecules? 2. Do different isoforms or splice variants of neurexins and neuroligins perform different functions? 3. Do these complexes have an effect on Aβ accumulation? 4. Does the impairment of neuroligin and neurexin processing and production play a role in the neuronal defects associated with a loss of PS/γ-secretase function in familial AD?

The answers to these questions will provide insight into the mechanisms of synaptic adhesion in AD and other cognitive diseases. If the involvement of this complex in AD is confirmed, new diagnostic and therapeutic approaches might emerge, such as manipulating the neuroligin–neurexin interaction to prevent Aβ accumulation in the brain, or perhaps preventing Aβ from disrupting neuroligin–neurexin complexes.

8 References

Addona, T. A., Abbatiello, S. E., Schilling, B., Skates, S. J., Mani, D. R., Bunk, D. M., Spiegelman, C. H., Zimmerman, L. J., Ham, A. J., Keshishian, H., Hall, S. C., Allen, S., Blackman, R. K., Borchers, C. H., Buck, C., Cardasis, H. L., Cusack, M. P., Dodder, N. G., Gibson, B. W., Held, J. M., Hiltke, T., Jackson, A., Johansen, E. B., Kinsinger, C. R., Li, J., Mesri, M., Neubert, T. A., Niles, R. K., Pulsipher, T. C., Ransohoff, D., Rodriguez, H., Rudnick, P. A., Smith, D., Tabb, D. L., Tegeler, T. J., Variyath, A. M., Vega-Montoto, L. J., Wahlander, A., Waldemarson, S., Wang, M., Whiteaker, J. R., Zhao, L., Anderson, N. L., Fisher, S. J., Liebler, D. C., Paulovich, A. G., Regnier, F. E., Tempst, P. & Carr, S. A. 2009. Multi-site assessment of the precision and reproducibility of multiple reaction monitoring-based measurements of proteins in plasma. *Nat. Biotechnol.*, 27, 633–41.

Agarwal, S., Tannenberg, R. K. & Dodd, P. R. 2008. Reduced expression of the inhibitory synapse scaffolding protein gephyrin in Alzheimer's disease. *J. Alzheimers Dis.*, 14, 313–21.

Akiyama, H., Kawamata, T., Dedhar, S. & Mcgeer, P. L. 1991. Immunohistochemical localization of vitronectin, its receptor and β-3 integrin in Alzheimer brain tissue. *J. Neuroimmunol.*, 32, 19–28.

Alonso, A. C., Zaidi, T., Grundke-Iqbal, I. & Iqbal, K. 1994. Role of abnormally phosphorylated tau in the breakdown of microtubules in Alzheimer disease. *Proc. Natl. Acad. Sci. U.S.A.*, 91, 5562–6.

Alonso-Nanclares, L., Merino-Serrais, P., Gonzalez, S. & Defelipe, J. 2013. Synaptic changes in the dentate gyrus of APP/PS1 transgenic mice revealed by electron microscopy. *J. Neuropathol. Exp. Neurol.*, 72, 386–95.

Altschul, S. F., Madden, T. L., Schaffer, A. A., Zhang, J., Zhang, Z., Miller, W. & Lipman, D. J. 1997. Gapped BLAST and PSI-BLAST: a new generation of protein database search programs. *Nucleic Acids Res.*, 25, 3389–402.

Alzheimer, A., Stelzmann, R. A., Schnitzlein, H. N. & Murtagh, F. R. 1995. An English translation of Alzheimer's 1907 paper, "Uber eine eigenartige Erkankung der Hirnrinde". *Clin. Anat.*, 8, 429–31.

Andin, J., Hallbeck, M., Mohammed, A. H. & Marcusson, J. 2007. Influence of environmental enrichment on steady-state mRNA levels for EAAC1, AMPA1 and NMDA2A receptor subunits in rat hippocampus. *Brain Res.*, 1174, 18–27.

Ando, K., Uemura, K., Kuzuya, A., Maesako, M., Asada-Utsugi, M., Kubota, M., Aoyagi, N., Yoshioka, K., Okawa, K., Inoue, H., Kawamata, J., Shimohama, S., Arai, T., Takahashi, R. & Kinoshita, A. 2011. N-cadherin regulates p38 MAPK signaling *via* association with JNK-associated leucine zipper protein: implications for neurodegeneration in Alzheimer disease. *J. Biol. Chem.*, 286, 7619–28.

Andres, C., Beeri, R., Friedman, A., Lev-Lehman, E., Henis, S., Timberg, R., Shani, M. & Soreq, H. 1997. Acetylcholinesterase-transgenic mice display embryonic modulations in spinal cord choline acetyltransferase and neurexin Iβ gene expression followed by late-onset neuromotor deterioration. *Proc. Natl. Acad. Sci. U.S.A.*, 94, 8173–8.

Andreyeva, A., Nieweg, K., Horstmann, K., Klapper, S., Müller-Schiffmann, A., Korth, C. & Gottmann, K. 2012. C-terminal fragment of N-cadherin accelerates synapse destabilization by amyloid-β. *Brain*, 135, 2140–54.

Anstey, K. J., Von Sanden, C., Salim, A. & O'Kearney, R. 2007. Smoking as a risk factor for dementia and cognitive decline: a meta-analysis of prospective studies. *Am. J. Epidemiol.*, 166, 367–78.

Antunez, C., Boada, M., Gonzalez-Perez, A., Gayan, J., Ramirez-Lorca, R., Marin, J., Hernandez, I., Moreno-Rey, C., Moron, F. J., Lopez-Arrieta, J., Mauleon, A., Rosende-Roca, M., Noguera-Perea, F., Legaz-Garcia, A., Vivancos-Moreau, L., Velasco, J., Carrasco, J. M., Alegret, M., Antequera-Torres, M., Manzanares, S., Romo, A., Blanca, I., Ruiz, S., Espinosa, A., Castano, S., Garcia, B., Martinez-Herrada, B., Vinyes, G., Lafuente, A., Becker, J. T., Galan, J. J., Serrano-Rios, M., Vazquez, E., Tarraga, L., Saez, M. E., Lopez, O. L., Real, L. M. & Ruiz, A. 2011. The membrane-spanning 4-domains, subfamily A (MS4A) gene cluster contains a common variant associated with Alzheimer's disease. *Genome Med.*, 3, 33.

Arendt, T. 2009. Synaptic degeneration in Alzheimer's disease. *Acta Neuropathol.*, 118, 167–79.

Asada-Utsugi, M., Uemura, K., Noda, Y., Kuzuya, A., Maesako, M., Ando, K., Kubota, M., Watanabe, K., Takahashi, M., Kihara, T., Shimohama, S., Takahashi, R., Berezovska, O. & Kinoshita, A. 2011. N-cadherin enhances APP dimerization at the extracellular domain and modulates Aβ production. *J. Neurochem.*, 119, 354–63.

Ashe, K. H. 2001. Learning and memory in transgenic mice modeling Alzheimer's disease. *Learn. Mem.*, 8, 301–8.

Ashford, J. W. 2004. *APOE* genotype effects on Alzheimer's disease onset and epidemiology. *J. Mol. Neurosci.*, 23, 157–65.

Bamji, S. X., Shimazu, K., Kimes, N., Huelsken, J., Birchmeier, W., Lu, B. & Reichardt, L. F. 2003. Role of β-catenin in synaptic vesicle localization and presynaptic assembly. *Neuron*, 40, 719–31.

Bancher, C., Braak, H., Fischer, P. & Jellinger, K. A. 1993. Neuropathological staging of Alzheimer lesions and intellectual status in Alzheimer's and Parkinson's disease patients. *Neurosci. Lett.*, 162, 179–82.

Bard, L. & Groc, L. 2011. Glutamate receptor dynamics and protein interaction: lessons from the NMDA receptor. *Mol. Cell. Neurosci.*, 48, 298–307.

Barrett, T., Troup, D. B., Wilhite, S. E., Ledoux, P., Rudnev, D., Evangelista, C., Kim, I. F., Soboleva, A., Tomashevsky, M. & Edgar, R. 2007. NCBI GEO: mining tens of millions of expression profiles — database and tools update. *Nucleic Acids Res.*, 35, D760–5.

Barria, A. & Malinow, R. 2002. Subunit-specific NMDA receptor trafficking to synapses. *Neuron*, 35, 345–53.

Bayes, A., Van De Lagemaat, L. N., Collins, M. O., Croning, M. D., Whittle, I. R., Choudhary, J. S. & Grant, S. G. 2011. Characterization of the proteome, diseases and evolution of the human postsynaptic density. *Nat. Neurosci.*, 14, 19–21.

Beel, A. J. & Sanders, C. R. 2008. Substrate specificity of γ-secretase and other intramembrane proteases. *Cell. Mol. Life Sci.*, 65, 1311–34.

Belichenko, P. V., Kleschevnikov, A. M., Masliah, E., Wu, C., Takimoto-Kimura, R., Salehi, A. & Mobley, W. C. 2009. Excitatory-inhibitory relationship in the fascia dentata in the Ts65Dn mouse model of Down syndrome. *J. Comp. Neurol.*, 512, 453–66.

Benson, D. L. & Tanaka, H. 1998. N-cadherin redistribution during synaptogenesis in hippocampal neurons. *J. Neurosci.*, 18, 6892–904.

Bertram, L., Mcqueen, M. B., Mullin, K., Blacker, D. & Tanzi, R. E. 2007. Systematic meta-analyses of Alzheimer disease genetic association studies: the AlzGene database. *Nat. Genet.*, 39, 17–23.

Bertram, L. & Tanzi, R. E. 2008. Thirty years of Alzheimer's disease genetics: the implications of systematic meta-analyses. *Nat. Rev. Neurosci.*, 9, 768–78.

Blundell, J., Tabuchi, K., Bolliger, M. F., Blaiss, C. A., Brose, N., Liu, X., Südhof, T. C. & Powell, C. M. 2009. Increased anxiety-like behavior in mice lacking the inhibitory synapse cell adhesion molecule neuroligin 2. *Genes Brain Behav.*, 8, 114–26.

Blundell, J., Blaiss, C. A., Etherton, M. R., Espinosa, F., Tabuchi, K., Walz, C., Bolliger, M. F., Südhof, T. C. & Powell, C. M. 2010. Neuroligin-1 deletion results in impaired spatial memory and increased repetitive behavior. *J. Neurosci.*, 30, 2115–29.

Bolliger, M. F., Frei, K., Winterhalter, K. H. & Gloor, S. M. 2001. Identification of a novel neuroligin in humans which binds to PSD-95 and has a widespread expression. *Biochem. J.*, 356, 581–8.

Bot, N., Schweizer, C., Ben Halima, S. & Fraering, P. C. 2011. Processing of the synaptic cell adhesion molecule neurexin-3β by Alzheimer disease α and γ-secretases. *J. Biol. Chem.*, 286, 2762–73.

Boucard, A. A., Chubykin, A. A., Comoletti, D., Taylor, P. & Südhof, T. C. 2005. A splice code for trans-synaptic cell adhesion mediated by binding of neuroligin 1 to α and β-neurexins. *Neuron*, 48, 229–36.

Boyles, J. K., Zoellner, C. D., Anderson, L. J., Kosik, L. M., Pitas, R. E., Weisgraber, K. H., Hui, D. Y., Mahley, R. W., Gebicke-Haerter, P. J., Ignatius, M. J. & Shooter, E. M. 1989. A role for

apolipoprotein E, apolipoprotein A-I, and low density lipoprotein receptors in cholesterol transport during regeneration and remyelination of the rat sciatic nerve. *J. Clin. Invest.*, 83, 1015–31.

Braak, H., Braak, E., Ohm, T. & Bohl, J. 1988. Silver impregnation of Alzheimer's neurofibrillary changes counterstained for basophilic material and lipofuscin pigment. *Stain Technol.*, 63, 197–200.

Braak, H. & Braak, E. 1991a. Neuropathological stageing of Alzheimer-related changes. *Acta Neuropathol.*, 82, 239–59.

Braak, H. & Braak, E. 1991b. Demonstration of amyloid deposits and neurofibrillary changes in whole brain sections. *Brain Pathol.*, 1, 213–6.

Braak, H., Thal, D. R., Ghebremedhin, E. & Del Tredici, K. 2011. Stages of the pathologic process in Alzheimer disease: age categories from 1 to 100 years. *J. Neuropathol. Exp. Neurol.*, 70, 960–9.

Brunden, K. R., Trojanowski, J. Q. & Lee, V. M. 2009. Advances in tau-focused drug discovery for Alzheimer's disease and related tauopathies. *Nat. Rev. Drug Discov.*, 8, 783–93.

Butner, K. A. & Kirschner, M. W. 1991. Tau protein binds to microtubules through a flexible array of distributed weak sites. *J. Cell. Biol.*, 115, 717–30.

Buttini, M., Akeefe, H., Lin, C., Mahley, R. W., Pitas, R. E., Wyss-Coray, T. & Mucke, L. 2000. Dominant negative effects of apolipoprotein E4 revealed in transgenic models of neurodegenerative disease. *Neuroscience*, 97, 207–10.

Buttini, M., Masliah, E., Barbour, R., Grajeda, H., Motter, R., Johnson-Wood, K., Khan, K., Seubert, P., Freedman, S., Schenk, D. & Games, D. 2005. β-amyloid immunotherapy prevents synaptic degeneration in a mouse model of Alzheimer's disease. *J. Neurosci.*, 25, 9096–101.

Cahill, L. 2006. Why sex matters for neuroscience. *Nat. Rev. Neurosci.*, 7, 477–84.

Carruth, L. L., Reisert, I. & Arnold, A. P. 2002. Sex chromosome genes directly affect brain sexual differentiation. *Nat. Neurosci.*, 5, 933–4.

Cartier, A. E., Djakovic, S. N., Salehi, A., Wilson, S. M., Masliah, E. & Patrick, G. N. 2009. Regulation of synaptic structure by ubiquitin C-terminal hydrolase L1. *J. Neurosci.*, 29, 7857–68.

Castano, E. M., Roher, A. E., Esh, C. L., Kokjohn, T. A. & Beach, T. 2006. Comparative proteomics of cerebrospinal fluid in neuropathologically-confirmed Alzheimer's disease and non-demented elderly subjects. *Neurol. Res.*, 28, 155–63.

Chang, R. Y., Nouwens, A. S., Dodd, P. R. & Etheridge, N. 2013. The synaptic proteome in Alzheimer's disease. *Alzheimers Dement.*, 9, 499–511.

Chang, R. Y., Etheridge, N., Dodd, P. & Nouwens, A. 2014a. Quantitative multiple reaction monitoring analysis of synaptic proteins from human brain. *J. Neurosci. Methods*, 227, 189–210.

Chang, R. Y., Etheridge, N., Dodd, P. R. & Nouwens, A. S. 2014b. Targeted quantitative analysis of synaptic proteins in Alzheimer's disease brain. *Neurochem. Int.*, 75, 66–75.

Chapman, P. F., Falinska, A. M., Knevett, S. G. & Ramsay, M. F. 2001. Genes, models and Alzheimer's disease. *Trends Genet.*, 17, 254–61.

Cheng, D., Hoogenraad, C. C., Rush, J., Ramm, E., Schlager, M. A., Duong, D. M., Xu, P., Wijayawardana, S. R., Hanfelt, J., Nakagawa, T., Sheng, M. & Peng, J. 2006. Relative and absolute quantification of postsynaptic density proteome isolated from rat forebrain and cerebellum. *Mol. Cell. Proteomics*, 5, 1158–70.

Chevyreva, I., Faull, R. L., Green, C. R. & Nicholson, L. F. 2008. Assessing RNA quality in postmortem human brain tissue. *Exp. Mol. Pathol.*, 84, 71–7.

Chih, B., Engelman, H. & Scheiffele, P. 2005. Control of excitatory and inhibitory synapse formation by neuroligins. *Science*, 307, 1324–8.

Chih, B., Gollan, L. & Scheiffele, P. 2006. Alternative splicing controls selective trans-synaptic interactions of the neuroligin–neurexin complex. *Neuron*, 51, 171–8.

Choi, Y. B., Li, H. L., Kassabov, S. R., Jin, I., Puthanveettil, S. V., Karl, K. A., Lu, Y., Kim, J. H., Bailey, C. H. & Kandel, E. R. 2011. Neurexin-neuroligin transsynaptic interaction mediates

learning-related synaptic remodeling and long-term facilitation in aplysia. *Neuron*, 70, 468–81.

Christensen, K., Thinggaard, M., Oksuzyan, A., Steenstrup, T., Andersen-Ranberg, K., Jeune, B., Mcgue, M. & Vaupel, J. W. 2013. Physical and cognitive functioning of people older than 90 years: a comparison of two Danish cohorts born 10 years apart. *Lancet*, 382, 1507–13.

Chubykin, A. A., Atasoy, D., Etherton, M. R., Brose, N., Kavalali, E. T., Gibson, J. R. & Südhof, T. C. 2007. Activity-dependent validation of excitatory versus inhibitory synapses by neuroligin-1 versus neuroligin-2. *Neuron*, 54, 919–31.

Cirrito, J. R., Yamada, K. A., Finn, M. B., Sloviter, R. S., Bales, K. R., May, P. C., Schoepp, D. D., Paul, S. M., Mennerick, S. & Holtzman, D. M. 2005. Synaptic activity regulates interstitial fluid amyloid-β levels *in vivo*. *Neuron*, 48, 913–22.

Clark, L. N., Poorkaj, P., Wszolek, Z., Geschwind, D. H., Nasreddine, Z. S., Miller, B., Li, D., Payami, H., Awert, F., Markopoulou, K., Andreadis, A., D'Souza, I., Lee, V. M., Reed, L., Trojanowski, J. Q., Zhukareva, V., Bird, T., Schellenberg, G. & Wilhelmsen, K. C. 1998. Pathogenic implications of mutations in the tau gene in pallido-ponto-nigral degeneration and related neurodegenerative disorders linked to chromosome 17. *Proc. Natl. Acad. Sci. U.S.A.*, 95, 13103–7.

Coba, M. P., Pocklington, A. J., Collins, M. O., Kopanitsa, M. V., Uren, R. T., Swamy, S., Croning, M. D., Choudhary, J. S. & Grant, S. G. 2009. Neurotransmitters drive combinatorial multistate postsynaptic density networks. *Sci. Signal.*, 2, ra19.

Comoletti, D., Flynn, R., Jennings, L. L., Chubykin, A., Matsumura, T., Hasegawa, H., Südhof, T. C. & Taylor, P. 2003. Characterization of the interaction of a recombinant soluble neuroligin-1 with neurexin-1β. *J. Biol. Chem.*, 278, 50497–505.

Corder, E. H., Saunders, A. M., Strittmatter, W. J., Schmechel, D. E., Gaskell, P. C., Small, G. W., Roses, A. D., Haines, J. L. & Pericak-Vance, M. A. 1993. Gene dose of apolipoprotein E type 4 allele and the risk of Alzheimer's disease in late onset families. *Science*, 261, 921–3.

Corder, E. H., Saunders, A. M., Risch, N. J., Strittmatter, W. J., Schmechel, D. E., Gaskell, P. C., Jr., Rimmler, J. B., Locke, P. A., Conneally, P. M., Schmader, K. E., Small, G. W., Roses, A. D., Haines, J. L. & Pericak-Vance, M. A. 1994. Protective effect of apolipoprotein E type 2 allele for late onset Alzheimer disease. *Nat. Genet.*, 7, 180–4.

Cotman, C. W. & Berchtold, N. C. 2002. Exercise: a behavioral intervention to enhance brain health and plasticity. *Trends Neurosci.*, 25, 295–301.

Craft, G. E., Chen, A. & Nairn, A. C. 2013. Recent advances in quantitative neuroproteomics. *Methods*, 61, 186–218.

Craig, A. M. & Kang, Y. 2007. Neurexin-neuroligin signaling in synapse development. *Curr. Opin. Neurobiol.*, 17, 43–52.

Cuevas, M. E., Haensgen, H., Sepulveda, F. J., Zegers, G., Roa, J., Opazo, C. & Aguayo, L. G. 2011. Soluble $A\beta_{1\text{-}40}$ peptide increases excitatory neurotransmission and induces epileptiform activity in hippocampal neurons. *J. Alzheimers Dis.*, 23, 673–87.

Cummings, J. L., Vinters, H. V., Cole, G. M. & Khachaturian, Z. S. 1998. Alzheimer's disease: etiologies, pathophysiology, cognitive reserve, and treatment opportunities. *Neurology*, 51, S2–17; discussion S65–7.

Dahlhaus, R., Hines, R. M., Eadie, B. D., Kannangara, T. S., Hines, D. J., Brown, C. E., Christie, B. R. & El-Husseini, A. 2010. Overexpression of the cell adhesion protein neuroligin-1 induces learning deficits and impairs synaptic plasticity by altering the ratio of excitation to inhibition in the hippocampus. *Hippocampus*, 20, 305–22.

Dalva, M. B., Takasu, M. A., Lin, M. Z., Shamah, S. M., Hu, L., Gale, N. W. & Greenberg, M. E. 2000. EphB receptors interact with NMDA receptors and regulate excitatory synapse formation. *Cell*, 103, 945–56.

Dalva, M. B., M^{c}Clelland, A. C. & Kayser, M. S. 2007. Cell adhesion molecules: signalling functions at the synapse. *Nat. Rev. Neurosci.*, 8, 206–20.

Darie, C. C., Deinhardt, K., Zhang, G., Cardasis, H. S., Chao, M. V. & Neubert, T. A. 2011. Identifying transient protein-protein interactions in EphB2 signaling by blue native PAGE and mass spectrometry. *Proteomics*, 11, 4514–28.

Davidsson, P. & Blennow, K. 1998. Neurochemical dissection of synaptic pathology in Alzheimer's disease. *Int. Psychogeriatr.*, 10, 11–23.

Davidsson, P., Paulson, L., Hesse, C., Blennow, K. & Nilsson, C. 2001. Proteome studies of human cerebrospinal fluid and brain tissue using a preparative two-dimensional electrophoresis approach prior to mass spectrometry. *Proteomics*, 1, 444–52.

Davies, C. A., Mann, D. M., Sumpter, P. Q. & Yates, P. O. 1987. A quantitative morphometric analysis of the neuronal and synaptic content of the frontal and temporal cortex in patients with Alzheimer's disease. *J. Neurol. Sci.*, 78, 151–64.

Davies, R. R., Graham, K. S., Xuereb, J. H., Williams, G. B. & Hodges, J. R. 2004. The human perirhinal cortex and semantic memory. *Eur. J. Neurosci.*, 20, 2441–6.

De Strooper, B., Annaert, W., Cupers, P., Saftig, P., Craessaerts, K., Mumm, J. S., Schroeter, E. H., Schrijvers, V., Wolfe, M. S., Ray, W. J., Goate, A. & Kopan, R. 1999. A presenilin-1-dependent γ-secretase-like protease mediates release of Notch intracellular domain. *Nature*, 398, 518–22.

Dekosky, S. T. & Scheff, S. W. 1990. Synapse loss in frontal cortex biopsies in Alzheimer's disease: Correlation with cognitive severity. *Ann. Neurol.*, 27, 457–64.

Dhanasekaran, S., Doherty, T. M. & Kenneth, J. 2010. Comparison of different standards for real-time PCR-based absolute quantification. *J. Immunol. Methods*, 354, 34–9.

Dinamarca, M. C., Colombres, M., Cerpa, W., Bonansco, C. & Inestrosa, N. C. 2008. β-Amyloid oligomers affect the structure and function of the postsynaptic region: role of the Wnt signaling pathway. *Neurodegener. Dis.*, 5, 149–52.

Dinamarca, M. C., Weinstein, D., Monasterio, O. & Inestrosa, N. C. 2011. The synaptic protein neuroligin-1 interacts with the amyloid β-peptide. Is there a role in Alzheimer's disease? *Biochemistry*, 50, 8127–37.

Dinamarca, M. C., Rios, J. A. & Inestrosa, N. C. 2012. Postsynaptic receptors for amyloid-β oligomers as mediators of neuronal damage in Alzheimer's disease. *Front. Physiol.*, 3, 464.

Dodd, P. R., Hardy, J. A., Baig, E. B., Kidd, A. M., Bird, E. D., Watson, W. E. & Johnston, G. A. 1986. Optimization of freezing, storage, and thawing conditions for the preparation of metabolically active synaptosomes from frozen rat and human brain. *Neurochem. Pathol.*, 4, 177–98.

Dodd, P. R., Buckley, S. T., Eckert, A. L., Foley, P. F. & Innes, D. J. 2006. Genes and gene expression in the brains of human alcoholics. *Ann. NY Acad. Sci.*, 1074, 104–15.

Dong, N., Qi, J. & Chen, G. 2007. Molecular reconstitution of functional GABAergic synapses with expression of neuroligin-2 and $GABA_A$ receptors. *Mol. Cell. Neurosci.*, 35, 14–23.

Dosemeci, A., Makusky, A. J., Jankowska-Stephens, E., Yang, X., Slotta, D. J. & Markey, S. P. 2007. Composition of the synaptic PSD-95 complex. *Mol. Cell. Proteomics*, 6, 1749–60.

Eng, J. K., Mccormack, A. L. & Yates, J. R. 1994. An approach to correlate tandem mass spectral data of peptides with amino acid sequences in a protein database. *J. Am. Soc. Mass Spectrom.*, 5, 976–89.

Etheridge, N., Lewohl, J. M., Mayfield, R. D., Harris, R. A. & Dodd, P. R. 2009. Synaptic proteome changes in the superior frontal gyrus and occipital cortex of the alcoholic brain. *Proteomics Clin. Appl.*, 3, 730–42.

Fannon, A. M. & Colman, D. R. 1996. A model for central synaptic junctional complex formation based on the differential adhesive specificities of the cadherins. *Neuron*, 17, 423–34.

Fenn, J. B., Mann, M., Meng, C. K., Wong, S. F. & Whitehouse, C. M. 1989. Electrospray ionization for mass spectrometry of large biomolecules. *Science*, 246, 64–71.

Fernandez, E., Collins, M. O., Uren, R. T., Kopanitsa, M. V., Komiyama, N. H., Croning, M. D., Zografos, L., Armstrong, J. D., Choudhary, J. S. & Grant, S. G. 2009. Targeted tandem affinity purification of PSD-95 recovers core postsynaptic complexes and schizophrenia susceptibility proteins. *Mol. Syst. Biol.*, 5, 269.

Ferrari, E., Tinti, M., Costa, S., Corallino, S., Nardozza, A. P., Chatraryamontri, A., Ceol, A., Cesareni, G. & Castagnoli, L. 2011. Identification of new substrates of the protein-tyrosine phosphatase PTP1B by Bayesian integration of proteome evidence. *J. Biol. Chem.*, 286, 4173–85.

Ferri, C. P., Prince, M., Brayne, C., Brodaty, H., Fratiglioni, L., Ganguli, M., Hall, K., Hasegawa, K., Hendrie, H., Huang, Y., Jorm, A., Mathers, C., Menezes, P. R., Rimmer, E. & Scazufca, M. 2005. Global prevalence of dementia: a Delphi consensus study. *Lancet*, 366, 2112–7.

Flerko, B. 1971. Steroid hormones and the differentiation of the central nervous system. *Curr. Top. Exp. Endocrinol.*, 1, 41–80.

Friedman, D. B., Hill, S., Keller, J. W., Merchant, N. B., Levy, S. E., Coffey, R. J. & Caprioli, R. M. 2004. Proteome analysis of human colon cancer by two-dimensional difference gel electrophoresis and mass spectrometry. *Proteomics*, 4, 793–811.

Friedman, D. B., Wang, S. E., Whitwell, C. W., Caprioli, R. M. & Arteaga, C. L. 2007. Multivariable difference gel electrophoresis and mass spectrometry: a case study on transforming growth factor-β and ERBB2 signaling. *Mol. Cell. Proteomics*, 6, 150–69.

Gant-Branum, R. L., Kerr, T. J. & Mclean, J. A. 2009. Labeling strategies in mass spectrometry-based protein quantitation. *Analyst*, 134, 1525–30.

Gebhardt, F. M., Scott, H. A. & Dodd, P. R. 2010. Housekeepers for accurate transcript expression analysis in Alzheimer's disease autopsy brain tissue. *Alzheimers Dement.*, 6, 465–74.

Gilbert, M., Smith, J., Roskams, A.-J. & Auld, V. J. 2001. Neuroligin 3 is a vertebrate gliotactin expressed in the olfactory ensheathing glia, a growth-promoting class of macroglia. *Glia*, 34, 151–64.

Gilbert, M. M. & Auld, V. J. 2005. Evolution of CLAMS (cholinesterase-like adhesion molecules): structure and function during development. *Front. Biosci.*, 10, 2177–92.

Gimbel, D. A., Nygaard, H. B., Coffey, E. E., Gunther, E. C., Lauren, J., Gimbel, Z. A. & Strittmatter, S. M. 2010. Memory impairment in transgenic Alzheimer mice requires cellular prion protein. *J. Neurosci.*, 30, 6367–74.

Glenner, G. G. & Wong, C. W. 1984a. Alzheimer's disease and Down's syndrome: sharing of a unique cerebrovascular amyloid fibril protein. *Biochem. Biophys. Res. Commun.*, 122, 1131–5.

Glenner, G. G. & Wong, C. W. 1984b. Alzheimer's disease: Initial report of the purification and characterization of a novel cerebrovascular amyloid protein. *Biochem. Biophys. Res. Commun.*, 120, 885–90.

Goate, A., Chartier-Harlin, M. C., Mullan, M., Brown, J., Crawford, F., Fidani, L., Giuffra, L., Haynes, A., Irving, N., James, L., Mant, R., Newton, P., Rooke, K., Roques, P., Talbot, C., Pericak-Vance, M., Roses, A., Williamson, R., Rossor, M., Owen, M. & Hardy, J. A. 1991. Segregation of a missense mutation in the amyloid precursor protein gene with familial Alzheimer's disease. *Nature*, 349, 704–6.

Gold, C. A. & Budson, A. E. 2008. Memory loss in Alzheimer's disease: implications for development of therapeutics. *Expert Rev. Neurother.*, 8, 1879–91.

Goode, B. L. & Feinstein, S. C. 1994. Identification of a novel microtubule binding and assembly domain in the developmentally regulated inter-repeat region of tau. *J. Cell. Biol.*, 124, 769–82.

Gräber, M. B., Kosel, S., Grasbon-Frodl, E., Moller, H. J. & Mehraein, P. 1998. Histopathology and APOE genotype of the first Alzheimer disease patient, Auguste D. *Neurogenetics*, 1, 223–8.

Graf, E. R., Zhang, X., Jin, S. X., Linhoff, M. W. & Craig, A. M. 2004. Neurexins induce differentiation of GABA and glutamate postsynaptic specializations *via* neuroligins. *Cell*, 119, 1013–26.

Graf, E. R., Kang, Y., Hauner, A. M. & Craig, A. M. 2006. Structure function and splice site analysis of the synaptogenic activity of the neurexin-1β LNS domain. *J. Neurosci.*, 26, 4256–65.

Greenamyre, J. T. & Young, A. B. 1989. Excitatory amino acids and Alzheimer's disease. *Neurobiol. Aging*, 10, 593–602.

Griffiths, J. R., Unwin, R. D., Evans, C. A., Leech, S. H., Corfe, B. M. & Whetton, A. D. 2007. The application of a hypothesis-driven strategy to the sensitive detection and location of acetylated lysine residues. *J. Am. Soc. Mass Spectrom.*, 18, 1423–8.

Guerreiro, R., Wojtas, A., Bras, J., Carrasquillo, M., Rogaeva, E., Majounie, E., Cruchaga, C., Sassi, C., Kauwe, J. S., Younkin, S., Hazrati, L., Collinge, J., Pocock, J., Lashley, T., Williams, J., Lambert, J. C., Amouyel, P., Goate, A., Rademakers, R., Morgan, K., Powell, J., St George-Hyslop, P., Singleton, A., Hardy, J. & Alzheimer Genetic Analysis Group 2013. TREM2 variants in Alzheimer's disease. *N. Engl. J. Med.*, 368, 117–27.

Gutala, R. V. & Reddy, P. H. 2004. The use of real-time PCR analysis in a gene expression study of Alzheimer's disease post-mortem brains. *J. Neurosci. Methods*, 132, 101–7.

Gygi, S. P., Rist, B., Gerber, S. A., Turecek, F., Gelb, M. H. & Aebersold, R. 1999. Quantitative analysis of complex protein mixtures using isotope-coded affinity tags. *Nat. Biotechnol.*, 17, 994–9.

Haass, C., Hung, A. & Selkoe, D. 1991. Processing of β-amyloid precursor protein in microglia and astrocytes favors a localization in internal vesicles over constitutive secretion. *J. Neurosci.*, 11, 3783–93.

Haass, C. & Selkoe, D. J. 2007. Soluble protein oligomers in neurodegeneration: lessons from the Alzheimer's amyloid β-peptide. *Nat. Rev. Mol. Cell Biol.*, 8, 101–12.

Hahn, C. G. 2010. A road less travelled: unpacking the complex traits of schizophrenia. *Brain Res. Bull.*, 83, 85.

Hall, A. C., Lucas, F. R. & Salinas, P. C. 2000. Axonal remodeling and synaptic differentiation in the cerebellum is regulated by WNT-7a signaling. *Cell*, 100, 525–35.

Halliday, G., Ng, T., Rodriguez, M., Harding, A., Blumbergs, P., Evans, W., Fabian, V., Fryer, J., Gonzales, M., Harper, C., Kalnins, R., Masters, C. L., Mclean, C., Milder, D. G., Pamphlett, R., Scott, G., Tannenberg, A. & Kril, J. 2002. Consensus neuropathological diagnosis of common dementia syndromes: testing and standardising the use of multiple diagnostic criteria. *Acta Neuropathol.*, 104, 72–8.

Hamos, J. E., Degennaro, L. J. & Drachman, D. A. 1989. Synaptic loss in Alzheimer's disease and other dementias. *Neurology*, 39, 355–61.

Harold, D., Abraham, R., Hollingworth, P., Sims, R., Gerrish, A., Hamshere, M. L., Pahwa, J. S., Moskvina, V., Dowzell, K., Williams, A., Jones, N., Thomas, C., Stretton, A., Morgan, A. R., Lovestone, S., Powell, J., Proitsi, P., Lupton, M. K., Brayne, C., Rubinsztein, D. C., Gill, M., Lawlor, B., Lynch, A., Morgan, K., Brown, K. S., Passmore, P. A., Craig, D., Mcguinness, B., Todd, S., Holmes, C., Mann, D., Smith, A. D., Love, S., Kehoe, P. G., Hardy, J., Mead, S., Fox, N., Rossor, M., Collinge, J., Maier, W., Jessen, F., Schurmann, B., Heun, R., Van Den Bussche, H., Heuser, I., Kornhuber, J., Wiltfang, J., Dichgans, M., Frolich, L., Hampel, H., Hull, M., Rujescu, D., Goate, A. M., Kauwe, J. S., Cruchaga, C., Nowotny, P., Morris, J. C., Mayo, K., Sleegers, K., Bettens, K., Engelborghs, S., De Deyn, P. P., Van Broeckhoven, C., Livingston, G., Bass, N. J., Gurling, H., Mcquillin, A., Gwilliam, R., Deloukas, P., Al-Chalabi, A., Shaw, C. E., Tsolaki, M., Singleton, A. B., Guerreiro, R., Muhleisen, T. W., Nothen, M. M., Moebus, S., Jockel, K. H., Klopp, N., Wichmann, H. E., Carrasquillo, M. M., Pankratz, V. S., Younkin, S. G., Holmans, P. A., O'donovan, M., Owen, M. J. & Williams, J. 2009. Genome-wide association study identifies variants at *CLU* and *PICALM* associated with Alzheimer's disease. *Nat. Genet.*, 41, 1088–93.

Harris, R. 1982. Genetics of Alzheimer's disease. *Br. Med. J.*, 284, 1065– 6.

Harrison, P. J., Procter, A. W., Barton, A. J., Lowe, S. L., Najlerahim, A., Bertolucci, P. H., Bowen, D. M. & Pearson, R. C. 1991. Terminal coma affects messenger RNA detection in post mortem human temporal cortex. *Brain Res. Mol. Brain Res.*, 9, 161–4.

Heindel, W., Jernigan Tl, Archibald Sl, Achim Cl, M. & E, W. C. 1994. The relationship of quantitative brain magnetic resonance imaging measures to neuropathologic indices of human immunodeficiency virus infection. *Arch. Neurol.*, 51, 1129–35.

Higuchi, R., Dollinger, G., Walsh, P. S. & Griffith, R. 1992. Simultaneous amplification and detection of specific DNA sequences. *Biotechnology (NY)*, 10, 413–7.

Hines, R. M., Wu, L., Hines, D. J., Steenland, H., Mansour, S., Dahlhaus, R., Singaraja, R. R., Cao, X., Sammler, E., Hormuzdi, S. G., Zhuo, M. & El-Husseini, A. 2008. Synaptic imbalance,

stereotypies, and impaired social interactions in mice with altered neuroligin 2 expression. *J. Neurosci.*, 28, 6055–67.

Hirao, K., Hata, Y., Ide, N., Takeuchi, M., Irie, M., Yao, I., Deguchi, M., Toyoda, A., Südhof, T. C. & Takai, Y. 1998. A novel multiple PDZ domain-containing molecule interacting with *N*-methyl-*D*-aspartate receptors and neuronal cell adhesion proteins. *J. Biol. Chem.*, 273, 21105–10.

Hishimoto, A., Liu, Q.-R., Drgon, T., Pletnikova, O., Walther, D., Zhu, X.-G., Troncoso, J. C. & Uhl, G. R. 2007. Neurexin 3 polymorphisms are associated with alcohol dependence and altered expression of specific isoforms. *Hum. Mol. Genet.*, 16, 2880–91.

Hoffman, R. C., Jennings, L. L., Tsigelny, I., Comoletti, D., Flynn, R. E., Südhof, T. C. & Taylor, P. 2004. Structural characterization of recombinant soluble rat neuroligin 1: mapping of secondary structure and glycosylation by mass spectrometry. *Biochemistry*, 43, 1496–506.

Hollingworth, P., Harold, D., Sims, R., Gerrish, A., Lambert, J. C., Carrasquillo, M. M., Abraham, R., Hamshere, M. L., Pahwa, J. S., Moskvina, V., Dowzell, K., Jones, N., Stretton, A., Thomas, C., Richards, A., Ivanov, D., Widdowson, C., Chapman, J., Lovestone, S., Powell, J., Proitsi, P., Lupton, M. K., Brayne, C., Rubinsztein, D. C., Gill, M., Lawlor, B., Lynch, A., Brown, K. S., Passmore, P. A., Craig, D., Mcguinness, B., Todd, S., Holmes, C., Mann, D., Smith, A. D., Beaumont, H., Warden, D., Wilcock, G., Love, S., Kehoe, P. G., Hooper, N. M., Vardy, E. R., Hardy, J., Mead, S., Fox, N. C., Rossor, M., Collinge, J., Maier, W., Jessen, F., Ruther, E., Schurmann, B., Heun, R., Kolsch, H., Van Den Bussche, H., Heuser, I., Kornhuber, J., Wiltfang, J., Dichgans, M., Frolich, L., Hampel, H., Gallacher, J., Hull, M., Rujescu, D., Giegling, I., Goate, A. M., Kauwe, J. S., Cruchaga, C., Nowotny, P., Morris, J. C., Mayo, K., Sleegers, K., Bettens, K., Engelborghs, S., De Deyn, P. P., Van Broeckhoven, C., Livingston, G., Bass, N. J., Gurling, H., Mcquillin, A., Gwilliam, R., Deloukas, P., Al-Chalabi, A., Shaw, C. E., Tsolaki, M., Singleton, A. B., Guerreiro, R., Muhleisen, T. W., Nothen, M. M., Moebus, S., Jockel, K. H., Klopp, N., Wichmann, H. E., Pankratz, V. S., Sando, S. B., Aasly, J. O., Barcikowska, M., Wszolek, Z. K., Dickson, D. W., Graff-Radford, N. R., Petersen, R. C., et al. 2011. Common variants at ABCA7, MS4A6A/MS4A4E,

EPHA1, CD33 and CD2AP are associated with Alzheimer's disease. *Nat. Genet.*, 43, 429–35.

Holmquist, M. 2000. α/β-hydrolase fold enzymes: structures, functions and mechanisms. *Curr. Protein Pept. Sci.*, 1, 209–35.

Honer, W. G., Dickson, D. W., Gleeson, J. & Davies, P. 1992. Regional synaptic pathology in Alzheimer's disease. *Neurobiol. Aging*, 13, 375–82.

Hong, M., Zhukareva, V., Vogelsberg-Ragaglia, V., Wszolek, Z., Reed, L., Miller, B. I., Geschwind, D. H., Bird, T. D., Mckeel, D., Goate, A., Morris, J. C., Wilhelmsen, K. C., Schellenberg, G. D., Trojanowski, J. Q. & Lee, V. M. 1998. Mutation-specific functional impairments in distinct tau isoforms of hereditary FTDP-17. *Science*, 282, 1914–7.

Hong, M. G., Alexeyenko, A., Lambert, J. C., Amouyel, P. & Prince, J. A. 2010. Genome-wide pathway analysis implicates intracellular transmembrane protein transport in Alzheimer disease. *J. Hum. Genet.*, 55, 707–9.

Hsia, A. Y., Masliah, E., Mcconlogue, L., Yu, G.-Q., Tatsuno, G., Hu, K., Kholodenko, D., Malenka, R. C., Nicoll, R. A. & Mucke, L. 1999. Plaque-independent disruption of neural circuits in Alzheimer's disease mouse models. *Proc. Natl. Acad. Sci. U.S.A.*, 96, 3228–33.

Hu, N.-W., Smith, I. M., Walsh, D. M. & Rowan, M. J. 2008. Soluble amyloid-β peptides potently disrupt hippocampal synaptic plasticity in the absence of cerebrovascular dysfunction *in vivo*. *Brain*, 131, 2414–24.

Hu, Y., Hosseini, A., Kauwe, J. S., Gross, J., Cairns, N. J., Goate, A. M., Fagan, A. M., Townsend, R. R. & Holtzman, D. M. 2007. Identification and validation of novel CSF biomarkers for early stages of Alzheimer's disease. *Proteomics Clin. Appl.*, 1, 1373–84.

Huang, Z. J. & Scheiffele, P. 2008. GABA and neuroligin signaling: linking synaptic activity and adhesion in inhibitory synapse development. *Curr. Opin. Neurobiol.*, 18, 77–83.

Hung, A. Y. & Selkoe, D. J. 1994. Selective ectodomain phosphorylation and regulated cleavage of β-amyloid precursor protein. *EMBO J.*, 13, 534–42.

Husi, H., Ward, M. A., Choudhary, J. S., Blackstock, W. P. & Grant, S. G. 2000. Proteomic analysis of NMDA receptor-adhesion protein signaling complexes. *Nat. Neurosci.*, 3, 661–9.

Hutton, M., Lendon, C. L., Rizzu, P., Baker, M., Froelich, S., Houlden, H., Pickering-Brown, S., Chakraverty, S., Isaacs, A., Grover, A., Hackett, J., Adamson, J., Lincoln, S., Dickson, D., Davies, P., Petersen, R. C., Stevens, M., De Graaff, E., Wauters, E., Van Baren, J., Hillebrand, M., Joosse, M., Kwon, J. M., Nowotny, P., Che, L. K., Norton, J., Morris, J. C., Reed, L. A., Trojanowski, J., Basun, H., Lannfelt, L., Neystat, M., Fahn, S., Dark, F., Tannenberg, T., Dodd, P. R., Hayward, N., Kwok, J. B. J., Schofield, P. R., Andreadis, A., Snowden, J., Craufurd, D., Neary, D., Owen, F., Oostra, B. A., Hardy, J., Goate, A., Van Swieten, J., Mann, D., Lynch, T. & Heutink, P. 1998. Association of missense and 5'-splice-site mutations in tau with the inherited dementia FTDP-17. *Nature*, 393, 702–5.

Hynd, M. R., Scott, H. L. & Dodd, P. R. 2001. Glutamate$_{NMDA}$ receptor NR1 subunit mRNA expression in Alzheimer's disease. *J. Neurochem.*, 78, 175–82.

Hynd, M. R., Lewohl, J. M., Scott, H. L. & Dodd, P. R. 2003. Biochemical and molecular studies using human autopsy brain tissue. *J. Neurochem.*, 85, 543–62.

Ichtchenko, K., Hata, Y., Nguyen, T., Ullrich, B., Missler, M., Moomaw, C. & Südhof, T. C. 1995. Neuroligin 1: A splice site-specific ligand for β-neurexins. *Cell*, 81, 435–43.

Ichtchenko, K., Nguyen, T. & Südhof, T. C. 1996. Structures, alternative splicing, and neurexin binding of multiple neuroligins. *J. Biol. Chem.*, 271, 2676–82.

Imbeaud, S., Graudens, E., Boulanger, V., Barlet, X., Zaborski, P., Eveno, E., Mueller, O., Schroeder, A. & Auffray, C. 2005. Towards standardization of RNA quality assessment using user-independent classifiers of microcapillary electrophoresis traces. *Nucleic Acids Res.*, 33, e56.

Inestrosa, N. C., Alvarez, A., Perez, C. A., Moreno, R. D., Vicente, M., Linker, C., Casanueva, O. I., Soto, C. & Garrido, J. 1996. Acetylcholinesterase accelerates assembly of amyloid-β-peptides into Alzheimer's fibrils: possible role of the peripheral site of the enzyme. *Neuron*, 16, 881–91.

Ingelsson, M., Fukumoto, H., Newell, K. L., Growdon, J. H., Hedley-Whyte, E. T., Frosch, M. P., Albert, M. S., Hyman, B. T. & Irizarry, M. C. 2004. Early β-amyloid accumulation and progressive synaptic loss, gliosis, and tangle formation in AD brain. *Neurology*, 62, 925–31.

Ishihara, T., Hong, M., Zhang, B., Nakagawa, Y., Lee, M. K., Trojanowski, J. Q. & Lee, V. M. 1999. Age-dependent emergence and progression of a tauopathy in transgenic mice overexpressing the shortest human tau isoform. *Neuron*, 24, 751–62.

Jackson, J., Chugh, D., Nilsson, P., Wood, J., Carlstrom, K., Lindvall, O. & Ekdahl, C. T. 2012. Altered synaptic properties during integration of adult-born hippocampal neurons following a seizure insult. *PLoS One*, 7, e35557.

Jamain, S., Quach, H., Betancur, C., Rastam, M., Colineaux, C., Gillberg, I. C., Soderstrom, H., Giros, B., Leboyer, M., Gillberg, C. & Bourgeron, T. 2003. Mutations of the X-linked genes encoding neuroligins NLGN3 and NLGN4 are associated with autism. *Nat. Genet.*, 34, 27–9.

Jamain, S., Radyushkin, K., Hammerschmidt, K., Granon, S., Boretius, S., Varoqueaux, F., Ramanantsoa, N., Gallego, J., Ronnenberg, A., Winter, D., Frahm, J., Fischer, J., Bourgeron, T., Ehrenreich, H. & Brose, N. 2008. Reduced social interaction and ultrasonic communication in a mouse model of monogenic heritable autism. *Proc. Natl. Acad. Sci. U.S.A.*, 105, 1710–5.

Janssen, J. C., Beck, J. A., Campbell, T. A., Dickinson, A., Fox, N. C., Harvey, R. J., Houlden, H., Rossor, M. N. & Collinge, J. 2003. Early onset familial Alzheimer's disease: Mutation frequency in 31 families. *Neurology*, 60, 235–9.

Jarrett, J. T., Berger, E. P. & Lansbury, P. T. 1993. The carboxy terminus of the β amyloid protein is critical for the seeding of amyloid formation: implications for the pathogenesis of Alzheimer's disease. *Biochemistry*, 32, 4693–7.

Joachim, C. L., Morris, J. H., Kosik, K. S. & Selkoe, D. J. 1987. Tau antisera recognize neurofibrillary tangles in a range of neurodegenerative disorders. *Ann. Neurol.*, 22, 514–20.

Johnson, L. A. & Ferris, J. a. J. 2002. Analysis of postmortem DNA degradation by single-cell gel electrophoresis. *Forensic Sci. Int.*, 126, 43–7.

Johnston, N. L., Cerevnak, J., Shore, A. D., Fuller Torrey, E. & Yolken, R. H. 1997. Multivariate analysis of RNA levels from postmortem human brains as measured by three different methods of RT-PCR. *J. Neurosci. Methods*, 77, 83–92.

Jones, L., Holmans, P. A., Hamshere, M. L., Harold, D., Moskvina, V., Ivanov, D., Pocklington, A., Abraham, R., Hollingworth, P., Sims, R., Gerrish, A., Pahwa, J. S., Jones, N., Stretton, A., Morgan, A. R., Lovestone, S., Powell, J., Proitsi, P., Lupton, M. K., Brayne, C., Rubinsztein, D. C., Gill, M., Lawlor, B., Lynch, A., Morgan, K., Brown, K. S., Passmore, P. A., Craig, D., M^{c}Guinness, B., Todd, S., Holmes, C., Mann, D., Smith, A. D., Love, S., Kehoe, P. G., Mead, S., Fox, N., Rossor, M., Collinge, J., Maier, W., Jessen, F., Schurmann, B., Heun, R., Kolsch, H., Van Den Bussche, H., Heuser, I., Peters, O., Kornhuber, J., Wiltfang, J., Dichgans, M., Frolich, L., Hampel, H., Hull, M., Rujescu, D., Goate, A. M., Kauwe, J. S., Cruchaga, C., Nowotny, P., Morris, J. C., Mayo, K., Livingston, G., Bass, N. J., Gurling, H., Mcquillin, A., Gwilliam, R., Deloukas, P., Al-Chalabi, A., Shaw, C. E., Singleton, A. B., Guerreiro, R., Muhleisen, T. W., Nothen, M. M., Moebus, S., Jockel, K. H., Klopp, N., Wichmann, H. E., Ruther, E., Carrasquillo, M. M., Pankratz, V. S., Younkin, S. G., Hardy, J., O'Donovan, M. C., Owen, M. J. & Williams, J. 2010. Genetic evidence implicates the immune system and cholesterol metabolism in the aetiology of Alzheimer's disease. *PLoS One*, 5, e13950.

Jorissen, E., Prox, J., Bernreuther, C., Weber, S., Schwanbeck, R., Serneels, L., Snellinx, A., Craessaerts, K., Thathiah, A., Tesseur, I., Bartsch, U., Weskamp, G., Blobel, C. P., Glatzel, M., De Strooper, B. & Saftig, P. 2010. The disintegrin/metalloproteinase ADAM10 is essential for the establishment of the brain cortex. *J. Neurosci.*, 30, 4833–44.

Jung, S. Y., Kim, J., Kwon, O. B., Jung, J. H., An, K., Jeong, A. Y., Lee, C. J., Choi, Y. B., Bailey, C. H., Kandel, E. R. & Kim, J. H. 2010. Input-specific synaptic plasticity in the amygdala is regulated by neuroligin-1 *via* postsynaptic NMDA receptors. *Proc. Natl. Acad. Sci. U.S.A.*, 107, 4710–5.

Kamenetz, F., Tomita, T., Hsieh, H., Seabrook, G., Borchelt, D., Iwatsubo, T., Sisodia, S. & Malinow, R. 2003. APP processing and synaptic function. *Neuron*, 37, 925–37.

Kanehisa, M. & Goto, S. 2000. KEGG: Kyoto encyclopedia of genes and genomes. *Nucleic Acids Res.*, 28, 27–30.

Karp, P. D. 2000. An ontology for biological function based on molecular interactions. *Bioinformatics*, 16, 269–85.

Kattenstroth, G., Tantalaki, E., Südhof, T. C., Gottmann, K. & Missler, M. 2004. Postsynaptic *N*-methyl-*D*-aspartate receptor function requires α-neurexins. *Proc. Natl. Acad. Sci. U.S.A.*, 101, 2607–12.

Keller, M. A., Gwinn, K., Nash, J., Horsford, J., Zhang, R., Rich, S. S. & Corriveau, R. A. 2007. Whole genome association studies of neuropsychiatric disease: An emerging era of collaborative genetic discovery. *Neuropsychiatr. Dis. Treat.*, 3, 613–8.

Kerrien, S., Alam-Faruque, Y., Aranda, B., Bancarz, I., Bridge, A., Derow, C., Dimmer, E., Feuermann, M., Friedrichsen, A., Huntley, R., Kohler, C., Khadake, J., Leroy, C., Liban, A., Lieftink, C., Montecchi-Palazzi, L., Orchard, S., Risse, J., Robbe, K., Roechert, B., Thorneycroft, D., Zhang, Y., Apweiler, R. & Hermjakob, H. 2007. IntAct — open source resource for molecular interaction data. *Nucleic Acids Res.*, 35, D561–5.

Keshishian, H., Addona, T., Burgess, M., Kuhn, E. & Carr, S. A. 2007. Quantitative, multiplexed assays for low abundance proteins in plasma by targeted mass spectrometry and stable isotope dilution. *Mol. Cell. Proteomics*, 6, 2212–29.

Keshishian, H., Addona, T., Burgess, M., Mani, D. R., Shi, X., Kuhn, E., Sabatine, M. S., Gerszten, R. E. & Carr, S. A. 2009. Quantification of cardiovascular biomarkers in patient plasma by targeted mass spectrometry and stable isotope dilution. *Mol. Cell. Proteomics*, 8, 2339–49.

Kim, J., Jung, S. Y., Lee, Y. K., Park, S., Choi, J. S., Lee, C. J., Kim, H. S., Choi, Y. B., Scheiffele, P., Bailey, C. H., Kandel, E. R. & Kim, J. H. 2008. Neuroligin-1 is required for normal expression of LTP and associative fear memory in the amygdala of adult animals. *Proc. Natl. Acad. Sci. U.S.A.*, 105, 9087–92.

Kim, J., Chang, A., Dudak, A., Federoff, H. J. & Lim, S. T. 2011. Characterization of nectin processing mediated by presenilin-dependent γ-secretase. *J. Neurochem.*, 119, 945–56.

Kingsbury, A. E., Foster, O. J., Nisbet, A. P., Cairns, N., Bray, L., Eve, D. J., Lees, A. J. & Marsden, C. D. 1995. Tissue pH as an indicator of mRNA preservation in human post-mortem brain. *Brain Res. Mol. Brain Res.*, 28, 311–8.

Kirvell, S. L., Esiri, M. & Francis, P. T. 2006. Down-regulation of vesicular glutamate transporters precedes cell loss and pathology in Alzheimer's disease. *J. Neurochem.*, 98, 939–50.

Klyubin, I., Walsh, D. M., Lemere, C. A., Cullen, W. K., Shankar, G. M., Betts, V., Spooner, E. T., Jiang, L., Anwyl, R., Selkoe, D. J. & Rowan, M. J. 2005. Amyloid β protein immunotherapy neutralizes amyloid β oligomers that disrupt synaptic plasticity *in vivo*. *Nat. Med.*, 11, 556–61.

Koffie, R. M., Meyer-Luehmann, M., Hashimoto, T., Adams, K. W., Mielke, M. L., Garcia-Alloza, M., Micheva, K. D., Smith, S. J., Kim, M. L., Lee, V. M., Hyman, B. T. & Spires-Jones, T. L. 2009. Oligomeric amyloid β associates with postsynaptic densities and correlates with excitatory synapse loss near senile plaques. *Proc. Natl. Acad. Sci. U.S.A.*, 106, 4012–7.

Koh, J. Y., Yang, L. L. & Cotman, C. W. 1990. β-Amyloid protein increases the vulnerability of cultured cortical neurons to excitotoxic damage. *Brain Res.*, 533, 315–20.

Köpke, E., Tung, Y. C., Shaikh, S., Alonso, A. C., Iqbal, K. & Grundke-Iqbal, I. 1993. Microtubule-associated protein tau. Abnormal phosphorylation of a non-paired helical filament pool in Alzheimer disease. *J. Biol. Chem.*, 268, 24374–84.

Krokhin, O. V., Craig, R., Spicer, V., Ens, W., Standing, K. G., Beavis, R. C. & Wilkins, J. A. 2004. An improved model for prediction of retention times of tryptic peptides in ion pair reversed-phase HPLC: its application to protein peptide mapping by off-line HPLC-MALDI MS. *Mol. Cell. Proteomics*, 3, 908–19.

Kudo, W., Lee, H. P., Zou, W. Q., Wang, X., Perry, G., Zhu, X., Smith, M. A., Petersen, R. B. & Lee, H. G. 2012. Cellular prion protein is essential for oligomeric amyloid-β induced neuronal cell death. *Hum. Mol. Genet.*, 21, 1138–44.

Kuhn, P. H., Wang, H., Dislich, B., Colombo, A., Zeitschel, U., Ellwart, J. W., Kremmer, E., Rossner, S. & Lichtenthaler, S. F. 2010. ADAM10 is the physiologically relevant,

constitutive α-secretase of the amyloid precursor protein in primary neurons. *EMBO J.*, 29, 3020–32.

Kurschner, C., Mermelstein, P. G., Holden, W. T. & Surmeier, D. J. 1998. CIPP, a novel multivalent PDZ domain protein, selectively interacts with Kir4.0 family members, NMDA receptor subunits, neurexins, and neuroligins. *Mol. Cell. Neurosci.*, 11, 161–72.

Laarakker, M. C., Reinders, N. R., Bruining, H., Ophoff, R. A. & Kas, M. J. 2012. Sex-dependent novelty response in neurexin-1α mutant mice. *PLoS One*, 7, e31503.

Lai, M. K., Chen, C. P., Hope, T. & Esiri, M. M. 2010. Hippocampal neurofibrillary tangle changes and aggressive behaviour in dementia. *Neuroreport*, 21, 1111–5.

Lambert, J. C., Heath, S., Even, G., Campion, D., Sleegers, K., Hiltunen, M., Combarros, O., Zelenika, D., Bullido, M. J., Tavernier, B., Letenneur, L., Bettens, K., Berr, C., Pasquier, F., Fievet, N., Barberger-Gateau, P., Engelborghs, S., De Deyn, P., Mateo, I., Franck, A., Helisalmi, S., Porcellini, E., Hanon, O., De Pancorbo, M. M., Lendon, C., Dufouil, C., Jaillard, C., Leveillard, T., Alvarez, V., Bosco, P., Mancuso, M., Panza, F., Nacmias, B., Bossu, P., Piccardi, P., Annoni, G., Seripa, D., Galimberti, D., Hannequin, D., Licastro, F., Soininen, H., Ritchie, K., Blanche, H., Dartigues, J. F., Tzourio, C., Gut, I., Van Broeckhoven, C., Alperovitch, A., Lathrop, M. & Amouyel, P. 2009. Genome-wide association study identifies variants at *CLU* and *CR1* associated with Alzheimer's disease. *Nat. Genet.*, 41, 1094–9.

Lambert, J. C., Grenier-Boley, B., Chouraki, V., Heath, S., Zelenika, D., Fievet, N., Hannequin, D., Pasquier, F., Hanon, O., Brice, A., Epelbaum, J., Berr, C., Dartigues, J. F., Tzourio, C., Campion, D., Lathrop, M. & Amouyel, P. 2010. Implication of the immune system in Alzheimer's disease: evidence from genome-wide pathway analysis. *J. Alzheimers Dis.*, 20, 1107–18.

Lange, V., Picotti, P., Domon, B. & Aebersold, R. 2008. Selected reaction monitoring for quantitative proteomics: a tutorial. *Mol. Syst. Biol.*, 4, 222.

Lassmann, H., Weiler, R., Fischer, P., Bancher, C., Jellinger, K., Floor, E., Danielczyk, W., Seitelberger, F. & Winkler, H. 1992. Synaptic pathology in Alzheimer's disease:

immunological data for markers of synaptic and large dense-core vesicles. *Neuroscience*, 46, 1–8.

Lauren, J., Gimbel, D. A., Nygaard, H. B., Gilbert, J. W. & Strittmatter, S. M. 2009. Cellular prion protein mediates impairment of synaptic plasticity by amyloid-β oligomers. *Nature*, 457, 1128–32.

Lawson-Yuen, A., Saldivar, J. S., Sommer, S. & Picker, J. 2008. Familial deletion within *NLGN4* associated with autism and Tourette syndrome. *Eur. J. Hum. Genet.*, 16, 614–8.

Leonard, S., Logel, J., Luthman, D., Casanova, M., Kirch, D. & Freedman, R. 1993. Biological stability of mRNA isolated from human postmortem brain collections. *Biol. Psychiatry*, 33, 456–66.

Leuba, G., Savioz, A., Vernay, A., Carnal, B., Kraftsik, R., Tardif, E., Riederer, I. & Riederer, B. M. 2008a. Differential changes in synaptic proteins in the Alzheimer frontal cortex with marked increase in PSD-95 postsynaptic protein. *J. Alzheimers Dis.*, 15, 139–51.

Leuba, G., Walzer, C., Vernay, A., Carnal, B., Kraftsik, R., Piotton, F., Marin, P., Bouras, C. & Savioz, A. 2008b. Postsynaptic density protein PSD-95 expression in Alzheimer's disease and okadaic acid induced neuritic retraction. *Neurobiol. Dis.*, 30, 408–19.

Leuba, G., Vernay, A., Kraftsik, R., Tardif, E., Riederer, B. M. & Savioz, A. 2014. Pathological reorganization of NMDA receptors subunits and postsynaptic protein PSD-95 distribution in Alzheimer's disease. *Curr. Alzheimer Res.*, 11, 86–96.

Levy-Lahad, E., Wasco, W., Poorkaj, P., Romano, D. M., Oshima, J., Pettingell, W. H., Yu, C. E., Jondro, P. D., Schmidt, S. D., Wang, K. & Et Al. 1995. Candidate gene for the chromosome 1 familial Alzheimer's disease locus. *Science*, 269, 973–7.

Li, B., Chohan, M. O., Grundke-Iqbal, I. & Iqbal, K. 2007. Disruption of microtubule network by Alzheimer abnormally hyperphosphorylated tau. *Acta Neuropathol.*, 113, 501–11.

Liang, W. S., Dunckley, T., Beach, T. G., Grover, A., Mastroeni, D., Ramsey, K., Caselli, R. J., Kukull, W. A., Mckeel, D., Morris, J. C., Hulette, C. M., Schmechel, D., Reiman, E. M., Rogers, J. & Stephan, D. A. 2008. Altered neuronal gene expression in brain regions

differentially affected by Alzheimer's disease: a reference data set. *Physiol. Genomics*, 33, 240–56.

Lisé, M. F. & El-Husseini, A. 2006. The neuroligin and neurexin families: from structure to function at the synapse. *Cell. Mol. Life Sci.*, 63, 1833–49.

Liu, C. C., Kanekiyo, T., Xu, H. & Bu, G. 2013. Apolipoprotein E and Alzheimer disease: risk, mechanisms and therapy. *Nat. Rev. Neurol.*, 9, 106–18.

Liu, G., Jiang, Y., Wang, P., Feng, R., Jiang, N., Chen, X., Song, H. & Chen, Z. 2012. Cell adhesion molecules contribute to Alzheimer's disease: multiple pathway analyses of two genome-wide association studies. *J. Neurochem.*, 120, 190–8.

Liu, J. P., Zhang, Q. X., Baldwin, G. & Robinson, P. J. 1996. Calcium binds dynamin I and inhibits its GTPase activity. *J. Neurochem.*, 66, 2074–81.

Liu, S. I., Prince, M., Chiu, M. J., Chen, T. F., Sun, Y. W. & Yip, P. K. 2005. Validity and reliability of a Taiwan Chinese version of the community screening instrument for dementia. *Am. J. Geriatr. Psychiatry*, 13, 581–8.

Lowry, O. H., Rosebrough, N. J., Farr, A. L. & Randall, R. J. 1951. Protein measurement with the Folin phenol reagent. *J. Biol. Chem.*, 193, 265–75.

Ludes, B., Pfitzinger, H. & Mangin, P. 1993. DNA fingerprinting from tissues after variable postmortem periods. *J. Forensic Sci.*, 38, 686–90.

Lukiw, W. J., Wong, L. & Mclachlan, D. R. 1990. Cytoskeletal messenger RNA stability in human neocortex: studies in normal aging and in Alzheimer's disease. *Int. J. Neurosci.*, 55, 81–8.

Mabb, A. M. & Ehlers, M. D. 2010. Ubiquitination in postsynaptic function and plasticity. *Annu. Rev. Cell Dev. Biol.*, 26, 179–210.

Maccoss, M. J., Wu, C. C. & Yates, J. R., 3rd 2002. Probability-based validation of protein identifications using a modified SEQUEST algorithm. *Anal. Chem.*, 74, 5593–9.

Mahley, R. W. 1988. Apolipoprotein E: cholesterol transport protein with expanding role in cell biology. *Science*, 240, 622–30.

Malinverno, M., Carta, M., Epis, R., Marcello, E., Verpelli, C., Cattabeni, F., Sala, C., Mulle, C., Di Luca, M. & Gardoni, F. 2010. Synaptic localization and activity of ADAM10 regulate excitatory synapses through N-cadherin cleavage. *J. Neurosci.*, 30, 16343–55.

Malkki, H. 2014. Neurodegenerative disease: Synaptic scaffolding protein neuroligin 1 links amyloid deposition, neuroinflammation and impaired memory. *Nat. Rev. Neurol.*, 10, 122.

Mann, M. 2006. Functional and quantitative proteomics using SILAC. *Nat. Rev. Mol. Cell Biol.*, 7, 952–8.

Marambaud, P., Shioi, J., Serban, G., Georgakopoulos, A., Sarner, S., Nagy, V., Baki, L., Wen, P., Efthimiopoulos, S., Shao, Z., Wisniewski, T. & Robakis, N. K. 2002. A presenilin-1/γ-secretase cleavage releases the E-cadherin intracellular domain and regulates disassembly of adherens junctions. *EMBO J.*, 21, 1948–56.

Martinez-Mir, A., González-Pérez, A., Gayán, J., Antúnez, C., Marín, J., Boada, M., Lopez-Arrieta, J. M., Fernández, E., Ramírez-Lorca, R., Sáez, M. E., Ruiz, A., Scholl, F. G. & Real, L. M. 2013. Genetic study of neurexin and neuroligin genes in Alzheimer's disease. *J. Alzheimers Dis.*, 35, 403–12.

Masliah, E., Terry, R. D., Alford, M., Deteresa, R. & Hansen, L. A. 1991. Cortical and subcortical patterns of synaptophysinlike immunoreactivity in Alzheimer's disease. *Am. J. Pathol.*, 138, 235–46.

Masliah, E., Mallory, M., Alford, M., Deteresa, R., Hansen, L. A., Mckeel, D. W., Jr. & Morris, J. C. 2001. Altered expression of synaptic proteins occurs early during progression of Alzheimer's disease. *Neurology*, 56, 127–9.

Masters, C. L., Simms, G., Weinman, N. A., Multhaup, G., Mcdonald, B. L. & Beyreuther, K. 1985. Amyloid plaque core protein in Alzheimer disease and Down syndrome. *Proc. Natl. Acad. Sci. U.S.A.*, 82, 4245–9.

Matsuda-Matsumoto, H., Iwazaki, T., Kashem, M. A., Harper, C. & Matsumoto, I. 2007. Differential protein expression profiles in the hippocampus of human alcoholics. *Neurochem. Int.*, 51, 370–6.

Matthews, F. E., Arthur, A., Barnes, L. E., Bond, J., Jagger, C., Robinson, L. & Brayne, C. 2013. A two-decade comparison of prevalence of dementia in individuals aged 65 years and older from three geographical areas of England: results of the Cognitive Function and Ageing Study I and II. *Lancet*, 382, 1405–12.

Maurer, K., Volk, S. & Gerbaldo, H. 1997. Auguste D and Alzheimer's disease. *Lancet*, 349, 1546–9.

Mckhann, G., Drachman, D., Folstein, M., Katzman, R., Price, D. & Stadlan, E. M. 1984. Clinical diagnosis of Alzheimer's disease: report of the NINCDS-ADRDA Work Group under the auspices of Department of Health and Human Services Task Force on Alzheimer's Disease. *Neurology*, 34, 939–44.

Mielke, M. M., Vemuri, P. & Rocca, W. A. 2014. Clinical epidemiology of Alzheimer's disease: assessing sex and gender differences. *Clin. Epidemiol.*, 6, 37–48.

Miller, G. E., Chen, E., Fok, A. K., Walker, H., Lim, A., Nicholls, E. F., Cole, S. & Kobor, M. S. 2009. Low early-life social class leaves a biological residue manifested by decreased glucocorticoid and increased proinflammatory signaling. *Proc. Natl. Acad. Sci. U.S.A.*, 106, 14716–21.

Mintun, M. A., Larossa, G. N., Sheline, Y. I., Dence, C. S., Lee, S. Y., Mach, R. H., Klunk, W. E., Mathis, C. A., Dekosky, S. T. & Morris, J. C. 2006. [^{11}C]PIB in a nondemented population: potential antecedent marker of Alzheimer disease. *Neurology*, 67, 446–52.

Mirnics, K., Middleton, F. A., Marquez, A., Lewis, D. A. & Levitt, P. 2000. Molecular characterization of schizophrenia viewed by microarray analysis of gene expression in prefrontal cortex. *Neuron*, 28, 53–67.

Mirnics, K. & Pevsner, J. 2004. Progress in the use of microarray technology to study the neurobiology of disease. *Nat. Neurosci.*, 7, 434–9.

Mirra, S. S., Hart, M. N. & Terry, R. D. 1993. Making the diagnosis of Alzheimer's disease. A primer for practicing pathologists. *Arch. Pathol. Lab. Med.*, 117, 132–44.

Missler, M., Fernandez-Chacon, R. & Südhof, T. C. 1998. The making of neurexins. *J. Neurochem.*, 71, 1339–47.

Mollah, S., Wertz, I. E., Phung, Q., Arnott, D., Dixit, V. M. & Lill, J. R. 2007. Targeted mass spectrometric strategy for global mapping of ubiquitination on proteins. *Rapid Commun. Mass Spectrom.*, 21, 3357–64.

Monastero, R., Cefalu, A. B., Camarda, C., Noto, D., Camarda, L. K., Caldarella, R., Imbornone, E., Averna, M. R. & Camarda, R. 2006. Association of estrogen receptor a gene with Alzheimer's disease: a case-control study. *J. Alzheimers Dis.*, 9, 273–8.

Morgan, D. 2010. Immunotherapy for Alzheimer's disease. *J. Intern. Med.*, 269, 54–63.

Mucke, L., Masliah, E., Yu, G. Q., Mallory, M., Rockenstein, E. M., Tatsuno, G., Hu, K., Kholodenko, D., Johnson-Wood, K. & Mcconlogue, L. 2000. High-level neuronal expression of Aβ1-42 in wild-type human amyloid protein precursor transgenic mice: synaptotoxicity without plaque formation. *J. Neurosci.*, 20, 4050–8.

Mullan, M., Houlden, H., Windelspecht, M., Fidani, L., Lombardi, C., Diaz, P., Rossor, M., Crook, R., Hardy, J. A., Duff, K. & Crawford, F. 1992. A locus for familial early-onset Alzheimer's disease on the long arm of chromosome 14, proximal to the α1-antichymotrypsin gene. *Nat. Genet.*, 2, 340–2.

Müller, B. M., Kistner, U., Kindler, S., Chung, W. J., Kuhlendahl, S., Fenster, S. D., Lau, L. F., Veh, R. W., Huganir, R. L., Gundelfinger, E. D. & Garner, C. C. 1996. SAP102, a novel postsynaptic protein that interacts with NMDA receptor complexes in vivo. *Neuron*, 17, 255–65.

Myers, R. H., Schaefer, E. J., Wilson, P. W., D'agostino, R., Ordovas, J. M., Espino, A., Au, R., White, R. F., Knoefel, J. E., Cobb, J. L., Mcnulty, K. A., Beiser, A. & Wolf, P. A. 1996. Apolipoprotein E ε4 association with dementia in a population-based study: The Framingham study. *Neurology*, 46, 673–7.

Nagy, Z., Esiri, M. M., Jobst, K. A., Johnston, C., Litchfield, S., Sim, E. & Smith, A. D. 1995. Influence of the apolipoprotein E genotype on amyloid deposition and neurofibrillary tangle formation in Alzheimer's disease. *Neuroscience*, 69, 757–61.

Namba, Y., Tomonaga, M., Kawasaki, H., Otomo, E. & Ikeda, K. 1991. Apolipoprotein E immunoreactivity in cerebral amyloid deposits and neurofibrillary tangles in Alzheimer's disease and kuru plaque amyloid in Creutzfeldt-Jakob disease. *Brain Res.*, 541, 163–6.

Nathan, B. P., Bellosta, S., Sanan, D. A., Weisgraber, K. H., Mahley, R. W. & Pitas, R. E. 1994. Differential effects of apolipoproteins E3 and E4 on neuronal growth *in vitro*. *Science*, 264, 850–2.

Ngounou Wetie, A. G., Sokolowska, I., Wormwood, K., Beglinger, K., Michel, T. M., Thome, J., Darie, C. C. & Woods, A. G. 2013. Mass spectrometry for the detection of potential psychiatric biomarkers. *J. Mol. Psychiatry*, 1, 8–16.

Nguyen, T. & Südhof, T. C. 1997. Binding properties of neuroligin 1 and neurexin 1β a reveal function as heterophilic cell adhesion molecules. *J. Biol. Chem.*, 272, 26032–9.

Niemitz, E. 2013. TREM2 and Alzheimer's disease. *Nat. Genet.*, 45, 11.

Nussbaum, J., Xu, Q., Payne, T. J., Ma, J. Z., Huang, W., Gelernter, J. & Li, M. D. 2008. Significant association of the neurexin-1 gene (*NRXN1*) with nicotine dependence in European- and African-American smokers. *Hum. Mol. Genet.*, 17, 1569–77.

Ono, S., Baux, G., Sekiguchi, M., Fossier, P., Morel, N. F., Nihonmatsu, I., Hirata, K., Awaji, T., Takahashi, S. & Takahashi, M. 1998. Regulatory roles of complexins in neurotransmitter release from mature presynaptic nerve terminals. *Eur. J. Neurosci.*, 10, 2143–52.

Palmer, A. M., Lowe, S. L., Francis, P. T. & Bowen, D. M. 1988. Are post-mortem biochemical studies of human brain worthwhile? *Biochem. Soc. Trans.*, 16, 472–5.

Paloneva, J., Manninen, T., Christman, G., Hovanes, K., Mandelin, J., Adolfsson, R., Bianchin, M., Bird, T., Miranda, R., Salmaggi, A., Tranebjaerg, L., Konttinen, Y. & Peltonen, L. 2002. Mutations in two genes encoding different subunits of a receptor signaling complex result in an identical disease phenotype. *Am. J. Hum. Genet.*, 71, 656–62.

Palop, J. J., Chin, J., Roberson, E. D., Wang, J., Thwin, M. T., Bien-Ly, N., Yoo, J., Ho, K. O., Yu, G. Q., Kreitzer, A., Finkbeiner, S., Noebels, J. L. & Mucke, L. 2007. Aberrant excitatory neuronal activity and compensatory remodeling of inhibitory hippocampal circuits in mouse models of Alzheimer's disease. *Neuron*, 55, 697–711.

Pedersen, N. L. 2010. Reaching the limits of genome-wide significance in Alzheimer disease: back to the environment. *JAMA*, 303, 1864–5.

Peixoto, R. T., Kunz, P. A., Kwon, H., Mabb, A. M., Sabatini, B. L., Philpot, B. D. & Ehlers, M. D. 2012. Transsynaptic signaling by activity-dependent cleavage of neuroligin-1. *Neuron*, 76, 396–409.

Peng, J., Kim, M. J., Cheng, D., Duong, D. M., Gygi, S. P. & Sheng, M. 2004. Semiquantitative proteomic analysis of rat forebrain postsynaptic density fractions by mass spectrometry. *J. Biol. Chem.*, 279, 21003–11.

Perdahl, E., Adolfsson, R., Alafuzoff, I., Albert, K. & Nestler, E. 1984. Synapsin I (protein I) in different brain regions in senile dementia of Alzheimer type and in multi-infarct dementia. *J. Neural Transm.*, 60, 133–41.

Pericak-Vance, M. A., Bebout, J. L., Gaskell, P. C., Jr., Yamaoka, L. H., Hung, W. Y., Alberts, M. J., Walker, A. P., Bartlett, R. J., Haynes, C. A., Welsh, K. A., Earl, N. L., Heyman, A., Clark, C. M. & Roses, A. D. 1991. Linkage studies in familial Alzheimer disease: evidence for chromosome 19 linkage. *Am. J. Hum. Genet.*, 48, 1034–50.

Perkins, D. N., Pappin, D. J., Creasy, D. M. & Cottrell, J. S. 1999. Probability-based protein identification by searching sequence databases using mass spectrometry data. *Electrophoresis*, 20, 3551–67.

Philibert, R. A., Winfield, S. L., Sandhu, H. K., Martin, B. M. & Ginns, E. I. 2000. The structure and expression of the human neuroligin-3 gene. *Gene*, 246, 303–10.

Piazza-Gardner, A. K., Gaffud, T. J. & Barry, A. E. 2013. The impact of alcohol on Alzheimer's disease: a systematic review. *Aging Ment. Health*, 17, 133–46.

Picotti, P., Aebersold, R. & Domon, B. 2007. The implications of proteolytic background for shotgun proteomics. *Mol. Cell. Proteomics*, 6, 1589–98.

Picotti, P., Bodenmiller, B., Mueller, L. N., Domon, B. & Aebersold, R. 2009. Full dynamic range proteome analysis of *S. cerevisiæ* by targeted proteomics. *Cell*, 138, 795–806.

Piersma, S. R., Warmoes, M. O., De Wit, M., De Reus, I., Knol, J. C. & Jimenez, C. R. 2013. Whole gel processing procedure for GeLC-MS/MS based proteomics. *Proteome Sci*, 11, 17.

Plant, L. D., Boyle, J. P., Smith, I. F., Peers, C. & Pearson, H. A. 2003. The production of amyloid β peptide is a critical requirement for the viability of central neurons. *J. Neurosci.*, 23, 5531–5.

Poulopoulos, A., Aramuni, G., Meyer, G., Soykan, T., Hoon, M., Papadopoulos, T., Zhang, M., Paarmann, I., Fuchs, C., Harvey, K., Jedlicka, P., Schwarzacher, S. W., Betz, H., Harvey, R. J., Brose, N., Zhang, W. & Varoqueaux, F. 2009. Neuroligin 2 drives postsynaptic assembly at perisomatic inhibitory synapses through gephyrin and collybistin. *Neuron*, 63, 628–42.

Proctor, D. T., Coulson, E. J. & Dodd, P. R. 2010. Reduction in post-synaptic scaffolding PSD-95 and SAP-102 protein levels in the Alzheimer inferior temporal cortex is correlated with disease pathology. *J. Alzheimers Dis.*, 21, 795–811.

Puglielli, L., Tanzi, R. E. & Kovacs, D. M. 2003. Alzheimer's disease: the cholesterol connection. *Nat. Neurosci.*, 6, 345–51.

Purcell, S., Cherny, S. S. & Sham, P. C. 2003. Genetic Power Calculator: design of linkage and association genetic mapping studies of complex traits. *Bioinformatics*, 19, 149–50.

Rebeck, G. W., Kindy, M. & Ladu, M. J. 2002. Apolipoprotein E and Alzheimer's disease: the protective effects of ApoE2 and E3. *J. Alzheimers Dis.*, 4, 145–54.

Reddy, P. H., Mcweeney, S., Park, B. S., Manczak, M., Gutala, R. V., Partovi, D., Jung, Y., Yau, V., Searles, R., Mori, M. & Quinn, J. 2004. Gene expression profiles of transcripts in amyloid precursor protein transgenic mice: up-regulation of mitochondrial metabolism and apoptotic genes is an early cellular change in Alzheimer's disease. *Hum. Mol. Genet.*, 13, 1225–40.

Reddy, P. H., Mani, G., Park, B. S., Jacques, J., Murdoch, G., Whetsell Jr, W., Kaye, J. & Manczak, M. 2005. Differential loss of synaptic proteins in Alzheimer's disease: implications for synaptic dysfunction. *J. Alzheimers Dis.*, 7, 103–17.

Rees, T., Hammond, P. I., Soreq, H., Younkin, S. & Brimijoin, S. 2003. Acetylcholinesterase promotes β-amyloid plaques in cerebral cortex. *Neurobiol. Aging*, 24, 777–87.

Reiss, K., Maretzky, T., Ludwig, A., Tousseyn, T., De Strooper, B., Hartmann, D. & Saftig, P. 2005. ADAM10 cleavage of N-cadherin and regulation of cell-cell adhesion and β-catenin nuclear signalling. *EMBO J.*, 24, 742–52.

Restituito, S., Khatri, L., Ninan, I., Mathews, P. M., Liu, X., Weinberg, R. J. & Ziff, E. B. 2011. Synaptic autoregulation by metalloproteases and γ-secretase. *J. Neurosci.*, 31, 12083–93.

Reynolds, G. P. 2001. Pharmacological management of neurological and psychiatric disorders. *Am. J. Psychiatry*, 158, 1539–40.

Rivera, S., Khrestchatisky, M., Kaczmarek, L., Rosenberg, G. A. & Jaworski, D. M. 2010. Metzincin proteases and their inhibitors: foes or friends in nervous system physiology? *J. Neurosci.*, 30, 15337–57.

Rocca, W. A., Petersen, R. C., Knopman, D. S., Hebert, L. E., Evans, D. A., Hall, K. S., Gao, S., Unverzagt, F. W., Langa, K. M., Larson, E. B. & White, L. R. 2011. Trends in the incidence and prevalence of Alzheimer's disease, dementia, and cognitive impairment in the United States. *Alzheimers Dement.*, 7, 80–93.

Rogaev, E. I., Sherrington, R., Rogaeva, E. A., Levesque, G., Ikeda, M., Liang, Y., Chi, H., Lin, C., Holman, K., Tsuda, T., Mar, L., Sorbi, S., Nacmias, B., Piacentini, S., Amaducci, L., Chumakov, I., Cohen, D., Lannfelt, L., Fraser, P. E., Rommens, J. M. & St George-Hyslop, P. H. 1995. Familial Alzheimer's disease in kindreds with missense mutations in a gene on chromosome 1 related to the Alzheimer's disease type 3 gene. *Nature*, 376, 775–8.

Roher, A. E., Lowenson, J. D., Clarke, S., Wolkow, C., Wang, R., Cotter, R. J., Reardon, I. M., Zürcher-Neely, H. A., Heinrikson, R. L. & Ball, M. J. 1993. Structural alterations in the

peptide backbone of β-amyloid core protein may account for its deposition and stability in Alzheimer's disease. *J. Biol. Chem.*, 268, 3072–83.

Ronicke, R., Mikhaylova, M., Ronicke, S., Meinhardt, J., Schroder, U. H., Fandrich, M., Reiser, G., Kreutz, M. R. & Reymann, K. G. 2011. Early neuronal dysfunction by amyloid β oligomers depends on activation of NR2B-containing NMDA receptors. *Neurobiol. Aging*, 32, 2219–28.

Rosenberg, M. E. & Silkensen, J. 1995. Clusterin: physiologic and pathophysiologic considerations. *Int. J. Biochem. Cell Biol.*, 27, 633–45.

Ross, P. L., Huang, Y. N., Marchese, J. N., Williamson, B., Parker, K., Hattan, S., Khainovski, N., Pillai, S., Dey, S., Daniels, S., Purkayastha, S., Juhasz, P., Martin, S., Bartlet-Jones, M., He, F., Jacobson, A. & Pappin, D. J. 2004. Multiplexed protein quantitation in *Saccharomyces cerevisiæ* using amine-reactive isobaric tagging reagents. *Mol. Cell. Proteomics*, 3, 1154–69.

Rowan, M. J., Klyubin, I., Cullen, W. K. & Anwyl, R. 2003. Synaptic plasticity in animal models of early Alzheimer's disease. *Philos. Trans. R. Soc. Lond., B, Biol. Sci.*, 358, 821–8.

Rowan, M. J., Klyubin, I., Wang, Q., Hu, N. W. & Anwyl, R. 2007. Synaptic memory mechanisms: Alzheimer's disease amyloid β-peptide-induced dysfunction. *Biochem. Soc. Trans.*, 35, 1219–23.

Rubenstein, J. L. & Merzenich, M. M. 2003. Model of autism: increased ratio of excitation/inhibition in key neural systems. *Genes Brain Behav.*, 2, 255–67.

Sadygov, R. G. & Yates, J. R. 2003. A hypergeometric probability model for protein identification and validation using tandem mass spectral data and protein sequence databases. *Anal. Chem.*, 75, 3792–8.

Saunders, A. M., Strittmatter, W. J., Schmechel, D., St. George-Hyslop, P. H., Pericak-Vance, M. A., Joo, S. H., Rosi, B. L., Gusella, J. F., Crapper-Maclachlan, D. R., Alberts, M. J., Hulette, C., Crain, B., Goldgaber, D. & Roses, A. D. 1993. Association of apolipoprotein E allele ε4 with late- onset familial and sporadic Alzheimer's disease. *Neurology*, 43, 1467.

Saura, C. A., Servián-Morilla, E. & Scholl, F. G. 2011. Presenilin/γ-secretase regulates neurexin processing at synapses. *PLoS One*, 6, e19430.

Scheff, S. W., Dekosky, S. T. & Price, D. A. 1990. Quantitative assessment of cortical synaptic density in Alzheimer's disease. *Neurobiol. Aging*, 11, 29–37.

Scheiffele, P., Fan, J., Choih, J., Fetter, R. & Serafini, T. 2000. Neuroligin expressed in nonneuronal cells triggers presynaptic development in contacting axons. *Cell*, 101, 657–69.

Schellenberg, G. D., Bird, T. D., Wijsman, E. M., Orr, H. T., Anderson, L., Nemens, E., White, J. A., Bonnycastle, L., Weber, J. L., Alonso, M. E. & Et Al. 1992. Genetic linkage evidence for a familial Alzheimer's disease locus on chromosome 14. *Science*, 258, 668–71.

Schellenberg, G. D. 1995. Genetic dissection of Alzheimer disease, a heterogeneous disorder. *Proc. Natl. Acad. Sci. U.S.A.*, 92, 8552–9.

Schmidt, R., Kienbacher, E., Benke, T., Dal-Bianco, P., Delazer, M., Ladurner, G., Jellinger, K., Marksteiner, J., Ransmayr, G., Schmidt, H., Stogmann, E., Friedrich, J. & Wehringer, C. 2008. [Sex differences in Alzheimer's disease]. *Neuropsychiatr.*, 22, 1–15.

Scholl, F. G. & Scheiffele, P. 2003. Making connections: cholinesterase-domain proteins in the CNS. *Trends Neurosci.*, 26, 618–24.

Schramm, M., Falkai, P., Tepest, R., Schneider-Axmann, T., Przkora, R., Waha, A., Pietsch, T., Bonte, W. & Bayer, T. A. 1999. Stability of RNA transcripts in post-mortem psychiatric brains. *J. Neural Transm.*, 106, 329–35.

Schrijvers, E. M., Verhaaren, B. F., Koudstaal, P. J., Hofman, A., Ikram, M. A. & Breteler, M. M. 2012. Is dementia incidence declining?: Trends in dementia incidence since 1990 in the Rotterdam Study. *Neurology*, 78, 1456–63.

Selkoe, D. J., Podlisny, M. B., Joachim, C. L., Vickers, E. A., Lee, G., Fritz, L. C. & Oltersdorf, T. 1988. β-Amyloid precursor protein of Alzheimer disease occurs as 110- to 135-kilodalton membrane-associated proteins in neural and nonneural tissues. *Proc. Natl. Acad. Sci. U.S.A.*, 85.

Selkoe, D. J. 1998. The cell biology of β amyloid precursor protein and presenilin in Alzheimer's disease. *Trends Cell Biol.*, 8, 447–53.

Selkoe, D. J. 2001. Alzheimer's disease: genes, proteins, and therapy. *Physiol. Rev.*, 81, 741–66.

Selkoe, D. J. 2002. Alzheimer's disease is a synaptic failure. *Science*, 298, 789–91.

Selkoe, D. J. 2008. Soluble oligomers of the amyloid β-protein impair synaptic plasticity and behavior. *Behav. Brain Res.*, 192, 106–13.

Sergeant, N., Delacourte, A. & Buee, L. 2005. Tau protein as a differential biomarker of tauopathies. *Biochim. Biophys. Acta*, 1739, 179–97.

Seshadri, S., Fitzpatrick, A. L., Ikram, M. A., Destefano, A. L., Gudnason, V., Boada, M., Bis, J. C., Smith, A. V., Carassquillo, M. M., Lambert, J. C., Harold, D., Schrijvers, E. M., Ramirez-Lorca, R., Debette, S., Longstreth, W. T., Jr., Janssens, A. C., Pankratz, V. S., Dartigues, J. F., Hollingworth, P., Aspelund, T., Hernandez, I., Beiser, A., Kuller, L. H., Koudstaal, P. J., Dickson, D. W., Tzourio, C., Abraham, R., Antunez, C., Du, Y., Rotter, J. I., Aulchenko, Y. S., Harris, T. B., Petersen, R. C., Berr, C., Owen, M. J., Lopez-Arrieta, J., Varadarajan, B. N., Becker, J. T., Rivadeneira, F., Nalls, M. A., Graff-Radford, N. R., Campion, D., Auerbach, S., Rice, K., Hofman, A., Jonsson, P. V., Schmidt, H., Lathrop, M., Mosley, T. H., Au, R., Psaty, B. M., Uitterlinden, A. G., Farrer, L. A., Lumley, T., Ruiz, A., Williams, J., Amouyel, P., Younkin, S. G., Wolf, P. A., Launer, L. J., Lopez, O. L., Van Duijn, C. M. & Breteler, M. M. 2010. Genome-wide analysis of genetic loci associated with Alzheimer disease. *JAMA*, 303, 1832–40.

Seubert, P., Oltersdorf, T., Lee, M. G., Barbour, R., Blomquist, C., Davis, D. L., Bryant, K., Fritz, L. C., Galasko, D., Thal, L. J., Lieberburg, I. & Schenk, D. B. 1993. Secretion of β-amyloid precursor protein cleaved at the amino terminus of the β-amyloid peptide. *Nature*, 361, 260–3.

Shankar, G. M., Bloodgood, B. L., Townsend, M., Walsh, D. M., Selkoe, D. J. & Sabatini, B. L. 2007. Natural oligomers of the Alzheimer amyloid-β protein induce reversible synapse loss by modulating an NMDA-type glutamate receptor-dependent signaling pathway. *J. Neurosci.*, 27, 2866–75.

Shannon, P., Markiel, A., Ozier, O., Baliga, N. S., Wang, J. T., Ramage, D., Amin, N., Schwikowski, B. & Ideker, T. 2003. Cytoscape: a software environment for integrated models of biomolecular interaction networks. *Genome Res.*, 13, 2498–504.

Shapiro, L. & Colman, D. R. 1999. The diversity of cadherins and implications for a synaptic adhesive code in the CNS. *Neuron*, 23, 427–30.

Sheckler, L. R., Henry, L., Sugita, S., Südhof, T. C. & Rudenko, G. 2006. Crystal structure of the second LNS/LG domain from neurexin 1a: Ca^{2+} binding and the effects of alternative splicing. *J. Biol. Chem.*, 281, 22896–905.

Shilov, I. V., Seymour, S. L., Patel, A. A., Loboda, A., Tang, W. H., Keating, S. P., Hunter, C. L., Nuwaysir, L. M. & Schaeffer, D. A. 2007. The Paragon Algorithm, a next generation search engine that uses sequence temperature values and feature probabilities to identify peptides from tandem mass spectra. *Mol. Cell. Proteomics*, 6, 1638–55.

Shipman, S. L. & Nicoll, R. A. 2012. A subtype-specific function for the extracellular domain of neuroligin 1 in hippocampal LTP. *Neuron*, 76, 309–16.

Simonian, N. A., Elvhage, T., Czernik, A. J., Greengard, P. & Hyman, B. T. 1994. Calcium/calmodulin-dependent protein kinase II immunostaining is preserved in Alzheimer's disease hippocampal neurons. *Brain Res.*, 657, 294–9.

Sindi, I. A., Tannenberg, R. K. & Dodd, P. R. 2014. A role for the neurexin-neuroligin complex in Alzheimer's disease. *Neurobiol. Aging*, 35, 746–56.

Snyder, E. M., Nong, Y., Almeida, C. G., Paul, S., Moran, T., Choi, E. Y., Nairn, A. C., Salter, M. W., Lombroso, P. J., Gouras, G. K. & Greengard, P. 2005. Regulation of NMDA receptor trafficking by amyloid-β. *Nat. Neurosci.*, 8, 1051–8.

Sokolowska, I., Ngounou Wetie, A. G., Wormwood, K., Thome, J., Darie, C. C. & Woods, A. G. 2013. The potential of biomarkers in psychiatry: focus on proteomics. *J. Neural Transm.*

Song, J.-Y., Ichtchenko, K., Südhof, T. C. & Brose, N. 1999. Neuroligin 1 is a postsynaptic cell-adhesion molecule of excitatory synapses. *Proc. Natl. Acad. Sci. U.S.A.*, 96, 1100–5.

Spellman, D. S., Deinhardt, K., Darie, C. C., Chao, M. V. & Neubert, T. A. 2008. Stable isotopic labeling by amino acids in cultured primary neurons: application to brain-derived neurotrophic factor-dependent phosphotyrosine-associated signaling. *Mol. Cell. Proteomics*, 7, 1067–76.

Spires, T. L., Meyer-Luehmann, M., Stern, E. A., Mclean, P. J., Skoch, J., Nguyen, P. T., Bacskai, B. J. & Hyman, B. T. 2005. Dendritic spine abnormalities in amyloid precursor protein transgenic mice demonstrated by gene transfer and intravital multiphoton microscopy. *J. Neurosci.*, 25, 7278–87.

St George-Hyslop, P., Haines, J., Rogaev, E., Mortilla, M., Vaula, G., Pericak-Vance, M., Foncin, J. F., Montesi, M., Bruni, A., Sorbi, S., Rainero, I., Pinessi, L., Pollen, D., Polinsky, R., Nee, L., Kennedy, J., Macciardi, F., Rogaeva, E., Liang, Y., Alexandrova, N., Lukiw, W., Schlumpf, K., Tanzi, R., Tsuda, T., Farrer, L., Cantu, J. M., Duara, R., Amaducci, L., Bergamini, L., Gusella, J., Roses, A. & Crapper Mclachlan, D. 1992. Genetic evidence for a novel familial Alzheimer's disease locus on chromosome 14. *Nat. Genet.*, 2, 330–4.

St George-Hyslop, P. H., Tanzi, R. E., Polinsky, R. J., Haines, J. L., Nee, L., Watkins, P. C., Myers, R. H., Feldman, R. G., Pollen, D., Drachman, D. & Et Al. 1987. The genetic defect causing familial Alzheimer's disease maps on chromosome 21. *Science*, 235, 885–90.

Stahl-Zeng, J., Lange, V., Ossola, R., Eckhardt, K., Krek, W., Aebersold, R. & Domon, B. 2007. High sensitivity detection of plasma proteins by multiple reaction monitoring of N-glycosites. *Mol. Cell. Proteomics*, 6, 1809–17.

Südhof, T. C. 2008. Neuroligins and neurexins link synaptic function to cognitive disease. *Nature*, 455, 903–11.

Sugita, S., Khvochtev, M. & Südhof, T. C. 1999. Neurexins are functional α-latrotoxin receptors. *Neuron*, 22, 489–96.

Sun, C., Cheng, M. C., Qin, R., Liao, D. L., Chen, T. T., Koong, F. J., Chen, G. & Chen, C. H. 2011. Identification and functional characterization of rare mutations of the neuroligin-2 gene (*NLGN2*) associated with schizophrenia. *Hum. Mol. Genet.*, 20, 3042–51.

Sun, C., Zhang, L. & Chen, G. 2013. An unexpected role of neuroligin-2 in regulating KCC2 and GABA functional switch. *Mol. Brain*, 6, 23.

Suzuki, K., Hayashi, Y., Nakahara, S., Kumazaki, H., Prox, J., Horiuchi, K., Zeng, M., Tanimura, S., Nishiyama, Y., Osawa, S., Sehara-Fujisawa, A., Saftig, P., Yokoshima, S., Fukuyama, T.,

Matsuki, N., Koyama, R., Tomita, T. & Iwatsubo, T. 2012. Activity-dependent proteolytic cleavage of neuroligin-1. *Neuron*, 76, 410–22.

Sze, C., Troncoso, J., Kawas, C., Mouton, P., Price, D. & Martin, L. 1997. Loss of the presynaptic vesicle protein synaptophysin in hippocampus correlates with cognitive decline in Alzheimer disease. *J. Neuropathol. Exp. Neurol.*, 56, 944–.

Tabuchi, K. & Südhof, T. C. 2002. Structure and evolution of neurexin genes: insight into the mechanism of alternative splicing. *Genomics*, 79, 849–59.

Talebizadeh, Z., Bittel, D. C., Veatch, O. J., Kibiryeva, N. & Butler, M. G. 2005. Brief report: non-random X chromosome inactivation in females with autism. *J. Autism Dev. Disord.*, 35, 675–81.

Tanaka, H., Shan, W., Phillips, G. R., Arndt, K., Bozdagi, O., Shapiro, L., Huntley, G. W., Benson, D. L. & Colman, D. R. 2000. Molecular modification of N-cadherin in response to synaptic activity. *Neuron*, 25, 93–107.

Tang, L., Hung, C. P. & Schuman, E. M. 1998. A role for the cadherin family of cell adhesion molecules in hippocampal long-term potentiation. *Neuron*, 20, 1165–75.

Taniguchi, H., Gollan, L., Scholl, F. G., Mahadomrongkul, V., Dobler, E., Limthong, N., Peck, M., Aoki, C. & Scheiffele, P. 2007. Silencing of neuroligin function by postsynaptic neurexins. *J. Neurosci.*, 27, 2815–24.

Tannenberg, R. K., Scott, H. L., Tannenberg, A. E. & Dodd, P. R. 2006. Selective loss of synaptic proteins in Alzheimer's disease: evidence for an increased severity with APOE ε4. *Neurochem. Int.*, 49, 631–9.

Tanzi, R. E. & Bertram, L. 2005. Twenty years of the Alzheimer's disease amyloid hypothesis: a genetic perspective. *Cell*, 120, 545–55.

Tebar, F., Bohlander, S. K. & Sorkin, A. 1999. Clathrin assembly lymphoid myeloid leukemia (CALM) protein: localization in endocytic-coated pits, interactions with clathrin, and the impact of overexpression on clathrin-mediated traffic. *Mol. Biol. Cell*, 10, 2687–702.

Tekin, S., Mega, M. S., Masterman, D. M., Chow, T., Garakian, J., Vinters, H. V. & Cummings, J. L. 2001. Orbitofrontal and anterior cingulate cortex neurofibrillary tangle burden is associated with agitation in Alzheimer disease. *Ann. Neurol.*, 49, 355–61.

Terry, R. D., Masliah, E., Salmon, D. P., Butters, N., Deteresa, R., Hill, R., Hansen, L. A. & Katzman, R. 1991. Physical basis of cognitive alterations in Alzheimer's disease: synapse loss is the major correlate of cognitive impairment. *Ann. Neurol.*, 30, 572–80.

Therianos, S., Zhu, M., Pyun, E. & Coleman, P. D. 2004. Single-channel quantitative multiplex reverse transcriptase-polymerase chain reaction for large numbers of gene products differentiates nondemented from neuropathological Alzheimer's disease. *Am. J. Pathol.*, 164, 795–806.

Theuns, J., Marjaux, E., Vandenbulcke, M., Van Laere, K., Kumar-Singh, S., Bormans, G., Brouwers, N., Van Den Broeck, M., Vennekens, K., Corsmit, E., Cruts, M., De Strooper, B., Van Broeckhoven, C. & Vandenberghe, R. 2006. Alzheimer dementia caused by a novel mutation located in the APP C-terminal intracytosolic fragment. *Hum. Mutat.*, 27, 888–96.

Thies, W. & Bleiler, L. 2013. 2013 Alzheimer's disease facts and figures. *Alzheimers Dement.*, 9, 208–45.

Thiriet, N., Amar, L., Toussay, X., Lardeux, V., Ladenheim, B., Becker, K. G., Cadet, J. L., Solinas, M. & Jaber, M. 2008. Environmental enrichment during adolescence regulates gene expression in the striatum of mice. *Brain Res.*, 1222, 31–41.

Ting, A. K., Chen, Y., Wen, L., Yin, D. M., Shen, C., Tao, Y., Liu, X., Xiong, W. C. & Mei, L. 2011. Neuregulin 1 promotes excitatory synapse development and function in GABAergic interneurons. *J. Neurosci.*, 31, 15–25.

Tippett, L. J., Meier, S. L., Blackwood, K. & Diaz-Asper, C. 2007. Category specific deficits in Alzheimer's disease: fact or artefact? *Cortex*, 43, 907–20.

Trabzuni, D., Ryten, M., Walker, R., Smith, C., Imran, S., Ramasamy, A., Weale, M. E. & Hardy, J. 2011. Quality control parameters on a large dataset of regionally dissected human control brains for whole genome expression studies. *J. Neurochem.*, 119, 275–82.

Uhlén, M. & Pontén, F. 2005. Antibody-based proteomics for human tissue profiling. *Mol. Cell. Proteomics*, 4, 384–93.

Ullrich, B., Ushkaryov, Y. A. & Südhof, T. C. 1995. Cartography of neurexins: more than 1000 isoforms generated by alternative splicing and expressed in distinct subsets of neurons. *Neuron*, 14, 497–507.

Umemori, H., Linhoff, M. W., Ornitz, D. M. & Sanes, J. R. 2004. FGF22 and its close relatives are presynaptic organizing molecules in the mammalian brain. *Cell*, 118, 257–70.

Unwin, R. D., Griffiths, J. R., Leverentz, M. K., Grallert, A., Hagan, I. M. & Whetton, A. D. 2005. Multiple reaction monitoring to identify sites of protein phosphorylation with high sensitivity. *Mol. Cell. Proteomics*, 4, 1134–44.

Ushkaryov, Y. A., Petrenko, A. G., Geppert, M. & Südhof, T. C. 1992. Neurexins: synaptic cell surface proteins related to the α-latrotoxin receptor and laminin. *Science*, 257, 50–6.

Ushkaryov, Y. A., Hata, Y., Ichtchenko, K., Moomaw, C., Afendis, S., Slaughter, C. A. & Südhof, T. C. 1994. Conserved domain structure of β-neurexins. Unusual cleaved signal sequences in receptor-like neuronal cell-surface proteins. *J. Biol. Chem.*, 269, 11987–92.

Van Gool, D., Carmeliet, G., Triau, E., Cassiman, J.-J. & Dom, R. 1994. Appearance of localized immunoreactivity for the α4 integrin subunit and for fibronectin in brains from Alzheimer's, Lewy body dementia patients and aged controls. *Neurosci. Lett.*, 170, 71–3.

Varoqueaux, F., Jamain, S. & Brose, N. 2004. Neuroligin 2 is exclusively localized to inhibitory synapses. *Eur. J. Cell Biol.*, 83, 449–56.

Varoqueaux, F., Aramuni, G., Rawson, R. L., Mohrmann, R., Missler, M., Gottmann, K., Zhang, W., Südhof, T. C. & Brose, N. 2006. Neuroligins determine synapse maturation and function. *Neuron*, 51, 741–54.

Vasilj, A., Gentzel, M., Ueberham, E., Gebhardt, R. & Shevchenko, A. 2012. Tissue proteomics by one-dimensional gel electrophoresis combined with label-free protein quantification. *J. Proteome Res.*, 11, 3680–9.

Vawter, M. P., Evans, S., Choudary, P., Tomita, H., Meador-Woodruff, J., Molnar, M., Li, J., Lopez, J. F., Myers, R., Cox, D., Watson, S. J., Akil, H., Jones, E. G. & Bunney, W. E. 2004. Gender-specific gene expression in post-mortem human brain: localization to sex chromosomes. *Neuropsychopharmacology*, 29, 373–84.

Verwer, R. W., Hermens, W. T., Dijkhuizen, P., Ter Brake, O., Baker, R. E., Salehi, A., Sluiter, A. A., Kok, M. J., Muller, L. J., Verhaagen, J. & Swaab, D. F. 2002. Cells in human postmortem brain tissue slices remain alive for several weeks in culture. *FASEB J.*, 16, 54–60.

Viard, I., Wehrli, P., Jornot, L., Bullani, R., Vechietti, J. L., Schifferli, J. A., Tschopp, J. & French, L. E. 1999. Clusterin gene expression mediates resistance to apoptotic cell death induced by heat shock and oxidative stress. *J. Invest. Dermatol.*, 112, 290–6.

Vina, J. & Lloret, A. 2010. Why women have more Alzheimer's disease than men: gender and mitochondrial toxicity of amyloid-β peptide. *J. Alzheimers Dis.*, 20 Suppl 2, S527–33.

Von Bernhardi, R., Ramirez, G., De Ferrari, G. V. & Inestrosa, N. C. 2003. Acetylcholinesterase induces the expression of the β-amyloid precursor protein in glia and activates glial cells in culture. *Neurobiol. Dis.*, 14, 447–57.

Walch-Solimena, C., Takei, K., Marek, K. L., Midyett, K., Südhof, T. C., De Camilli, P. & Jahn, R. 1993. Synaptotagmin: a membrane constituent of neuropeptide-containing large dense-core vesicles. *J. Neurosci.*, 13, 3895–903.

Walikonis, R. S., Jensen, O. N., Mann, M., Provance, D. W., Jr., Mercer, J. A. & Kennedy, M. B. 2000. Identification of proteins in the postsynaptic density fraction by mass spectrometry. *J. Neurosci.*, 20, 4069–80.

Weidemann, A., König, G., Bunke, D., Fischer, P., Salbaum, J. M., Masters, C. L. & Beyreuther, K. 1989. Identification, biogenesis, and localization of precursors of Alzheimer's disease A4 amyloid protein. *Cell*, 57, 115–26.

Welberg, L. 2012. Synaptic plasticity: neuroligin 1 does the splits. *Nat. Rev. Neurosci.*, 13, 811.

West, H. L., Rebeck, G. W. & Hyman, B. T. 1994. Frequency of the apolipoprotein E ε2 allele is diminished in sporadic Alzheimer disease. *Neurosci. Lett.*, 175, 46–8.

Williamson, B. L., Marchese, J. & Morrice, N. A. 2006. Automated identification and quantification of protein phosphorylation sites by LC/MS on a hybrid triple quadrupole linear ion trap mass spectrometer. *Mol. Cell. Proteomics,* 5, 337–46.

Wolfe, M. S. 2008. γ-Secretase inhibition and modulation for Alzheimer's disease. *Curr. Alzheimer Res.*, 5, 158–64.

Wong, P., Taillefer, D., Lakins, J., Pineault, J., Chader, G. & Tenniswood, M. 1994. Molecular characterization of human TRPM-2/clusterin, a gene associated with sperm maturation, apoptosis and neurodegeneration. *Eur. J. Biochem.*, 221, 917–25.

Wood, J. G., Mirra, S. S., Pollock, N. J. & Binder, L. I. 1986. Neurofibrillary tangles of Alzheimer disease share antigenic determinants with the axonal microtubule-associated protein tau (τ). *Proc. Natl. Acad. Sci. U.S.A.*, 83, 4040–3.

Woods, A. G., Sokolowska, I., Taurines, R., Gerlach, M., Dudley, E., Thome, J. & Darie, C. C. 2012. Potential biomarkers in psychiatry: focus on the cholesterol system. *J. Cell. Mol. Med.*, 16, 1184–95.

Wright, S., Malinin, N. L., Powell, K. A., Yednock, T., Rydel, R. E. & Griswold-Prenner, I. 2007. α2β1 and αlVβ1 integrin signaling pathways mediate amyloid-β-induced neurotoxicity. *Neurobiol. Aging*, 28, 226–37.

Yamada, M., Saisu, H., Ishizuka, T., Takahashi, H. & Abe, T. 1999. Immunohistochemical distribution of the two isoforms of synaphin/complexin involved in neurotransmitter release: localization at the distinct central nervous system regions and synaptic types. *Neuroscience,* 93, 7–18.

Yan, J., Oliveira, G., Coutinho, A., Yang, C., Feng, J., Katz, C., Sram, J., Bockholt, A., Jones, I. R., Craddock, N., Cook, E. H., Jr., Vicente, A. & Sommer, S. S. 2005. Analysis of the neuroligin 3 and 4 genes in autism and other neuropsychiatric patients. *Mol. Psychiatry,* 10, 329–32.

Yang, G. P., Ross, D. T., Kuang, W. W., Brown, P. O. & Weigel, R. J. 1999. Combining SSH and cDNA microarrays for rapid identification of differentially expressed genes. *Nucleic Acids Res.*, 27, 1517–23.

Yao, P. J., Zhu, M., Pyun, E. I., Brooks, A. I., Therianos, S., Meyers, V. E. & Coleman, P. D. 2003. Defects in expression of genes related to synaptic vesicle trafficking in frontal cortex of Alzheimer's disease. *Neurobiol. Dis.*, 12, 97–109.

Yasojima, K., Mcgeer, E. G. & Mcgeer, P. L. 2001. High stability of mRNAs postmortem and protocols for their assessment by RT-PCR. *Brain Res. Brain Res. Protoc.*, 8, 212–8.

Ylisaukko-Oja, T., Rehnstrom, K., Auranen, M., Vanhala, R., Alen, R., Kempas, E., Ellonen, P., Turunen, J. A., Makkonen, I., Riikonen, R., Nieminen-Von Wendt, T., Von Wendt, L., Peltonen, L. & Jarvela, I. 2005a. Analysis of four neuroligin genes as candidates for autism. *Eur. J. Hum. Genet.*, 13, 1285–92.

Ylisaukko-Oja, T., Rehnström, K., Auranen, M., Vanhala, R., Alen, R., Kempas, E., Ellonen, P., Turunen, J. A., Makkonen, I., Riikonen, R., Nieminen-Von Wendt, T., Von Wendt, L., Peltonen, L. & Järvelä, I. 2005b. Analysis of four neuroligin genes as candidates for autism. *Eur. J. Hum. Genet.*, 13, 1285–92.

Zannis, V. I., Just, P. W. & Breslow, J. L. 1981. Human apolipoprotein E isoprotein subclasses are genetically determined. *Am. J. Hum. Genet.*, 33, 11–24.

Zeev-Ben-Mordehai, T., Rydberg, E. H., Solomon, A., Toker, L., Auld, V. J., Silman, I., Botti, S. & Sussman, J. L. 2003. The intracellular domain of the drosophila cholinesterase-like neural adhesion protein, gliotactin, is natively unfolded. *Proteins*, 53, 758–67.

Zhou, J., Jones, D. R., Duong, D. M., Levey, A. I., Lah, J. J. & Peng, J. 2013. Proteomic analysis of postsynaptic density in Alzheimer's disease. *Clin. Chim. Acta*, 420, 62–8.

Ziff, E. B. 1997. Enlightening the postsynaptic density. *Neuron*, 19, 1163–74.

Zuo, L., Van Dyck, C. H., Luo, X., Kranzler, H. R., Yang, B. Z. & Gelernter, J. 2006. Variation at *APOE* and *STH* loci and Alzheimer's disease. *Behav. Brain Funct.*, 2, 13.

9 Appendix

9.1 Appendix for Chapter 2

Human *NLGN1* and *NLGN2* wild-type sequences were gained from the NCBI database (Accession No: NP_055747 and NP_065846 respectively).

9.1.1.1 NLGN1

```
   1  ccaccgactc ctgcccgcct caacacaatg ccttacctgt gaagcttgag gccactcaag
  61  ttccaaattt gtgacaaatc ccccagggct cactggagtg gcagatatag acctgcagct
 121  aactggattt gatttataag agagaaatct gcagtcaatg cccactcttg ccacactgct
 181  aatatggaaa acagaatgtt caataggata tggtctgata aatagtgatg attgaagatg
 241  ctgctccaat acatgtgaaa tcaatgggag atatctgctg tctgaagatc tttcagagct
 301  tttctcgaca agctcccctg taagaaatcg gaggtatatt ctaccattat acagtctttc
 361  tcaagtggat ataaatacgt ttgcctcact gtaaccagac aactagacaa ctaatgtggg
 421  accatggcac tgcccagatg cacgtggcca aattatgttt ggagagcagt gatggcatgc
 481  ttggtacacc ggggattggg tgccccattg actctctgta tgttgggatg tttgcttcag
 541  gctggccatg tgctatcaca aaaattggat gatgtggacc cactggtggc taccaacttt
 601  ggaaagataa gagggattaa gaaggaactc aataatgaaa ttttggggcc tgttattcaa
 661  tttcttgggg ttccatatgc agccccacca acaggggaac gtcgttttca gcctccagaa
 721  ccaccatctc cctggtcaga tatcagaaat gccactcaat ttgctcctgt gtgtccccag
 781  aatatcattg atggcagatt gccagaagtc atgcttcctg tgtggtttac taataacttg
 841  gatgtggttt catcatatgt gcaagaccag agcgaagact gcctatattt aaatatatat
 901  gtcccgactg aggatgatat tcgggacagt gggggtccca aaccagtgat ggtgtatatc
 961  catggtggct catatatgga aggtactgga aatttatatg atggaagtgt cttggcaagt
1021  tatggcaatg tgatcgtcat cacagtcaac tatcgacttg gagtactcgg tttcttgagt
1081  acaggcgatc aggctgcaaa ggggaactat ggactccttg atctcataca agctttaaga
1141  tggactagtg aaaacattgg attctttggt ggtgacccct taagaatcac tgtttttgga
1201  tctggtgctg ggggttcatg tgtcaacctg ctgactttat cccattattc tgaaggtaac
```

1261 cgttggagca attcaaccaa aggacttttt caacgagcaa tagctcaaag tggaacagcc

1321 ctttccagct gggctgttag ttttcaacct gcaaaatatg ctagaatgtt ggccacaaaa

1381 gttggttgca atgtttcaga tacagtagag ttagtggaat gcctacagaa gaagccttac

1441 aaagaacttg ttgaccaaga tattcaacca gctcgatacc acatagcctt tggacctgtg

1501 attgatggtg atgtaatacc agacgacccc cagatattga tggagcaagg agagtttctc

1561 aactatgata taatgttagg agtgaaccaa ggggaagggt taaaatttgt tgaaaatata

1621 gtagatagcg atgatggtat atcagctagt gattttgact ttgctgtttc aaattttgtt

1681 gataatttat atggatatcc tgaaggcaaa gatgttttga gagaaaccat taagttcatg

1741 tatactgact gggctgaccg tcataaccct gaaaccagaa gaaagacatt actggctttg

1801 tttacggacc atcagtgggt ggcaccagct gtagccacag cggatcttca ctcaaacttt

1861 ggttcaccta cgtacttcta tgccttttac catcattgcc aaacagatca ggttccagct

1921 tgggctgatg cagcccacgg agacgaggtt ccctatgtac tgggaatccc catgattggc

1981 cctacagagt tatttccttg caatttctcc aaaaatgatg tgatgctgag tgcagttgta

2041 atgacatact ggacaaattt tgctaaaact ggtgacccaa atcaaccagt ccctcaagac

2101 acgaaattca ttcataccaa acccaaccgt tttgaagaag tagcatggac cagatattcc

2161 cagaaagacc aactttatct ccatattgga ttaaaaccaa gagttaaaga acattacaga

2221 gccaataagg tgaacctctg gttggagttg gtacctcatc tgcataatct caatgacatt

2281 tctcagtata cctctacaac aactaaagtg ccatcaactg acatcacttt cagacctacg

2341 agaaaaaatt ctgtacctgt cacgtcagcc tttcccactg ccaagcagga tgatcccaaa

2401 caacaaccaa gtccattttc agtggatcaa agggactact caacagagct gagtgtcact

2461 attgcagttg gagcatcact gctgtttctg aacatcttgg cctttgcagc cctgtactac

2521 aaaaaggata agaggagaca tgatgttcac aggagatgca gccctcagcg cactactacc

2581 aatgatctaa cccatgcaca agaagaggaa atcatgtccc tccaaatgaa gcacactgat

2641 ttggatcatg aatgtgagtc cattcatcca catgaggtgg ttcttcggac cgcctgtccc

2701 ccagattaca cactagctat gaggaggtca cctgatgatg ttcccttaat gacacccaac

2761 accattacaa tgattcccaa cactatacca gggattcagc ccttacacac attcaataca

2821 tttactggag gacagaacaa tactctgccc catccccatc cccaccccca ttcacattca

2881 acaaccaggg tatagccaga taagagaaac aaactatttt ttttgatgga ttgcagtaaa

2941 cgatcactga agattccttg gctttcaacc tacaagactt actatttaaa taaggaggaa

3001 tattatgtga atatacatat caagaacttt gggggttttg aaaaaaatga attgtatata

3061 tacaaatcaa ctttaaaaac aaatttcaat tgcttgaagc aattgttctg aatgatactt

3121 tttcattcac attcaagaat taatttttg aagatttaag ttacataatg gaattaggca

3181 tgtggaacac caaacaggaa agaactatgt ctgaaatata aaaaataaaa ataaaaaaac

3241 aactatgaat atgcacaagg gacacaccag tggaatgtca gataattttc accagttttt

3301 atttggagcc gttttattgt gtagaccata tttacatatt tggataagta cacaaagcgt

3361 caatgctgtt aatggcctta gcaaaggctc atgctgaaat ttgccagtaa aacaaagaag

3421 tttaaagact ggcaggtaca ccattatcac ataagtgctg tcagtataaa gttgtgggga

3481 taaaggaaac tggatatttt tagcacgatg tgcatgataa tttatatgct tggtggctgt

3541 gctgctgatt aagccgtaat taaaattctt ctcatcccat tggagttttt aatagaagct

3601 tcctccatca attggcagaa cctaaagaag attttaaggg gcaaaagtaa ttacaataaa

3661 ataattcaca gtagtttcaa tatagaagga attagctatt aaaggtattt gaagaaacta

3721 taggtatagt ggtgaatact cgctgatatg aatcccagaa aaaaatttcc tgtttttaat

3781 gttcttttca atcccatcta gataatttat agaaatataa ccctaattgg acatgtggta

3841 caggatctat aagttgctgt gttttttgt tactctgtat tttgttcctt ttggtaaggt

3901 gaagtgtgtc caaagagtta cttgcaacag tctttcatga tatgaggatg cccccgtatt

3961 accactctga ttatagttct gagttctttg atttactcat gctgcatgac aaaatgttta

4021 ctaataacaa ttcattataa agttatatcc ctctttacat cacttatctt tctcactgag

4081 gttcattcac tggaatttac tcacgcaatc tcagtagagt acaacgtaga tacagaacct

4141 aggagagtca acatctggag gattttagtc tttcttacac atatgtgtga ttttaaacga

4201 atattctcag accacaggaa actcttcatc cccctgttgt ttaccagtaa cagtatatca

4261 cagacctttc caaatgtttg tatatgtaat cagatgtaca tttatattga aaaacaaatg

4321 agatggactt aaagagcaca tcctgataaa tactttctct ctcacctgta ctatatttct

4381 attagactaa agttatgtga ttttttttt acatttttc agatgactag caattttgat

4441 agtttataag ataatgcaaa gaactttctc tgacaaacta actgcagtaa cagaaacctt

```
4501  tcttttcagt  tactcttttt  caagaatgaa  agattattat  acaaaaaatt  gtatactact

4561  tgatggaacc  aactttgtac  atcttggcca  tgtcactggt  cattgtgtga  aataaagata

4621  atctggataa  tgactattag  tccaatgcta  agaaacatga  tctttgctca  ttaaagagct

4681  aaaatgttta  ttgctgtttt  gtctttcttt  tttctaaaaa  aagaaaaaaa  agaaaaaaag

4741  gaaaagaaga  acaaagaaac  atgactgtct  caaagagtaa  tttttctaga  ttagaccagt

4801  caggtttttg  aagacatata  ggtaacttcc  acagaaaaca  caaacatgta  tttaaaggca

4861  agtctcatct  aagatgaaac  tcataaaaat  tatttaatgt  ttgttatgaa  tttaaaag
```

9.1.1.2 Compute pI/Mw

Theoretical pI/Mw (average) for the user-entered sequence

```
        10          20          30          40          50          60
TMALPRCTWP  NYVWRAVMAC  LVHRGLGAPL  TLCMLGCLLQ  AGHVLSQKLD  DVDPLVATNF
        70          80          90         100         110         120
GKIRGIKKEL  NNEILGPVIQ  FLGVPYAAPP  TGERRFQPPE  PPSPWSDIRN  ATQFAPVCPQ
       130         140         150         160         170         180
NIIDGRLPEV  MLPVWFTNNL  DVVSSYVQDQ  SEDCLYLNIY  VPTEDDIRDS  GGPKPVMVYI
       190         200         210         220         230         240
HGGSYMEGTG  NLYDGSVLAS  YGNVIVITVN  YRLGVLGFLS  TGDQAAKGNY  GLLDLIQALR
       250         260         270         280         290         300
WTSENIGFFG  GDPLRITVFG  SGAGGSCVNL  LTLSHYSEGN  RWSNSTKGLF  QRAIAQSGTA
       310         320         330         340         350         356
LSSWAVSFQP  AKYARMLATK  VGCNVSDTVE  LVECLQKKPY  KELVDQDIQP      ARYHIA
```

Theoretical pI/Mw: 5.97 / 38921.59

9.1.1.3 NLGN2

```
   1  tccctctccc  ccccttctct  ctctctccga  gggggggggg  tcccagggag  ggaggggggg

  61  tcccccgatc  agcatgtggc  tcctggcgct  gtgtctggtg  gggctggcgg  gggctcaacg

 121  cgggggaggg  ggtcccggcg  gcggcgcccc  gggcggcccc  ggcctgggcc  tcggcagcct

 181  cggcgaggag  cgcttcccgg  tggtgaacac  ggcctacggg  cgagtgcgcg  gtgtgcggcg

 241  cgagctcaac  aacgagatcc  tgggccccgt  cgtgcagttc  ttgggcgtgc  cctacgccac

 301  gccgcccctg  ggcgcccgcc  gcttccagcc  gcctgaggcg  cccgcctcgt  ggcccggcgt

 361  gcgcaacgcc  accaccctgc  cgcccgcctg  cccgcagaac  ctgcacgggg  cgctgcccgc

 421  catcatgctg  cctgtgtggt  tcaccgacaa  cttggaggcg  gccgccacct  acgtgcagaa

 481  ccagagcgag  gactgcctgt  acctcaacct  ctacgtgccc  accgaggacg  gtccgctcac

 541  aaaaaaacgt  gacgaggcga  cgctcaatcc  gccagacaca  gatatccgtg  accctgggaa
```

601 gaagcctgtg atgctgtttc tccatggcgg ctcctacatg gaggggaccg gaaacatgtt

661 cgatggctca gtcctggctg cctatggcaa cgtcattgta gccacgctca actaccgtct

721 tggggtgctc ggttttctca gcaccgggga ccaggctgca aaaggcaact atgggctcct

781 ggaccagatc caggccctgc gctggctcag tgaaaacatc gcccactttg ggggcgaccc

841 cgagcgtatc accatctttg gttccggggc aggggcctcc tgcgtcaacc ttctgatcct

901 ctcccaccat tcagaagggc tgttccagaa ggccatcgcc cagagtggca ccgccatttc

961 cagctggtct gtcaactacc agccgctcaa gtacacgcgg ctgctggcag ccaaggtggg

1021 ctgtgaccga gaggacagcg ctgaagctgt ggagtgtctg cgccggaagc cctcccggga

1081 gctggtggac caggacgtgc agcctgcccg ctaccacatc gcctttgggc ccgtggtgga

1141 tggcgacgtg gtccccgatg accctgagat cctcatgcag cagggagaat tcctcaacta

1201 cgacatgctc atcggcgtca accagggaga gggcctcaag ttcgtggagg actctgcaga

1261 gagcgaggac ggtgtgtctg ccagcgcctt tgacttcact gtctccaact ttgtggacaa

1321 cctgtatggc tacccggaag gcaaggatgt gcttcgggag accatcaagt ttatgtacac

1381 agactgggcc gaccgggaca atggcgaaat gcgccgcaaa accctgctgg cgctctttac

1441 tgaccaccaa tgggtggcac cagctgtggc cactgccaag ctgcacgccg actaccagtc

1501 tcccgtctac ttttacacct tctaccacca ctgccaggcg gagggccggc ctgagtgggc

1561 agatgcggcg cacggggatg aactgcccta tgtctttggc gtgcccatgg tgggtgccac

1621 cgacctcttc ccctgtaact tctccaagaa tgacgtcatg ctcagtgccg tggtcatgac

1681 ctactggacc aacttcgcca agactgggga ccccaaccag ccggtgccgc aggataccaa

1741 gttcatccac accaagccca atcgcttcga ggaggtggtg tggagcaaat tcaacagcaa

1801 ggagaagcag tatctgcaca taggcctgaa gccacgcgtg cgtgacaact accgcgccaa

1861 caaggtggcc ttctggctgg agctcgtgcc ccacctgcac aacctgcaca cggagctctt

1921 caccaccacc acgcgcctgc ctccctacgc cacgcgctgg ccgcctcgtc cccccgctgg

1981 cgccccgggc acacgccggc ccccgccgcc tgccaccctg cctcccgagc ccgagcccga

2041 gcccggccca agggcctatg accgcttccc cggggactca cgggactact ccacggagct

2101 gagcgtcacc gtggccgtgg gtgcctccct cctcttcctc aacatcctgg cctttgctgc

2161 cctctactac aagcgggacc ggcggcagga gctgcggtgc aggcggctta gcccacctgg

2221 cggctcaggc tctggcgtgc ctggtggggg ccccctgctc cccgccgcgg gccgtgagct

2281 gccaccagag gaggagctgg tgtcactgca gctgaagcgg ggtggtggcg tcggggcgga

2341 ccctgccgag gctctgcgcc ctgcctgccc gcccgactac accctggccc tgcgccgggc

2401 accggacgat gtgcctctct tggcccccgg ggccctgacc ctgctgccca gtggcctggg

2461 gccaccgcca cccccaccgc ccccctccct tcatcccttc gggcccttcc ccccgccccc

2521 tcccaccgcc accagccaca acaacacgct accccacccc cactccacca ctcgggtata

2581 gggggtgggt ggggaggccc tcctccccgg ccctccctgg cccggccact ccgaaggcag

2641 ggaggaggac ttggcaactg gcttttctcc tgtggagtcg tcacacgcca tccagcagcg

2701 ctaaggtgga catgggattc ctccctgcga tgcgtgtctt tcccacgcag agaagcccag

2761 tctcttctct ggatctgggc ctttgaacaa ctgggggggcg ttttctcccc cccattggga

2821 caccagtctt cggtgtgtgg aatgtggtat tttcccgcgt ggaggtgtgc tttctcacaa

2881 cggggtgtgt tttcccatgt gcagggtgag gttttttttt gccaccctgg acacatgttg

2941 gccccctcaa agaatttctg tggggatttg taccccagaa tcctgttccc ccatcccttc

3001 tcccacctcc tcccctctcc ctccccctgg agaccctgga agtggtgtgt tcacatacag

3061 tgacccttgg ccaccagacc acagaggatg gagcctggga agcagcgagg aaatcacagc

3121 cccctcgccc ctgcctccct tgcccctacc ccggcgaagc atgttccccc cgacgccccc

3181 cttggcacaa gtcagatgaa gcacgttctg ccggggaggc cctcaccttc cagagaggac

3241 agacacagat ttcctgctgg gggagggagg agtccacgca tcctgatgct gcctggaagc

3301 ttattttccc gtggccagga cgcatttctc tgagtggaaa caggttcttg catgtggatg

3361 tgtgtttccc caggcagacg gcccctctct tcccagcact tccctgcctc ccccaggcct

3421 caggcccagc acccagttcc tcctcacatg gcaggtgagc acagacttct agttggcagg

3481 agctgaggag ggtgaacaaa ccccgaggga ggcccggccc ttgctcccga gttgggggga

3541 gggggtgtgg caacgtgccc cccgcagagg ccacgcatgt ttgaccaaag ccctcattgt

3601 ggtccgagga cagccttttc cccaggcctc agagcattgc tcatccgtgc caaactgggt

3661 aggtggattt gagcggaaag actcccaaaa tgtgccaaga atttcccagt cccaggcagg

3721 gcaggggaaa ctaagggcaa gcaggataca gggcgaggga tgtggcaggt gaggggctc

3781 ccgcctgtgc cccttctcct caccatgtct cccccaccct gcctcagttc tccgttcccc

```
3841  ttcatctccg  tccccctctt  tgaagctgtc  cccatctcag  tgtcagacca  gccttctcct

3901  cagctgacca  ccctcctctg  acccacgccc  cctccttgtc  tgaaagaaag  gagccttgaa

3961  tggtggaggg  aggcagtggg  gagaaaggtc  tcaccggaca  ggttgggaga  atgaggtcag

4021  cggtgctggg  gaacagatgg  agggggcagt  ggggacaggg  cttgggcaga  caccagcagg

4081  aataatttga  aatgtgtgag  gtgactcccc  ggagggcctt  gggcttgggc  atttgggaaa

4141  agaatgatgt  ctggaagggc  ttaagggaca  cagtggacga  ggggagagtc  ctcatctgct

4201  ggcattttgt  ggggtgttag  tgccaaactt  gaataggggc  tggggtgctg  tcttccactg

4261  acacccaaat  ccagaatccc  tggtcttgag  tccccagaac  tttgcctctt  gactgtccct

4321  tctcttccta  cctccatcca  tggaaaatta  gttatttttct  gatcctttcc  cctgcctggt

4381  ctagctcctc  tccaaacagc  catgccctcc  aaatgctaga  gacctgggcc  ctgaaccctg

4441  tagacagatg  ccctcagaat  tggggcatgg  gaggggggct  gggggacccc  atgattcagc

4501  cacggactcc  aatgcccagc  tcctctcccc  aaaacaatcc  cgacaatccc  ttatccctac

4561  cccaaccctt  tgcggctctg  tacacatttt  taaacctggc  aaaagatgaa  gagaatattg

4621  taaatataaa  agtttaactg  tt
```

9.1.1.4 Compute pI/Mw

Theoretical pI/Mw (average) for the user-entered sequence

```
        10          20          30          40          50          60
TYVQNQSEDC  LYLNLYVPTE  DGPLTKKRDE  ATLNPPDTDI  RDPGKKPVML  FLHGGSYMEG
        70          80          90         100         110         120
TGNMFDGSVL  AAYGNVIVAT  LNYRLGVLGF  LSTGDQAAKG  NYGLLDQIQA  LRWLSENIAH
       130         140         150         160         170         180
FGGDPERITI  FGSGAGASCV  NLLILSHHSE  GLFQKAIAQS  GTAISSWSVN  YQPLKYTRLL
       190         200         210         220         230         240
AAKVGCDRED  SAEAVECLRR  KPSRELVDQD  VQPARYHIAF  GPVVDGDVVP  DDPEILMQQG
       250         260         270         280         290         300
EFLNYDMLIG  VNQGEGLKFV  EDSAESEDGV  SASAFDFTVS  NFVDNLYGYP  EGKDVLRETI
       310         320         330         340         350
KFMYTDWADR  DNGEMRRKTL  LALFTDHQWV  APAVATAKLH     ADYQSPV
```

Theoretical pI/Mw: 4.66 / 38192.81

9.1.2 Forward primer

BLASTN 1.8.4-Paracel [2010-10-31], (Altschul et al., 1997)

Query= 5F_H06 (1039 letters)

Database: genbank

9,537,552 sequences; 28,719,530,764 total letters

Sequences producing significant alignments:	(bits)	Value	Score	E
gi|123980671|gb|DQ891239.2| Synthetic construct clone IMAGE:1000...	1750		0.0	
gi|157928141|gb|EU176566.1| Synthetic construct *H. sapiens* clo...	1750		0.0	
gi|21595790|gb|BC032555.1| *H. sapiens* Neuroligin-1, mRNA (cDNA...	1748		0.0	
gi|5689476|dbj|AB028993.1| *H. sapiens* mRNA for KIAA1070 protei...	1748		0.0	
gi|31317253|ref|NM_014932.2| *H. sapiens* Neuroligin-1 (NLGN1)...	1748		0.0	
gi|168278798|dbj|AB385423.1| Synthetic construct DNA, clone: pF1...	1746		0.0	
gi|114590433|ref|XM_001166397.1| PREDICTED: Pan troglodytes simi...	1725		0.0	
gi|114590431|ref|XM_001166321.1| PREDICTED: Pan troglodytes simi...	1725		0.0	
gi|114590435|ref|XM_001166442.1| PREDICTED: Pan troglodytes simi...	1629		0.0	
gi|109044231|ref|XM_001082898.1| PREDICTED: Macaca mulatta Neuro...	1606		0.0	
gi|109044228|ref|XM_001082770.1| PREDICTED: Macaca mulatta Neuro...	1606		0.0	
gi|109044234|ref|XM_001083506.1| PREDICTED: Macaca mulatta Neuro...	1511		0.0	
gi|149731113|ref|XM_001494392.1| PREDICTED: Equus caballus Neuro...	1376		0.0	
gi|194222596|ref|XM_001494331.2| PREDICTED: Equus caballus Neuro...	1376		0.0	
gi|74003762|ref|XM_545297.2| PREDICTED: Canis familiaris similar...	1344		0.0	
gi|113912208|gb|BC122827.1| Bos taurus Neuroligin-1, mRNA (cDNA...	1225		0.0	
gi|194664213|ref|XM_608505.4| PREDICTED: Bos taurus Neuroligin-1...	1225		0.0	
gi|17105267|gb|AC092967.5| *H. sapiens* 3 BAC RP11-521A24 (Roswe...	983		0.0	
gi|114590437|ref|XM_001166231.1| PREDICTED: Pan troglodytes simi...	975		0.0	
gi|114590429|ref|XM_001166258.1| PREDICTED: Pan troglodytes simi...	975		0.0	
gi|114590427|ref|XM_001166019.1| PREDICTED: Pan troglodytes simi...	975		0.0	
gi|114590425|ref|XM_001166092.1| PREDICTED: Pan troglodytes simi...	975		0.0	
gi|114590423|ref|XM_001166352.1| PREDICTED: Pan troglodytes simi...	975		0.0	
gi|114590421|ref|XM_526383.2| PREDICTED: Pan troglodytes similar...	975		0.0	

gi|114590419|ref|XM_001166291.1| PREDICTED: Pan troglodytes simi...	975	0.0
gi|164693376|dbj|AK307813.1| *H. sapiens* cDNA, FLJ97761	975	0.0
gi|254281190|ref|NM_001163387.1| Mus musculus Neuroligin-1 (Nlgn...	924	0.0
gi|68533534|gb|BC098461.1| Mus musculus Neuroligin-1, mRNA (cDNA...	916	0.0
gi|109044244|ref|XM_001083140.1| PREDICTED: Macaca mulatta Neuro...	864	0.0
gi|109044240|ref|XM_001082256.1| PREDICTED: Macaca mulatta Neuro...	864	0.0

>5F_H06

AATAATTTTGTTTACTTTAAGAAGGAGATATACATATGCGGGGTTCTCATCATCATCATCAT
CATGGTATGGCTAGCATGACTGGTGGACAGCAAATGGGTCGGGATCTGTACGACGATGAC
GATAAGGATCATCCCTTCACCATGGCACTGCCCAGATGCACGTGGCCAAATTATGTTTGGA
GAGCAGTGATGGCATGCTTGGTACACCGGGGATTGGGTGCCCCATTGACTCTCTGTATGT
TGGGATGTTTGCTTCAGGCTGGCCATGTGCTATCACAAAAATTGGATGATGTGGACCCAC
TGGTGGCTACCAACTTTGGAAAGATAAGAGGGATTAAGAAGGAACTCAATAATGAAATTT
TGGGGCCTGTTATTCAATTTCTTGGGGTTCCATATGCAGCCCCACCAACAGGGGAACGTC
GTTTTCAGCCTCCAGAACCACCATCTCCCTGGTCAGATATCAGAAATGCCACTCAATTTGC
TCCTGTGTGTCCCCAGAATATCATTGATGGCAGATTGCCAGAAGTCATGCTTCCTGTGTGG
TTTACTAATAACTTGGATGTGGTTTCATCATATGTGCAAGACCAGAGCGAAGACTGCCTAT
ATTTAAATATATATGTCCCGACTGAGGATGATATTCGGGACAGTGGGGGTCCCAAACCAGT
GATGGTGTATATCCATGGTGGCTCATATATGGAAGGTACTGGAAATTTATATGATGGAAGTG
TCTTGGCAAGTTATGGCAATGTGATCGTCATCACAGTCAACTATCGACTTGGAGTACTCGG
TTTCTTGAGTACAGGCGATCAGGCTGCAAAGGGGAACTATGGACTCCTTGATCTCATACA
AGCTTTAAGATGGACTAGTGAAAACATTGGATTCTTTGGTGGTGACCCCTTAAGAATCAC
TGTTTTTGGATCTGGTGCTGGGGGTTCATGTGTCAACCTGCTGACTTTATCCCATTATTCTG
AAAGTAACCCGTTGGAGCAATTCACCCAAAGGACTTTTTCAACGAGCAATAGCTCAAAG
TGGAACAA

9.1.3 NLGN1 reverse primer

BLASTN 1.8.4-Paracel [2010-10-31], (Altschul et al., 1997).

Query= 6R_H07 (1106 letters)

Database: genbank

9,537,552 sequences; 28,719,530,764 total letter

Sequences producing significant alignments:	(bits) Value	Score	E
gi|21595790|gb|BC032555.1| *H. sapiens* Neuroligin-1, mRNA (cDNA...	2089	0.0	
gi|5689476|dbj|AB028993.1| *H. sapiens* mRNA for KIAA1070 protei...	2089	0.0	
gi|31317253|ref|NM_014932.2| *H. sapiens* Neuroligin-1 (NLGN1)...	2089	0.0	
gi|123980671|gb|DQ891239.2| Synthetic construct clone IMAGE:1000...	2089	0.0	
gi|157928141|gb|EU176566.1| Synthetic construct *H. sapiens* clo...	2089	0.0	
gi|168278798|dbj|AB385423.1| Synthetic construct DNA, clone: pF1...	2089	0.0	
gi|114590433|ref|XM_001166397.1| PREDICTED: Pan troglodytes simi...	2058	0.0	
gi|114590431|ref|XM_001166321.1| PREDICTED: Pan troglodytes simi...	2058	0.0	
gi|109044231|ref|XM_001082898.1| PREDICTED: Macaca mulatta Neuro...	1939	0.0	
gi|109044228|ref|XM_001082770.1| PREDICTED: Macaca mulatta Neuro...	1939	0.0	
gi|149731113|ref|XM_001494392.1| PREDICTED: Equus caballus Neuro...	1685	0.0	
gi|194222596|ref|XM_001494331.2| PREDICTED: Equus caballus Neuro...	1685	0.0	
gi|74003762|ref|XM_545297.2| PREDICTED: Canis familiaris similar...	1661	0.0	
gi|114590435|ref|XM_001166442.1| PREDICTED: Pan troglodytes simi...	1604	0.0	
gi|113912208|gb|BC122827.1| Bos taurus Neuroligin-1, mRNA (cDNA...	1542	0.0	
gi|194664213|ref|XM_608505.4| PREDICTED: Bos taurus Neuroligin-1...	1542	0.0	
gi|109044234|ref|XM_001083506.1| PREDICTED: Macaca mulatta Neuro...	1485	0.0	
gi|114590427|ref|XM_001166019.1| PREDICTED: Pan troglodytes simi...	1114	0.0	
gi|114590425|ref|XM_001166092.1| PREDICTED: Pan troglodytes simi...	1114	0.0	
gi|114590421|ref|XM_526383.2| PREDICTED: Pan troglodytes similar...	1114	0.0	
gi|109044240|ref|XM_001082256.1| PREDICTED: Macaca mulatta Neuro...	1106	0.0	
gi|109044225|ref|XM_001082382.1| PREDICTED: Macaca mulatta Neuro...	1106	0.0	
gi|164693376|dbj|AK307813.1| *H. sapiens* cDNA, FLJ97761	955	0.0	

gi|17105267|gb|AC092967.5| *H. sapiens* 3 BAC RP11-521A24 (Roswe...	954	0.0
gi|114590437|ref|XM_001166231.1| PREDICTED: Pan troglodytes simi...	946	0.0
gi|114590429|ref|XM_001166258.1| PREDICTED: Pan troglodytes simi...	946	0.0
gi|114590423|ref|XM_001166352.1| PREDICTED: Pan troglodytes simi...	946	0.0
gi|114590419|ref|XM_001166291.1| PREDICTED: Pan troglodytes simi...	946	0.0
gi|254281190|ref|NM_001163387.1| Mus musculus Neuroligin-1 (Nlgn...	898	0.0
gi|224060830|ref|XM_002197701.1| PREDICTED: Taeniopygia guttata...	894	0.0

>6R_H07

GCAGCCGGATCGTTGAGCTCGCCCTTTTAGGCTATGTGGTATCGAGCTGGTTGAATATCTT
GGTCAACAAGTTCTTTGTAAGGCTTCTTCTGTAGGCATTCCACTAACTCTACTGTATCTGA
AACATTGCAACCAACTTTTGTGGCCAACATTCTAGCATATTTTGCAGGTTGAAAACTAAC
AGCCCAGCTGGAAAGGGCTGTTCCACTTTGAGCTATTGCTCGTTGAAAAAGTCCTTTGGT
TGAATTGCTCCAACGGTTACCTTCAGAATAATGGGATAAAGTCAGCAGGTTGACACATGA
ACCCCCAGCACCAGATCCAAAAACAGTGATTCTTAAGGGGTCACCACCAAAGAATCCAA
TGTTTTCACTAGTCCATCTTAAAGCTTGTATGAGATCAAGGAGTCCATAGTTCCCCTTTGC
AGCCTGATCGCCTGTACTCAAGAAACCGAGTACTCCAAGTCGATAGTTGACTGTGATGAC
GATCACATTGCCATAACTTGCCAAGACACTTCCATCATATAAATTTCCAGTACCTTCCATAT
ATGAGCCACCATGGATATACACCATCACTGGTTTGGGACCCCCACTGTCCCGAATATCATC
CTCAGTCGGGACATATATATTTAAATATAGGCAGTCTTCGCTCTGGTCTTGCACATATGATG
AAACCACATCCAAGTTATTAGTAAACCACACAGGAAGCATGACTTCTGGCAATCTGCCAT
CAATGATATTCTGGGGACACACAGGAGCAAATTGAGTGGCATTTCTGATATCTGACCAGG
GAGATGGTGGTTCTGGAGGCTGAAAACGACGTTCCCCTGTTGGTGGGGCTGCATATGGA
ACCCCAAGAAATTGAATAACAGGCCCCAAAATTTCATTATTGAGTTCCTTCTTAATCCCTC
TTATCTTTCCAAAGTTGGTAGCCACCAGTGGGTCCACATCATCCAATTTTTGTGATAGCAC
ATGGCCAGCCTGAAGCAAACATCCCAACATACAGAGAGTCAATGGGGCACCCAATCCCC
GGTGTACCAAGCATGCCATCACTGCTCTCCAAACATAATTTGGGCCACGTGCATCTGGGG
CAGTGCCATGGGTGAAGGG

9.2 Appendix for Chapter 4

Table 4.3. Membrane proteins identified using in-solution detection.

Abbrev[1]	Description[2]	Score[3]	Mol Mass[4]	Mc [5]	Ms [6]	Sq [7]	Ss [8]	Cov [9]	Lngt [10]
TBB4B[1]	Tubulin β-4B chain; *TUBB4B*	14852	50255	493	423	49	46	87.9	445
TBB4A[1]	Tubulin β-4A chain; *TUBB4A*	14487	50010	491	411	48	44	88.1	444
TBB2A[1]	Tubulin β-2A chain; *TUBB2A*	13826	50274	448	393	47	46	87.9	445
TBB5[1]	Tubulin β chain; *TUBB*	13058	50095	445	386	49	47	88.1	444
TBB3[1]	Tubulin β-3 chain; *TUBB3*	9705	50856	304	259	34	29	69.3	450
TBB6[1]	Tubulin β-6 chain; *TUBB6*	4914	50281	161	128	23	19	46.2	446
TBB8[1]	Tubulin β-8 chain; *TUBB8*	3176	50257	166	120	18	14	32.9	444
TBB1[1]	Tubulin β-1 chain; *TUBB1*	782	50865	35	28	6	5	11.1	451
TBB2B[1]	Tubulin β-2B chain; *TUBB2B*	12629	50377	429	373	46	45	84.3	445
TBB8L[1]	Tubulin β-8 chain-like protein LOC260334	2672	50168	133	108	15	12	31.3	444
YI016[5]	Putative tubulin β chain-like protein ENSP00000290377	1623	42204	69	59	10	8	14.6	
TBA1A[1]	Tubulin α-1A chain; *TUBA1A*	10156	50788	266	244	42	39	74.5	451
TBA4A[1]	Tubulin α-4A chain; *TUBA4A*	9298	50634	249	232	40	39	75	448
TBA8[1]	Tubulin α-8 chain; *TUBA8*	5698	50746	143	124	19	19	37.9	449
TBA1B[1]	Tubulin α-1B chain; *TUBA1B*	10684	50804	285	260	44	41	74.5	451
TBA3C[1]	Tubulin α-3C/D chain; *TUBA3C*	8278	50612	194	186	28	27	55.6	450
TBA1C[1]	Tubulin α-1C chain; *TUBA1C*	8097	50548	238	216	38	35	65.7	449
TBA3E[1]	Tubulin α-3E chain; *TUBA3E*	5962	50568	146	133	22	20	46	450
TBAL3[1]	Tubulin α chain-like 3; *TUBAL3*	1001	50675	46	40	6	4	13.5	446
TBA4B[5]	Putative tubulin-like protein α-4B; *TUBA4B*	571	27819	13	12	2	2	10.8	241
ATPB[1]	ATP synthase subunit β, mitochondrial; *ATP5B*	8652	56525	242	216	40	37	80.7	529
DPYL2[1]	Dihydropyrimidinase-related protein 2; *DPYSL2*	6512	62711	184	156	38	34	80.4	572
DPYL1[1]	Dihydropyrimidinase-related protein 1; *CRMP1*	931	62487	27	25	10	9	25.5	572
DPYL3[1]	Dihydropyrimidinase-related protein 3; *DPYSL3*	491	62323	16	11	7	4	16.3	570
DPYS[1]	Dihydropyrimidinase; *DPYS*	71	57107	5	4	2	1	6.6	519
AT1A3[1]	Na^+/K^+-transporting ATPase subunit α–3; *ATP1A3*	6442	113102	199	173	46	39	51.3	1013
AT1A1[1]	Na^+/K^+-transporting ATPase subunit α-1; *ATP1A1*	6387	114135	167	152	38	33	37.8	1023
AT1A2[1]	Na^+/K^+-transporting ATPase subunit α-2; *ATP1A2*	4269	113505	126	105	29	26	36.5	1020
AT1A4[1]	Na^+/K^+-transporting ATPase subunit α-4; *ATP1A4*	1569	115119	69	53	13	10	14.4	1029
AT12A[1]	K^+-transporting ATPase α chain 2; *ATP12A*	547	116292	33	24	7	4	5.3	1039
ATP4A[2]	K^+-transporting ATPase α chain 1; *ATP4A*	135	115756	8	7	2	2	2.7	1035
ACTB[1]	Actin, cytoplasmic 1; *ACTB*	5799	42052	189	176	28	25	78.9	375
ACTC[1]	Actin, α cardiac muscle 1; *ACTC1*	4116	42334	150	138	20	18	42.2	377

ACTA[1]	Actin, aortic smooth muscle; *ACTA2*	3877	42381	138	126	17	15	39.3	377
POTEE[1]	POTE ankyrin domain family member E; *POTEE*	1726	122882	72	58	11	7	11.7	1075
POTEF[1]	POTE ankyrin domain family member F; *POTEF*	1714	123020	74	56	8	5	8	1075
POTEI[3]	POTE ankyrin domain family member I; *POTEI*	1142	122858	54	47	8	4	9	1075
ACTBM[5]	Putative β-actin-like protein 3; *POTEKP*	768	42331	16	16	2	2	7.2	375
ACTBL[1]	β-actin-like protein 2; *ACTBL2*	708	42318	36	19	7	5	19.7	376
POTEJ[3]	POTE ankyrin domain family member J; *POTEJ*	289	118740	28	11	8	2	11.8	1038
G3P[1]	Glyceraldehyde-3-phosphate dehydrogenase; *GAPDH*	5506	36201	156	140	26	24	67.2	335
MDHM[1]	Malate dehydrogenase, mitochondrial; *MDH2*	5231	35937	112	101	26	22	78.1	338
HBB[1]	Hemoglobin subunit β; *HBB*	4991	16102	147	139	18	18	96.6	147
HBD[1]	Hemoglobin subunit δ; *HBD*	1426	16159	54	50	9	9	80.3	147
HBE[1]	Hemoglobin subunit ε; *HBE1*	307	16249	18	14	3	1	25.2	147
SPTN1[1]	Spectrin α chain, non-erythrocytic 1; *SPTAN1*	4837	285163	163	122	62	45	33.7	2472
AP1G2[1]	AP-1 complex subunit g-like 2; *AP1G2*	23	87917	3	1	2	1	2.3	785
SPTB2[1]	Spectrin β chain, non-erythrocytic 1; *SPTBN1*	4742	275237	133	122	48	43	25.2	2364
SPTN2[1]	Spectrin β chain, non-erythrocytic 2; *SPTBN2*	64	272526	12	2	9	2	4.8	2390
SPTB1[1]	Spectrin β chain, erythrocytic; *SPTB*	39	247171	14	1	10	1	5.9	2137
KCRB[1]	Creatine kinase B-type; *CKB*	4638	42902	132	119	26	25	80.3	381
KPYM[1]	Pyruvate kinase isozymes M1/M2; *PKM*	3904	58470	140	121	30	27	62.5	531
KPYR[1]	Pyruvate kinase isozymes R/L; *PKLR*	260	62191	15	12	4	2	6.4	574
GNAO[1]	Guanine nucleotide-binding protein G_o subunit α; *GNAO1*	3882	40595	86	79	16	14	43.8	354
GNAI2[1]	Guanine nucleotide-binding protein G_i subunit α-2; *GNAI2*	1294	40995	35	32	8	6	23.4	355
GNAI1[1]	Guanine nucleotide-binding protein Gi subunit α-1; *GNAI1*	1130	40905	34	31	6	5	14.1	354
GNAI3[1]	Guanine nucleotide-binding protein Gk subunit α; *GNAI3*	1026	41076	35	27	6	3	13.6	354
GNAL[1]	Guanine nucleotide-binding protein Golf subunit α; *GNAL*	910	44794	25	23	3	2	5.2	381
GNA12[1]	Guanine nucleotide-binding protein subunit α-12; *GNA12*	726	44422	18	17	2	1	7.6	381
ENOA[1]	α-enolase; *ENO1*	3730	47481	107	95	26	23	81.1	434
ENOG[1]	γ-enolase; *ENO2*	2874	47581	86	73	21	20	63.8	434
ENOB[1]	β-enolase; *ENO3*	1036	47299	32	22	11	7	33.9	434
ATPA[1]	ATP synthase subunit α, mitochondrial; *ATP5A1*	3653	59828	134	111	28	22	45.6	553
STXB1[1]	Syntaxin-binding protein 1; *STXBP1* pe 1	3118	67925	120	103	30	26	56.1	594
CH60[1]	60 kDa heat shock protein, mitochondrial; *HSPD1*	2996	61187	78	63	21	16	54.1	573
PPIA[1]	Peptidyl-prolyl cis-trans isomerase A; *PPIA*	2753	18229	84	77	13	12	93.9	165
PAL4A[1]	Peptidyl-prolyl cis-trans isomerase A-like 4A/B/C; *PPIAL4A*	344	18398	7	7	1	1	8.5	164
ALDOA[1]	Fructose-bisphosphate aldolase A; *ALDOA*	2753	39851	80	69	20	15	79.1	364
ALDOC[1]	Fructose-bisphosphate aldolase C; *ALDOC*	1963	39830	58	45	15	11	40.7	364
NSF[1]	Vesicle-fusing ATPase; *NSF*	2485	83055	83	72	22	20	41.1	744
GBB1[1]	Guanine nucleotide-binding protein G_i/G_s/G_t subunit β-1; *GNB1*	2435	38151	60	51	17	15	61.5	340

GBB2[1]	Guanine nucleotide-binding protein $G_i/G_s/G_t$ subunit β-2; *GNB2*	1118	38048	38	29	15	11	47.6	340
GBB4[1]	Guanine nucleotide-binding protein subunit β-4; *GNB4*	96	38284	7	4	5	2	24.7	340
SYN1[1]	Synapsin-1; *SYN1*	2364	74237	90	76	30	27	52.2	705
SYN2[1]	Synapsin-2; *SYN2*	903	63093	27	25	7	7	13.6	582
SRGP3[1]	SLIT-ROBO ρ GTPase-activating protein 3; *SRGAP3*	33	125395	8	2	2	1	1	1099
KCC2A[1]	Ca^{2+}/calmodulin-dependent protein kinase II subunit α; *CAMK2A*	2354	54624	84	77	21	20	46	478
KCC2B[1]	Ca^{2+}/calmodulin-dependent protein kinase II subunit β; *CAMK2B*	1106	73544	44	33	15	12	32.1	666
KCC2G[1]	Ca^{2+}/calmodulin-dependent protein kinase II subunit γ; *CAMK2G*	949	63311	34	28	11	8	28.5	558
KCC2D[1]	Ca^{2+}/calmodulin-dependent protein kinase II subunit δ; *CAMK2D*	825	56961	37	26	14	10	40.3	499
VATB2[1]	V-type proton ATPase subunit B, brain isoform; *ATP6V1B2*	2248	56807	54	49	13	11	48.1	511
VATB1[1]	V-type proton ATPase subunit B, kidney isoform; *ATP6V1B1*	642	57196	18	15	4	3	12.7	513
DYN1[1]	Dynamin-1; *DNM1*	2225	97746	89	76	26	20	38.2	864
DYN3[1]	Dynamin-3; *DNM3*	988	98084	43	36	9	7	14	869
DYN2[1]	Dynamin-2; *DNM2*	235	98345	19	15	6	4	9.9	870
HXK1[1]	Hexokinase-1; *HK1*	2116	103561	66	57	18	18	23.2	917
HKDC1[1]	Putative hexokinase HKDC1; *HKDC1*	77	103790	12	4	6	2	10.1	917
HXK2[1]	Hexokinase-2; *HK2*	55	103739	16	3	5	1	6.1	917
HSP7C[1]	Heat shock cognate 71 kDa protein; *HSPA8*	2103	71082	71	63	21	19	37.2	646
HSP71[1]	Heat shock 70 kDa protein 1A/1B; *HSPA1A*	466	70294	19	13	9	8	18.3	641
HSP72[1]	Heat shock-related 70 kDa protein 2; *HSPA2*	713	70263	29	22	9	6	16.3	639
HS71L[1]	Heat shock 70 kDa protein 1-like; *HSPA1L*	323	70730	15	9	6	5	9.4	641
HSP76[1]	Heat shock 70 kDa protein 6; *HSPA6*	292	71440	10	10	4	4	8.4	643
HSP77[5]	Putative heat shock 70 kDa protein 7; *HSPA7*	58	40448	3	3	2	2	6.8	367
MBP[1]	Myelin basic protein; *MBP*	2072	33097	130	103	19	14	37.2	304
CN37[1]	2',3'-cyclic-nucleotide 3'-phosphodiesterase; *CNP*	2034	47948	102	75	22	18	68.4	421
PP2BA[1]	Serine/threonine-protein phosphatase 2B catalytic subunit α isoform; *PPP3CA*	109	59335	18	14	5	2	18.8	521
PP2BC[1]	Serine/threonine-protein phosphatase 2B catalytic subunit γ isoform; *PPP3CC*	80	58777	14	12	2	1	4.5	512
CLH1[1]	Clathrin heavy chain 1; *CLTC* pe 1	1963	193260	81	64	30	23	21.7	1675
CLH2[1]	Clathrin heavy chain 2; *CLTCL1*	92	189020	8	5	6	3	4	1640
VATA[1]	V-type proton ATPase catalytic subunit A; *ATP6V1A*	1785	68660	54	46	16	13	36.8	617
SHPS1[1]	Tyrosine-protein phosphatase non-receptor type substrate 1; *SIRPA*	1744	55446	61	49	14	12	36.5	504

SIRBL[1]	Signal-regulatory protein β-1 isoform 3; *SIRPB1*	731	43674	39	28	8	6	23.9	398
SIRB1[1]	Signal-regulatory protein β-1; *SIRPB1*	250	43640	11	9	3	3	10.3	398
SIRPG[1]	Signal-regulatory protein γ; *SIRPG*	102	42870	10	7	4	3	10.1	387
VATE1[1]	V-type proton ATPase subunit E 1; *ATP6V1E1*	1728	26186	52	46	11	9	48.2	226
TPPP[1]	Tubulin polymerization-promoting protein; *TPPP*	1725	23850	40	38	9	8	50.7	219
ACON[1]	Aconitate hydratase, mitochondrial; *ACO2*	1722	86113	60	47	16	15	29.4	780
1433Z[1]	14-3-3 protein ζ/δ; *YWHAZ*	1549	27899	46	44	11	10	45.3	245
1433G[1]	14-3-3 protein g; *YWHAG*	1167	28456	55	41	16	13	62.3	247
1433B[1]	14-3-3 protein β/α; *YWHAB*	738	28179	41	28	9	6	45.1	246
1433E[1]	14-3-3 protein ε; *YWHAE*	590	29326	15	11	5	4	32.5	255
1433F[1]	14-3-3 protein η; *YWHAH*	460	28372	31	21	10	7	42.3	246
1433T[1]	14-3-3 protein θ; *YWHAQ*	80	28032	10	6	5	3	26.5	245
1433S[1]	14-3-3 protein sigma; *SFN*	50	27871	4	2	2	1	6.5	248
NCAM1[1]	Neural cell adhesion molecule 1; *NCAM1*	1540	95370	63	49	15	11	23	858
IGSF8[1]	Immunoglobulin superfamily member 8; *IGSF8*	1382	65621	37	32	13	11	36.4	613
KCRU[1]	Creatine kinase U-type, mitochondrial; *CKMT1A*	1345	47406	52	39	18	14	57.8	417
HBA[1]	Hemoglobin subunit α; *HBA1*	1339	15305	58	46	10	10	69.7	142
ANK2[1]	Ankyrin-2; *ANK2*	1326	435957	58	40	28	18	10.3	3957
ANK3[1]	Ankyrin-3; *ANK3*	28	482394	16	1	13	1	4.7	4377
CNTN1[1]	Contactin-1; *CNTN1*	1276	114104	62	49	19	16	22.1	1018
PGK1[1]	Phosphoglycerate kinase 1; *PGK1*	1250	44985	46	38	18	14	64.3	417
PGK2[1]	Phosphoglycerate kinase 2; *PGK2*	128	45166	6	4	4	2	24.7	417
GFAP[1]	Glial fibrillary acidic protein; *GFAP*	1206	49907	48	39	18	16	55.1	432
K2C1[1]	Keratin, type II cytoskeletal 1; *KRT1*	44	66170	3	1	3	1	5.9	644
HS90A[1]	Heat shock protein HSP 90-α; *HSP90AA1*	1183	85006	24	21	9	8	13	732
HS90B[1]	Heat shock protein HSP 90-β; *HSP90AB1*	1090	83554	23	19	10	8	14.2	724
ENPL[1]	Endoplasmin; *HSP90B1*	87	92696	2	2	2	2	3.1	803
TRAP1[1]	Heat shock protein 75 kDa, mitochondrial; *TRAP1*	220	80345	10	3	2	1	3.7	704
H90B3[5]	Putative heat shock protein HSP 90-β-3; *HSP90AB3P*	162	68624	4	3	3	2	4.5	597
H90B4[5]	Putative heat shock protein HSP 90-β 4; *HSP90AB4P*	149	58855	3	2	2	1	6.7	505
HS904[5]	Putative heat shock protein HSP 90-α A4; *HSP90AA4P*	129	47796	3	2	2	1	5.3	418
H90B2[1]	Putative heat shock protein HSP 90-β 2; *HSP90AB2P*	101	44492	2	2	1	1	3.1	381
G6PI[1]	Glucose-6-phosphate isomerase; *GPI*	1175	63335	38	30	12	9	37.3	558
CSPG2[1]	Versican core protein; *VCAN*	1163	374585	42	32	15	8	8.5	3396
PRDX2[1]	Peroxiredoxin-2; *PRDX2*	1159	22049	51	41	12	9	40.9	198
PRDX1[1]	Peroxiredoxin-1; *PRDX1*	1139	22324	37	36	6	5	34.2	199
PRDX4[1]	Peroxiredoxin-4; *PRDX4*	270	30749	7	7	1	1	4.4	271
STX1B[1]	Syntaxin-1B; *STX1B*	1139	33452	40	32	12	10	36.8	288
STX1A[1]	Syntaxin-1A; *STX1A*	450	33174	20	16	8	6	35.8	288

STX2[1]	Syntaxin-2; *STX2*	40	33377	5	2	2	1	5.9	288
UCHL1[1]	Ubiquitin carboxyl-terminal hydrolase isozyme L1; *UCHL1*	1115	25151	40	32	12	8	78.5	223
AT1B1[1]	Na^+/K^+-transporting ATPase subunit β-1; *ATP1B1*	1094	35438	37	32	8	6	32.3	303
GLNA[1]	Glutamine synthetase; *GLUL*	1094	42665	22	22	5	5	23.3	373
PHB[1]	Prohibitin; *PHB*	1089	29843	30	26	11	10	68.4	272
NFASC[1]	Neurofascin; *NFASC*	1042	150789	44	36	16	13	15.5	1347
THY1[1]	Thy-1 membrane glycoprotein; *THY1*	1036	18151	31	30	4	4	18	161
NFL[1]	Neurofilament light polypeptide; *NEFL*	1023	61536	39	32	15	13	37.8	543
AINX[1]	α-internexin; *INA*	309	55528	26	15	12	8	29.5	499
NFM[1]	Neurofilament medium polypeptide; *NEFM*	247	102468	22	12	11	4	18.7	916
NFH[1]	Neurofilament heavy polypeptide; *NEFH*	209	112639	12	8	5	2	4	1026
DESM[1]	Desmin; *DES*	23	53560	3	1	2	1	5.7	470
GRP75[1]	Stress-70 protein, mitochondrial; *HSPA9*	1006	73920	29	23	9	7	18	679
VAMP2[1]	Vesicle-associated membrane protein 2; *VAMP2*	996	12712	19	19	5	5	43.1	116
VAMP3[1]	Vesicle-associated membrane protein 3; *VAMP3*	226	11359	7	7	2	2	33	100
VAMP1[1]	Vesicle-associated membrane protein 1; *VAMP1*	113	13008	5	5	1	1	7.6	118
MIF[1]	Macrophage migration inhibitory factor; *MIF*	988	12639	39	32	6	5	46.1	115
MDHC[1]	Malate dehydrogenase, cytoplasmic; *MDH1*	984	36631	21	20	6	5	20.4	334
MYPR[1]	Myelin proteolipid protein; *PLP1*	962	30855	27	24	5	4	18.1	277
COX5A[1]	Cytochrome c oxidase subunit 5A, mitochondrial; *COX5A*	940	16923	37	28	10	8	58	150
CX6B1[1]	Cytochrome c oxidase subunit 6B1; *COX6B1*	931	10414	32	29	6	5	84.9	86
ATPO[1]	ATP synthase subunit O, mitochondrial; *ATP5O*	920	23377	33	30	10	7	52.1	213
EAA1[1]	Excitatory amino acid transporter 1; *SLC1A3*	919	59705	20	17	4	3	9.4	542
TENR[1]	Tenascin-R; *TNR*	914	151805	31	26	10	9	13.6	1358
AATM[1]	Aspartate aminotransferase, mitochondrial; *GOT2*	898	47886	36	33	13	11	37.2	430
TKT[1]	Transketolase; *TKT*	890	68519	33	26	9	9	23.1	623
ATP5H[1]	ATP synthase subunit δ, mitochondrial; *ATP5H*	851	18537	34	26	9	7	62.7	161
PGAM1[1]	Phosphoglycerate mutase 1; *PGAM1*	847	28900	33	27	11	7	46.9	254
PGAM4[1]	Probable phosphoglycerate mutase 4; *PGAM4*	649	28930	27	21	9	5	34.3	254
PGAM2[1]	Phosphoglycerate mutase 2; *PGAM2* pe 1	295	28919	12	8	4	2	17.8	253
COF1[1]	Cofilin-1; *CFL1*	844	18719	25	24	6	6	56.6	166
COF2[1]	Cofilin-2; *CFL2*	237	18839	10	10	3	3	19.9	166
SNP25[1]	Synaptosomal-associated protein 25; *SNAP25*	824	23528	27	21	11	8	61.7	206
EAA2[1]	Excitatory amino acid transporter 2; *SLC1A2*	822	62577	28	25	9	8	21.3	574
TPIS[1]	Triosephosphate isomerase; *TPI1*	795	31057	46	31	17	13	70.6	286
VDAC1[1]	Voltage-dependent anion-selective channel protein 1; *VDAC1*	789	30868	34	25	12	7	50.2	283
VPP1[1]	V-type proton ATPase 116 kDa subunit α isoform 1; *ATP6V0A1*	788	97148	36	28	15	12	20.1	837
PRDX5[1]	Peroxiredoxin-5, mitochondrial; *PRDX5*	777	22301	32	27	10	6	72.9	214

MOG[1]	Myelin-oligodendrocyte glycoprotein; *MOG*	766	28574	13	13	3	3	16.2	247
VDAC2[1]	Voltage-dependent anion-selective channel protein 2; *VDAC2*	761	32060	35	30	6	6	25.9	294
ATP5I[1]	ATP synthase subunit e, mitochondrial; *ATP5I*	742	7928	24	20	7	4	71	69
SEPT7[1]	Septin-7; *SEPT7*	740	50933	27	24	8	7	24.3	437
SEPT8[1]	Septin-8; *SEPT8*	321	56234	15	14	4	4	11.8	483
SEPT6[1]	Septin-6; *SEPT6*	288	50084	18	14	6	5	18.2	434
SEP11[1]	Septin-11; *SEPT11*	338	49652	17	14	5	4	14.2	429
SEP14[1]	Septin-14; *SEPT14*	173	50449	12	8	2	1	4.2	432
SEP10[1]	Septin-10; *SEPT10*	105	53016	2	2	1	1	5.1	454
ODPB[1]	Pyruvate dehydrogenase E1 component subunit β, mitochondrial; *PDHB*	739	39550	26	26	6	6	32.6	359
ICAM5[1]	Intercellular adhesion molecule 5; *ICAM5* pe 1	731	98766	18	16	7	5	10.8	924
PCSK1[1]	ProSAAS; *PCSK1N*	700	27413	16	16	3	3	20	260
PIN1[1]	Peptidyl-prolyl cis-trans isomerase NIMA-interacting 1; *PIN1*	691	18346	15	15	4	4	43.6	163
ADT3[1]	ADP/ATP translocase 3; *SLC25A6*	674	33073	31	24	10	10	38.6	298
ADT2[1]	ADP/ATP translocase 2; *SLC25A5*	499	33059	26	22	7	7	24.2	298
ADT1[1]	ADP/ATP translocase 1; *SLC25A4*	478	33271	29	18	11	9	38.9	298
ADT4[1]	ADP/ATP translocase 4; *SLC25A31*	58	35285	3	1	2	1	6	315
PACN1[1]	Protein kinase C and casein kinase substrate in neurons protein 1; *PACSIN1* pe 1	648	51276	22	21	10	9	32.2	444
CATD[1]	Cathepsin D; *CTSD*	634	45037	21	18	7	6	22.6	412
L1CAM[1]	Neural cell adhesion molecule L1; *L1CAM*	631	140885	19	17	9	7	10.7	1257
DHE3[1]	Glutamate dehydrogenase 1, mitochondrial; *GLUD1*	622	61701	30	23	15	10	30.6	558
DHE4[1]	Glutamate dehydrogenase 2, mitochondrial; *GLUD2*	361	61738	13	11	6	4	14	558
DHPR[1]	Dihydropteridine reductase; *QDPR*	614	26001	18	17	7	6	38.1	244
KAP3[1]	cAMP-dependent protein kinase type II-β regulatory subunit; *PRKAR2B*	599	46672	20	15	8	4	22.2	418
KAP2[1]	cAMP-dependent protein kinase type II-α regulatory subunit; *PRKAR2A*	102	45832	6	3	4	2	13.9	404
STMN1[1]	Stathmin; *STMN1*	586	17292	9	8	2	1	18.1	149
AT2B4[1]	Plasma membrane Ca^{2+}-transporting ATPase 4; *ATP2B4*	582	139030	39	26	15	12	17.2	1241
AT2B2[1]	Plasma membrane Ca^{2+}-transporting ATPase 2; *ATP2B2*	389	137987	20	14	8	7	8.6	1243
AT2B1[1]	Plasma membrane Ca^{2+}-transporting ATPase 1; *ATP2B1*	297	139637	26	15	9	8	10.4	1258
AT2B3[1]	Plasma membrane Ca^{2+}-transporting ATPase 3; *ATP2B3*	162	135253	26	9	8	6	8.5	1220
PIMT[1]	Protein-L-isoaspartate(D-aspartate) O-methyltransferase; *PCMT1*	581	24792	13	10	5	3	41.4	227
MAP1B[1]	Microtubule-associated protein 1B; *MAP1B*	573	271665	52	19	19	9	13.4	2468
MAP1A[1]	Microtubule-associated protein 1A; *MAP1A*	196	306781	15	8	9	4	5.2	2803

DHSA[1]	Succinate dehydrogenase [ubiquinone] flavoprotein subunit, mitochondrial; *SDHA*	572	73672	8	8	2	2	4.6	
QCR1[1]	Cytochrome b-c1 complex subunit 1, mitochondrial; *UQCRC1*	564	53297	23	21	10	9	36	480
MAP2[1]	Microtubule-associated protein 2; *MAP2*	560	199860	23	15	12	6	34.1	478
COX5B[1]	Cytochrome c oxidase subunit 5B, mitochondrial; *COX5B*	539	13915	32	23	6	5	54.3	129
ACTN1[1]	α-actinin-1; *ACTN1*	507	103563	25	15	10	8	20.1	892
ACTN4	α-actinin-4; *ACTN4*	403	105245	9	9	3	3	4.1	911
ACTN2	α-actinin-2; *ACTN2*	44	104358	3	1	2	1	2.6	894
SFXN1[1]	Sideroflexin-1; *SFXN1*	494	35881	18	13	8	5	46.9	322
SFXN3[2]	Sideroflexin-3; *SFXN3*	338	36298	10	9	4	4	17.2	325
GRP78[1]	78 kDa glucose-regulated protein; *HSPA5*	483	72402	16	14	9	7	22.2	654
CADM2[2]	Cell adhesion molecule 2; *CADM2*	480	47980	14	13	4	3	17.5	435
QCR2[1]	Cytochrome b-c1 complex subunit 2, mitochondrial; *UQCRC2*	475	48584	13	12	5	4	22.7	453
BASP1[1]	Brain acid soluble protein 1; *BASP1*	474	22680	13	8	4	2	44.5	227
EHD3[1]	EH domain-containing protein 3; *EHD3*	472	60906	12	11	5	4	15.3	535
PEBP1[1]	Phosphatidylethanolamine-binding protein 1; *PEBP1*	472	21158	19	14	8	4	71.7	187
VATL[1]	V-type proton ATPase 16 kDa proteolipid subunit; *ATP6V0C*	469	15725	4	4	1	1	20	155
LSAMP[1]	Limbic system-associated membrane protein; *LSAMP*	466	37883	18	13	6	4	26.9	338
E41L3[1]	Band 4.1-like protein 3; *EPB41L3*	459	121458	14	12	9	7	11.8	1087
DYHC1[1]	Cytoplasmic dynein 1 heavy chain 1; *DYNC1H1*	456	534809	40	19	25	11	9.6	4646
AP2M1[1]	AP-2 complex subunit μ; *AP2M1*	424	49965	15	12	4	4	12	435
CAP2[1]	Adenylyl cyclase-associated protein 2; *CAP2*	420	53076	12	7	4	3	11.7	477
GDIA[1]	Rab GDP dissociation inhibitor α; *GDI1*	417	51177	16	14	4	4	10.7	447
GDIB[1]	Rab GDP dissociation inhibitor β; *GDI2*	247	51087	9	8	2	2	4.9	445
SCOT1[1]	Succinyl-CoA:3-ketoacid coenzyme A transferase 1, mitochondrial; *OXCT1*	414	56578	17	12	9	6	23.1	520
SCOT2[2]	Succinyl-CoA:3-ketoacid coenzyme A transferase 2, mitochondrial; *OXCT2*	95	56731	2	2	1	1	2.3	517
THIL[1]	Acetyl-CoA acetyltransferase, mitochondrial; *ACAT1*	412	45456	13	12	5	5	30.9	427
OPA1[1]	Dynamin-like 120 kDa protein, mitochondrial; *OPA1*	407	112131	14	9	7	4	12.6	960
RAB3A[1]	Ras-related protein Rab-3A; *RAB3A*	407	25196	8	7	3	3	10.9	220
RAB3D[1]	Ras-related protein Rab-3D; *RAB3D*	33	24480	2	1	1	1	3.7	219
RAC1[1]	Ras-related C3 botulinum toxin substrate 1; *RAC1*	402	21835	19	16	7	5	28.1	192
RAC2[1]	Ras-related C3 botulinum toxin substrate 2; *RAC2*	100	21814	6	4	3	2	17.2	192
OPCM[1]	Opioid-binding protein/cell adhesion molecule; *OPCML*	391	38496	25	14	8	4	29.6	345
TMOD2[1]	Tropomodulin-2; *TMOD2*	389	39571	9	9	3	3	16	351
PARK7[1]	Protein DJ-1; *PARK7*	388	20050	12	11	4	4	19	189

TCPE[1]	T-complex protein 1 subunit ε; *CCT5*	378	60089	22	9	9	5	31.2	541
UCRI[1]	Cytochrome b-c1 complex subunit Rieske, mitochondrial; *UQCRFS1*	373	29934	18	16	3	3	21.2	274
UCRIL[5]	Putative cytochrome b-c1 complex subunit Rieske-like protein 1; *UQCRFS1P1*	368	31081	17	15	2	2	12	283
RAP2A[1]	Ras-related protein Rap-2a; *RAP2A*	368	20830	7	7	2	2	15.3	183
CADM3[1]	Cell adhesion molecule 3; *CADM3*	364	43729	14	12	4	4	21.4	398
RAP1A[1]	Ras-related protein Rap-1A; *RAP1A*	363	21316	9	9	2	2	7.6	184
HSPB1[1]	Heat shock protein β-1; *HSPB1*	358	22826	9	9	3	3	21	205
SEPT5[1]	Septin-5; *SEPT5*	350	43206	17	14	7	6	30.9	369
DCTN2[1]	Dynactin subunit 2; *DCTN2*	348	44318	9	8	4	3	14.5	401
NDUA5[1]	NADH dehydrogenase [ubiquinone] 1 α subcomplex subunit 5; *NDUFA5*	345	13507	20	17	8	7	82.8	116
MMSA[1]	Methylmalonate-semialdehyde dehydrogenase [acylating], mitochondrial; *ALDH6A1*	342	58259	13	12	6	6	23	535
NCAM2[1]	Neural cell adhesion molecule 2; *NCAM2*	341	93786	9	8	3	2	5.1	837
SYT1[1]	Synaptotagmin-1; *SYT1*	336	47885	13	10	5	4	17.5	422
EF1A2[1]	Elongation factor 1-α 2; *EEF1A2*	336	50780	19	10	8	4	35	463
EF1A1[1]	Elongation factor 1-α 1; *EEF1A1*	334	50451	17	10	7	3	31	462
AT1B2[1]	Na^+/K^+-transporting ATPase subunit β-2; *ATP1B2*	335	33745	15	15	4	4	25.5	290
SSBP[1]	Single-stranded DNA-binding protein, mitochondrial; *SSBP1*	331	17249	13	10	5	3	44.6	148
AP2A1[1]	AP-2 complex subunit α-1; *AP2A1*	324	108561	16	13	8	6	10.8	977
AP2A2[1]	AP-2 complex subunit α-2; *AP2A2*	261	104807	16	12	8	5	14	939
4F2[1]	4F2 cell-surface antigen heavy chain; *SLC3A2*	318	68180	12	10	3	3	6.8	630
DDAH1[1]	N(G),N(G)-dimethylarginine dimethylaminohydrolase 1; *DDAH1*	315	31444	15	14	4	3	35.1	285
K6PP[1]	6-phosphofructokinase type C; *PFKP*	310	86454	18	11	9	5	13.1	784
FUMH[1]	Fumarate hydratase, mitochondrial; *FH*	308	54773	12	9	6	3	24.7	510
HECAM[1]	Hepatocyte cell adhesion molecule; *HEPACAM*	308	46226	11	7	5	3	22.8	416
LEG1[1]	Galectin-1; *LGALS1*	304	15048	7	7	2	2	33.3	135
GBG2[1]	Guanine nucleotide-binding protein $G_i/Gs/G_o$ subunit γ-2; *GNG2*	295	7959	6	6	1	1	19.7	71
NDUA8[1]	NADH dehydrogenase [ubiquinone] 1 α subcomplex subunit 8; *NDUFA8*	291	20548	12	10	4	3	27.9	172
SEPT2[1]	Septin-2; *SEPT2*	289	41689	14	8	7	4	33.2	361
SNAG[1]	γ-soluble NSF attachment protein; *NAPG*	288	35066	11	7	5	3	25.6	312
ATP5L[1]	ATP synthase subunit γ, mitochondrial; *ATP5L*	285	11421	8	8	3	3	40.8	103
ATPG[1]	ATP synthase subunit γ, mitochondrial; *ATP5C1*	281	33032	11	9	4	3	25.5	298
SEPT3[1]	Neuronal-specific septin-3; *SEPT3*	280	40963	13	11	4	3	17.9	358

NDUAD[1]	NADH dehydrogenase [ubiquinone] 1 α subcomplex subunit 13; *NDUFA13*	280	16688	18	16	4	3	51.4	144
PRDX6[1]	Peroxiredoxin-6; *PRDX6*	280	25133	6	5	2	1	15.2	224
TCPB[1]	T-complex protein 1 subunit β; *CCT2*	278	57794	15	8	6	3	20.4	535
NNTM[1]	NAD(P) transhydrogenase, mitochondrial; *NNT*	277	114564	10	9	5	4	8.7	1086
PRIO[1]	Major prion protein; *PRNP*	274	27871	5	5	1	1	4.7	253
PRDX3[1]	Thioredoxin-dependent peroxide reductase, mitochondrial; *PRDX3*	272	28017	10	9	4	3	21.1	256
PDXK[1]	Pyridoxal kinase; *PDXK*	271	35308	11	9	3	2	13.8	312
AP2B1[1]	AP-2 complex subunit β; *AP2B1*	269	105398	20	12	10	6	15.5	937
AP1B1[1]	AP-1 complex subunit β-1; *AP1B1*	79	105482	12	2	5	1	7.9	949
SH3G2[1]	Endophilin-A1; *SH3GL2*	269	40108	13	13	5	5	13.1	352
SH3G1[1]	Endophilin-A2; *SH3GL1*	105	41692	5	5	1	1	3.3	368
SSDH[1]	Succinate-semialdehyde dehydrogenase, mitochondrial; *ALDH5A1*	269	58034	12	7	7	3	22.6	535
TAU[1]	Microtubule-associated protein tau; *MAPT*	268	79108	21	13	7	6	12.5	758
NDUA2[1]	NADH dehydrogenase [ubiquinone] 1 α subcomplex subunit 2; *NDUFA2*	266	11029	10	8	3	3	45.5	99
LDHB[1]	L-lactate dehydrogenase B chain; *LDHB*	264	36900	19	15	6	4	37.7	334
K6PF[1]	6-phosphofructokinase, muscle type; *PFKM*	260	85984	8	3	3	1	5.8	780
2AAA[1]	Serine/threonine-protein phosphatase 2A 65 kDa regulatory subunit A α isoform; *PPP2R1A*	259	66065	9	6	5	4	15.6	589
2AAB[1]	Serine/threonine-protein phosphatase 2A 65 kDa regulatory subunit A β isoform; *PPP2R1B*	90	66799	3	1	3	1	8.3	601
NDUS7[1]	NADH dehydrogenase [ubiquinone] Fe-S protein 7, mitochondrial; *NDUFS7*	258	23833	4	3	2	1	17.8	213
GPM6A[1]	Neuronal membrane glycoprotein M6A; *GPM6A*	258	31930	11	8	5	3	14.7	278
CH10[1]	10 kDa heat shock protein, mitochondrial; *HSPE1*	257	10925	17	15	5	4	45.1	102
NEGR1[1]	Neuronal growth regulator 1; *NEGR1*	255	39379	11	7	5	4	15.8	354
CISD1[1]	CDGSH Fe-S domain-containing protein 1; *CISD1*	255	12362	5	5	1	1	16.7	108
BRK1[1]	Protein BRICK1; *BRK1*	254	8796	5	4	2	1	29.3	75
CNTP1[1]	Contactin-associated protein 1; *CNTNAP1*	254	158220	8	4	5	2	5.3	1384
IMMT[1]	Mitochondrial inner membrane protein; *IMMT*	253	84026	17	9	7	5	16.5	758
TERA[1]	Transitional endoplasmic reticulum ATPase; *VCP*	252	89950	19	11	9	6	18.1	806
S12A5[2]	Solute carrier family 12 member 5; *SLC12A5*	249	127470	10	6	5	2	4.3	1139
S12A4[1]	Solute carrier family 12 member 4; *SLC12A4*	180	121712	5	4	2	1	2.1	1085
NIPS1[1]	Protein NipSnap homolog 1; *NIPSNAP1*	248	33460	8	7	4	3	15.1	284
EFTU[1]	Elongation factor Tu, mitochondrial; *TUFM*	244	49852	14	9	8	6	19.9	452
AATC[1]	Aspartate aminotransferase, cytoplasmic; *GOT1*	243	46447	12	8	6	4	20.1	413
COX7C[1]	Cytochrome c oxidase subunit 7C, mitochondrial; *COX7C*	239	7298	8	7	3	3	65.1	63
CISY[1]	Citrate synthase, mitochondrial; *CS*	239	51908	11	8	4	3	19.1	466

SATT[1]	Neutral amino acid transporter A; *SLC1A4*	238	56087	8	7	3	2	11.3	532
GBG3[2]	Guanine nucleotide-binding protein $G_i/G_s/G_o$ subunit γ-3; *GNG3*	235	8527	7	7	2	2	41.3	75
COX41[1]	Cytochrome c oxidase subunit 4 isoform 1, mitochondrial; *COX4I1*	231	19621	15	14	5	4	40.8	169
RALB[1]	Ras-related protein Ral-B; *RALB*	231	23508	6	5	2	1	9.7	206
FA49B[1]	Protein FAM49B; *FAM49B*	230	37010	5	4	2	1	8	324
PGCB[1]	Brevican core protein; *BCAN*	230	100539	13	9	3	2	4.3	911
E41L1[1]	Band 4.1-like protein 1; *EPB41L1*	230	99012	10	8	5	3	9.6	881
AOFB[1]	Amine oxidase [flavin-containing] B; *MAOB*	227	59238	11	8	5	4	14.4	520
C1QBP[1]	Complement component 1 Q subcomponent-binding protein, mitochondrial; *C1QBP*	225	31742	5	4	2	1	6.4	282
CMC1[1]	Ca^{2+}-binding mitochondrial carrier protein Aralar1; *SLC25A12*	221	75114	11	8	5	3	12.8	678
RAB10[1]	Ras-related protein Rab-10; *RAB10*	221	22755	9	9	2	2	9	200
CY1[1]	Cytochrome c1, heme protein, mitochondrial; *CYC1*	220	35741	12	11	3	3	13.8	325
SYPH[1]	Synaptophysin; *SYP*	220	34109	7	7	4	4	22.7	313
ATP5J[1]	ATP synthase-coupling factor 6, mitochondrial; *ATP5J*	215	12580	12	7	7	5	69.4	108
HCDH[1]	Hydroxyacyl-coenzyme A dehydrogenase, mitochondrial; *HADH*	214	34329	8	6	2	2	9.6	314
HS12A[1]	Heat shock 70 kDa protein 12A; *HSPA12A*	211	75217	12	8	6	3	14.5	675
FLOT1[1]	Flotillin-1; *FLOT1*	211	47554	9	5	5	2	16.2	427
UBA1[1]	Ubiquitin-like modifier-activating enzyme 1; *UBA1*	211	118858	6	5	5	4	8.9	1058
FLOT2[1]	Flotillin-2; *FLOT2*	208	47434	7	6	2	1	9.1	428
AT2A2[1]	Sarcoplasmic/endoplasmic reticulum Ca^{2+} ATPase 2; *ATP2A2*	206	116336	15	11	7	4	11	1042
AT2A1[1]	Sarcoplasmic/endoplasmic reticulum Ca^{2+} ATPase 1; *ATP2A1*	159	111550	10	7	3	1	3.3	1001
ARP5L[1]	Actin-related protein 2/3 complex subunit 5-like protein; *ARPC5L*	203	16931	6	6	3	3	25.5	153
SYFA[1]	Phenylalanine—tRNA ligase α subunit; *FARSA*	203	57585	4	4	1	1	2.8	508
GNAQ[1]	Guanine nucleotide-binding protein G_q subunit α; *GNAQ*	203	42400	15	6	4	2	17.3	359
GNA11[1]	Guanine nucleotide-binding protein subunit α-11; *GNA11*	70	42382	12	3	3	2	13.1	359
MAP6[1]	Microtubule-associated protein 6; *MAP6* pe 1	199	86680	6	4	4	2	7.1	813
MGST3[1]	Microsomal glutathione S-transferase 3; *MGST3*	197	16734	7	4	3	2	35.5	152
MPCP[1]	Phosphate carrier protein, mitochondrial; *SLC25A3*	197	40525	12	11	4	3	13.5	362
PEA15[1]	Astrocytic phosphoprotein PEA-15; *PEA15* pe 1	196	15088	6	6	2	2	21.5	130
RAB7A[1]	Ras-related protein Rab-7a; *RAB7A*	190	23760	4	3	3	2	16.9	207
PURA[1]	Transcriptional activator protein Pur-α; *PURA*	190	35003	6	5	2	2	8.4	322
NB5R3[1]	NADH-cytochrome b5 reductase 3; *CYB5R3*	190	34441	5	4	2	1	10.3	301

ECHA[1]	Trifunctional enzyme subunit α, mitochondrial; *HADHA*	187	83688	16	10	8	4	15.2	763
NDUS8[1]	NADH dehydrogenase [ubiquinone] Fe-S protein 8, mitochondrial; *NDUFS8*	187	24203	10	10	3	3	17.6	210
VISL1[1]	Visinin-like protein 1; *VSNL1*	187	22299	10	9	3	3	23	191
NDKB[1]	Nucleoside diphosphate kinase B; *NME2*	186	17401	11	9	3	3	31.6	152
NDKA[1]	Nucleoside diphosphate kinase A; *NME1*	175	17309	8	8	2	2	19.1	152
NDK8[1]	Putative nucleoside diphosphate kinase; *NME2P1*	109	15690	9	5	3	2	34.3	137
CAZA2[1]	F-actin-capping protein subunit α-2; *CAPZA2*	186	33157	6	6	2	2	9.8	286
CAZA1[1]	F-actin-capping protein subunit α-1; *CAPZA1*	135	33073	5	4	2	1	9.1	286
IDHP[1]	Isocitrate dehydrogenase [NADP], mitochondrial; *IDH2*	185	51333	13	10	6	4	18.4	452
NDRG2[1]	Protein NDRG2; *NDRG2*	184	41114	14	12	4	3	28.8	371
BIN1[1]	Myc box-dependent-interacting protein 1; *BIN1*	181	64887	11	7	4	2	8.1	593
RAB5B[1]	Ras-related protein Rab-5B; *RAB5B*	177	23920	4	4	1	1	6.5	215
DCLK1[1]	Serine/threonine-protein kinase DCLK1; *DCLK1*	175	82743	6	4	3	2	5	740
VATG2[1]	V-type proton ATPase subunit G 2; *ATP6V1G2*	175	13653	6	5	2	1	35.6	118
RLA1[1]	60S acidic ribosomal protein P1; *RPLP1*	175	11621	4	4	1	1	14	114
ETFA	Electron transfer flavoprotein subunit α, mitochondrial; *ETFA*	174	35400	6	4	3	1	18.9	333
PHB2[1]	Prohibitin-2; *PHB2*	173	33276	11	9	6	4	29.8	299
CLCB[1]	Clathrin light chain B; *CLTB*	169	25289	5	5	3	3	13.5	229
COX6C[1]	Cytochrome c oxidase subunit 6C; *COX6C*	169	8776	8	7	3	3	28	75
SHLB2[1]	Endophilin-B2; *SH3GLB2*	169	44175	5	5	5	5	20.3	395
VA0D1[1]	V-type proton ATPase subunit d 1; *ATP6V0D1*	167	40759	11	9	3	2	11.1	351
IMB1[1]	Importin subunit β-1; *KPNB1*	167	98420	4	4	2	2	3.4	876
ECHM[1]	Enoyl-CoA hydratase, mitochondrial; *ECHS1*	167	31823	11	9	4	3	21.7	290
PPT1[1]	Palmitoyl-protein thioesterase 1; *PPT1*	167	34627	4	4	2	2	13.7	306
CAPZB[1]	F-actin-capping protein subunit β; *CAPZB*	166	31616	6	6	2	2	17.3	277
CSRP1[1]	Cysteine and glycine-rich protein 1; *CSRP1*	165	21409	4	3	1	1	7.8	193
PROF1[1]	Profilin-1; *PFN1*	164	15216	3	3	2	2	22.9	140
CBR1[1]	Carbonyl reductase [NADPH] 1; *CBR1*	162	30641	17	8	5	3	24.9	277
CBR3[1]	Carbonyl reductase [NADPH] 3; *CBR3*	76	31230	4	3	2	1	10.1	277
MK01[1]	Mitogen-activated protein kinase 1; *MAPK1*	162	41762	6	4	2	2	10.3	360
SNAB[1]	β-soluble NSF attachment protein; *NAPB*	160	33878	9	5	5	2	24.8	298
SNAA[1]	α-soluble NSF attachment protein; *NAPA*	153	33667	5	4	2	1	14.2	295
VATH[1]	V-type proton ATPase subunit H; *ATP6V1H*	159	56417	8	7	3	2	12.6	483
PALM[1]	Paralemmin-1; *PALM*	157	42221	8	4	4	2	18.3	387
ATPK[1]	ATP synthase subunit f, mitochondrial; *ATP5J2*	157	11025	5	4	1	1	11.7	94
IDH3A[1]	Isocitrate dehydrogenase [NAD] subunit α, mitochondrial; *IDH3A*	156	40022	6	4	3	1	10.1	366

NDUA6[1]	NADH dehydrogenase [ubiquinone] 1 α subcomplex subunit 6; *NDUFA6*	155	17973	3	3	1	1	10.4	154
GTR3[1]	Solute carrier family 2, facilitated glucose transporter member 3; *SLC2A3*	151	54345	3	3	1	1	4	496
RTN4[1]	Reticulon-4; *RTN4*	148	130250	13	6	3	1	4.9	1192
PTGDS[1]	Prostaglandin-H2 D-isomerase; *PTGDS*	148	21243	3	2	1	1	8.4	190
NPTN[1]	Neuroplastin; *NPTN*	146	44702	10	8	3	1	9.5	398
FSCN1[1]	Fascin; *FSCN1*	145	55123	5	3	3	1	13.4	493
NDE1[1]	Nuclear distribution protein nudE homolog 1; *NDE1*	144	38842	4	2	2	1	8.1	346
TCPQ[1]	T-complex protein 1 subunit θ; *CCT8*	144	60153	6	4	4	3	11.7	548
M2OM[1]	Mitochondrial 2-oxoglutarate/malate carrier protein; *SLC25A11*	143	34211	11	8	4	2	14.3	314
ALBU[1]	Serum albumin; *ALB*	140	71317	10	6	7	4	15.8	609
DLG2[1]	Disks large homolog 2; *DLG2*	139	97948	6	4	4	2	6.8	870
DLG4[1]	Disks large homolog 4; *DLG4* pe 1	105	80788	5	4	3	2	8	724
DLG1[1]	Disks large homolog 1; *DLG1*	106	100678	3	3	1	1	2.8	904
NDUS6[1]	NADH dehydrogenase [ubiquinone] Fe-S protein 6, mitochondrial; *NDUFS6*	138	14045	2	2	1	1	19.4	124
TAGL3[1]	Transgelin-3; *TAGLN3*	137	22629	13	6	4	4	25.1	199
NDUA9[1]	NADH dehydrogenase [ubiquinone] 1 α subcomplex subunit 9, mitochondrial; *NDUFA9*	136	42654	9	3	3	1	11.1	377
COX2[1]	Cytochrome c oxidase subunit 2; *MT-CO2*	134	25719	5	5	3	3	19.4	227
NRCAM[1]	Neuronal cell adhesion molecule; *NRCAM*	133	144655	8	6	5	3	5.7	1304
CRYAB[1]	α-crystallin B chain; *CRYAB*	132	20146	7	4	5	4	48	175
ACO13[1]	Acyl-coenzyme A thioesterase 13; *ACOT13*	131	15065	7	3	4	1	22.9	140
CD81[1]	CD81 antigen; *CD81*	131	26476	6	4	2	1	16.5	236
AP180[1]	Clathrin coat assembly protein AP180; *SNAP91*	128	92672	6	5	2	1	4.1	907
NIPS2[1]	Protein NipSnap homolog 2; *GBAS*	127	33949	6	3	4	1	21.7	286
NDUB1[1]	NADH dehydrogenase [ubiquinone] 1 β subcomplex subunit 1; *NDUFB1*	125	7014	4	4	2	2	32.8	58
CRYM[1]	Thiomorpholine-carboxylate dehydrogenase; *CRYM*	125	33925	6	5	2	2	13.4	314
ADDB[1]	β-adducin; *ADD2*	124	81260	8	7	4	3	5.9	726
ADDA[1]	α-adducin; *ADD1*	53	81304	8	5	4	2	7.6	737
CNRP1[1]	CB1 cannabinoid receptor-interacting protein 1; *CNRIP1*	123	18751	8	6	4	2	45.1	164
PTPRZ[1]	Receptor-type tyrosine-protein phosphatase ζ; *PTPRZ1*	122	255683	4	3	2	1	1.9	2315
ARPC3[1]	Actin-related protein 2/3 complex subunit 3; *ARPC3*	121	20761	2	2	1	1	13.5	178
TPM3L[5]	Putative tropomyosin α-3 chain-like protein	121	26595	6	4	3	1	15.7	
PSD3[1]	PH and SEC7 domain-containing protein 3; *PSD3*	120	116646	8	3	7	2	8.8	1048
AMPH[1]	Amphiphysin; *AMPH*	119	76381	6	4	5	3	12.4	695

TPM4[1]	Tropomyosin α-4 chain; *TPM4*	118	28619	11	7	5	2	30.6	248
TPM1[1]	Tropomyosin α-1 chain; *TPM1*	100	32746	8	5	4	1	21.8	284
TOM70[1]	Mitochondrial import receptor subunit TOM70; *TOMM70A*	118	68096	6	3	2	1	4.9	608
NDUB4[1]	NADH dehydrogenase [ubiquinone] 1 β subcomplex subunit 4; *NDUFB4*	117	15256	5	4	2	1	17.8	129
QCR7[1]	Cytochrome b-c1 complex subunit 7; *UQCRB*	117	13522	9	6	6	4	71.2	111
OPALI[2]	Opalin; *OPALIN*	117	15787	5	4	1	1	5.7	141
STX7[1]	Syntaxin-7; *STX7*	117	29911	3	2	2	1	12.6	261
QCR6[1]	Cytochrome b-c1 complex subunit 6, mitochondrial; *UQCRH*	117	11017	4	4	2	2	34.1	91
VGF[1]	Neurosecretory protein VGF; *VGF*	116	67275	5	4	3	2	10.9	615
MOES[1]	Moesin; *MSN*	116	67892	6	3	4	1	8.8	577
TOM22[1]	Mitochondrial import receptor subunit TOM22 homolog; *TOMM22*	115	15512	5	5	1	1	17.6	142
RS7[1]	40S ribosomal protein S7; *RPS7*	114	22113	10	4	3	2	22.2	194
QCR8[1]	Cytochrome b-c1 complex subunit 8; *UQCRQ*	114	9900	3	2	2	1	29.3	82
APOD[1]	Apolipoprotein D; *APOD*	112	21547	3	3	2	2	17.5	189
AL4A1[1]	δ-1-pyrroline-5-carboxylate dehydrogenase, mitochondrial; *ALDH4A1*	111	62137	6	4	3	2	7.5	563
RAB1B[1]	Ras-related protein Rab-1B; *RAB1B*	110	22328	5	2	3	1	19.9	201
NEUM[1]	Neuromodulin; *GAP43*	108	24902	8	3	3	1	18.5	238
TCPH[1]	T-complex protein 1 subunit η; *CCT7*	107	59842	6	3	5	2	12.2	543
RAB14[1]	Ras-related protein Rab-14; *RAB14*	106	24110	2	2	1	1	7	215
PA1B3[1]	Platelet-activating factor acetylhydrolase IB subunit γ; *PAFAH1B3*	106	25832	3	2	2	1	14.3	231
ACTY[1]	β-centractin; *ACTR1B*	105	42381	4	4	2	2	9	376
TLN1[1]	Talin-1; *TLN1*	103	271766	20	2	8	1	3.8	2541
CPLX2[1]	Complexin-2; *CPLX2*	102	15499	7	5	2	2	9	134
VATC1[1]	V-type proton ATPase subunit C 1; *ATP6V1C1*	102	44085	15	3	6	1	26.2	382
EF2[1]	Elongation factor 2; *EEF2*	101	96246	4	3	3	2	8.9	858
KGUA[1]	Guanylate kinase; *GUK1*	100	21769	2	1	2	1	12.7	197
BSN[1]	Protein bassoon; *BSN*	99	418324	19	4	15	3	8.2	3926
WDR37[2]	WD repeat-containing protein 37; *WDR37*	98	55316	4	4	2	2	5.7	494
KAD1[1]	Adenylate kinase isoenzyme 1; *AK1*	96	21735	15	6	5	4	35.1	194
MYH10[1]	Myosin-10; *MYH10*	95	229827	14	4	8	3	5.9	1976
S6A17[2]	Na^+-dependent neutral amino acid transporter SLC6A17; *SLC6A17*	95	81747	5	2	3	1	6.9	727
GABT[1]	4-aminobutyrate aminotransferase, mitochondrial; *ABAT*	94	57087	7	2	5	2	16.2	500
CAH2[1]	Carbonic anhydrase 2; *CA2*	91	29285	4	3	1	1	6.2	260
SNG1[1]	Synaptogyrin-1; *SYNGR1*	91	25667	4	4	1	1	5.2	233

CYFP1[1]	Cytoplasmic FMR1-interacting protein 1; *CYFIP1*	91	146742	4	3	3	2	2.9	1253
CYFP2[1]	Cytoplasmic FMR1-interacting protein 2; *CYFIP2*	73	150298	4	2	3	1	5.4	1278
NPTX1[2]	Neuronal pentraxin-1; *NPTX1*	90	47606	4	3	2	1	7.4	432
CLCA[1]	Clathrin light chain A; *CLTA*	90	27174	4	3	2	1	12.5	248
LDHA[1]	L-lactate dehydrogenase A chain; *LDHA*	90	36950	8	5	4	2	21.1	332
LDH6B[1]	L-lactate dehydrogenase A-like 6B; *LDHAL6B*	16	42372	5	1	3	1	11	381
LRC47[1]	Leucine-rich repeat-containing protein 47; *LRRC47*	90	64004	6	2	4	1	10.6	583
KPCG[1]	Protein kinase C g type; *PRKCG*	89	79652	4	3	3	2	6	697
KPCA[1]	Protein kinase C α type; *PRKCA*	70	77841	5	4	3	2	5.7	672
GLO2[1]	Hydroxyacylglutathione hydrolase, mitochondrial; *HAGH*	88	34240	2	1	2	1	8.8	308
FKBP8[1]	Peptidyl-prolyl cis-trans isomerase FKBP8; *FKBP8*	88	44990	2	2	1	1	7	412
PI42A[1]	Phosphatidylinositol 5-phosphate 4-kinase type-2 α; *PIP4K2A*	88	46424	4	4	1	1	2.5	406
NCEH1[1]	Neutral cholesterol ester hydrolase 1; *NCEH1*	87	46064	3	2	2	1	12	408
TPPP3[1]	Tubulin polymerization-promoting protein family member 3; *TPPP3*	87	19145	3	2	3	2	30.7	176
RASK[1]	GTPase KRas; *KRAS*	87	21927	8	6	3	1	21.7	189
MYL6[1]	Myosin light polypeptide 6; *MYL6*	84	17090	8	3	2	1	19.2	151
PCBP2[1]	Poly(rC)-binding protein 2; *PCBP2*	84	38955	5	4	3	2	16.4	365
TPP1[1]	Tripeptidyl-peptidase 1; *TPP1*	83	61723	6	5	2	2	5	563
RAB5C[1]	Ras-related protein Rab-5C; *RAB5C*	83	23696	3	2	2	2	16.2	216
RAB5A[1]	Ras-related protein Rab-5A; *RAB5A*	51	23872	3	2	1	1	6.5	215
PGRC1[1]	Membrane-associated progesterone receptor component 1; *PGRMC1*	83	21772	3	3	2	2	14.4	195
SODM[1]	Superoxide dismutase [Mn], mitochondrial; *SOD2*	83	24878	3	2	2	1	10.4	222
GSTT1[1]	Glutathione S-transferase θ-1; *GSTT1*	82	27489	4	4	1	1	4.2	240
CX7A2[1]	Cytochrome c oxidase subunit 7A2, mitochondrial; *COX7A2*	82	9390	9	5	3	2	60.2	83
SV2A[1]	Synaptic vesicle glycoprotein 2A; *SV2A*	81	83440	7	2	4	1	7	742
MTCH2[1]	Mitochondrial carrier homolog 2; *MTCH2*	81	33936	3	3	2	2	10.2	303
CTNB1[1]	Catenin β-1; *CTNNB1*	79	86069	4	1	3	1	4.6	781
RAN[1]	GTP-binding nuclear protein Ran; *RAN*	79	24579	3	2	2	1	13.9	216
DHSB[1]	Succinate dehydrogenase [ubiquinone] Fe-S subunit, mitochondrial; *SDHB*	79	32407	5	5	2	2	11.5	
CYB5B[1]	Cytochrome b5 type B; *CYB5B*	78	16436	2	2	1	1	8.9	146
MAON[2]	NADP-dependent malic enzyme, mitochondrial; *ME3*	78	67653	2	2	1	1	3.8	604
PROF2[1]	Profilin-2; *PFN2*	78	15378	2	2	1	1	10	140
ALDH2[1]	Aldehyde dehydrogenase, mitochondrial; *ALDH2*	77	56859	3	2	2	1	6.4	517
VAT1[1]	Synaptic vesicle membrane protein VAT-1 homolog; *VAT1*	77	42122	2	1	1	1	3.1	393

NTRI[1]	Neurotrimin; *NTM*	77	38518	5	3	3	2	9.3	344
FBX2[1]	F-box only protein 2; *FBXO2*	77	33706	4	2	2	2	9.8	296
SCG2[1]	Secretogranin-2; *SCG2*	75	70897	5	2	3	1	9.2	617
SNG3[2]	Synaptogyrin-3; *SYNGR3*	75	24768	2	2	1	1	5.2	229
PRRT2[1]	Proline-rich transmembrane protein 2; *PRRT2*	74	35208	5	4	1	1	3.5	340
MYO5A	Unconventional myosin-Va; *MYO5A* pe 1	73	216979	9	4	6	3	4.3	1855
MYO5C	Unconventional myosin-Vc; *MYO5C*	24	203994	11	1	4	1	3.5	1742
NDUS1	NADH-ubiquinone oxidoreductase 75 kDa subunit, mitochondrial; *NDUFS1*	73	80443	9	6	4	2	11.3	727
PDIA3	Protein disulfide-isomerase A3; *PDIA3*	72	57146	5	2	4	1	7.1	505
UBP5	Ubiquitin carboxyl-terminal hydrolase 5; *USP5*	71	96638	8	6	5	5	10.4	858
UBP13[1]	Ubiquitin carboxyl-terminal hydrolase 13; *USP13*	23	98006	3	1	3	1	3.7	863
COR1A[1]	Coronin-1A; *CORO1A*	71	51678	1	1	1	1	3.5	461
GBG7[1]	Guanine nucleotide-binding protein $G_i/G_s/G_o$ subunit γ-7; *GNG7*	71	7631	2	2	1	1	20.6	68
IF4A1[1]	Eukaryotic initiation factor 4A-I; *EIF4A1*	70	46353	6	2	3	1	8.4	406
GDIR1[1]	ρ GDP-dissociation inhibitor 1; *ARHGDIA*	69	23250	3	1	2	1	27.5	204
PDCD5[1]	Programmed cell death protein 5; *PDCD5*	69	14276	2	2	1	1	10.4	125
SYUB[1]	β-synuclein; *SNCB*	69	14279	7	3	3	2	45.5	134
AL7A1[1]	α-aminoadipic semialdehyde dehydrogenase; *ALDH7A1*	68	59020	3	3	2	2	6.9	539
RAB1A[1]	Ras-related protein Rab-1A; *RAB1A*	68	22891	7	4	5	4	31.7	205
CADM4[1]	Cell adhesion molecule 4; *CADM4*	67	43215	5	2	3	1	10.1	388
GELS[1]	Gelsolin; *GSN*	67	86043	3	2	2	1	9.6	782
GNAZ[2]	Guanine nucleotide-binding protein G_z subunit α; *GNAZ*	66	41411	4	2	3	1	10.1	355
IQEC1[1]	IQ motif and SEC7 domain-containing protein 1; *IQSEC1*	65	109103	8	2	4	1	4.9	963
DLRB1[1]	Dynein light chain roadblock-type 1; *DYNLRB1*	65	10915	1	1	1	1	12.5	96
PHIPL[2]	Phytanoyl-CoA hydroxylase-interacting protein-like; *PHYHIPL*	64	43029	2	2	1	1	2.4	376
TIM13[1]	Mitochondrial import inner membrane translocase subunit Tim13; *TIMM13*	64	10721	2	1	2	1	23.2	95
NEBL[1]	Nebulette; *NEBL*	64	116609	11	2	5	1	6	1014
MAG[1]	Myelin-associated glycoprotein; *MAG*	63	69880	4	3	2	1	3.7	626
GDAP1[1]	Ganglioside-induced differentiation-associated protein 1; *GDAP1*	63	41548	2	2	1	1	3.4	358
UK114[1]	Ribonuclease UK114; *HRSP12*	62	14542	5	4	3	2	34.3	137
BACH[1]	Cytosolic acyl coenzyme A thioester hydrolase; *ACOT7*	61	42454	3	2	2	1	9.7	380
K0513[2]	Uncharacterized protein KIAA0513; *KIAA0513*	60	47066	1	1	1	1	3.4	411
GPM6B[1]	Neuronal membrane glycoprotein M6-b; *GPM6B*	60	29882	4	4	1	1	4.9	265

ES1[1]	ES1 protein homolog, mitochondrial; *C21orf33*	60	28495	3	2	2	1	10.1	268
NFS1[1]	Cysteine desulfurase, mitochondrial; *NFS1* pe 1	59	50563	4	2	2	1	7.2	457
SEPT9[1]	Septin-9; *SEPT9*	59	65646	6	2	4	1	6.7	586
NPM[1]	Nucleophosmin; *NPM1*	59	32726	3	3	1	1	7.1	294
NPY[1]	Pro-neuropeptide Y; *NPY*	59	10902	2	2	1	1	13.4	97
PPAC[1]	Low molecular weight phosphotyrosine protein phosphatase; *ACP1*	58	18487	1	1	1	1	7.6	158
AT5EL[1]	ATP synthase subunit ε-like protein, mitochondrial; *ATP5EP2*	58	5860	2	1	1	1	15.7	51
HNRPK[1]	Heterogeneous nuclear ribonucleoprotein K; *HNRNPK*	57	51230	4	3	1	1	3.7	463
LY6H[2]	Lymphocyte antigen 6H; *LY6H*	57	15286	5	3	2	1	21.4	140
KPCB[1]	Protein kinase C β type; *PRKCB*	56	77960	7	5	3	2	6	671
HSP74[1]	Heat shock 70 kDa protein 4; *HSPA4*	56	95127	4	2	3	2	4.5	840
HS105[1]	Heat shock protein 105 kDa; *HSPH1*	55	97716	6	1	4	1	6.4	858
KCY[1]	UMP-CMP kinase; *CMPK1*	56	22436	1	1	1	1	6.6	196
IF4H[1]	Eukaryotic translation initiation factor 4H; *EIF4H*	56	27425	7	4	3	2	26.6	248
EPN1[1]	Epsin-1; *EPN1*	55	60370	9	1	4	1	8.2	576
GLU2B[1]	Glucosidase 2 subunit β; *PRKCSH*	55	60357	1	1	1	1	1.9	528
NDUS3[1]	NADH dehydrogenase [ubiquinone] Fe-S protein 3, mitochondrial; *NDUFS3*	54	30337	2	1	2	1	14	264
AUXI[1]	Putative tyrosine-protein phosphatase auxilin; *DNAJC6*	54	100675	5	2	3	2	6.1	913
SCRN1[1]	Secernin-1; *SCRN1*	53	46980	11	2	3	2	11.4	414
NMDZ1[1]	Glutamate receptor ionotropic, NMDA 1; *GRIN1*	52	105990	2	1	2	1	2.2	938
STRAP[1]	Serine-threonine kinase receptor-associated protein; *STRAP*	52	38756	1	1	1	1	6	350
GLSK[1]	Glutaminase kidney isoform, mitochondrial; *GLS*	52	74269	5	3	4	2	10.3	669
RTN3[1]	Reticulon-3; *RTN3*	51	113169	2	2	1	1	1.5	1032
PCBP1[1]	Poly(rC)-binding protein 1; *PCBP1*	51	37987	6	4	3	2	21.9	356
DLDH[1]	Dihydrolipoyl dehydrogenase, mitochondrial; *DLD*	51	54713	4	4	2	2	6.7	509
DOPD[1]	D-dopachrome decarboxylase; *DDT*	51	12818	5	3	2	2	27.1	118
DDTL[2]	D-dopachrome decarboxylase-like protein; *DDTL*	41	14414	2	2	1	1	15.7	134
K1045[1]	Protein KIAA1045; *KIAA1045*	51	45905	4	1	4	1	15.5	400
MTMR5[1]	Myotubularin-related protein 5; *SBF1*	50	210294	7	2	3	1	2.6	1867
ARPC4[1]	Actin-related protein 2/3 complex subunit 4; *ARPC4*	50	19768	4	2	2	1	13.7	168
NCKP1[1]	Nck-associated protein 1; *NCKAP1*	50	130018	4	1	3	1	5.2	1128
NDUAA[1]	NADH dehydrogenase [ubiquinone] 1 α subcomplex subunit 10, mitochondrial; *NDUFA10*	50	41067	3	1	2	1	9	355
DEST[1]	Destrin; *DSTN*	50	18950	6	3	4	2	31.5	165
SCG1[1]	Secretogranin-1; *CHGB*	49	78343	2	2	1	1	1.8	677

ARP2[1]	Actin-related protein 2; *ACTR2*	49	45017	5	1	4	1	12.7	394
NDUS2[1]	NADH dehydrogenase [ubiquinone] Fe-S protein 2, mitochondrial; *NDUFS2*	48	52911	5	3	3	2	13.2	463
CX04A[1]	Protein CXorf40A; *CXorf40A*	47	18051	5	3	1	1	8.9	158
AP2S1[1]	AP-2 complex subunit sigma; *AP2S1*	47	17178	2	2	1	1	8.5	142
SH3L3[1]	SH3 domain-binding glutamic acid-rich-like protein 3; *SH3BGRL3*	47	10488	1	1	1	1	20.4	93
ODPA[1]	Pyruvate dehydrogenase E1 component subunit α, somatic form, mitochondrial; *PDHA1*	47	43952	2	2	1	1	3.1	390
RHOB[1]	ρ-related GTP-binding protein ρB; *RHOB*	46	22565	4	1	2	1	7.1	196
NAC2[2]	Na^+/Ca^{2+} exchanger 2; *SLC8A2*	46	101388	5	2	2	1	3	921
MACF1[1]	Microtubule-actin cross-linking factor 1, isoforms 1/2/3/5; *MACF1*	46	843033	37	2	19	1	2.9	7388
ST134[5]	Putative protein FAM10A4; *ST13P4*	45	27561	3	1	2	1	12.1	240
NDRG1[1]	Protein NDRG1; *NDRG1*	45	43264	2	2	1	1	9.4	394
PLEC[1]	Plectin; *PLEC*	45	533462	35	1	21	1	5	4684
BAIP2[1]	Brain-specific angiogenesis inhibitor 1-associated protein 2; *BAIAP2*	45	61115	5	2	4	2	10.7	552
H2B1D[1]	Histone H2B type 1-D; *HIST1H2BD*	45	13928	3	1	2	1	22.2	126
VGLU3[1]	Vesicular glutamate transporter 3; *SLC17A8*	44	65861	3	1	3	1	6.6	589
GHC1[1]	Mitochondrial glutamate carrier 1; *SLC25A22*	44	34904	3	3	1	1	6.8	323
SCPDL	Saccharopine dehydrogenase-like oxidoreductase; *SCCPDH*	43	47464	2	1	1	1	8.2	429
OMGP[1]	Oligodendrocyte-myelin glycoprotein; *OMG*	43	50032	6	3	2	1	8.4	440
SYAC[1]	Alanine–tRNA ligase, cytoplasmic; *AARS*	42	107484	6	1	6	1	7.4	968
IGS21[2]	Immunoglobulin superfamily member 21; *IGSF21*	42	52202	3	1	3	1	16.5	467
RL6[1]	60S ribosomal protein L6; *RPL6*	41	32765	2	2	2	2	9	288
CALX[1]	Calnexin; *CANX*	41	67982	2	1	2	1	8.1	592
EF1B[1]	Elongation factor 1-β; *EEF1B2*	41	24919	1	1	1	1	5.8	225
MPP2[1]	MAGUK p55 subfamily member 2; *MPP2*	41	64882	2	1	2	1	6.4	576
TTYH1[2]	Protein tweety homolog 1; *TTYH1*	40	49704	3	1	2	1	6.4	450
KCD16[2]	BTB/POZ domain-containing protein KCTD16; *KCTD16*	39	49962	1	1	1	1	2.8	428
DREB[1]	Drebrin; *DBN1*	39	71842	2	1	2	1	4	649
MARE3[1]	Microtubule-associated protein RP/EB family member 3; *MAPRE3*	39	32247	3	2	2	1	10	281
CDC42[1]	Cell division control protein 42 homolog; *CDC42*	38	21587	2	2	1	1	12.6	191
RLA2[1]	60S acidic ribosomal protein P2; *RPLP2*	38	11658	1	1	1	1	18.3	115
SERA[1]	D-3-phosphoglycerate dehydrogenase; *PHGDH*	38	57356	3	1	2	1	4.5	533
CUTA[1]	Protein CutA; *CUTA*	36	19218	4	3	3	2	41.9	179
ERP29[1]	Endoplasmic reticulum resident protein 29; *ERP29*	36	29032	1	1	1	1	3.8	261

MARE2[1]	Microtubule-associated protein RP/EB family member 2; *MAPRE2*	36	37236	1	1	1	1	4	327
UN45B[2]	Protein unc-45 homolog B; *UNC45B*	36	104979	2	1	2	1	2.7	931
NDUBA[1]	NADH dehydrogenase [ubiquinone] 1 β subcomplex subunit 10; *NDUFB10*	36	21048	2	2	2	2	17.4	172
CAD13[1]	Cadherin-13; *CDH13*	36	78694	1	1	1	1	3.1	713
RTCB[1]	tRNA-splicing ligase RtcB homolog; *C22orf28*	35	55688	3	2	2	1	3.8	505
TCPG[1]	T-complex protein 1 subunit g; *CCT3*	35	61066	5	2	4	1	13.8	545
TIM8A[1]	Mitochondrial import inner membrane translocase subunit Tim8 A; *TIMM8A*	34	11219	1	1	1	1	17.5	97
CD47[1]	Leukocyte surface antigen CD47; *CD47*	33	35590	9	1	3	1	10.2	323
PYGB[1]	Glycogen phosphorylase, brain form; *PYGB*	33	97319	3	2	2	1	5.5	843
CAP1[1]	Adenylyl cyclase-associated protein 1; *CAP1*	32	52325	5	2	2	1	8.8	475
TTYH3	Protein tweety homolog 3; *TTYH3*	32	58477	12	1	2	1	4.2	523
PP2AA[1]	Serine/threonine-protein phosphatase 2A catalytic subunit α isoform; *PPP2CA*	32	36142	2	1	2	1	12.6	309
NDUS5[1]	NADH dehydrogenase [ubiquinone] Fe-S protein 5; *NDUFS5*	32	12737	1	1	1	1	11.3	106
PVRL1[1]	Poliovirus receptor-related protein 1; *PVRL1*	31	57465	3	1	2	1	8.9	517
DPYL5[1]	Dihydropyrimidinase-related protein 5; *DPYSL5*	31	61952	4	2	4	2	14.9	564
IDH3B[1]	Isocitrate dehydrogenase [NAD] subunit β, mitochondrial; *IDH3B*	31	42442	2	1	2	1	11.7	385
CTRO[1]	Citron ρ-interacting kinase; *CIT*	31	233339	15	4	9	1	6.4	2027
SGTA[1]	Small glutamine-rich tetratricopeptide re-peat-containing protein α; *SGTA*	31	34270	1	1	1	1	4.8	313
UB2V1[1]	Ubiquitin-conjugating enzyme E2 variant 1; *UBE2V1*	31	16598	16	1	3	1	23.8	147
LGUL[1]	Lactoylglutathione lyase; *GLO1*	31	20992	2	2	1	1	8.7	184
LASP1[1]	LIM and SH3 domain protein 1; *LASP1*	31	30097	3	2	2	1	9.2	261
PFD3[1]	Prefoldin subunit 3; *VBP1*	30	22815	1	1	1	1	5.1	197
NDUB9[1]	NADH dehydrogenase [ubiquinone] 1 β subcomplex subunit 9; *NDUFB9*	30	22045	2	1	1	1	8.9	179
NDUAC[1]	NADH dehydrogenase [ubiquinone] 1α subcomplex subunit 12; *NDUFA12*	30	17104	1	1	1	1	12.4	145
BDH2[1]	3-hydroxybutyrate dehydrogenase type 2; *BDH2*	30	27049	1	1	1	1	8.6	245
KAD5[1]	Adenylate kinase isoenzyme 5; *AK5*	30	63863	7	1	3	1	7.1	562
WDR1[1]	WD repeat-containing protein 1; *WDR1*	29	66836	2	1	2	1	9.1	606
ARP3B[1]	Actin-related protein 3B; *ACTR3B*	29	48090	4	2	2	1	4.5	418
CX6A1[1]	Cytochrome c oxidase subunit 6A1, mitochondrial; *COX6A1*	29	12147	3	1	3	1	53.2	109
RBP2[1]	E3 SUMO-protein ligase RanBP2; *RANBP2*	29	362365	14	1	7	1	2.2	3224
TOLIP[1]	Toll-interacting protein; *TOLLIP*	29	30490	4	1	2	1	9.1	274

CHL1[1]	Neural cell adhesion molecule L1-like protein; *CHL1*	29	136070	4	2	3	1	3.6	1208
DEMA[1]	Dematin; *EPB49*	29	45600	2	1	2	1	6.2	405
NDUB6[1]	NADH dehydrogenase [ubiquinone] 1 β subcomplex subunit 6; *NDUFB6*	29	15479	2	1	1	1	19.5	128
TF[1]	Tissue factor; *F3*	29	33332	1	1	1	1	5.1	295
ODO1[1]	2-oxoglutarate dehydrogenase, mitochondrial; *OGDH*	28	117059	5	1	3	1	4.4	1023
MPC2[1]	Mitochondrial pyruvate carrier 2; *MPC2*	28	14327	4	1	3	1	43.3	127
OTUB1[1]	Ubiquitin thioesterase OTUB1; *OTUB1*	28	31492	1	1	1	1	7	271
LRC8B[2]	Leucine-rich repeat-containing protein 8B; *LRRC8B*	28	93528	2	1	1	1	1.7	803
GLP1R[1]	Glucagon-like peptide 1 receptor; *GLP1R*	28	53960	4	1	1	1	1.9	463
SYNPO[1]	Synaptopodin; *SYNPO*	27	99915	10	1	6	1	9.6	929
NDUA4[1]	NADH dehydrogenase [ubiquinone] 1 α subcomplex subunit 4; *NDUFA4*	27	9421	3	1	1	1	12.3	81
DNM1L[1]	Dynamin-1-like protein; *DNM1L*	27	82339	11	2	5	2	9.1	736
HUWE1[1]	E3 ubiquitin-protein ligase HUWE1; *HUWE1*	27	485523	4	1	3	1	0.9	4374
MLP3B[1]	Microtubule-associated proteins 1A/1B light chain 3B; *MAP1LC3B*	27	14679	2	1	1	1	12.8	125
CAMKV[2]	CaM kinase-like vesicle-associated protein; *CAMKV*	27	54662	1	1	1	1	5.2	501
SIM2[1]	Single-minded homolog 2; *SIM2*	26	73914	8	1	4	1	9.9	667
NP1L1[1]	Nucleosome assembly protein 1-like 1; *NAP1L1*	26	45631	2	1	1	1	2.8	391
C1TC[1]	C-1-tetrahydrofolate synthase, cytoplasmic; *MTHFD1*	26	102180	3	1	3	1	5.3	935
GIT1[1]	ARF GTPase-activating protein GIT1; *GIT1*	26	85030	2	1	1	1	1.8	761
AT8A1[1]	Probable phospholipid-transporting ATPase IA; *ATP8A1*	26	132597	5	1	5	1	6.3	1164
ODB2[1]	Lipoamide acyltransferase component of branched-chain α-keto acid dehydrogenase complex, mitochondrial; *DBT*	26	53852	4	2	3	1	11	482
WDR13[1]	WD repeat-containing protein 13; *WDR13*	26	54289	2	1	2	1	6.6	485
ODO2[1]	Dihydrolipoyllysine-residue succinyltransferase component of 2-oxoglutarate dehydrogenase complex, mitochondrial; *DLST*	26	49067	3	2	2	1	9.1	453
HPLN2[1]	Hyaluronan and proteoglycan link protein 2; *HAPLN2*	26	38378	3	1	2	1	6.5	340
FXYD7[2]	FXYD domain-containing ion transport regulator 7; *FXYD7*	25	8689	2	1	1	1	20	80
CADM1[1]	Cell adhesion molecule 1; *CADM1*	25	48935	1	1	1	1	5.2	442
RUFY1[1]	RUN & FYVE domain-containing protein 1; *RUFY1*	25	80851	3	1	2	1	3.8	708
AAK1[1]	AP2-associated protein kinase 1; *AAK1*	25	104562	6	1	5	1	8.8	961
ACLY[1]	ATP-citrate synthase; *ACLY*	24	121674	7	1	4	1	5.5	1101
RTN1[1]	Reticulon-1; *RTN1*	24	83851	2	2	1	1	3	776
TBCA[1]	Tubulin-specific chaperone A; *TBCA*	24	12904	2	1	2	1	17.6	108

ITSN1[1]	Intersectin-1; *ITSN1*	23	196155	5	1	3	1	2.8	1721
CD59[1]	CD59 glycoprotein; *CD59*	23	14795	2	1	1	1	10.2	128
PUS7[1]	Pseudouridylate synthase 7 homolog; *PUS7*	23	75330	2	1	1	1	1.7	661
HINT2[1]	Histidine triad nucleotide-binding protein 2, mitochondrial; *HINT2*	23	17208	2	1	2	1	20.9	163
DPY30[1]	Protein dpy-30 homolog; *DPY30*	23	11243	1	1	1	1	20.2	99
LHPP[1]	Phospholysine phosphohistidine inorganic pyrophosphate phosphatase; *LHPP*	23	29432	1	1	1	1	10.7	270
CHCH3[1]	Coiled-coil-helix-coiled-coil-helix domain-containing protein 3, mitochondrial; *CHCHD3*	23	26421	2	1	2	1	9.3	227
TUSC2[1]	Tumor suppressor candidate 2; *TUSC2*	23	12066	3	1	2	1	40.9	110
D39U1[1]	Epimerase family protein SDR39U1; *SDR39U1*	22	34840	4	2	2	1	9.1	319
PAP1L[2]	Polyadenylate-binding protein 1-like; *PABPC1L*	22	68976	5	2	4	1	10.1	614
MYL6B[1]	Myosin light chain 6B; *MYL6B*	22	22864	3	2	2	1	13.9	208
ATP6[1]	ATP synthase subunit α; *MT-ATP6*	22	24801	1	1	1	1	4.4	226
ABI1[1]	Abl interactor 1; *ABI1*	22	55161	3	1	1	1	3.7	508
AT5F1[1]	ATP synthase subunit β, mitochondrial; *ATP5F1*	22	28947	6	2	2	1	10.5	256
RM12[1]	39S ribosomal protein L12, mitochondrial; *MRPL12*	22	21563	1	1	1	1	12.6	198
PKHA8[1]	Pleckstrin homology domain-containing family A member 8; *PLEKHA8*	21	58908	5	1	5	1	12.1	519
PRAF2[1]	PRA1 family protein 2; *PRAF2*	21	19588	2	2	2	2	16.3	178
DECR[1]	2,4-dienoyl-CoA reductase, mitochondrial; *DECR1*	21	36330	2	1	2	1	11	335
CXA1[1]	Gap junction α-1 protein; *GJA1*	21	43494	2	1	1	1	5.2	382
ADDG[1]	γ-adducin; *ADD3*	21	79447	2	1	2	1	4.7	706
AFG32[1]	AFG3-like protein 2; *AFG3L2*	20	88984	6	1	5	1	11.4	797
CRBG3[2]	β/γ crystallin domain-containing protein 3; *CRYBG3*	20	117378	6	1	3	1	2.7	1022
RSSA[1]	40S ribosomal protein SA; *RPSA*	20	32947	4	2	3	1	17.3	295
GLOD4[1]	Glyoxalase domain-containing protein 4; *GLOD4*	20	35170	4	1	4	1	16.6	313
NDUV1[1]	NADH dehydrogenase [ubiquinone] flavoprotein 1, mitochondrial; *NDUFV1*	20	51469	2	1	2	1	8.2	464
HPLN4[2]	Hyaluronan & proteoglycan link protein 4; *HAPLN4*	19	43402	3	2	1	1	4.7	402
PDC6I[1]	Programmed cell death 6-interacting protein; *PDCD6IP*	19	96590	2	1	1	1	3.9	868
SLN11[1]	Schlafen family member 11; *SLFN11*	19	104309	1	1	1	1	1.3	901
PK1L2[1]	Polycystic kidney disease protein 1-like 2; *PKD1L2*	19	275595	4	1	2	1	1.5	2459
TCPZ[1]	T-complex protein 1 subunit ζ; *CCT6A*	18	58444	4	1	4	1	10.2	531
RDH14[1]	Retinol dehydrogenase 14; *RDH14*	18	37184	2	1	2	1	6.5	336
PKHH1[2]	Pleckstrin homology domain-containing family H member 1; *PLEKHH1*	18	152733	11	1	6	1	5.9	1364

NDUA7[1]	NADH dehydrogenase [ubiquinone] 1 α subcomplex subunit 7; *NDUFA7*	17	12601	1	1	1	1	20.4	113
QOR[1]	Quinone oxidoreductase; *CRYZ*	17	35356	3	1	1	1	3.3	329
CAND2[1]	Cullin-associated NEDD8-dissociated protein 2; *CAND2*	17	136653	3	1	2	1	2.1	1236
ODP2[1]	Dihydrolipoyllysine-residue acetyltransferase component of pyruvate dehydrogenase complex, mitochondrial; *DLAT*	17	69466	13	1	4	1	9.6	647
COTL1[1]	Coactosin-like protein; *COTL1*	17	16049	1	1	1	1	11.3	142
AK1A1[1]	Alcohol dehydrogenase [$NADP^+$]; *AKR1A1*	17	36892	2	1	2	1	6.5	325
PCCB[1]	Propionyl-CoA carboxylase β chain, mitochondrial; *PCCB*	17	58806	1	1	1	1	2.4	539
CG025[1]	UPF0415 protein C7orf25; *C7orf25*	16	46707	3	1	2	1	7.8	421
HPRT[1]	Hypoxanthine-guanine phosphoribosyl-transferase; *HPRT1*	16	24792	1	1	1	1	10.6	218
DBNL[1]	Drebrin-like protein; *DBNL*	16	48463	4	1	3	1	13.3	430
AK1BA[1]	Aldo-keto reductase family 1 member B10; *AKR1B10*	16	36225	1	1	1	1	5.4	316
PI42C[1]	Phosphatidylinositol 5-phosphate 4-kinase type-2γ; *PIP4K2C*	16	47441	3	1	2	1	9.3	421
CLCN4[1]	H^+/Cl^- exchange transporter 4; *CLCN4*	16	85774	19	2	2	1	2.9	760
NDRG3[1]	Protein NDRG3; *NDRG3*	16	41896	1	1	1	1	9.9	375
KCNG2[1]	K^+ voltage-gated channel subfamily G member 2; *KCNG2*	16	52176	6	1	1	1	4.7	466
ANXA6[1]	Annexin A6; *ANXA6*	16	76168	3	1	3	1	5.8	673
ITIH3[1]	Inter-α-trypsin inhibitor heavy chain H3; *ITIH3*	15	100072	2	1	2	1	4.3	890
SYUA[1]	α-synuclein; *SNCA*	15	14451	4	1	2	1	22.1	140
GCSH[1]	Glycine cleavage system H protein, mitochondrial; *GCSH*	15	19101	1	1	1	1	13.3	173
UBP20[1]	Ubiquitin carboxyl-terminal hydrolase 20; *USP20*	15	103763	4	1	2	1	2.8	914
CCD19[1]	Coiled-coil domain-containing protein 19, mitochondrial; *CCDC19*	15	65803	19	1	3	1	7.3	551
DMXL2[1]	DmX-like protein 2; *DMXL2*	15	342962	17	1	10	1	4.6	3036
AQP8[2]	Aquaporin-8; *AQP8*	15	27706	1	1	1	1	6.1	261
TIM9[1]	Mitochondrial import inner membrane translocase subunit Tim9; *TIMM9*	15	10599	2	1	1	1	16.9	89
THIM[1]	3-ketoacyl-CoA thiolase, mitochondrial; *ACAA2*	15	42354	1	1	1	1	7.1	397
PRAF3[1]	PRA1 family protein 3; *ARL6IP5*	15	21600	3	1	2	1	18.1	188
SYNE1[1]	Nesprin-1; *SYNE1*	14	1017127	29	1	21	1	3.5	8797
REC8[2]	Meiotic recombination protein REC8 homolog; *REC8*	14	62916	20	1	2	1	4.8	547
F86C2[5]	Putative protein FAM86C2P; *FAM86C2P*	14	18865	3	1	3	1	26.7	165
SORCN[1]	Sorcin; *SRI*	14	21947	3	1	2	1	17.2	198
PAPS2[1]	Bifunctional 3'-phosphoadenosine 5'-phospho-sulfate synthase 2; *PAPSS2*	14	70027	6	1	1	1	2.6	614

RL11[1]	60S ribosomal protein L11; *RPL11*	13	20468	1	1	1	1	7.9	178
SV2B[2]	Synaptic vesicle glycoprotein 2B; *SV2B*	13	78248	2	1	2	1	4.4	683
THIC[1]	Acetyl-CoA acetyltransferase, cytosolic; *ACAT2*	13	41838	3	1	3	1	18.9	397
RIF1[1]	Telomere-associated protein RIF1; *RIF1*	13	276461	11	1	5	1	3.2	2472
RPB1[1]	DNA-directed RNA polymerase II subunit RPB1; *POLR2A*	13	218408	5	1	4	1	1.9	1970
FETA[1]	α-fetoprotein; *AFP*	13	70458	1	1	1	1	2.6	609

Notes: The MASCOT software arranges the proteins in order of their score, and then groups similar proteins in score order below each initial entry. [1], Abbreviated protein name; all names in this table had the suffix "_HUMAN"; the superscripted number after the name gives the protein existence (PE) score in the Uniprot database, for which 5 levels of evidence are provided: 1, evidence at the protein level, 2, evidence at the transcript level, 3, inferred from homology, 4, predicted, 5, uncertain; [2], All descriptions contained the entry OS=*Homo sapiens*; gene names in *CAPITAL ITALICS*; [3], Score; [4], Molecular Mass, Da; [5], Nº of Matches; [6], Nº of significant matches; [7], Nº of sequences found; [8], Nº of significant sequences found; [9], % Cover of the sequence; [10], Length in Nº of amino acid residues.

Table 4.4. Proteins identified by MASCOT search using SCX fractionation

Abbrev[1]	Description[2]	Score [3]	Mol Mass[4]	Mc [5]	Ms [6]	Sq [7]	Ss [8]	Cov [9]	Lngt [10]
HS90A[1]	Heat shock protein HSP 90-α; *HSP90AA1*	2316	85006	109	86	25	20	32	732
HS90B[1]	Heat shock protein HSP 90-β; *HSP90AB1*	2117	83554	105	77	27	20	35.1	724
ENPL[1]	Endoplasmin; *HSP90B1*	542	92696	36	24	13	9	19.7	803
TRAP1[1]	Heat shock protein 75 kDa, mitochondrial; *TRAP1*	594	80345	14	12	1	1	2	704
HS904[5]	Putative heat shock protein HSP 90-α A4; *HSP90AA4P*	430	47796	17	17	2	2	5.7	418
H90B3[5]	Putative heat shock protein HSP 90-β-3; *HSP90AB3P*	401	68624	39	21	12	8	14.4	597
HS902[1]	Putative heat shock protein HSP 90-α A2; *HSP90AA2*	331	39454	17	14	3	3	9.3	343
H90B2[1]	Putative heat shock protein HSP 90-β 2; *HSP90AB2P*	327	44492	23	15	7	4	16	381
H90B4[5]	Putative heat shock protein HSP 90-β 4; *HSP90AB4P*	217	58855	8	8	2	2	5.5	505
HS905[1]	Putative heat shock protein HSP 90-α A5; *HSP90AA5P*	53	38942	12	5	6	3	15.3	334
ENPLL[5]	Putative endoplasmin-like protein; *HSP90B2P*	14	46343	2	1	2	1	5	399
AT1A1[1]	Na^+/K^+-transporting ATPase subunit α-1; *ATP1A1*	2165	114135	79	62	21	18	20.9	1023
AT1A3[1]	Na^+/K^+-transporting ATPase subunit α-3; *ATP1A3*	1798	113102	74	57	22	19	23.2	1013
AT1A2[1]	Na^+/K^+-transporting ATPase subunit α-2; *ATP1A2*	1381	113505	55	40	20	16	21.7	1020
AT1A4[1]	Na^+/K^+-transporting ATPase subunit α-4; *ATP1A4*	180	115119	18	10	5	5	4.4	1029
ATP4A[1]	K^+-transporting ATPase α chain 1; *ATP4A*	158	115756	7	3	5	2	6.5	1035
AT12A[1]	K^+-transporting ATPase α chain 2; *ATP12A*	133	116292	14	8	4	4	3.3	1039
HXK1[1]	Hexokinase-1; *HK1*	2134	103561	129	90	40	33	39.1	917
HKDC1[2]	Putative hexokinase HKDC1; *HKDC1*	53	103790	10	3	4	1	4.7	917
HXK2[1]	Hexokinase-2; *HK2*	43	103739	8	2	5	2	6.2	917
HXK3[1]	Hexokinase-3; *HK3*	38	100616	6	1	4	1	5.3	923
CLH1[1]	Clathrin heavy chain 1; *CLTC*	1623	193260	76	55	29	23	21.5	1675
CLH2[1]	Clathrin heavy chain 2; *CLTCL1*	482	189020	17	13	7	5	4.1	1640
DYN1[1]	Dynamin-1; *DNM1*	1503	97746	104	67	28	24	35.1	864
DYN3[1]	Dynamin-3; *DNM3*	341	98084	38	19	11	7	15.7	869
DYN2[1]	Dynamin-2; *DNM2*	357	98345	31	19	6	5	7.2	870
ACON[1]	Aconitate hydratase, mitochondrial; *ACO2*	1185	86113	54	38	16	13	27.4	780
UBA1[1]	Ubiquitin-like modifier-activating enzyme 1; *UBA1*	914	118858	33	27	14	13	18.9	1058
MYPR[1]	Myelin proteolipid protein; *PLP1*	876	30855	41	30	6	5	24.9	277
SPTB2[1]	Spectrin β chain, non-erythrocytic 1; *SPTBN1*	777	275237	50	31	27	14	15.1	2364
SPTN2[1]	Spectrin β chain, non-erythrocytic 2; *SPTBN2*	54	272526	13	3	6	2	3.1	2390
ACTN1[1]	α-actinin-1; *ACTN1*	703	103563	33	24	10	7	15.1	892
ACTN4[1]	α-actinin-4; *ACTN4*	684	105245	37	23	13	6	18.8	911
ACTN2[1]	α-actinin-2; *ACTN2*	194	104358	8	5	5	2	8.1	894
ACTN3[1]	α-actinin-3; *ACTN3*	149	103917	5	3	3	1	4.2	901
NNTM[1]	NAD(P) transhydrogenase, mitochondrial; *NNT*	633	114564	47	29	15	11	18.8	1086

PYGB[1]	Glycogen phosphorylase, brain form; *PYGB*	633	97319	44	29	18	12	23	843
PYGM[1]	Glycogen phosphorylase, muscle form; *PYGM*	267	97487	29	16	11	7	14.5	842
PYGL[1]	Glycogen phosphorylase, liver form; *PYGL*	187	97486	13	10	3	3	2.7	847
SPTN1[1]	Spectrin α chain, non-erythrocytic 1; *SPTAN1*	610	285163	65	34	36	16	17.4	2472
GELS[1]	Gelsolin; *GSN*	513	86043	20	14	5	5	9.2	782
CAND1[1]	Cullin-associated *NEDD8*-dissociated protein 1; *CAND1*	504	137999	32	24	15	10	14.8	1230
UBP5[1]	Ubiquitin carboxyl-terminal hydrolase 5; *USP5*	462	96638	29	20	12	9	18.3	858
TERA[1]	Transitional endoplasmic reticulum ATPase; *VCP*	436	89950	35	14	15	7	22.8	806
KATL2[2]	Katanin p60 ATPase-containing subunit A-like 2; *KATNAL2*	126	61557	7	4	2	1	4.8	538
AP2A1[1]	AP-2 complex subunit α-1; *AP2A1*	432	108561	38	23	15	14	17.6	977
AP2A2[1]	AP-2 complex subunit α-2; *AP2A2*	376	104807	27	18	14	10	18.6	939
E41L3[1]	Band 4.1-like protein 3; *EPB41L3*	397	121458	24	13	14	8	17.8	1087
ICAM5[1]	Intercellular adhesion molecule 5; *ICAM5*	375	98766	19	14	9	6	13.1	924
HS74L[1]	Heat shock 70 kDa protein 4L; *HSPA4L*	373	95479	22	14	11	6	16.2	839
HS105[1]	Heat shock protein 105 kDa; *HSPH1*	327	97716	25	15	15	8	22.8	858
HSP74[1]	Heat shock 70 kDa protein 4; *HSPA4*	192	95127	20	8	12	6	19	840
VPP1[1]	V-type proton ATPase 116 kDa subunit a isoform 1; *ATP6V0A1*	349	97148	36	18	12	8	16.1	837
AMPH[1]	Amphiphysin; *AMPH*	329	76381	28	15	10	8	17.6	695
EAA1[1]	Excitatory amino acid transporter 1; *SLC1A3*	313	59705	10	7	5	2	12.9	542
EF2[1]	Elongation factor 2; *EEF2*	300	96246	17	12	9	5	12.8	858
NFASC[1]	Neurofascin; *NFASC*	292	150789	17	12	6	4	5.4	1347
CNTN1[1]	Contactin-1; *CNTN1*	289	114104	37	21	13	9	16.7	1018
PSA[1]	Puromycin-sensitive aminopeptidase; *NPEPPS*	277	103895	39	18	19	12	21.8	919
PSAL[2]	Puromycin-sensitive aminopeptidase-like protein; *NPEPPSL1*	58	54226	11	4	9	3	20.9	478
CSPG2[1]	Versican core protein; *VCAN*	274	374585	16	9	8	4	3	3396
EAA2[1]	Excitatory amino acid transporter 2; *SLC1A2*	272	62577	7	4	4	2	9.6	574
ODO1[1]	2-oxoglutarate dehydrogenase, mitochondrial; *OGDH*	253	117059	29	13	12	9	13.1	1023
OGDHL[1]	2-oxoglutarate dehydrogenase-like, mitochondrial; *OGDHL*	89	115264	20	10	10	7	12.4	1010
DPP6[1]	Dipeptidyl aminopeptidase-like protein 6; *DPP6*	246	98154	17	9	6	4	9.5	865
ANK2[1]	Ankyrin-2; *ANK2*	227	435957	33	10	21	6	6.7	3957
ANK1[1]	Ankyrin-1; *ANK1*	16	207334	4	1	3	1	2.6	1881
PYC[1]	Pyruvate carboxylase, mitochondrial; *PC*	223	130293	19	10	8	4	9.2	1178
SYAC[1]	Alanine--tRNA ligase, cytoplasmic; *AARS*	217	107484	8	7	4	3	5.6	968
ADDA[1]	α-adducin; *ADD1*	216	81304	9	6	5	3	9.5	737
4F2[1]	4F2 cell-surface antigen heavy chain; *SLC3A2*	207	68180	16	10	9	5	17.3	630
AL1L1[1]	Cytosolic 10-formyltetrahydrofolate dehydrogenase; *ALDH1L1*	205	99622	17	9	11	6	15.5	902

MAG[1]	Myelin-associated glycoprotein; *MAG*	202	69880	12	8	6	4	14.1	626
TBA1A[1]	Tubulin α-1A chain; *TUBA1A*	199	50788	14	8	5	4	17.7	451
TBA3C[1]	Tubulin α-3C/D chain; *TUBA3C*	49	50612	9	4	4	3	14.4	450
TBA4A[1]	Tubulin α-4A chain; *TUBA4A*	42	50634	8	3	4	2	15.6	448
TBA8[1]	Tubulin α-8 chain; *TUBA8*	27	50746	5	1	4	1	13.1	449
UBB[1]	Polyubiquitin-B; *UBB*	199	25803	8	6	3	2	14.4	229
LONM[1]	Lon protease homolog, mitochondrial; *LONP1*	197	106936	20	9	12	5	13.2	959
KCRB[1]	Creatine kinase B-type; *CKB*	193	42902	6	4	3	2	10	381
NCAM1[1]	Neural cell adhesion molecule 1; *NCAM1*	192	95370	14	9	8	6	13.5	858
TENR[1]	Tenascin-R; *TNR*	179	151805	10	3	6	2	5.4	1358
C1TC[1]	C-1-tetrahydrofolate synthase, cytoplasmic; *MTHFD*	176	102180	13	8	9	5	13.7	935
SV2A[1]	Synaptic vesicle glycoprotein 2A; *SV2A*	162	83440	8	8	3	3	3.6	742
ADDB[1]	β-adducin; *ADD2*	159	81260	7	4	2	2	3.6	726
NFM[1]	Neurofilament medium polypeptide; *NEFM*	158	102468	7	4	4	2	4.9	916
NFH[1]	Neurofilament heavy polypeptide; *NEFH*	158	112639	5	3	3	1	2.8	1026
GANAB[1]	Neutral α-glucosidase AB; *GANAB*	150	107263	13	6	6	3	8.2	944
IMB1[1]	Importin subunit β-1; *KPNB1*	150	98420	4	3	2	1	3.7	876
EPHA4[1]	Ephrin type-A receptor 4; *EPHA4*	149	111443	10	7	4	3	5.3	986
EPHA3[1]	Ephrin type-A receptor 3; *EPHA3*	36	111714	2	2	1	1	1.3	983
EPHA2[1]	Ephrin type-A receptor 2; *EPHA2*	32	109679	4	1	3	1	4.6	976
NCAM2[1]	Neural cell adhesion molecule 2; *NCAM2*	147	93786	9	4	6	2	9.8	837
NCKP1[1]	Nck-associated protein 1; *NCKAP1*	138	130018	12	6	7	4	7.9	1128
SYIM[1]	Isoleucine--tRNA ligase, mitochondrial; *IARS2*	126	114688	8	3	6	2	8.7	1012
CYFP2[1]	Cytoplasmic FMR1-interacting protein 2; *CYFIP2*	123	150298	10	6	5	2	4.4	1278
CYFP1[1]	Cytoplasmic FMR1-interacting protein 1; *CYFIP1*	104	146742	9	3	3	1	3.4	1253
IMMT[1]	Mitochondrial inner membrane protein; *IMMT*	117	84026	17	8	8	5	13.5	758
E41L1[1]	Band 4.1-like protein 1; *EPB41L1*	116	99012	20	11	9	8	13.2	881
MAP1B[1]	Microtubule-associated protein 1B; *MAP1B*	115	271665	12	7	7	4	4.3	2468
CALX[1]	Calnexin; *CANX*	115	67982	8	8	3	3	5.2	592
MOG[1]	Myelin-oligodendrocyte glycoprotein; *MOG*	114	28574	4	3	2	2	10.1	247
MYO1D[1]	Unconventional myosin-Id; *MYO1D*	114	116927	10	4	6	1	9.7	1006
MAP2[1]	Microtubule-associated protein 2; *MAP2*	113	199860	9	3	7	2	18.4	478
NRCAM[1]	Neuronal cell adhesion molecule; *NRCAM*	110	144655	6	4	4	3	4.4	1304
KIF5C[1]	Kinesin heavy chain isoform 5C; *KIF5C*	108	109997	17	8	11	4	15.5	957
KIF5A[1]	Kinesin heavy chain isoform 5A; *KIF5A*	97	118161	10	5	5	2	5.9	1032
CTNB1[1]	Catenin β-1; *CTNNB1*	105	86069	11	6	7	4	12.7	781
AP180[1]	Clathrin coat assembly protein AP180; *SNAP91*	94	92672	7	2	4	1	5.3	907
TBB2A[1]	Tubulin β-2A chain; *TUBB2A*	82	50274	5	4	3	2	7.9	445
TBB2B[1]	Tubulin β-2B chain; *TUBB2B*	64	50377	3	2	2	1	4.3	445

DLG4[1]	Disks large homolog 4; *DLG4*	81	80788	13	6	8	5	14.6	724
LPHN1[1]	Latrophilin-1; *LPHN1*	80	164609	3	2	2	1	1.8	1474
AP2B1[1]	AP-2 complex subunit β; *AP2B1*	77	105398	11	5	8	3	10	937
ESYT1[1]	Extended synaptotagmin-1; *ESYT1*	76	123293	2	2	1	1	1.2	1104
ACTB[1]	Actin, cytoplasmic 1; *ACTB*	73	42052	6	2	3	1	15.2	375
CNTP1[1]	Contactin-associated protein 1; *CNTNAP1*	70	158220	3	2	2	1	1.7	1384
AT2A2[1]	Sarcoplasmic/endoplasmic reticulum Ca^{2+} ATPase 2; *ATP2A2*	69	116336	9	3	5	2	6.3	1042
AT2A1[1]	Sarcoplasmic/endoplasmic reticulum Ca^{2+} ATPase 1; *ATP2A1*	40	111550	5	1	3	1	3.2	1001
EF1A2[1]	Elongation factor 1-α 2; *EEF1A2*	66	50780	4	2	3	1	10.8	463
L2GL1[1]	Lethal(2) giant larvæ protein homolog 1; *LLGL1*	62	116657	2	2	1	1	1.1	1064
HIP1R[1]	Huntingtin-interacting protein 1-related protein; *HIP1R*	61	119999	8	2	5	1	6.5	1068
PLEC[1]	Plectin; *PLEC*	61	533462	19	3	18	3	5	4684
PGCB[1]	Brevican core protein; *BCAN*	60	100539	3	1	2	1	2.5	911
CTND2[1]	Catenin δ-2; *CTNND2*	60	133658	7	2	5	1	5.9	1225
DYHC1[1]	Cytoplasmic dynein 1 heavy chain 1; *DYNC1H1*	59	534809	13	4	9	1	2.5	4646
OMGP[1]	Oligodendrocyte-myelin glycoprotein; *OMG*	59	50032	7	4	2	2	6.6	440
MAP1A[1]	Microtubule-associated protein 1A; *MAP1A*	58	306781	13	3	11	2	5.2	2803
ADA22[1]	Disintegrin and metalloproteinase domain-containing protein 22; *ADAM22*	58	102991	1	1	1	1	1.5	906
PREP[1]	Presequence protease, mitochondrial; *PITRM1* pe 1	58	118407	2	2	1	1	1.2	1037
PDE2A[1]	cGMP-dependent 3',5'-cyclic phosphodiesterase; *PDE2A* pe 1	57	107360	5	4	3	2	4.5	941
E41L2[1]	Band 4.1-like protein 2; *EPB41L2*	54	113032	7	3	3	2	3.5	1005
AT2B1[1]	Plasma membrane Ca^{2+}-transporting ATPase 1; *ATP2B1*	51	139637	6	1	6	1	6.2	1258
ATPA[1]	ATP synthase subunit α, mitochondrial; *ATP5A1*	50	59828	4	1	3	1	8.1	553
NLGN3[1]	Neuroligin-3; *NLGN3*	50	94463	3	1	3	1	5.2	848
AT1B1[1]	Na^+/K^+-transporting ATPase subunit β-1; *ATP1B1*	48	35438	6	4	3	2	12.9	303
LIGO1[1]	Leucine-rich repeat and immunoglobulin-like domain-containing nogo receptor-interacting protein 1; *LINGO1*	47	70687	5	2	3	1	4.7	620
BRSK1[1]	Serine/threonine-protein kinase BRSK1; *BRSK1*	47	85604	7	1	5	1	8.1	778
WDR47[1]	WD repeat-containing protein 47; *WDR47*	47	103424	6	1	5	1	7.8	919
EFR3B[2]	Protein EFR3 homolog B; *EFR3B*	46	93397	2	1	2	1	3.1	817
SND1[1]	Staphylococcal nuclease domain-containing protein 1; *SND1*	45	102618	9	2	5	1	6.5	910
SC6A1[1]	Na^+- and Cl^--dependent GABA transporter 1; *SLC6A1*	44	67827	4	2	2	1	5.5	599
CAD13[1]	Cadherin-13; *CDH13*	44	78694	4	3	3	2	4.2	713
AUXI[1]	Putative tyrosine-protein phosphatase auxilin; *DNAJC6*	43	100675	5	2	5	2	8	913
BIN1[1]	Myc box-dependent-interacting protein 1; *BIN1*	43	64887	8	2	4	1	10.1	593
ACLY[1]	ATP-citrate synthase; *ACLY*	43	121674	5	3	4	2	5.4	1101
EXOC4[1]	Exocyst complex component 4; *EXOC4*	42	111170	4	2	3	1	4.7	974
SV2B[2]	Synaptic vesicle glycoprotein 2B; *SV2B*	40	78248	3	2	2	1	4.1	683

NELL2[1]	Protein kinase C-binding protein NELL2; *NELL2*	39	96359	1	1	1	1	1.1	816
CTNA2[1]	Catenin α-2; *CTNNA2*	37	106045	9	1	9	1	12.9	953
GRIA2[1]	Glutamate receptor 2; *GRIA2*	37	99385	8	4	4	4	5.9	883
GRIA1[1]	Glutamate receptor 1; *GRIA1*	34	102240	8	2	4	2	5.5	906
EEA1[1]	Early endosome antigen 1; *EEA1*	37	163337	2	1	2	1	1.8	1411
BCAS3[1]	Breast carcinoma-amplified sequence 3; *BCAS3*	36	102484	4	1	3	1	3.8	928
HGS[1]	Hepatocyte growth factor-regulated tyrosine kinase substrate; *HGS*	35	86708	1	1	1	1	1.5	777
KIF2A[1]	Kinesin-like protein KIF2A; *KIF2A*	35	80589	5	2	4	1	5.7	706
GIT1[1]	ARF GTPase-activating protein GIT1; *GIT1*	35	85030	4	2	2	2	3.9	761
SNG1[1]	Synaptogyrin-1; *SYNGR1*	34	25667	1	1	1	1	5.2	233
K2C1[1]	Keratin, type II cytoskeletal 1; *KRT1*	34	66170	5	2	3	2	5	644
GFAP[1]	Glial fibrillary acidic protein; *GFAP*	22	49907	5	2	4	2	11.1	432
K2C4[1]	Keratin, type II cytoskeletal 4; *KRT4*	22	57649	4	1	2	1	3.7	534
FAK2[1]	Protein-tyrosine kinase 2-β; *PTK2B*	33	117112	15	3	9	2	12.2	1009
ANFY1[1]	Ankyrin repeat & FYVE domain-containing protein 1; *ANKFY1*	32	129915	4	1	4	1	5	1169
NMDZ1[1]	Glutamate receptor ionotropic, NMDA 1; *GRIN1*	32	105990	7	1	4	1	5.9	938
SYGP1[1]	Ras GTPase-activating protein SynGAP; *SYNGAP1*	32	149160	7	1	5	1	6.1	1343
USO1[1]	General vesicular transport factor p115; *USO1*	31	108740	2	2	2	2	2.3	962
TPPC9[1]	Trafficking protein particle complex subunit 9; *TRAPPC9*	31	129817	2	1	1	1	0.8	1148
ITAV[1]	Integrin α-V; *ITGAV*	31	117048	3	1	3	1	4.5	1048
NMD3A[1]	Glutamate receptor ionotropic, NMDA 3A; *GRIN3A*	31	126525	34	1	1	1	0.6	1115
COPG2[1]	Coatomer subunit γ-2; *COPG2*	30	98700	8	1	4	1	5.7	871
PLCA[2]	1-acyl-sn-glycerol-3-phosphate acyltransferase α; *AGPAT1*	30	32038	2	1	1	1	3.5	283
IPO5[1]	Importin-5; *IPO5*	29	125032	3	2	2	2	2.3	1097
TBCD[1]	Tubulin-specific chaperone D; *TBCD*	29	134283	5	1	3	1	3.8	1192
ADDG[1]	γ-adducin; *ADD3*	28	79447	3	2	2	1	3.4	706
INP4A[1]	Type I inositol 3,4-bisphosphate 4-phosphatase; *INPP4A*	28	111539	3	1	3	1	4.6	977
NED4L[1]	E3 ubiquitin-protein ligase NEDD4-like; *NEDD4L*	28	112204	6	2	3	1	3.8	975
SGIP1[1]	SH3-containing GRB2-like protein 3-interacting protein 1; *SGIP1*	27	89453	6	3	3	2	4	828
GRIA3[1]	Glutamate receptor 3; *GRIA3*	26	101662	3	1	2	1	4	894
UTRO[1]	Utrophin; *UTRN*	26	396444	7	1	6	1	2.3	3433
BASP1[1]	Brain acid soluble protein 1; *BASP1*	26	22680	1	1	1	1	12.3	227
IQEC1[1]	IQ motif & SEC7 domain-containing protein 1; *IQSEC1*	26	109103	1	1	1	1	1.5	963
SRCN1[1]	SRC kinase signaling inhibitor 1; *SRCIN1*	25	112670	9	1	6	1	10.2	1055
SORT[1]	Sortilin; *SORT1*	25	92979	4	1	3	1	4.5	831
MLL4[1]	Histone-lysine *N*-methyltransferase MLL4; *WBP7*	25	297664	10	1	5	1	2.8	
XPO2[1]	Exportin-2; *CSE1L*	25	111145	5	1	4	1	4.5	971
CRNS1[1]	Carnosine synthase 1; *CARNS1*	24	89910	1	1	1	1	1.3	827

KPCE[1]	Protein kinase C ε type; *PRKCE*	24	84989	2	2	1	1	2.4	737
AP3B2[1]	AP-3 complex subunit β-2; *AP3B2*	24	119612	2	1	1	1	1.3	1082
DICER[1]	Endoribonuclease Dicer; *DICER1*	24	221279	3	1	1	1	0.4	1922
LR10B[4]	Leucine-rich repeat-containing protein 10B; *LRRC10B*	24	32864	4	1	3	1	14.7	292
SYNE3[1]	Nesprin-3; *SYNE3*	23	112774	4	1	4	1	6.4	975
MVP[1]	Major vault protein; *MVP*	23	99551	4	1	3	1	4.1	893
FOLH1[1]	Glutamate carboxypeptidase 2; *FOLH1*	22	84506	3	1	3	1	5.7	750
PTPRS[1]	Receptor-type tyrosine-protein phosphatase S; *PTPRS*	22	218159	7	2	5	1	4.1	1948
A4[1]	Amyloid βA4 protein; *APP*	22	87914	4	2	3	1	5.6	770
MBP[1]	Myelin basic protein; *MBP*	22	33097	4	1	1	1	3.9	304
SYN1[1]	Synapsin-1; *SYN1*	22	74237	2	1	2	1	5.8	705
IL25[1]	Interleukin-25; *IL25*	21	20887	5	2	1	1	5.6	177
EMC1[1]	ER membrane protein complex subunit 1; *EMC1*	21	112145	2	1	1	1	1.3	993
SPTN4[1]	Spectrin β chain, non-erythrocytic 4; *SPTBN4*	21	290005	9	1	7	1	3.8	2564
DPP10[1]	Inactive dipeptidyl peptidase 10; *DPP10*	21	91401	2	1	2	1	3.6	796
APOB[1]	Apolipoprotein B-100; *APOB*	20	516651	4	1	4	1	1.2	4563
DDX58[1]	Probable ATP-dependent RNA helicase DDX58; *DDX58*	19	108014	14	2	4	1	3.9	925
ZMYM3[1]	Zinc finger MYM-type protein 3; *ZMYM3*	18	156101	4	1	4	1	2.7	1370
LPIN1[2]	Phosphatidate phosphatase LPIN1; *LPIN1*	18	99287	4	1	3	1	6.2	890
UBE4A[1]	Ubiquitin conjugation factor E4 A; *UBE4A*	17	123565	5	1	3	1	4.1	1066
PLLP[1]	Plasmolipin; *PLLP*	17	20087	1	1	1	1	12.6	182
CCL28[1]	C-C motif chemokine 28; *CCL28*	17	14670	3	1	3	1	18.9	127
TAU[1]	Microtubule-associated protein tau; *MAPT*	17	79108	4	1	2	1	3.2	758
NXPE2[2]	NXPE family member 2; *NXPE2*	16	65601	5	1	1	1	3	559
DSCL1[1]	Down syndrome cell adhesion molecule-like protein 1; *DSCAML1*	15	226147	2	1	2	1	1.1	2053
DYH9[1]	Dynein heavy chain 9, axonemal; *DNAH9*	15	515599	17	1	16	1	4.4	4486
MK06[1]	Mitogen-activated protein kinase 6; *MAPK6*	15	83256	4	1	3	1	6.4	721
LRC52[1]	Leucine-rich repeat-containing protein 52; *LRRC52*	14	35731	2	1	2	1	12.5	313
FBX47[2]	F-box only protein 47; *FBXO47*	13	52846	20	1	2	1	8	452
CO2A1[1]	Collagen α-1(II) chain; *COL2A1*	13	142782	3	1	2	1	2.4	1487

Notes as for Table 4.3